The Effects of Cerebral Ischaemia on Pericytes and Neurovascular Function

Ain A. Neuhaus
St John's College
University of Oxford

A thesis submitted for the degree of
Doctor of Philosophy

October 2016

Abstract

Acute ischaemic stroke is a major cause of morbidity and mortality in the developed world, yet the treatment options available are limited to therapies that restore vessel patency. Recanalisation of the occluded artery does not necessarily result in reperfusion of the downstream microvasculature, however, and the pathomechanisms involved in this are incompletely understood. One putative mediator of this is the capillary pericyte, a vascular mural cell type that may constrict under ischaemic conditions. The overarching aim of this thesis was to characterise vascular function following cerebral ischaemia, using *in vivo*, *ex vivo* and *in vitro* approaches. First, I demonstrated that ischaemia reduced both ipsilateral and contralateral cerebral blood flow responses to hypercapnia, and diminished reactivity of isolated pressurised arteries. I then developed a novel assay to characterise human pericyte contractility *in vitro*, and demonstrated that they are responsive to vasoactive substances even in the absence of αSMA expression. In this assay, chemical ischaemia caused pericyte contraction and subsequent death, consistent with *in vivo* reports describing their role in the no-reflow phenomenon. Finally, I explored whether the voltage-gated Ca^{2+} channel antagonist nimodipine could improve reperfusion in cerebral ischaemia, and found that rats treated with nimodipine exhibited improved post-ischaemic cerebral blood flow and ameliorated neurological impairment. However, I did not find a direct effect of nimodipine on pericyte contractility during chemical ischaemia *in*

vitro, indicating that nimodipine may be targeting other cell types in the vasculature. Together, these data highlight the importance of vascular function following stroke and shed light on putative vasculoprotective approaches, which have translational potential to improve reperfusion in patients receiving recanalisation therapy.

Statement of Authorship

The work presented in this thesis does not contain material written or published by any other person, except where indicated in the text. Contributions from other researchers to the design, conduct and analysis of experiments are as follows:

Chapter 1: Dr. Yvonne Couch (University of Oxford) assisted in preparing Figure 1.

Chapter 2: Dr. Brad Sutherland assisted with the design of *in vivo* experiments. Dr. Zuzana Broskova (Augusta University) performed most of the vessel isolation experiments and data analysis, presented in Figure 2.10, using animals that I had operated on; I performed the final statistical analysis. I analysed cerebral blood flow and eletrophysiology data presented in Figures 2.3-2.9 using custom software previously developed by Dr. Chris Martin (University of Sheffield).

Chapter 3: I designed, conducted and analysed the experiments jointly with Dr. Couch. Most of the work has been published, with Dr. Couch and I as co-first authors (Neuhaus et al., 2016).

Chapter 4: I designed and analysed the experiments independently. Dr. Couch assisted with blinding and the behavioural studies presented in Figures 4.2, 4.3 and 4.5.

Chapter 5: none.

Acknowledgements

I am deeply grateful for the opportunity to have worked with so many incredible scientists, who supported me through difficult times of self-doubt and slow scientific progress. My supervisors, Alastair Buchan and Daniel Anthony, have been outstanding role models in their approach to research. I can only hope that I make the most of the important lessons they have taught me.

The experiments described in this thesis would not have been possible without help from a number of people. I would particularly like to thank Zoran Redzic, who was incredibly generous with his time and patience, accrued a lot of frequent flyer miles over his many trips to Oxford, and provided a great deal of counsel regarding the cell culture experiments chapters 3 and 4.

Zuzana Broskova was pivotal in conducting the isolated vessel experiments in chapter 2. Clare Howarth, Chris Martin, Aisling Spain, Sebastien Serres and Manuel Sarmiento Soto (all from Nicola Sibson's laboratory), Brad Sutherland, and Judith Schweimer very kindly shared their expertise and equipment to allow me to perform the blood flow imaging and electrophysiology experiments in chapter 2.

The experiments described in chapter 4 were part of a collaboration with David Attwell, whose advice (and generosity with sharing his confocal microscopes!) I greatly appreciate. Catherine Hall and Fergus O'Farrell

from the Attwell lab provided crucial help with designing and conducting pericyte death experiments in acute brain slices.

I am also grateful to all the members and collaborators of the Buchan and Anthony labs, for their help in the lab and camaraderie outside of it: Brad Sutherland, Michalis Papadakis, Tamer Rabie, Jim Peeling, Gabriele De Luca, Zonghang Zhao, Scarlett Harris, Giacomo Bertuzzi, Nareg Kalajian, Inês Sá Pereira, Jay Roodselaar, Fay Probert, Christina Simoglou Karagli. A special thanks goes to Pramodi Majithia, whose ability to organise things at a moment's notice has been absolutely invaluable over the years.

Gina Hadley, my contemporary DPhil student in the lab, has been a great friend and mentor, and I am honoured to have been the other half of "team 4-VO" – for my ineptitude as a scrub nurse, I can only apologise. She demonstrates every day that it is possible, if frequently stressful, to combine clinical practice with an interest in understanding the fundamental biology underpinning what we see in patients.

I am forever indebted to Yvonne Couch. Without her, this thesis would never have been completed – her pragmatic and logical approach to science has been a true inspiration, and her willingness to spend time providing informal psychotherapy to stressed students is the stuff of legend. She has been an amazing friend and should be considered as a third supervisor to this thesis.

Finally, I would like to thank my family for their support, patience, and unwavering faith in me.

Contents

List of Figures

List of Tables

Chapter 1

Introduction

1.1 Stroke

Stroke—a neurological deficit associated with focal brain injury arising from vascular causes—is a leading cause of morbidity and mortality (Sacco et al., 2013). Recent US statistics rank stroke as the 5th most common cause of death, accounting for approximately 1 in every 20 deaths; globally, it may account for as many as 11.8% or 6.5 million deaths annually (Mozaffarian et al., 2015; GBD 2013 Mortality and Causes of Death Collaborators, 2015). Although stroke mortality and incidence have been declining in recent decades, the rising average age of the population in developed countries and increasing prevalence of risk factors (such as diabetes and hypertension) in low- and middle-income countries will result in 12 million annual stroke deaths and in excess of 200 million disability-adjusted life years lost globally by 2030, based on current trends (Feigin et al., 2014). As such, strategies for stroke prevention and improved management of patients in both the acute and chronic phases of stroke form major priorities of contemporary medical research (Mendis et al., 2015; Hachinski et al., 2010).

Broadly, stroke can be divided into ischaemic and haemorrhagic subtypes, where the underlying vascular cause is occlusion or rupture of a cerebral vessel, respectively. Approximately 87% of strokes are ischaemic (Mozaffarian et al., 2015), with 68% of infarcts located in the carotid territory (see section 1.3.1); of these, 96% affect the

middle cerebral artery (MCA) territory (Bogousslavsky et al., 1988). The clinical presentation of ischaemic stroke varies immensely, depending on the functions of the cerebral regions supplied by the occluded artery: in MCA strokes, typical symptoms include contralateral hemiplegia/hemiparesis, hemisensory loss and, in the case of left hemisphere strokes, aphasia (Ferro and Fonseca, 2014). The morbidity and mortality of ischaemic stroke are greatly exacerbated by further neurological and medical complications, including haemorrhagic transformation, cerebral oedema, epileptic seizures, and infections due to immunosuppression (Balami et al., 2011; Langhorne et al., 2000).

Despite the immense clinical need, there is a dearth of therapeutic options in stroke. Currently, only five interventions have adequate evidence of improving outcomes:

- endovascular thrombectomy (EVT) to recanalise the affected vessel, in particular by mechanical withdrawal of the clot using stent-retrievers (Balami et al., 2015; Badhiwala et al., 2015);
- thrombolysis with intravenous recombinant tissue-type plasminogen activator (IV-rt-PA) to degrade the thrombus (The National Institute of Neurological Disorders and Stroke rt-PA Stroke Study Group (NINDS), 1995; Wardlaw et al., 2012);
- early administration of aspirin to reduce stroke recurrence (Chen et al., 2000);
- hemicraniectomy in the case of malignant space-occupying MCA infarctions (Schwab et al., 1998);
- treatment of patients in a specialised stroke unit/ward (Stroke Unit Trialists Collaboration, 1997).

While interventions to prevent secondary recurrence are quite widely used, the two

acute treatments—IT-rt-PA and EVT— are administered to relatively few patients, with only 2-5% receiving IV-rt-PA in most centres (Donnan et al., 2011). Nonetheless, IV-rt-PA was the first true revolution in stroke care, as it provided a means to interfere in in the ongoing pathological process of infarction and restore cerebral blood flow (CBF) to the affected region, rather than simply dealing with the consequences and preventing recurrence. The reasons behind the underuse of thrombolytic therapy include the 4.5 hour window following stroke onset in which it can be administered, as well as various other risk factors (including severe hypertension, hyperglycaemia, and combination antiplatelet drugs), necessitating careful imaging-based selection to ensure only appropriate cases are treated (Balami et al., 2013). In addition, IV-rt-PA is relatively inefficient at disrupting large occlusions in proximal vessels, leading to poor recanalisation rates (Bhatia et al., 2010).

The new gold standard therapy, EVT using stent-retrievers to mechanically remove the clot, yields superior results for large artery recanalisation, but this comes at the cost of much greater procedural complexity and the need for considerable resources and infrastructure. As such, it is performed far more infrequently than thrombolysis with IV-rt-PA, although recent successes from clinical trials will likely lead to a substantial increase in the availability of EVT (Wardlaw and Dennis, 2015). There are also several important unanswered questions surrounding EVT, including exact contraindications and patient selection criteria (Wardlaw and Dennis, 2015). Despite this, the advent of recanalisation methods with relatively high efficacy has brought stroke intervention into a new era. Further improvements may well be made to the organisation of stroke emergency management and the design of EVT devices, which could increase the number of patients who reach stroke centres in time to benefit from more efficient recanalisation of the artery.

Nonetheless, it is inevitable that not all patients will be recanalised before the infarct has fully developed and no salvageable tissue remains. Indeed, a key concept

in stroke pathophysiology is the distinction between the penumbra—a region of electrically silent hypoperfused tissue that remains viable if reperfused in time—and the core, an area of irreversible injury due to total energy depletion and the catastrophic loss of ion homoeostasis that follows (Dirnagl et al., 1999). While viable, the penumbra will still have ongoing ischaemic signalling cascades, which result in a progressive loss of cells through a host of mechanisms, including spreading depolarisations (see section 1.6), inflammation, and apoptosis (Dirnagl et al., 1999). As such, the penumbra will be converted into irreversibly damaged tissue over time. The aim of all acute stroke therapies is to prevent this conversion process from occurring, through restoration of blood flow or direct protection of neurons (Minnerup et al., 2012). Once the penumbra is lost, recanalisation is futile and potentially dangerous due to increased risk of haemorrhagic transformation (Balami et al., 2013). This patient population will benefit only from neurorehabilitation and neurorepair strategies, which form another major focus of stroke research (Cramer, 2008a,b).

Even in the recanalised patients, however, there is considerable scope to improve recovery and ameliorate pathological processes on a cellular level (see section 1.6.1). The focus of this thesis will be on the microvasculature (in particular the capillary pericyte) and its interactions with other cell types in the ischaemic and reperfused brain, with the aim of both describing changes to constituent cell types of the cerebral microvasculature as well as investigating putative vasculoprotective compounds to enhance its function and survival.

1.2 Neurovascular unit

In recent decades, there has been an increasing focus on the roles of glial cells and the vasculature in CNS function (Aguzzi et al., 2013; Tsacopoulos and Magistretti, 1996; Araque et al., 1999; Tremblay et al., 2011; Perea et al., 2009). Of particular interest is the neurovascular unit (NVU), the interface between vascular and neural tissue, which

has two critical roles: first, it must provide the brain parenchyma with nutrients and remove by-products of cerebral metabolism, given the reliance of neurons on oxidative phosphorylation and the limited store of energy substrates in the brain (Harris et al., 2013). Simultaneously, the markedly different composition of blood cannot disturb the delicate ionic homeostasis needed for neural transmission. Therefore, the NVU must provide protection from uncontrolled diffusion of ions as well as exogenous substances that could affect neurotransmission or cause neurotoxic effects. This impermeable endothelial phenotype is termed the blood-brain barrier (BBB; Neuwelt et al., 2011; Abbott et al., 2010, 2006), and it is induced and maintained by capillary pericytes during development and through adulthood (Armulik et al., 2010; Daneman et al., 2010; Bell et al., 2010). As a result of this tight integration, it is unsurprising that numerous structural and functional changes in the neurovascular unit have been described in a host of clinical conditions including Alzheimer's disease (Nicolakakis et al., 2011), diabetes (Mishra and Newman, 2010), multiple sclerosis (MS; Errede et al., 2012) and stroke (Yang and Rosenberg, 2011).

The canonical constituent cell types of the NVU are neurons, astrocytes, vascular smooth muscle (VSM) cells, pericytes and endothelial cells (Lecrux and Hamel, 2011); however, microglia and perivascular macrophages can also be included as part of the NVU, partly due to their potent effects on barrier function in inflammation (Vangilder et al., 2011). Our understanding of the signalling mechanisms that operate between these cells has expanded immensely over the last 20 years, and we are now able to attribute particular functions to specific cell types in the NVU, some of which will be discussed in greater details below (sections 1.3.3, 1.4.1 and 1.4.3). This plethora of interactions has direct implications for neuronal function, including regulation neurogenesis during development and adulthood by the vascular niche (Stubbs et al., 2009; Goldman and Chen, 2011; Andreone et al., 2015); more speculatively, it has been suggested that vascular mechanisms can directly influence neuronal

information processing (Moore and Cao, 2008). Conversely, neuronal activity affects the other constituents of the NVU: there is a well-characterised relationship between synaptic activity and astrocytic (Perea et al., 2009; Araque et al., 1999; Nedergaard and Verkhratsky, 2012; Sun et al., 2013), microglial (Tremblay et al., 2011) and oligodendrocytic responses (Fields, 2008). While these are indubitably important for normal CNS homoeostasis, the main interaction explored in this thesis is the regulation of nutrient supply via the vasculature to meet metabolic demand in the parenchyma.

1.3 Neurovascular coupling

Effectively by definition, the NVU is the structure mediating neurovascular coupling (NVC) – the regulation of regional cerebral perfusion in response to local neural activity. In parallel to understanding the interactions between the information-processing elements of the brain and the vasculature, using blood flow as a functional read-out of CNS activity, as extrapolated through assumptions regarding NVC, has become a crucial tool in our understanding of neural processing since the pioneering studies of Kety, Ingvar and others in the mid-20$^{\text{th}}$ century regarding quantitative CBF changes in humans (Raichle and Mintun, 2006; Raichle, 2009). These observations have contributed immensely to the emergence of cognitive and social neuroscience, where complex behaviours can be correlated with neurobiological changes in a non-invasive manner, thus making it suitable for use in human subjects (Raichle and Mintun, 2006).

1.3.1 Cerebrovascular anatomy

Cerebral blood supply is provided by two bilateral sets of large vessels, the carotid and vertebral arteries, which conduct approximately 15% of cardiac output (Hirsch et al., 2012) to meet the considerable energy demands of the brain, amounting to 20%

of resting energy consumption despite forming only 2% of body mass (Attwell et al., 2010). These vessels contribute to the circle of Willis, an anastomotic structure at the base of the brain giving rise to arteries supplying well-defined regions of tissue, with limited overlap in their feeding territories (Hirsch et al., 2012). A pial network composed of large arteries then undergoes ramification and forms the descending arteries and arterioles, which dive into the parenchyma itself and subdivide (Hirsch et al., 2012). Beyond this point, the terminology and precise classifications become more contentious, with distinctions between small arterioles and large capillaries relatively difficult to make (see section 1.4.3; Fernández-Klett et al., 2010; Hill et al., 2015; Dalkara and Alarcon-Martinez, 2015), but in either case, it can be said that there is a general progressive reduction in mural cell coverage of the tunica intima until only pericytes remain atop the endothelium and within its associated basal lamina (Hamilton et al., 2010; Dalkara and Alarcon-Martinez, 2015). A similar pattern then occurs in reverse, with venous drainage consolidating into progressively larger vessels and emerging from the parenchyma into a pial network (Hirsch et al., 2012). In addition, anastomotic interactions are seen at all levels within the arterial and venous networks (Hirsch et al., 2012). These anatomical and topological features are also relevant to the mechanisms of NVC, as the maximal spatial resolution of CBF regulation depends on the site where it occurs along the microvasculature (see section 1.4.3).

1.3.2 Historical studies

NVC was first observed through openings in the cranium in neurosurgical patients by Mosso in the 1870s, when he described an increase in pulsatile activity during mental arithmetic tasks (Raichle, 2009). However, such measurements were fraught with methodological difficulties and inconsistencies due to an inability to simultaneously measure systemic arterial and venous pressure at the time, which could alter

perfusion independently of changes in local vessels (Roy and Sherrington, 1890). This necessitated the use of animal models, which enabled Roy and Sherrington to describe NVC in much greater detail using sensory or chemical stimulation in dogs, cats and rabbits, and thus confirm that "the brain possesses an intrinsic mechanism by which its vascular supply can be varied locally in correspondence with local variations of functional activity" (Roy and Sherrington, 1890).

NVC was originally explained as a feedback mechanism, evoked by increased utilisation of glucose during neuronal activity. The accumulation of metabolites such as lactate was assumed to cause vasodilation and increase CBF in the active region (Roy and Sherrington, 1890), similarly to other tissues such as skeletal muscle. This was supported by early studies of functional imaging in humans, showing good correlations between cerebral O_2 metabolism ($CMRO_2$) and CBF, as revealed by positron emission tomography (PET; Raichle et al., 1976). However, it was subsequently demonstrated that the functional hyperaemic response (ΔCBF) during a visual task exceeds $\Delta CMRO_2$ approximately 6-fold (Fox and Raichle, 1986), which the authors described as "physiological uncoupling" of flow and metabolism and suggested this was a feedforward mechanism. Nonetheless, their results did not exclude precise coupling between CBF and another indicator of activity, such as accumulation of K^+ or neurotransmitter metabolites in the microvascular milieu, or direct neurogenic regulation of vessel tone.

1.3.3 Neural correlates of flow

It is universally accepted that functional hyperaemia is a consequence of neural activity, but the nature of the process triggering this response is less clear, including which aspect of neuronal physiology contributes most to evoking blood flow (Attwell and Iadecola, 2002). *A priori*, the regulation of blood supply should match the processes that are most energy-demanding. It has been estimated that the

majority of adenosine triphosphate (ATP) utilised by neurons is due to postsynaptic mechanisms downstream of glutamate receptors, with smaller contributions from action potentials, resting potentials and neurotransmitter handling, which suggests that synaptic transmission is the most relevant parameter for CBF regulation (Attwell and Laughlin, 2001; Howarth et al., 2012). In white matter, there is a much greater contribution of housekeeping processes to energy demand, followed by resting potentials and a small contribution from synaptic transmission and action potentials (Harris and Attwell, 2012). The seminal work of Logothetis et al. in the macaque visual cortex demonstrated that, using simultaneous electrophysiological recordings and blood oxygen level-dependent functional magnetic resonance imaging (BOLD-fMRI) signal (see section 1.5.3), local field potentials (LFPs) correlated more closely with BOLD signal than multi-unit activity (MUA Logothetis et al., 2001). As LFPs primarily reflect synaptic activity and MUA indicates spiking activity, this further supported the hypothesis that synaptic transmission is the main reason for NVC.

However, as noted previously with regard to physiological uncoupling, CBF need not be directly coupled to energy demand. Indeed, work by numerous groups has suggested that the flow increase is tightly correlated with both presynaptic and postsynaptic activity and downstream mechanisms such as changes in intracellular Ca^{2+} concentration ($[Ca^{2+}]_i$), but not with spike rate or potential changes per se (Lauritzen, 2001; Caesar et al., 2003; Hoffmeyer et al., 2007). Nonetheless, many questions regarding the exact correlation of vascular responses and their neural substrates remain poorly understood, including the linearity or non-linearity of CBF increases in relation to electrophysiological changes (Sheth et al., 2003, 2004; Devor et al., 2003; Norup Nielsen and Lauritzen, 2001), laminar (Goense et al., 2012) and inter-areal variations of quantitative and qualitative aspects of NVC (Attwell et al., 2010), pathway-specific features of coupling within the same region (Enager et al., 2009), and the existence of multiple haemodynamic response components, such as

anticipatory responses in the absence of sensory stimulation (Sirotin and Das, 2009; Logothetis, 2010).

1.4 Mechanisms of blood flow control

Our understanding of CBF control in terms of its cellular and molecular basis has expanded vastly in the past three decades, albeit in a non-unified manner: there is ample evidence from slice preparations and *in vivo* pharmacological experiments implicating a diverse—and occasionally contradictory—list of mediators in NVC (Fig. 1), with numerous attempts to provide integrative explanations to account for this observed heterogeneity and inconsistency (Attwell et al., 2010; Hillman, 2014). There are three key ambiguities that have caused controversy in the field, as views have undulated between extremes regarding whether or not certain mechanisms are involved in NVC.

1.4.1 Cellular mechanisms of NVC initiation

The first of these dichotomies is the cell type that signals to the vasculature to evoke dilation. Direct neurovascular transmission would seem the optimal mechanism, providing the most precise spatiotemporal coupling. In acute brain slices, changes in microvessel diameter have been observed in response to stimulation of perivascular interneurons (Cauli et al., 2004). The same group demonstrated that interfering with signalling through excitatory N-methyl-D-aspartate (NMDA) glutamatergic receptors, inhibitory γ-aminobutyric acid (GABA) type A ($GABA_A$) receptors or inhibiting the production of vasodilatory prostaglandins by cyclooxygenase-2 (COX-2) reduced CBF responses to whisker stimulation (Lecrux and Hamel, 2011). Cyclooxygenase-1 (COX-1) inhibitors had no effect and they were unable to find COX-2 expression in non-neuronal cells in the parenchyma, implying the regulatory cells were COX-2-expressing neurons. According to this model, NVC is dependent on

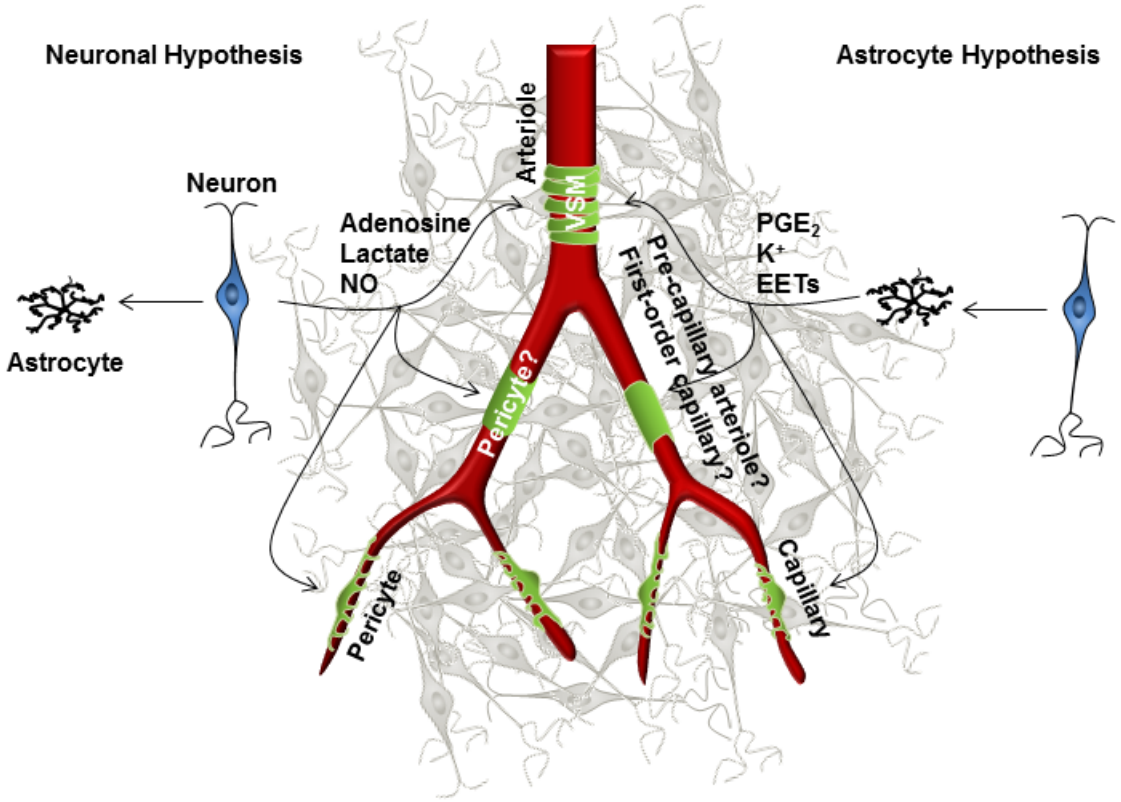

Figure 1.1: Major signalling pathways implicated in neurovascular coupling. Adapted from Attwell et al. (2010).

a glutamatergic-GABAergic neural network, with neurons acting either directly on vessels, or via astrocyte-mediated release of epoxyeicosatrienoic acids (EETs; Lecrux et al., 2011; Lecrux and Hamel, 2011). The involvement of nitric oxide (NO), produced by the neuronal isoform of nitric oxide synthase (nNOS), has also been suggested in NVC (Dirnagl et al., 1993, 1994; Lindauer et al., 1999), but the interpretation of these data is more complex (see section 1.4.2).

The main problem with the neuronal hypothesis is the relative paucity of direct neurovascular contacts (Vaucher and Hamel, 1995; Estrada et al., 1993; Mathiisen et al., 2010), which would severely limit the maximal resolution of NVC as relatively large regions would need to receive an increase in CBF to accommodate what might only be a small population of active cells. Conversely, astrocytes provide much denser coverage of the microvasculature (Mathiisen et al., 2010; Koehler et al., 2009). The first clear indications of astrocytes as mediators of NVC came from cortical slice experiments, where stimulation of astrocytes or neuronal afferents resulted in an increased $[Ca^{2+}]_i$ in astrocytes as well as vasodilation in adjacent microvessels (Zonta et al., 2003). Importantly, trans-1-amino-1,3-dicarboxycyclopentane (tACPD), an agonist of metabotropic glutamate receptors (mGluRs), produced comparable increases in astrocytic $[Ca^{2+}]_i$ and vessel diameter, whereas the mGluR antagonists LY367385 and 2-methyl-6-(phenylethynyl)pyridine (MPEP) abolished both astrocytic $[Ca^{2+}]_i$ elevations and vasodilation, without detectably affecting neuronal $[Ca^{2+}]_i$. This was further supported by *in vivo* suppression of forepaw stimulation CBF responses after MPEP and LY367385 administration, although they could not directly show this was as a consequence of astrocyte signalling (Zonta et al., 2003).

MacVicar's group noted that Ca^{2+} uncaging in astrocytes triggered propagating astrocytic Ca^{2+} waves and vasoconstriction via arachidonic acid metabolites (Mulligan and MacVicar, 2004), which seemingly contradicted the aforementioned conclusion of astrocytes inducing vasodilation (Zonta et al., 2003), whilst further

supporting the case of astrocytic involvement in CBF regulation. The controversy has since been reconciled by the discovery of O_2-dependent changes in the polarity of vascular responses and different conditions used in the two papers: Zonta et al. (2003) used oxygen pressures more closely mimicking the physiological situation *in vivo* and observed vasodilation, whereas Mulligan and MacVicar (2004) used much higher oxygen pressures, resulting in astrocyte-mediated vasoconstriction (Gordon et al., 2008). Most of the earlier work on astrocytic $[Ca^{2+}]_i$ and its effects on the cerebral microvasculature was done in hippocampal or cortical slices from rodents; however, Ca^{2+} waves also correlated with vascular changes in the cerebellum during motor activity (Nimmerjahn et al., 2009) and in the somatosensory cortex during whisker stimulation (Wang et al., 2006b). Moreover, uncaging Ca^{2+} in astrocytic endfeet in vivo caused vasodilation in adjacent vessels, with a clear correlation between the $[Ca^{2+}]_i$-dependent fluorescent signal and diameter changes (Takano et al., 2006).

Although there is a general consensus that astrocytic responses must be involved in NVC at least to some extent (Lecrux and Hamel, 2011; Attwell et al., 2010; Koehler et al., 2009; Petzold and Murthy, 2011; Iadecola and Nedergaard, 2007; Cauli and Hamel, 2010), there are disagreements regarding the relative importances and contributions to astrocytes and neurons, and in determining the pathways through which they operate (Lecrux and Hamel, 2011; Cauli and Hamel, 2010). For instance, the temporal dynamics of astrocytic Ca^{2+} waves are unclear: in one experiment, whole-cell responses were delayed relative to neuronal voltage changes and CBF increases in the somatosensory cortex, although this was not necessarily representative of changes in the endfeet domains (Ghosh et al., 2013). Other studies using genetically encoded Ca^{2+} indicators (GECIs) have altogether failed to find $[Ca^{2+}]_i$ rises during visual stimulation, despite robust hyperaemia (Bonder and McCarthy, 2014).

Even in studies that support astrocytic involvement in NVC, local uncaging of Ca^{2+} in astrocyte endfeet resulted in vasodilation with a 1-2 second latency (Takano

et al., 2006), whereas others have found using optical imaging that blood flow increases approximately 600 ms after stimulation (Devor et al., 2003). Similarly, *in vivo* 2-PM work specifically examining Ca^{2+} endfeet found that $[Ca^{2+}]_i$ increases were delayed by 3–6 seconds relative to LFPs (Wang et al., 2006b). Studies using transgenic mice lacking the gene encoding inositol-3-phosphate receptor 2 ($IP_3R_2^{-/-}$) have further argued against the astrocyte hypothesis, as this ostensibly prevents mGluR-mediated signalling; CBF responses to somatosensory stimulation, however, were unaffected (Nizar et al., 2013; Takata et al., 2013). The corollary experiment, where astrocytes were selectively activated using designer receptors exclusively activated by designer drugs (DREADDs), also failed to affect cortical blood flow (Bonder and McCarthy, 2014). Recent evidence suggests that astrocytic $[Ca^{2+}]_i$ responses to glutamate are dependent on the developmental stage of the animal and appear to be more prominent in the first 3 weeks of life in mice (Sun et al., 2013). This could call some of the previously obtained evidence from slices into question, as juvenile animals are typically used to harvest slices due to their improved viability *ex vivo*.

These diverging data are potentially reconciled by more detailed understanding of the compartmentalisation of $[Ca^{2+}]_i$ rises in astrocytes, and the extent to which these are altered in different experimental settings. It has become clear that $IP_3R_2^{-/-}$ astrocytes continue to have elaborate $[Ca^{2+}]_i$ variations in their endfeet, thus invalidating the argument that these mice cannot have astrocyte-mediated NVC (Srinivasan et al., 2015). Development of more elaborate image analysis techniques has also enabled detailed examination of endfoot $[Ca^{2+}]_i$; during whisker stimulation, Ca^{2+} transients in astrocyte endfeet correlated much more closely with whisker stimulation-induced CBF than transients in neuronal somata or the neuropil (Lind et al., 2013). Similar observations have also been made in the olfactory bulb (Otsu et al., 2015). As such, the controversies regarding astrocyte contribution to NVC have not been fully resolved, but the compartmentalisation hypothesis may provide

a unifying theory (Bazargani and Attwell, 2016).

1.4.2 Molecular mechanisms of NVC

The difficulties in precisely defining the initiating cell types involved in NVC have inevitably complicated the identification of signalling cascades underlying the phenomenon. Nonetheless, experiments utilising pharmacological antagonism or knockout of signalling-associated proteins (such as the putative mediator itself in the case of peptides, synthetic enzymes in the case of small molecules or lipids, or the receptors on target cells) have revealed a number of agents contributing to NVC (Figure 1.1). Firstly, a number of neurotransmitters have been associated with blood flow regulation, including glutamate (Busija and Leffler, 1989; Faraci and Breese, 1993), GABA, vasoactive intestinal peptide (VIP), somatostatin, neuropeptide Y (NPY; Cauli et al., 2004), serotonin or 5-hydroxytryptamine (5-HT), acetylcholine (ACh; Scremin et al., 1973) and others (for a comprehensive review, see Iadecola and Nedergaard 2007). However, given the uncertainties regarding the cell types involved, it is unsurprising that the list of known or suspected mediators extend far beyond classical neurotransmitters (Attwell et al., 2010; Cauli and Hamel, 2010).

In terms of alternative neuronal products, the most thoroughly characterised is NO, in particular that derived from nNOS in response to elevations of neuronal $[Ca^{2+}]_i$ after activation of NMDA receptors (Knowles et al., 1989; Faraci and Breese, 1993; Domoki et al., 2002). NO acts as a potent vasodilator via cyclic GMP (cGMP Bredt and Snyder, 1989) and protein kinase G (Archer et al., 1994), or via direct actions on Ca^{2+}-activated K^+ channels (Archer et al., 1994; Bolotina et al., 1994). Inhibition of NOS (in an non-isoform-specific way) reduced functional hyperaemia in response to whisker stimulation without altering vascular reactivity to NO donors (Dirnagl et al., 1993, 1994), suggesting it was signalling from the parenchyma to the vessel wall. This was later verified using an nNOS-specific blocker, which also decreased

CBF responses without affecting cerebral glucose utilisation, an indicator of neuronal activity (Cholet et al., 1997). However, it was subsequently shown that NO donors (i.e. an activity-independent increase in NO concentration) also restored NVC after NOS blockade, which is not consistent with its role as a direct mediator; rather, it must function as a modulator of other signalling mechanisms (Lindauer et al., 1999). Some of these conclusions have been criticised as not taking into account confounding factors—including effects of NO inhibition on neural activity (Stefanovic et al., 2007), regional heterogeneity (Yang et al., 2003; Gotoh et al., 2001) and other factors—which complicate analysis of the roles of NO in the cerebral microvasculature (Duchemin et al., 2012). More recently, it has been suggested based on slice experiments that NMDA-dependent activation of endothelial nitric oxide synthase (eNOS) could be implicated in NVC (Stobart and Anderson, 2013; LeMaistre et al., 2012), but given the previous negative results in piglet in vivo eNOS inhibition experiments (Domoki et al., 2002) and eNOS mouse knockout models (Ayata et al., 1996), eNOS is unlikely to be a key mediator.

In addition to NO, the agents that have been examined most thoroughly in the setting of NVC are arachidonic acid (AA) metabolites, derived from membrane phospholipids and processed into a number of structurally related but pharmacologically distinct products (Needleman et al., 1986). The best-characterised of these is the COX pathway, producing prostaglandin H_2 (PGH_2), which can then be converted into PGD_2, PGE_2, PGI_2, PGF_2 or thromboxane A_2 (TXA_2) by specific synthase enzymes (Attwell et al., 2010). The main effect observed with COX inhibition is a diminution of vasodilation, usually assumed to be due to reductions in the strongly vasodilatory PGE_2 (Zonta et al., 2003; Gordon et al., 2008; Davis et al., 2004), although prostaglandins PGD_2, PGI_2 and PGG_2 are also vasodilators (Ellis et al., 1979) and PGD_2 appears to be produced in relatively large quantities in cultured astrocytes (Amruthesh et al., 1993). Their pharmacology is incompletely understood,

but the main vasodilatory mechanism is thought to be $G_{\alpha s}$-coupled PGE_2 receptor 4 activation, leading to cyclic adenosine monophosphate (cAMP) production and subsequent inactivation of the contractile apparatus in VSM cells (Davis et al., 2004; Hata and Breyer, 2004), or acting indirectly to upregulate endothelial NO production (Hristovska et al., 2007). It should be noted that PGE_2 has recently been reported to be a vasoconstrictor in isolated rat and mouse parenchymal arterioles, due to activation of PGE_2 receptor 1, which is thought to be $G_{\alpha q}$-coupled (Dabertrand et al., 2013); however, this has not yet been replicated and in any case bears less relevance to the *in vivo* setting than previous experiments done in acute brain slices (Zonta et al., 2003; Gordon et al., 2008).

There is nonetheless considerable controversy regarding the isoform of COX that is involved in cerebral prostaglandin production. As noted before, work on direct neuronal mediation of NVC also found that COX-1 inhibition had no effect during whisker stimulation (Lecrux and Hamel, 2011) or basal forebrain stimulation (known to increase CBF via cholinergic projections; Lecrux et al., 2012). NVC was also impaired in COX-$2^{-/-}$ mice (Niwa et al., 2000), but not COX-$1^{-/-}$ mice, although the latter do show abnormal responses to other vasodilatory stimuli, notably hypercapnia (Niwa et al., 2001). Conversely, direct PGE_2 application appeared to partly restore functional hyperaemia following COX-2 inhibition, suggesting a modulatory role rather than direct control, akin to NO (Stefanovic et al., 2006). Other groups have successfully altered coupling in response to stimulation in the presence COX-1 antagonists, both *ex vivo*, and *in vivo* in the cerebral cortex (Takano et al., 2006) and olfactory bulb (Petzold et al., 2008), whilst failing to detect COX-2 expression in neurons or astrocytes near the vasculature and finding no effect with COX-2 inhibitors (Takano et al., 2006). It is conceivable that there are inherent interspecies differences, with some evidence to suggest that rats require COX-1 for normal NVC, whereas mice utilise COX-1-independent mechanisms (Liu et al., 2012). COX-1 polymorphisms

that reduce enzyme activity have been found to reduce haemodynamic responses in the occipital cortex following visual tasks in human subjects, indirectly supporting its role in human NVC (Hahn et al., 2011).

The other class of AA-derived dilators most closely associated with neurovascular coupling are EETs, produced in astrocytes by cytochrome P450 (CYP450) epoxygenases, especially the CYP2C and CYP2J families (Imig et al., 2011). The exact mechanism by which they function is uncertain, but thought to involve both modulation of astrocytic (Gebremedhin et al., 2003) or VSM cell Ca^{2+}-activated K^+ channels (Gebremedhin et al., 1992; Campbell et al., 1996; Behm et al., 2009), as well as interactions with other NVC signalling mechanisms such as TXA_2 receptor antagonism (Behm et al., 2009). In the retina, inhibition of epoxygenase reduced the likelihood of vasodilatory responses to uncaging of astrocytic Ca^{2+}, application of ATP or exposure to light, whereas COX inhibition had no effect (Metea and Newman, 2006). Two mechanistically different epoxygenase inhibitors also reduced CBF responses to vibrissal stimulation in the barrel cortex, again independently of COX isoforms (Peng et al., 2002). The effect of EET blockade was not synergistic with $GABA_A$ or NMDA receptor antagonists in one set of experiments, and all three provided a similar degree of NVC attenuation, suggesting it is produced downstream of neurons during somatosensory activity or basal forebrain stimulation (Lecrux and Hamel, 2011; Lecrux et al., 2012). There is also crosstalk between COX and EET signalling, as mGluR-induced CBF responses were attenuated by COX-2 and EET inhibitors, whereas COX-1 and NO inhibition only had an effect on baseline CBF (Liu et al., 2011).

Adenosine and lactate have well-described vasodilatory properties, but their roles in NVC are unclear. On the one hand, they would be ideal candidates due to their metabolism-dependent production mechanisms, thus providing a direct feedback mechanism based on metabolic demand (which, as previously noted, is not always

coupled to flow). Neuronal activity can result in the extracellular release of ATP (Newman, 2003), which is progressively hydrolysed to remove phosphate residues and results in adenosine accumulation (Zimmermann and Braun, 1996). It is known that adenosine antagonists reduce hyperaemia during sciatic nerve (Ko et al., 1990) or whisker stimulation in rats (Dirnagl et al., 1994), whereas inhibitors of adenosine uptake increase the response amplitude (Ko et al., 1990). Despite the known effects of adenosine on $G_{\alpha s}$-coupled A_2 receptors (Pelligrino et al., 2011), others have failed to demonstrate the effect of adenosine in NVC (Takano et al., 2006). However, it may be exerting an indirect influence via its interactions with prostaglandin-dependent signalling (Gordon et al., 2008).

The role of lactate as a similar feedback mediator was hypothesised already by Roy and Sherrington (1890), and it has subsequently been demonstrated that lactate release into the extracellular space in the cerebellum correlates with CBF increase (Caesar et al., 2008). The mechanistic explanation is unclear, but may feature nitric oxide, with downstream cGMP and ATP-sensitive K^+ channel signalling (Hein et al., 2006). Again, however, the effect of lactate has been attributed to its influences on other pathways such as PGE_2 clearance from the extracellular space via prostaglandin transporters (which are inhibited by lactate), thereby providing a metabolic control mechanism over vascular response polarity following astrocytic activation (Gordon et al., 2008).

An alternative that has been proposed to these pathways is K^+, which is normally found at very low concentrations (approximately 3–4 mM) extracellularly, but increases during neuronal depolarisation. Although the effect is relatively minor when viewed on a tissue-wide level (Somjen, 1979), local perivascular concentrations can increase much more considerably (Filosa et al., 2006). Although elevations beyond approximately 20 mM would evoke direct depolarisation (as predicted by the Nernst equation), $[K^+]$ of $<$20 mM has been shown to have a hyperpolarising effect on VSM

cells due to the presence of Ca^{2+}-activated large conductance K^+ (BK) channels on astrocytes, which release K^+ into the perivascular space and therefore activate inward rectifying K^+ (K_{ir}) channels on VSM cells, thus hyperpolarising and relaxing them (Filosa et al., 2006). The same group demonstrated the polarity of this response was dependent on the amplitude of $[Ca^{2+}]_i$ elevation in the astrocyte, with moderate levels producing BK- and K_{ir}-dependent vasodilation, whereas high elevations produced BK-dependent, K_{ir}-independent vasoconstriction, consistent with the biphasic response model (Girouard et al., 2010). *In vivo*, pharmacological inhibition of BK and K_{ir} channels was non-additive, further suggesting a sequential mode of action (Girouard et al., 2010).

BK/K_{ir} inhibition reduced somatosensory evoked CBF responses by approximately 50%, with the remaining component attributed to COX-derived mediators. However, even in studies using combinations of NOS, COX and CYP450 epoxygenase inhibitors with adenosine receptor and K_{ir} antagonists, forepaw stimulation-induced functional hyperaemia was only reduced by approximately 65%, while evoked potentials and $\Delta CMRO_2$ were unchanged (Leithner et al., 2010). Similar observations have been made with combined COX, nNOS, EET, NMDA receptor and adenosine receptor blockade, resulting in a 60% decrease in ΔCBF (Liu et al., 2012). It is therefore evident that there is considerable functional redundancy and/or hitherto unidentified mediators involved in evoking dilations in the microvasculature.

1.4.3 Primary site of CBF regulation

In addition to controversy regarding where and by which mechanisms NVC is initiated, the vascular site where the parenchymal signal is first converted into a change of vascular tone is also unclear. Clearly, the observed spatial changes of CBF during stimulation limit the potential sites for change to the microvasculature (Attwell et al., 2010; Berwick et al., 2008), but this could involve either arteriolar

VSM, capillary pericytes or both. Traditionally, VSM cells have been considered the main contractile cell type in the vasculature, and initial descriptions of the molecular basis of NVC assumed that the target was smooth muscle, due to its expression of numerous receptors for implicated mediators and its well-described contractile apparatus including α-smooth muscle actin (αSMA). However, it was suggested by Vimtrup already in 1922 that pericytes appeared to constrict capillaries in living larvae (Krueger and Bechmann, 2010). Attwell's group demonstrated that at least in cerebellar and retinal slices, pericytes can respond to a variety of neurotransmitters and regulate the diameter of their underlying capillaries (Peppiatt et al., 2006). They subsequently replicated this *in vivo*, using two-photon microscopy (2-PM) to show that somatosensory stimulation evokes a capillary dilation that precedes the dilation of its parent arteriole, suggesting capillary dilation is an active phenomenon rather than passive distention following an upsteam rise in flow (Hall et al., 2014).

This arrangement is advantageous from the point of view of blood flow optimisation, as the mean capillary-to-neuron distance in the hippocampus—approximately 8 to 19 µm in different hippocampal fields—is much smaller than the arteriole-to-neuron distance, approximately 70 to 162 µm (Hamilton et al., 2010; Lovick et al., 1999). Moreover, this response can propagate along the vessel, thus providing a potential mechanism whereby locally initiated signals can progress upstream and evoke further responses in larger vessels or in other capillaries (Hamilton et al., 2010; Peppiatt et al., 2006; Itoh and Suzuki, 2012), and could thus elegantly account for the increase in parenchymal blood volume seen during functional hyperaemia (Berwick et al., 2008; Stefanovic et al., 2008). The capillary dilation mechanism is also attractive due to its powerful influence on the passage of circulating erythrocytes and leukocytes cells through the lumen. As capillary diameters are small enough to require blood cell deformation during passage, the effects of dilation on capillary flow are not accurately estimated by Poiseuille's law and actually exceed the r^4 effect of vessel radius on

flow (Attwell et al., 2010); therefore, even a very small dilation would have a very pronounced effect on flow. Finally, it has been argued that pericytes would have a critical role due to their potential to regulate capillary transit time heterogeneity and the accompanying differences in oxygen extraction efficiency (Jespersen and Østergaard, 2012). Recent evidence supports this position, as flow homogenisation in the capillary bed exceeds what might be expected from a passive vasculature and is consistent with active capillary dilation (Gutiérrez-Jiménez et al., 2016).

Conversely, arguments have also been presented against the role of pericytes in CBF regulation, especially as the evidence for their regulatory function has thus far been demonstrated primarily *in vitro*, which lacks physiological levels of basal flow through the vasculature. The group of Lindauer specifically examined this question using *in vivo* 2-PM and found that although capillaries dilated during bicuculline-induced activity or electrical stimulation and contracted in response to TXA_2 analogues, this did not correlate with the presence of pericytes, suggesting a passive mechanism (Fernández-Klett et al., 2010). The most elegant contradictory study to date used a variety of transgenic mice to ascertain morphological and functional differences between VSM cells and pericytes, and showed that capillary diameter did not change at what they defined as pericyte locations, in response to spontaneous $[Ca^{2+}]_i$ oscillations, somatosensory stimuli or optogenetic activation; pericytes also lacked αSMA expression, suggesting the absence of a contractile apparatus (Hill et al., 2015).

This contentious issue is further complicated by disagreement, or at least inconsistency, regarding definitions and the distinction between precapillary arterioles and large capillaries, as determined by the transition from VSM cells to pericytes. The studies arguing against pericytes are perhaps guilty of circular reasoning, as their *a priori* definitions of pericytes could, at least to some extent, result in all contractile cells being labelled as VSM cells: any αSMA^+ cells with large

circumferential processes were defined as VSM, despite the discontinuous appearance that is inconsistent with classical notions of arteriolar VSM (Hill et al., 2015; Attwell et al., 2016). Indeed, proponents of the pericyte hypothesis vociferously argued that pericyte heterogeneity along the vascular tree is to be expected, and it is logical that 'transitional'pericytes closer to the arteriolar side would be more likely to regulate vessel diameter (Attwell et al., 2016). As such, a consensus will hopefully emerge that regardless of nomenclature, the primary site of CBF regulation is at small vessels covered by spatially separated, αSMA$^+$ contractile mural cells.

1.5 Tools for studying NVC

Of course, such advances in our understanding of NVC would not have been possible without corresponding developments in experimental methodology. The tools available for experimentally determining CBF have evolved beyond recognition from Mosso's crude plethysmography through cranial defects and now encompass a variety of optical and other methods, including magnetic resonance imaging (MRI; Raichle, 2009). However, to estimate NVC rather than simply flow, we require direct measurements of neuronal or astrocytic activity such as LFP recordings, the use of voltage-sensitive or Ca^{2+}-sensitive dyes, or non-invasive methods such as electroencephalography (EEG).

1.5.1 Optical methods

One of the first reliable methods for quantitative determination of blood flow was the injection of a tracer, such as fluorescent microspheres or [^{14}C]-iodoantipyrine, followed by decapitation and imaging or autoradiography (Jay et al., 1988). However, this is very limited in its use due to methodological difficulties and the limitation of only one timepoint per animal. In an experimental context, Laser Doppler flowmetry (LDF) is probably the most widely used method, utilised in several hundred publications

annually (Rajan et al., 2009). LDF provides accurate measurements of perfusion changes at a given point (with full-field cameras becoming available more recently; see Draijer et al., 2009; Boas and Dunn, 2010)) based on the well-understood Doppler effect of light, causing a shift in wavelength based on the movement of the reflecting substrate (i.e. primarily erythrocytes) in relation to the probe. However, it does not provide means of determining absolute flow, nor can depth information be derived from the signal, limiting its use to cortical measurements unless the probe is invasively inserted into deeper structures (Rajan et al., 2009; Devor et al., 2012).

Laser speckle contrast imaging (LSCI) provides a full-field view, but the underlying physics are less clear—the measurement is based on contrast and decorrelation time of 'speckles' resulting from back-scattered photons captured by a charge-coupled device camera, but extracting blood flow information from this requires a number of assumptions, which limit its quantitative accuracy (Rajan et al., 2009; Draijer et al., 2009; Boas and Dunn, 2010; Dunn, 2012). Unlike LDF, where multiple probes can be inserted into the brain at different depths, (thereby partly evading the problem of lack of depth information; Norup Nielsen and Lauritzen, 2001) LSCI is limited to depths of a few hundred microns (Rajan et al., 2009). Other scatter-related phenomena can also be used for cerebrovascular investigations, including optical coherence tomography, diffuse correlation spectroscopy (Devor et al., 2012) and Doppler ultrasound (Rajan et al., 2009).

Optical intrinsic signal imaging (OISI) relies on differential absorption of light at particular wavelengths by haemoglobin (Hb) in its different oxygenation states – oxygenated (HbO), deoxygenated (HbR) or total (HbT) – which can consequently be distinguished depending on the chosen wavelength of light (Devor et al., 2012). This enables determination of cerebral blood volume (CBV), assumed to correlate proportionally with HbT (Jones et al., 2001). It also allows for greater spatiotemporal detail due to differences between the changes of the different parameters, with the

transient increase in deoxygenated Hb ('deoxy-dip') reportedly providing the most localised haemodynamic response (Vanzetta and Grinvald, 2001), although this has not been definitively established (Berwick et al., 2008). Moreover, when used in conjunction with flow measurements, OISI facilitates estimations of $CMRO_2$, as oxygen extraction can be determined from the change in HbR and HbT (Devor et al., 2012).

The third major contrast mechanism is fluorescence, (Devor et al., 2012) achieved either through the injection of exogenous dyes including Ca^{2+}-sensitive dyes specific for astrocytes (Takano et al., 2006; Chuquet et al., 2007; Nimmerjahn et al., 2004; Schummers et al., 2008) or labelling neurons and astrocytes non-selectively (Chuquet et al., 2007; Schummers et al., 2008), voltage-sensitive dyes for imaging electrical activity (Sweetnam and Brown, 2012; Wyss et al., 2011), dyes for labelling the vascular lumen (Takano et al., 2007; Shih et al., 2012; Stefanovic et al., 2008) or vessel wall (Shen et al., 2012), or even O_2 tension (pO_2) indicators (Lecoq et al., 2011). In addition, we can exploit intrinsically fluorescent compounds such as nicotinamide adenine dinucleotide (NADH), a coenzyme involved in both mitochondrial and glycolytic energy production (Kasischke et al., 2004).

When used in conjunction with 2-PM, fluorescent dyes enable simultaneous investigation of various aspects of metabolism, neuronal and glial activity, and vascular responses both in vitro (Zonta et al., 2003; Mulligan and MacVicar, 2004) and in vivo (Wang et al., 2006b; Takano et al., 2006) at extremely high resolutions and to greater depths than most optical imaging tools (Shih et al., 2012). However, 2-PM is technically much more laborious and costly than most other optical techniques, and cannot provide overviews of large areal changes (Shih et al., 2012), making combination of different imaging methods advantageous in many situations (Mathiesen et al., 2011; Hillman, 2007).

1.5.2 Electrophysiological methods

Any attempts to definitively establish neurovascular coupling require the use of electrophysiological recordings to obtain information regarding neural activity, thus enabling to quantitatively assess its relationship with perfusion changes (Iannetti and Wise, 2007). Although animal studies have the advantage of being less limited in restrictions on invasiveness, thus allowing for the aforementioned optical recording methods of electrical and ionic activity, it is much more common, less laborious and often more reliable to quantify local activity through the use of electrodes (Sheth et al., 2003, 2004; Devor et al., 2003; Norup Nielsen and Lauritzen, 2001; Berwick et al., 2008). There are a number of methods that can be used for estimating different aspects of neuronal signalling. LFP recordings (obtained by applying a low-pass filter to the extracellular field potential) reflect mainly synaptic potentials, spike after-potentials and voltage-dependent membrane potential oscillations (Logothetis and Wandell, 2004; Logothetis, 2003). MUA is a direct measurement of spiking, obtained by applying a high-pass filter to the extracellular field potential recordings. If arrays of electrodes are used, current source density can be calculated, thus providing greater detail regarding laminar locations of recording sites (Devor et al., 2003). In terms of non-invasive methods, EEG is the most widely used, but has poor spatial resolution; the same is true of magnetoencephalography, although the resolution can be considerably improved through the use of model-based methods such as electrophysiological source imaging (He et al., 2011) .

1.5.3 Magnetic resonance imaging

Although PET studies have provided some of the most important historical data on neurovascular coupling (e.g. Fox and Raichle, 1986), the technique has relatively poor temporal/spatial resolution and requires the use of a cyclotron, greatly restricting its widespread utilisation (Raichle, 2009). The methods that are of greatest clinical

value in determining cerebrovascular function include various MRI protocols, such as BOLD-fMRI, arterial spin labelling (ASL) to measure CBF and vascular space occupancy (VASO) to measure CBV (Logothetis, 2008; Donahue et al., 2012). Of these, BOLD-fMRI is by far the most prevalent and thoroughly characterised, with over 25 years of data from animal models and human subjects (Bandettini, 2012). BOLD is based on Pauling's observation that unlike HbO, HbR had paramagnetic properties (Pauling and Coryell, 1936), which led to its subsequent use as an endogenous MRI contrast agent (Bandettini, 2012). Due to the excess of ΔCBF in comparison to $\Delta CMRO_2$, there is an increase in Hb oxygenation and a concomitant quadratic decrease in T2* MR signal (Logothetis and Wandell, 2004). The existence of an early 'deoxy-dip' where oxygenation decreases due to the latency of CBF responses is hotly contested (Villringer, 2012).

In macaques, BOLD responses to visual stimulation have been shown to correlate with LFPs, whereas MUA showed much faster adaptation and decayed back to baseline long before the stimulus was terminated (Logothetis et al., 2001). It is therefore assumed that like CBF control in general (see section 1.3.3), BOLD-fMRI reflects synaptic activity (Attwell and Iadecola, 2002; Logothetis and Wandell, 2004). However, the multiple factors determining BOLD signal (CBV, CBF, oxygenation status of haemoglobin, differentiating between microvascular and venous signals) make it more difficult to draw straightforward conclusions regarding the links between neural physiology and vascular responses (Logothetis and Wandell, 2004; Logothetis, 2008; Menon, 2012).

Recent work using combined ultrahigh-field MRI with sensory and optogenetic stimulation showed that BOLD originates primarily in venular voxels, whereas CBV increases are mainly in arteriolar voxels (Yu et al., 2016). It has been suggested that multimodal imaging using simultaneous measurements of BOLD, CBV (as determined by VASO) and CBF (as determined by ASL) provide a more reliable estimate of

overall vascular responses to activity, particularly in case of cerebrovascular pathology (see section 1.6.1; Blicher et al., 2012) but BOLD-fMRI remains the most popular method for functional neuroimaging. To establish the relevance of BOLD signal to NVC, simultaneous EEG-fMRI is now used, albeit in a relatively small number of studies (Ritter and Villringer, 2006). In animal models, magnetic field strengths of 20T and beyond are now available to provide greater spatial resolution, and multimodal approaches have been developed to allow simultaneous high field strength imaging with optical imaging of Ca^{2+} signal (Schulz et al., 2012), thus providing a much more direct avenue to explore the physiological basis of fMRI.

1.6 Neurovascular coupling in pathology

Despite the plethora of methods available in the preclinical setting, there are fundamental limitations of resolution for non-invasive measurements of neural activity in patients. It is therefore tacitly assumed in most functional imaging studies that NVC operates as described in previous human experiments or animal models, and the vascular response (typically detected as an alteration in the BOLD signal) is taken as the only read-out of activity (Iannetti and Wise, 2007). However, there is an increasing body of evidence suggesting that this assumption is invalid in a number of scenarios. For instance, it has been known since the 1970s that patients with "multi-infarct" (vascular) dementia exhibit abnormal CBF patterns (Hachinski et al., 1975), which was originally associated with a lack of demand for blood flow in the affected tissue. Subsequently, it has become clear that vascular changes precede clinical dementia in Alzheimer's disease, suggesting that vascular factors are more broadly involved in the development of dementia (Ruitenberg et al., 2005). This conclusion is further supported by observations of altered vascular reactivity in patients and in animal models of Alzheimer's disase, even before overt neuropathology can be detected (Nicolakakis et al., 2011; Iadecola, 2004; Park et al., 2013; Rombouts et al.,

2005; Takano et al., 2007). Furthermore, evidence also exists for altered vascular responses in schizophrenia (Ford et al., 2005; Song et al., 2012), community-acquired pneumonia (Rosengarten et al., 2012), epilepsy (Ma et al., 2012), diabetes (Mishra and Newman, 2010; Mishra et al., 2011) and normal aging (D'Esposito et al., 2003).

This is particularly relevant for cerebrovascular disorders, where there are ongoing pathophysiological signalling cascades occurring within the NVU, in addition to the obvious haemodynamic derangement caused by disruption of major arteries in the case of stroke (Zhang et al., 2012b). The phenomenon of pathophysiological uncoupling is perhaps best characterised in cortical spreading depression (CSD), a propagating wave of depolarisation associated with stroke, migraine and traumatic brain injury (Chuquet et al., 2007). CSD spreads across the cortex at 3-5 mm/s and leaves it in an electrophysiologically silenced state for a prolonged period (Guiou et al., 2005). It is known that CSD evokes a multiphasic CBF response, including hyperaemia during extracellular current shifts and a subsequent long-term oligaemia (Fabricius et al., 1995). but cortical spreading ischaemia (CSI) has also been observed in humans (Dreier et al., 2009). Similarly, mice subjected to CSD exhibit an altered relationship between electrophysiological activity and OISI responses during CSD, which does not recover for periods upward of one hour (Chang et al., 2010). There is analogous evidence that after CSD, both CBF and CBV responses to sensory stimulation are reduced in rats (Guiou et al., 2005; Enager et al., 2004; Piilgaard and Lauritzen, 2009). The same has been described in models of subarachnoid haemorrhage (SAH), another disorder which features CSD in its proposed pathophysiology: after injection of blood into the cisterna magna, brain slices from rats exhibited an inversion of vascular responses to astrocytic activity, indicative of abnormal signalling in the NVU (Koide et al., 2012).

1.6.1 Dysfunction of the NVU in ischaemic stroke

It is unsurprising that the NVU would be altered in ischaemic stroke, as its constituent cells are also susceptible to ischaemic damage—although there is heterogeneity in their relative vulnerabilities (Redzic et al., 2015). In addition, the mechanisms underlying NVC (as described in section 1.4.2) have considerable overlap with the 'ischaemic cascade', a series of biochemical and signalling events occurring as a consequence of nutrient and oxygen deprivation, and ultimately leading to cell damage or death (Lipton, 1999; Sutherland et al., 2012). Importantly, the ischaemic cascade in the microvasculature and parenchyma can potentially interfere with NVC. It was observed in the 1980s by Kågström and colleagues that following global ischaemia (induced via injection of excess cerebrospinal fluid (CSF) or via bilateral occlusion of common carotid arteries), rats exhibited attenuated CBF responses to hypercapnia and hypoxia (Kågström et al., 1983a). They subsequently demonstrated that transient CSF compression or 4-vessel occlusion (4-VO; bilateral carotid and vertebral occlusion) caused initial hyperaemia when the cerebral circulation was restored; however, this was converted into a delayed hypoperfusion within 60 minutes of reperfusion, suggesting long-lasting alterations in vascular function (Kagstrom et al., 1983). The same phenomenon was seen with incomplete global ischaemia (Kågström et al., 1983b).

It was shown by Ueki et al. that 4-VO also impaired CBF and glucose metabolism responses to forepaw stimulation, despite partial recovery of somatosensory evoked potentials (SEP) and EEG over 3 hours of reperfusion, again indicative of uncoupling (Ueki et al., 1988). LDF has revealed altered temporal characteristics of functional hyperaemia following carotid occlusion (Ances et al., 2000) while LSCI showed extensive postischaemic hypoperfusion, diminished area of activation and increased time-to-peak after bilateral carotid occlusion, despite a normal peak flow response (Zhou et al., 2008). There is also data on the level of impairment in relation to

severity of ischaemia, including characterisations of differential vulnerability of CBF and SEP during graded cerebral ischaemia: when animals were binned according to the severity of CBF reduction, optical imaging of CBF, HbR and HbO showed a significant decline at 80% ischaemia relative to normalised SEP changes, whereas SEP and estimates of $CMRO_2$ remained coupled (Baker et al., 2013).

These results suggest that in models of global ischaemia, the relationship between neural activity and vascular regulation is altered. This is not without controversy, particularly insofar as detailed relationships between severity of the insult and subsequent outcomes are concerned. Work by Schmitz et al., using a model of cardiac arrest in rats, demonstrated abnormalities in MRI signal after forepaw stimulation: perfusion-weighted responses recovered more slowly than BOLD responses, whereas apparent diffusion coefficient as an indicator of oedema and (in an indirect manner) metabolic activity returned to baseline within 1 hour, which was interpreted as an early suppression of neurovascular coupling that normalised by 24 hours, despite residual impairments in functional activity (Schmitz et al., 1998). The same group found no evidence of uncoupling using electrode recordings and LDF in response to forepaw stimulation, as both somatosensory evoked potentials and CBF responses recovered with similar temporal dynamics (Schmitz et al., 1997).

Similar controversies exist in focal models of ischaemia, where most of the cerebral blood supply remains intact, but regions supplied by a single distal artery are damaged following transient or permanent occlusion of the supplying vessel. The most common form of this is middle cerebral artery occlusion (MCAO), due to the relative ease of access to the MCA via the carotid system, as well as the cerebral regions located in its territory of supply—in particular the somatosensory cortex, which provides an easy model of evoking activity via tactile stimulation. Permanent MCAO has been reported to reduce BOLD-fMRI responses to bilateral forepaw stimulation in rats (Reese et al., 2000; Sauter et al., 2002), but there is also a BOLD impairment

following transient MCAO and somatosensory stimulation (Sicard et al., 2006) or pharmacological induction of neural activity (Reese et al., 2002).

However, these studies did not utilise direct measurements of neuronal activity and in others the evidence suggests the contrary: Weber and colleagues were not able to detect loss of NVC after 60 minutes of MCAO, as diminished BOLD responses correlated with SEP impairment over a 7-week period (Weber et al., 2008). Deficits in BOLD and CBF responses to forepaw stimulation have been found after permanent, but not 15-minute transient MCAO; however, this experiment did not directly measure electrophysiological responses or functional impairment in either model (Shen et al., 2005). Less common methods for reducing cortical perfusion such as controlled graded compression of cerebral tissue in rats (admittedly fraught with the caveat of non-ischaemic brain damage) have shown a similar vulnerability of both vascular and neural responses to ischaemia (Burnett et al., 2005). There is also conflicting evidence whether or not cerebrovascular reactivity to non-neural stimuli such as exogenously applied ACh (Winters et al., 2012) or CO_2 inhalation is altered following MCAO (Shen et al., 2005; Sicard et al., 2006; Dijkhuizen et al., 2001, 2003).

Ultimately, the heterogeneity of preclinical models—global vs. focal, duration of ischaemia, stimuli used etc.—do not necessarily reflect the situation in patients. Indeed, there is evidence from clinical studies that cerebrovascular disease is associated with abnormal NVC. It was observed that patients with lacunar strokes showed an impaired BOLD response in non-infarcted regions during a finger tapping task, indicative of diffuse widespread NVC dysfunction (Pineiro et al., 2002). Despite the lack of electrophysiological investigations in that study, BOLD signal diminution or absence has been demonstrated in patients with a history of stroke and transient ischaemic attacks (TIA), despite a relatively smaller defect in MEG signal (Rossini et al., 2004).

The findings of altered haemodynamic responses were further validated in patients

with frontal lobe strokes, who displayed reduced BOLD responses to unimanual or bimanual tasks and hyperventilation; (Krainik et al., 2005) similar observations have been made by others (Mazzetto-Betti et al., 2010). In subacute stroke patients who had BOLD-fMRI silencing during a tactile exploration task, transcranial magnetic stimulation evoked normal motor potentials in the interosseus muscle, suggesting retained neural activity in the absence of haemodynamic responses; in chronic patients, the BOLD response reappeared (Binkofski and Seitz, 2004). These effects are possibly not restricted to the lesion, as acute stroke patients performing a visual task have reduced perilesional BOLD despite normal behavioural responses (de Haan et al., 2013a).

The extent of NVC impairment appears to depend on severity of ischaemia, leading to altered haemoglobin oxygenation and content changes in severe chronic stroke or symptomatic intracranial/extracranial arterial stenosis patients (Murata et al., 2006; Röther et al., 2002; Nakamura et al., 2010; Roc et al., 2006; Hund-Georgiadis et al., 2003), whereas patients with moderate posterior cerebral stenosis have normal NVC (Fritzsch et al., 2010). It is also possible that the size and location of the infarct determine whether haemodynamic responses are altered, with cortical infarcts having more of an effect than subcortical strokes (Promjunyakul et al., 2013). Time from onset plays a role as well, as subacute stroke patients have a delayed time-to-peak in BOLD-fMRI using language tasks, demonstrating that even in a given patient, the interpretation of functional imaging is not necessarily straightforward in a pathological context (Altamura et al., 2009). Recent work has suggested that CBF is a more reliable measurement of neural activity in chronic stroke, and multimodal imaging can be used to compensate for altered cerebrovascular responses (Blicher et al., 2012), but in any case there appear to be fundamental changes in the physiology of the NVU following stroke in humans.

Alterations of BOLD/CBF are potentially of diagnostic or even prognostic use

on their own, as both hypercapnia-induced (Bouvier et al., 2015) and resting-state BOLD-fMRI can give information regarding perfusion deficit, penumbral location and cerebrovascular reserve (Lv et al., 2013; Tsai et al., 2014; Zhang et al., 2011). However, if the ultimate goal is to extract information regarding alterations in neural activity, these studies raise considerable issues with our interpretation of functional imaging in cerebrovascular disease patients. Moreover, it is possible that abnormal vascular responses further exacerbate the pathology due to inadequate nutrient supply (Bonakdarpour et al., 2015), emphasising the importance of understanding, and correcting, post-ischaemic deficits in CBF regulation and NVC.

1.6.2 Mechanisms of neurovascular uncoupling

The observations of altered coupling have now become well-established in multiple contexts, yet there is very little data on which of the known changes best account for—and provide therapeutic avenues to ameliorate—the uncoupling phenomenon in this heterogeneous set of pathological conditions. Uncoupling has been relatively widely studied in SAH/CSD models for several reasons. Firstly, CSD provides an in-built neuronal activity paradigm due to the silencing and subsequent recovery, with very clear changes in electrophysiological readouts. Secondly, as there is no obstruction or loss of patency in larger vessels as a direct consequence of experimental methods, any changes in vascular supply would presumably be accounted for by neuronal/NVU changes and downstream effects. Thirdly, the spreading nature of the wave allows for very clear conclusions regarding spatial and temporal correlations between neural and vascular activity.

Comparatively less research has been done on uncoupling in animal models of stroke; consequently, proposed mechanisms are much more speculative. On the one hand, mechanical factors such as exhausted cerebrovascular reserve capacity (CVRC) are probably involved: the severe ischaemia prompts a compensatory vasodilation in

vessels downstream of the occlusion, which prevents further dilation and therefore does not allow for a change in BOLD signal (Derdeyn et al., 1999; D'Esposito et al., 2003). Numerous publications demonstrate that in extreme cases of stenosis-related failure of cerebral autoregulation, the impairment of CVRC correlates with inverse or impaired BOLD changes (a more marked initial 'dip' and diminished subsequent increase) due to increased oxygen consumption and extraction fraction causing a corresponding decrease in HbO, as opposed to the normally overwhelming increase due to elevated CBF (Röther et al., 2002; Hamzei et al., 2003).

However, CSD is a potentially useful model for examining neurovascular function in stroke, as similar depolarising waves are known to occur during ischaemia (Shin et al., 2006). Indeed, there is considerable overlap in the experimental data investigating mechanisms of uncoupling in the two disorders, with commonly implicated pathways including abnormal mitochondrial function, the production of free radicals, release of vasoconstrictive mediators and, importantly, abnormal calcium handling.

1.6.2.1 Signalling changes in neurovascular pathology

Results from a rat model of CSD suggest that the mechanism underlying oligaemia involves mitochondrial permeability transition pore (MPTP) formation and calcineurin activation, as inhibitors of calcineurin (cyclosporine A, FK506) or MPTP (cyclosporine A, NIM811) restore the evoked CBF response to control levels after transcallosal stimulation (Piilgaard et al., 2011). The exact pathway by which MPTP formation and calcineurin exert these effects is unknown in this context, although there are numerous potential candidates. For instance, it is known that FK506 inhibits NOS dephosphorylation (and subsequent activation) via its effects on calcineurin, which is the purported basis for its neuroprotective properties in models of excitotoxicity (Dawson et al., 1991, 1993), but would also carry implications for NVC. Indeed, the protective effect of FK506 has partly been attributed to a reduction

of reperfusion injury in a transient MCAO model, as it had no difference with vehicle in permanent MCAO animals (Bochelen et al., 1999); this could plausibly be explained as an improvement in flow, but the existing literature is inadequate to draw clear conclusions (Nakai et al., 1997; Sierra-Paredes and Sierra-Marcuño, 2008). Inhibiting MPTP formation would prevent release of mitochondrial calcium and apoptotic factors, which contribute to derangement or destruction of neurons or other components of the NVU (Rasola and Bernardi, 2011).

Another consequence of MPTP opening is the loss of inner mitochondrial membrane potential, failure of oxidative metabolism and concomitant production of reactive oxygen species (ROS) and other free radicals (Chan, 2001). There is a well-known increase in ROS and NO (derived from inducible NOS) generation during ischaemia (Lipton, 1999; Rasola and Bernardi, 2011) and reperfusion, which is known to contribute to vascular damage (Iadecola and Anrather, 2011). This has implications for NVC, as well as BBB function and structural integrity. However, the production of ROS is regulated by some of the same mediators that control NVC, including NO (Rasola and Bernardi, 2011) and prostaglandins (Lipton, 1999), making it more difficult to dissociate any direct effects from ROS-dependent mechanisms.

There are also alterations to the physiological NVC pathways described in section 1.4.2. In SAH (and, potentially, CSD), excess K^+ release leads to direct depolarisation of VSM cells and subsequent vasospasm, which would account for diminished reactivity in that context (Koide et al., 2012). Specifically, it was demonstrated that Ca^{2+} uncaging in astrocytes caused a constriction of vessels in slices from SAH rats, whereas controls responded with vasodilation. The effect was also mimicked by moderate elevations in superfusate $[K^+]$ and reverted by BK channel blockade, highly suggestive of excess BK activity leading to excess perivascular $[K^+]$ and constriction (Koide et al., 2012). This experiment would imply a defect in the astrocytes rather than a purely vascular mechanism. In addition, it has been suggested that during

SAH-associated CSD, the coupling defect may be a consequence of high $[K^+]$ or low glucose levels acting in conjunction with products of haemolysis (Dreier et al., 2000), in particular NO scavenging by haemoglobin, as NOS inhibition and elevated $[K^+]$ were able to mimic the effect observed during application of Hb onto the cortex (Dreier et al., 1998).

Another putative mediator of Hb-induced CSI is endothelin-1 (ET-1), a potent vasoconstrictor (Yanagisawa et al., 1988) that can influence the NVU through binding to ET_A and ET_B receptors located primarily on vascular smooth muscle cells (Seo et al., 1994), but also via a complex interaction associated with reductions in Na^+/K^+-ATPase activity (Petzold et al., 2003). It has been reported that ET-1 is also increased in both ischaemic stroke patients (Ziv et al., 1992) and multiple rat models of cerebral ischaemia (Barone et al., 1994), although other contradictory reports suggest no increase in circulating ET-1 concentration in stroke patients (which does not exclude increased local concentrations in the NVU; Haapaniemi et al., 2000)

Excess production of 20-hydroxyeicosatetraenoic acid (20-HETE) has also been implicated in CBF dysregulation. 20-HETE is an arachidonic acid derivative produced primarily by the CYP4A family enzymes, with a smaller contribution from CYP4F isoforms (Imig et al., 2011). The cellular sources of 20-HETE in the NVU include astrocytes (Amruthesh et al., 1993) and VSM cells (Gebremedhin et al., 1998). 20-HETE is a potent vasoconstrictor, through its inhibition BK channel activity (Zou et al., 1996) and enhancement of L-type voltage-gated Ca^{2+} channel conductance (Gebremedhin et al., 1998). Its production forms a significant component of the cerebral autoregulatory response, whereby elevations in transmural pressure result in vasoconstriction to prevent excessive flow through downstream vessels (Gebremedhin et al., 2000). Although 20-HETE does not play a substantial role in NVC under physiological conditions, due to its inhibition by basal NO production (Lindauer et al., 1999; Roman, 2002)it is known to be upregulated at multiple timepoints during

the first day after transient MCAO (Tanaka et al., 2007), with increased CYP4A expression detectable at 3 and 7 days following ischaemia (Kawasaki et al., 2012).

Inhibitors of 20-HETE synthesis have well-documented neuroprotective properties in both filament (Tanaka et al., 2007; Kawasaki et al., 2012; Omura et al., 2006; Poloyac et al., 2006; Renic et al., 2009) and photothrombotic models of transient ischaemia, and they ameliorate post-ischaemic microvascular hypoperfusion (Marumo et al., 2010). The vascular benefits of 20-HETE antagonism in transient MCAO have been confirmed by other groups, despite differing conclusions regarding whether 20-HETE is actually upregulated or not (Poloyac et al., 2006). In particular, reducing 20-HETE levels appears to prevent a secondary decrease in perfusion rather than influencing CBF during ischaemia or early reperfusion (Renic et al., 2009). TTC infarct volumes were diminished, even when the inhibitor was administered 4 hours after stroke; due to this delayed protection, it has been argued that 20-HETE inhibition prevents neuronal death by interfering with the ischaemic cascade, and the improvement in late reperfusion could be an epiphenomenon of improved tissue survival (Omura et al., 2006).

The role of 20-HETE in post-ischaemic NVC has not been elucidated in detailed fashion. What is known is that following CSD induced via a potassium acetate needle stab to the rat neocortex, antagonism of 20-HETE synthesis reduces long-term hypoperfusion compared to CSD-controls without altering $CMRO_2$ or tissue pO_2 (Fordsmann et al., 2013). Moreover, the hyperaemic response to transcallosal stimulation was impaired following CSD regardless of treatment group, which revealed a persistent neurovascular coupling defect when ΔCBF was plotted against stimulation frequency or summed excitatory postsynaptic potentials (Fordsmann et al., 2013). However, while CSD-like phenomena are clearly implicated in stroke pathophysiology (Nakamura et al., 2010; Shin et al., 2006), the possibility that 20-HETE causes stroke-specific vascular and NVC derangements cannot be excluded.

One major convergence point of several distinct pathways involved in the ischaemic cascade is Ca^{2+} (Lipton, 1999). The main focus on Ca^{2+} in the context of cerebral ischaemia has been on excitotoxicity in neurons, caused by excessive NMDA receptor activation by glutamate and resulting in uncontrolled Ca^{2+} influx (Szydlowska and Tymianski, 2010). However, this is relevant to the vasculature as well: in an *ex vivo* model of ischaemia in brain slices, pericyte survival was improved by the removal of Ca^{2+} from the bath solution (Hall et al., 2014). This is of particular interest, as Ca^{2+} appears to not only regulate vascular mural cell survival, but is also inherently linked to their contractile function through calmodulin-mediated activation of myosin light chain kinase and subsequent constriction. There are numerous mechanisms leading to Ca^{2+} rises in vascular cells, including L-type voltage-gated Ca^{2+} channels, non-selective cation channels, Ca^{2+}-induced Ca^{2+} release and exchange pumps (Karaki et al., 1997). Not only might there be excess Ca^{2+} influx into vascular mural cells, but this could operate synergistically with enhanced Ca^{2+} sensitivity in the contractile apparatus, through aberrant Rho kinase activity (Shin et al., 2007). However, the exact contributions of these mechanisms to ischaemic vascular $[Ca^{2+}]_i$ changes have not yet been elucidated.

It is clear that many of the signalling pathways implicated in ischaemic damage are inextricably linked to vascular function as well, making it difficult to establish whether the primary effect of interfering with these cascades is through improvement of intrinsic tissue survival or reduced severity of ischaemic through amelioration of oligaemia. Determining the precise roles these pathways play in neurovascular interactions during stroke will be a key question for the development of therapeutic agents targeting the microvasculature.

1.6.2.2 Cellular Basis of uncoupling in ischaemia

A particularly relevant aspect of changes to the NVU in ischaemia relates to the controversies described in section 1.4.3, i.e. which cell type is the primary regulator

of CBF in the cerebral microvasculature. Already in the 1960s, it was observed that microvascular flow—as detected based on India ink perfusion—was not fully restored following global ischaemia, a phenomenon termed 'no-reflow' (Ames et al., 1968). Numerous mechanisms have been proposed to underlie this: stasis as a consequence of increased viscosity (Fischer et al., 1979), glial and/or endothelial swelling leading to capillary compression (Chiang et al., 1968), and adhesion of leukocytes (including neutrophils) to the affected vessels resulting in luminal obstruction (Mori et al., 1992).

More recently, active and irreversible constriction of the microvasculature has been proposed as an alternative explanation. It was observed that following transient MCAO in mice, luminal constrictions were evident in capillaries at various times following reperfusion; these co-localised with pericytes, defined based on apperance in brightfield and differential interference contrast microscopy, as well as immunohistochemistry for αSMA (Yemisci et al., 2009). Notably, this constriction was prevented by ROS scavengers, which also reduced infarct volumes. This hypothesis of pericyte-mediated no-reflow was subsequently modified in a combined *ex vivo*/*in vivo* study, where application of chemical ischaemia to acute brain slices caused pericytes to die in a constricted state (Hall et al., 2014). This was not ameliorated by ROS inhibition, but blockade of ionotropic glutamate receptors and removal of Ca^{2+} from the bath solution reduced pericyte death. *In vivo*, rat pericytes also died following 90-minute MCAO, although changes in capillary diameter were not investigated (Hall et al., 2014).

As might be expected from the disagreements concerning the primary site of CBF regulation, the pericyte constriction hypothesis has also proven controversial (Vates et al., 2010). The most direct refutation has come from a study that examined pericyte responses to CSD as well as MCAO (Hill et al., 2015). Despite finding clear evidence vasomotion in CSD and vascular blockage following reperfusion in MCAO, they attributed this to "pre-capillary arterioles" and "terminal [VSM cells]"; at locations of

cells they defined as pericytes (αSMA$^-$ cells with elongated morphology), there were no detectable changes in vessel diameter (Hill et al., 2015). These findings were partly replicated in a recent study showing that while capillary RBC flux preceded arteriolar flow changes, capillary diameter did not change during somatosensory stimulation (Wei et al., 2016). As discussed extensively in section 1.4.3, this could be a largely terminological issue, and the data of Hill et al. (2015) in fact provide some of the strongest evidence to suggest that microvascular mural cells, located on small branches toward the arteriolar side, are key mediators of no-reflow (Dalkara and Alarcon-Martinez, 2015; Hill et al., 2015). Pharmacological interventions targeting these cells, with the aim of preventing no-reflow, should therefore be considered an emerging priority in preclinical stroke research.

1.7 Caveats of translational stroke research

When discussing any novel treatment strategy based on preclinical hypotheses, rather than clinical first principles (e.g. removal or dissolution of the clot to allow recanalisation), it is impossible to omit mentioning the abysmal track record that has plagued stroke research. Despite preclinical data successfully predicting phenomena such as the penumbra and peri-infarct depolarisations, there has been a failure of translation in stroke therapeutics. A notable systematic review found that between 1957 and 2003, a total of 1,026 compounds had been tested as putative stroke therapies, including 114 that reached clinical trials; of these, only one (tPA) has shown unequivocal benefit in a clinical setting (O'Collins et al., 2006). There are numerous explanations for the high attrition rate of candidate drugs in preclinical studies, including:

— inadequate sample sizes and lack of power calculations, resulting in underpowered studies prone to spurious results (Howells and Macleod, 2013);

— failure to randomise animals and blind experimenters to treatment groups, introducing bias (Sena et al., 2007);

— publication bias, when only positive results are reported while negative results remain unpublished, unbalancing the information available in the literature (Sena et al., 2010);

— ignoring physiological variables such as core temperature that affect outcomes (Buchan and Pulsinelli, 1990; Buchan et al., 1992);

— inappropriate selection of models depending on which aspect of stroke pathophysiology is being investigated (Neuhaus et al., 2014).

Paradoxically, this is perhaps the great advantage of preclinical stroke research: due to the immense clinical interest and plethora of promising targets involved, we have already made—and taken steps to correct—the mistakes that other fields have yet to go through. Certainly, the problem of false positives and irreproducible data is not unique to stroke (Begley and Ioannidis, 2015), but the response to these problems has been very encouraging. For example, the Stroke Therapy Academic Industry Roundtable (STAIR) criteria were published with the aim of increasing preclinical research quality through both improved experimental and statistical design as well as models that more closely mimic human stroke patients (Stroke Therapy Academic Industry Roundtable (STAIR), 1999; Fisher et al., 2009). It has been observed that reporting of potential sources of bias in *in vivo* studies has substantially improved over the past decade, as a consequence of STAIR criteria and similar initiatives in other disorders (Macleod et al., 2015b). Preclinical phase III trials, where candidate drugs are investigated in multiple centres with highly standardised protocols, are also being pioneered in the stroke field (Dirnagl et al., 2013; Llovera et al., 2015). Therefore, despite the ignominious failures of the past, the future of stroke research is nonetheless promising due to the increased emphasis on study quality.

1.8 Central aims of the thesis

In this thesis, I have studied changes to the pericyte population in ischaemia using a number of complementary experimental approaches, ranging from isolated cell cultures *in vitro* to blood flow imaging *in vivo*. The central hypothesis is that transient focal cerebral ischaemia results in vascular dysfunction that worsens outcome, and that this is at least partly mediated through dysfunction of capillary pericytes. The specific questions posed in the thesis are:

1. What is the impact of MCAO on stimulation-evoked CBF responses in the rat, and on isolated arterial reactivity *ex vivo* (chapter 2)?

2. Can pericyte contractility be modelled *in vitro* and does it enable us to accurately evaluate the effects of compounds known to have vasoactive properties *in vivo* (chapter 3)?

3. What effect does ischaemia have on pericytes, and to what extent can this be altered by treatment with a calcium channel antagonist (chapter 4)?

Chapter 2

Neurovascular Coupling and Vascular Reactivity Following Stroke

2.1 Introduction

The brain has an extremely high level of vascularisation and perfusion, necessary to meet its metabolic demands. As discussed in chapter 1, cerebral nutrient supply accounts for approximately 11% of cardiac output and 20% of oxygen metabolism ($CMRO_2$), despite the brain forming only 2% of body weight (Raichle and Mintun, 2006). In terms of biological importance, an increase in cerebral blood flow (CBF) during neural activity is necessary to meet (and exceed, in order to provide a safety margin) the metabolic needs of the active tissue, termed neurovascular coupling (NVC).

There are controversies regarding regional (Attwell et al., 2010; Devonshire et al., 2012), laminar (Goense et al., 2012), and pathway-specific (Enager et al., 2009) variations in NVC, suggesting that the underlying mechanism of CBF regulation exhibits physiological variability. There is also evidence for pathophysiological interference with NVC in a wide range of neurological and neuropsychiatric disorders, such as Alzheimer's disease (Nicolakakis et al., 2011), schizophrenia (Song et al., 2012) and epilepsy (Ma et al., 2012), but also in more systemic non-neurological disorders,

such as diabetes (Mishra and Newman, 2010) and lower respiratory tract infections (Rosengarten et al., 2012). This is most often described as a diminution of ΔCBF, in the absence of, or disproportionate to, any alteration in neural activity.

In parallel to NVC, CBF is coupled to arterial blood gases as an indicator of systemic oxygenation status. The arterial partial pressures of oxygen (P_aO_2) and carbon dioxide (P_aCO_2) are very tightly regulated under normal conditions. If gas exchange is impaired for some reason and P_aO_2 falls below the critical level of approximately 50 mmHg—corresponding to the end of the oxygen dissociation curve plateau, i.e. the point where arterial O_2 content begins to decline—CBF increases to ensure oxygen delivery to the brain (Johnston et al., 2003). The cerebral vasculature is also exquisitely sensitive to increases in P_aCO_2, indicative of hypoventilation or excessive metabolic demand. Inhalation of 5-7% CO_2 evokes a 75% rise in CBF (Kety and Schmidt, 1948), and it has been estimated that CBF rises by 0.24 ml/100 g/min per kPa of P_aCO_2 increase (Grubb et al., 1974).

Importantly, long-lasting changes in CBF regulation have been observed in stroke and cortical spreading depression (CSD; Veldsman et al., 2015). In stroke, the affected area can be divided into two main regions. The core features severe ischaemia, failure of ion gradients, anoxic depolarisation (similar to CSD) and irreversible processes leading to cell death (Dirnagl et al., 1999). The penumbra, conversely, is a region of hypoperfusion in the absence of detectable tissue damage, although pathophysiological processes in the penumbra (reduced protein synthesis, inflammation, alterations in gene expression) can lead to delayed cell death. Unless flow is restored via thrombolytic drugs, mechanical means or spontaneous reperfusion, over time the core will progressively extend and replace the penumbra (Dirnagl et al., 1999).

The pathophysiological uncoupling of neural activity and vascular responses is relevant to stroke pathophysiology for multiple reasons. First, in the short-term

context, it can exacerbate cerebral ischaemia by preventing the physiological increase in perfusion during periods of elevated neuronal and glial metabolic demands, such as the aberrant activity seen during CSD-like peri-infarct depolarisations (PID). Indeed, PIDs have been associated with enlargement of ischaemic brain lesions in multiple animal models as well as patients (Nakamura et al., 2010), and CSD induction in rats can lead to spreading ischaemia – an inverted CBF response to activity leading to further tissue damage (Dreier et al., 2002; Shin et al., 2006; Strong et al., 2007).

Second, NVC is also relevant in the chronic stages of stroke due to its importance in functional imaging. Since the search for neuroprotective therapies in stroke has thus far been unsuccessful, despite numerous promising preclinical findings (O'Collins et al., 2006; Neuhaus et al., 2014), there has been an increasing emphasis on repair strategies involving neurorehabilitation and neuroplasticity (Cramer, 2008a,b). The effect of such approaches, e.g. whether or not activity of a particular brain region is improved following treatment, is often evaluated using blood oxygen level-dependent functional magnetic resonance imaging (BOLD-fMRI) or other functional imaging modalities, which in their most typical configurations are fundamentally reliant on vascular responses (Carey et al., 2007). Therefore, long-term alterations in NVC complicate the analysis of these findings, which has implications for the accurary of assessing the effectiveness of rehabilitative interventions.

Studies in a variety of focal and global models of ischaemic stroke, as well as in the clinical setting, have thus far provided conflicting evidence whether CBF regulation is disrupted by stroke and cerebrovascular disease (Baker et al., 2013; Weber et al., 2008). Nonetheless, there is considerable evidence from a wide variety of paradigms that components of the neurovascular unit (NVU)—including pericytes (Yemisci et al., 2009), arteriolar smooth muscle (Cipolla and Bullinger, 2008), astrocytes (Duffy and MacVicar, 1996) and endothelial cells (Marrelli, 2002)—are functionally altered following cerebral ischaemia. Similarly, while countless distinct pathways are

activated or inhibited following stroke (Lipton, 1999), it has been difficult to link them directly to changes in NVC. The alterations could be occurring either in the signalling between neurons/astrocytes and the vasculature, or as a consequence of direct vascular changes. For example, it has been demonstrated that CSD features both neurovascular uncoupling and diminished basal flow; however, the production of the potent vasoconstrictor 20-hydroxyeicosatetraenoic acid (20-HETE) only accounted for the hypoperfusion, but not the impairment in NVC (Fordsmann et al., 2013).

2.1.1 Aims

The work described in this chapter investigated the following questions:

1. Are haemodynamic responses to somatosensory stimulation and/or hypercapnia altered following ischaemic stroke in rats?

2. Is the responsiveness of isolated middle cerebral arteries altered following stroke?

3. Could an increase in 20-HETE production account for these effects?

2.2 Materials & methods

2.2.1 Animal care

All procedures were conducted in accordance with the Animals (Scientific Procedures) Act of 1986, under a valid project licence and personal licence, and approved by the University of Oxford Animal Ethics Committee. Male Wistar rats (approximately 250-330 g; Harlan, UK) were housed in individually ventilated cages under a 12:12 hour light-dark cycle, with *ad libitum* access to standard food pellets and water unless otherwise specified.

2.2.2 Laser Doppler flowmetry

Laser Doppler flowmetry (LDF) was used for confirmation of MCAO and detection of peri-infarct depolarisations during ischaemia. Briefly, a small aseptic incision was made near the location of bregma. The scalp was retracted and a small area of skull (approximately 4 mm lateral and 1.5 mm caudal to bregma) was thinned with a surgical microdrill. A fiberoptic probe connected to an OxyFlo 2000 or OxyLab laser Doppler flow monitor (Oxford Optronix, UK) was attached to the thinned window using cyanoacrylate glue. At the end of the session, the probe was removed and the wound closed with silk suture and cyanoacrylate. LDF traces were recorded onto a Windows XP workstation running WinDaq (Dataq Instruments, USA).

2.2.3 Focal cerebral ischaemia

A modified variant of the transient middle cerebral artery occlusion (tMCAO) model of focal cerebral ischaemia was used, as previously described in other publications (Sutherland and Buchan, 2013; Hall et al., 2014). Rats were induced in 4-5% isoflurane (V/V) in a 30% O_2/70% N_2O carrier gas. Having verified anaesthesia with loss of righting and corneal reflexes, rats were maintained at 2% for the surgical procedure and given 0.03 mg/kg of subcutaneous buprenorphine for further analgaesia and

sedation. A rectal probe attached to a homoeothermic blanket (Harvard Apparatus, UK) was inserted and the rats were maintained at 37±0.5 °C.

The neck was shaved and disinfected with 70% ethanol and 4% chlorhexidine. An incision was made to the right of the midline starting above the level of the manubrium and extending 2-3 cm rostrally. Following dissection and retraction of the sternomastoid, cleidomastoid and caudal part of the digastricus, to allow visualisation of the right carotid bifurcation, the external carotid artery (ECA) was permanently ligated and cauterised above the superior thyroid artery. The superior thyroid and occipital arteries were also cauterised and cut. The common carotid artery (CCA) was temporarily ligated and the internal carotid artery (ICA) clamped, with a loose ligature placed on the ECA close to the bifurcation. The ECA was cut distal to the permanent ligation, and an incision made between the two ligatures on the ECA, through which the filament was inserted.

The ECA was manipulated to bring it into alignment with the ICA, and the filament was advanced past the pterygopalatine branch into the circle of Willis, where it occluded the origins of the middle cerebral artery (MCA). The rats were subjected to 90 minutes of ischaemia under 1.5% isoflurane anaesthesia, followed by retraction of the filament, permanent ligation of the proximal ECA ligature and removal of the CCA ligature. Recanalisation was verified via LDF. The wound was then closed with silk sutures, clips or cyanoacrylate, depending on the experiment.

For permanent MCAO (pMCAO), the producedure was performed as described, except the filament and CCA ligature were left in place and the wound closed. For sham ischaemic animals, the surgery was identical except that the filament was not advanced into the ICA, but allowed to enter the pterygopalatine branch or, if it appeared to naturally advance into the ICA, stopped at the bifurcation. The filament was withdrawn and the wound closed.

Animals were randomly allocated to sham or tMCAO groups by flipping a coin.

Due to a lack of preliminary data to estimate effect sizes, it was not possible to carry out power calculations and to determine sample sizes.

2.2.4 TTC staining

Lesions were identified using 2,3,5-triphenyltetrazolium chloride (TTC), which stains viable grey matter red, while dead regions remain uncoloured (Bederson et al., 1986a). Rats were induced in 4-5% isoflurane and killed by cervical dislocation. Brains were removed, cut into 2 mm sections on an ice-cold stainless steel matrix (Kent Scientific, UK) and immersed into a solution of 2% TTC in 37°C phosphate-buffered saline (PBS). After 30 minutes, sections were removed and imaged with a digital camera (Digital IXUS 870 IS, Canon, Japan).

2.2.5 Haemodynamic response imaging

After approximately 3 or 21 hours of recovery from transient or sham ischaemia (for the 6-hour and 24-hour groups, respectively), anaesthesia was re-induced with 4-5% isoflurane, and maintained at 2% isoflurane in air for the duration of further surgical procedures. The femoral artery was cannulated with polyethylene tubing (outer/inner ⌀ 0.8/0.4 mm; filled with heparinised saline) for assessment of blood gases. The rats were tracheotomised and artificially ventilated at approximately 60 strokes/minute with a 3.5 mL tidal volume (adjusted as necessary, based on the initial arterial blood gas reading). Having been placed into a stereotaxic frame (Kopf Instruments, USA), a midline incision was made on the dorsal aspect of the skull to reveal the full extent of the sagittal suture. The scalp was retracted bilaterally, and the parietal bones were thinned with a surgical microdrill. Laser speckle contrast imaging (LSCI) of the barrel cortex was performed with a dedicated infrared camera (Moor Instruments, UK; Fig. 2.1), starting at 6 or 24 hours following MCAO onset, with the full protocol lasting approximately 90 minutes. LSCI data were recorded using Moor LFPI software (Moor Instruments) running on a Windows 7 workstation.

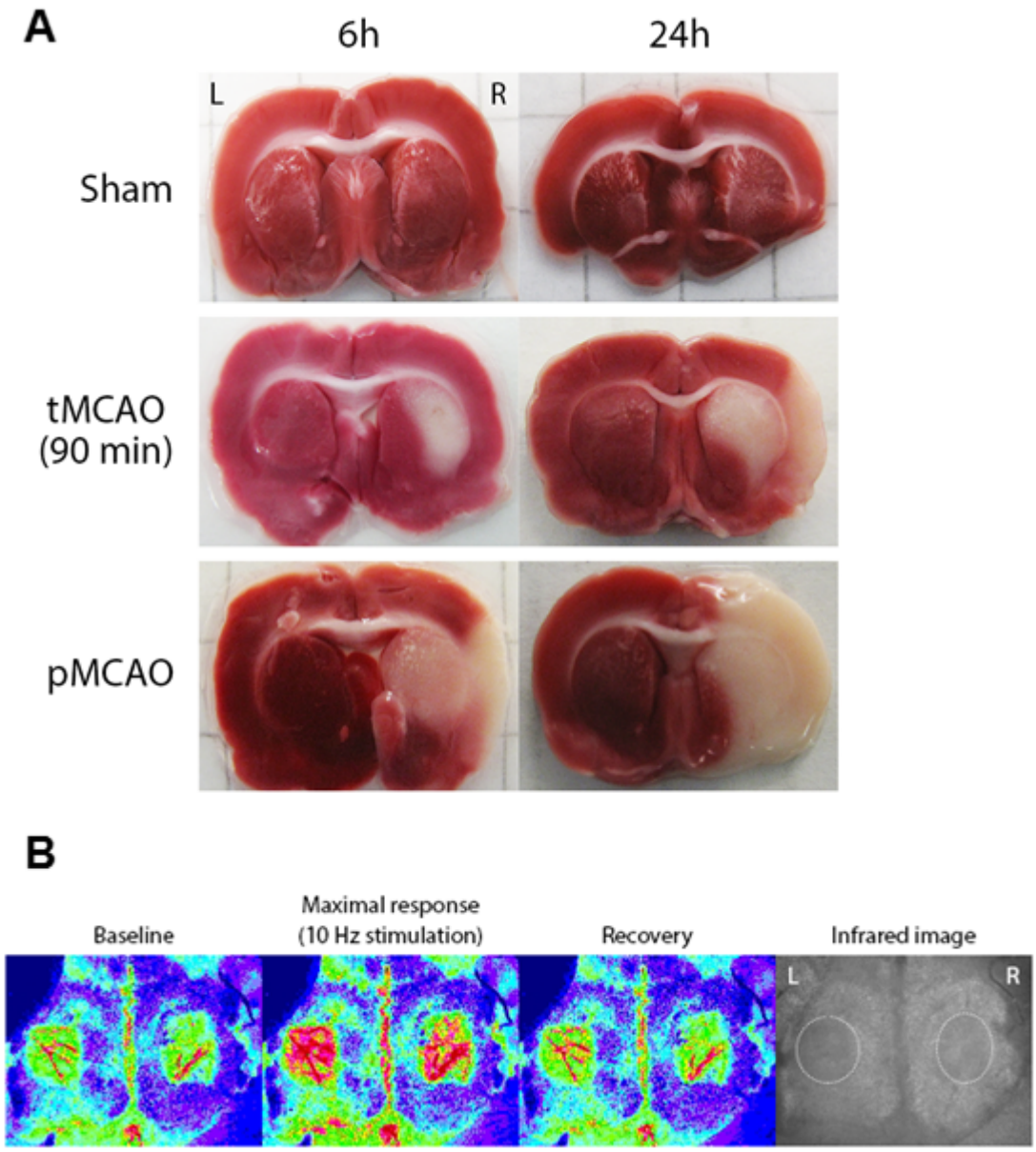

Figure 2.1: Example lesions and laser speckle imaging setup. **(A)** TTC staining for tissue death at 6 and 24 h following MCAO. Sham animals do not have evidence of lesion development, whereas 90 min tMCAO results in striatal tissue loss at 6 h, with additional cortical lesion development by 24 h, primarily in the lateral cortex. By contrast, pMCAO results in early striatal and cortical lesions, and near-hemispheric tissue death by 24 h. **(B)** False-coloured images of laser speckle contrast during baseline, stimulation and recovery, with an infrared image showing the cranial windows. Note that the imaging is performed in the superomedial cortex, distant to the lesion at 6 hours after tMCAO and only partially affected at 24 hours.

2.2.6 Somatosensory evoked potential recordings

After the thinned skull preparation was completed, bilateral burr holes were made inferior to the temporal ridge, using a combination of drilling and removal of the bone with a surgical probe. Somatosensory evoked potentials (SEPs) were unilaterally recorded with platinum-iridium electrodes (Bilaney, Germany), a CED 1902 preamplifier and a CED 1401 converter (Cambridge Electronic Designs, UK). Electrophysiological data were recorded using Spike2 software (Cambridge Electronic Designs) running on a Windows 7 workstation.

2.2.7 Stimulation

10 sets of 16-second stimulation trains were delivered to the contralateral whisker pad with a bipolar stimulating electrode (Grass Instruments, USA), with a 60-second interstimulus interval. The stimulation protocol started with 3 Hz stimulation followed by 10 Hz stimulation. The starting point varied between the left (i.e. contralateral to the stroke) or right (ipsilateral) whisker pad; changeovers between sides were made at each frequency (e.g. 3 Hz left $\rightarrow$ 3 Hz right $\rightarrow$ 10 Hz left $\rightarrow$ 10 Hz right). At the end of the electrical stimulation protocol, rats were subjected to 4 sets of 30-second hypercapnia (10% CO2), with a 3-minute interstimulus interval.

2.2.8 Arterial blood gas measurements

In the LSCI cohort, arterial blood samples were collected onto i-STAT cartridges and analysed on the i-STAT 1 platform (Point Of Care Testing).

2.2.9 Behavioural outcomes

Animals were evaluated for overall welfare and neurological function. The assessor was aware of the surgical group allocation, due to obvious differences in impairment between sham and tMCAO animals.

2.2.9.1 Neurological assessment

Neurological impairment following MCAO was assessed with a modified Neuroscore protocol (Garcia et al., 1995), as described in table 2.1.

2.2.9.2 Welfare assessment

General welfare was evaluated according to a composite score, as described in table 2.2. Rats scoring >7 points were considered severely impaired, whereas scores of <4 points were considered indicative of mild impairment.

Table 2.1: Neurological impairment scoring system (Neuroscore), comprised of 6 tests. Modified from Garcia et al. (1995).

Spontaneous activity, evaluted for 5 minutes in the home cage	
0	Moves and approaches at least three sides of cage
1	Moves but does not approach at least three sides of cage
2	Barely moves
3	No movement
Symmetry of movements when suspended by the tail	
0	Both sides move symmetrically
1	Contralateral side moves slowly
2	Contralateral side shows slight movement
3	Contralateral side shows no movement
Symmetry of forelimb movement when hindlimbs are suspended	
0	Symmetrical outreach
1	Contralateral forepaw shows slightly diminished movement
2	Contralateral forepaw shows severely diminished movement
3	Contralateral forepaw does not move
Climbing a 1 centimetre wire grid	
0	Normal climbing
1	Able to climb but contralateral side is weaker
2	Failure to climb
Reaction to touch on either side of trunk	
0	Symmetrical response
1	Slower or less sensitive response on the contralateral side
2	No response on the contralateral side
Response to vibrissal touch on either side	
0	Symmetrical response
1	Slower or less sensitive response on the contralateral side
2	No response on the contralateral side

Table 2.2: Welfare scoring system, comprised of 5 categories.

Appearance	
0	Normal
1	Lack of grooming
2	Coat staring/ocular discharge/nasal discharge
4	Piloerection/hunched posture
Food and water intake	
0	Maintaining body weight within 5% of baseline weight
1	Weight loss 5-10%
2	Weight loss 10-15%
4	Weight loss >10-15%
12	Weight loss >10-15%, sustained for $\geq$48 hours
Natural behaviour	
0	Normal
1	Minor change in spontaneous activity
2	Substantial change in spontaneous activity
4	Restless or very still
12	Chewing limb, lameness, loss of blood supply to leg
Cerebral function	
0	Normal
2	Minor/moderate circling and/or hemiparesis
6	Severe circling and/or hemiparesis/hemiplegia
12	Fitting or ataxia
Postoperative complications	
4	Difficulty in breathing
4	Excessive bleeding
4	Infection
4	Wound breakdown

2.2.10 Isolated vessel studies

Isolated vessel experiments were conducted in collaboration with Dr. Zuzana Broskova (Augusta University) and performed as previously described (Broskova et al., 2013). Briefly, anaesthesia was re-induced with 4-5% isoflurane at 48 hours following MCAO, and the rats were killed by decapitation. The brains were removed and placed into ice-cold Ca^{2+}-free Krebs buffer. M1 and M2 branches of the MCA, approximately 2 mm in length, were identified under a dissection microscope (Leica, Germany), gently isolated from the brain, transferred to an organ bath, and attached to glass capillaries at both ends with silk thread. The organ bath was continuously perfused with Krebs buffer containing 120 mM NaCl, 5.9 mM KCl, 1.2 mM NaH_2PO_4, 1.2 mM $MgCl_2$, 15.4 mM $NaHCO_3$, 1.25 mM $CaCl_2$, and 5.5 mM glucose. The vessels were then pressurised to approximately 80 mmHg and allowed to develop tone for 1 hour; if the vessel diameter did not decrease over that period, the vessels were discarded. Subsequently, histamine, sodium nitroprusside (SNP), serotonin (5-hydroxytryptamine; 5-HT) and/or bradykinin (all from Sigma, USA) were added in increasing concentrations (10^{-10} to 10^{-7} M for bradykinin; 10^{-9} to 10^{-6} M for histamine, SNP and 5-HT) and vessel responses recorded for 3 minutes. Each vessel was exposed to no more than 2 drugs, with extensive washes and rest periods in between. Vessel responses were recorded using a brightfield microscope with a 20× water-immersed objective (Nikon, UK) coupled to an ultra-fast imaging system (Till Photonics, UK).

2.2.11 20-HETE measurement

Anaesthesia was induced in 4-5% isoflurane and rats were killed by cervical dislocation. Brains were removed and cut into 1 mm sections on an ice-cold stainless steel matrix (Kent Scientific). Cortices and striata were dissected out from both hemispheres on ice, placed into 10 µM triphenylphosphine solution, and frozen in

liquid nitrogen. Sample processing and enzyme-linked immunosorbent assay (ELISA) for 20-HETE were carried out according to manufacturer's instructions (Detroit R&D, USA). Striatal and cortical results were normalised to the mean sham striatal and cortical values, respectively.

2.2.12 Analysis

LDF, behavioural, neurological and welfare data were analysed in Excel 2010 (Microsoft, USA) and Prism 6.0 (Graphpad, USA). Electrophysiological data and LSCI recordings were analysed in Matlab 8.1 (Mathworks, USA), using custom software written by Dr. Chris Martin (University of Sheffield). Area under the curve (AUC) measurements were quantified over 40 seconds from onset of whisker stimulation, and 130 seconds from onset of CO_2 inhalation, to account for the persistence of CBF changes even after stimulation had stopped. Isolated vessel responses were analysed with Arivis Browser (Till Photonics). The significance level was set at α=0.05 for Mann-Whitney U tests (Neuroscore, welfare), nonlinear regression with extra sum-of-squares F-tests (LSCI traces, isolated vessel dose-response curves), and 2-way ANOVA with Sidak's post-hoc testing (all other comparisons). Results are presented as mean $\pm$ 95% confidence intervals for Neuroscore and welfare, and mean $\pm$ standard error (SEM) for other results, unless otherwise specified.

2.3 Results

2.3.1 Surgery for imaging does not affect arterial blood gases

To exclude arterial blood gas abnormalities as a confounding factor for CBF measurements in the artificially ventilated LSCI cohort, arterial blood sampling was carried out prior to stimulation and at the end of the protocol (Table 2.3). Although base excess and bicarbonate were elevated, P_aCO_2 and P_aO_2 were stably within reference range in both MCAO and sham groups, and there was no evidence of pH disturbances.

Table 2.3: Arterial blood gases during laser speckle contrast imaging, sampled immediately following vessel cannulation (baseline) or at the end of the imaging protocol (post-imaging). The measured parameters included pH, partial pressures of oxygen (P_aO_2) and carbon dioxide (P_aCO_2), standard base excess (cBase(ECF)), bicarbonate concentration ($[HCO_3^-]$), and total CO_2 content. Mean ± SEM; n=3 animals per group.

	Sham		**MCAO**	
Parameter	**Baseline**	**Post-imaging**	**Baseline**	**Post-imaging**
pH	7.45±0.02	7.43±0.03	7.48±0.01	7.46±0.01
P_aCO_2 (kPa)	40.65±1.95	44.85±4.05	40.05±3.53	40.05±3.00
P_aO_2 (mmHg)	107.41±6.38	122.04±7.13	122.04±6.38	112.73±17.48
cBase(ECF)	4.17±0.75	4.67±0.37	6.00±1.53	5.33±2.33
HCO_3^- (mmol/L)	28.03±0.52	29.27±0.62	29.40±2.00	29.23±2.09
TCO_2 (mmol/L)	29.33±0.56	30.67±0.68	30.67±2.33	30.67±2.03
O_2 saturation	98.17±0.31%	98.33±0.40%	99.00±0.00%	98.33±0.67%

2.3.2 tMCAO increases neurological impairment

The functional status of animals subjected to sham or tMCAO was evaluated in both the 6-hour and 24-hour groups. Due to the small sample size (n=3 in all groups), non-parametric Mann-Whitney testing did not show a significant difference between any groups. Sham animals showed effectively no neurological impairment at 6 hours, and only scored points due to a lack of spontaneous activity, attributable to the brevity of their recovery period after surgery (approximately 3 h).

In contrast, all tMCAO animals exhibited at least moderate neurological dysfunction (Fig. 2.2A; p=0.1). Welfare scores exhibited a trend towards increase in tMCAO animals at 6 hours (Fig. 2.2B; p=0.3). The differences were greater at 24 hours, when tMCAO animals showed substantial trend towards neurological impairment (Fig. 2.2C; p=0.1) and worsened welfare scores (Fig. 2.2D; p=0.1), whereas shams were unimpaired in both test batteries.

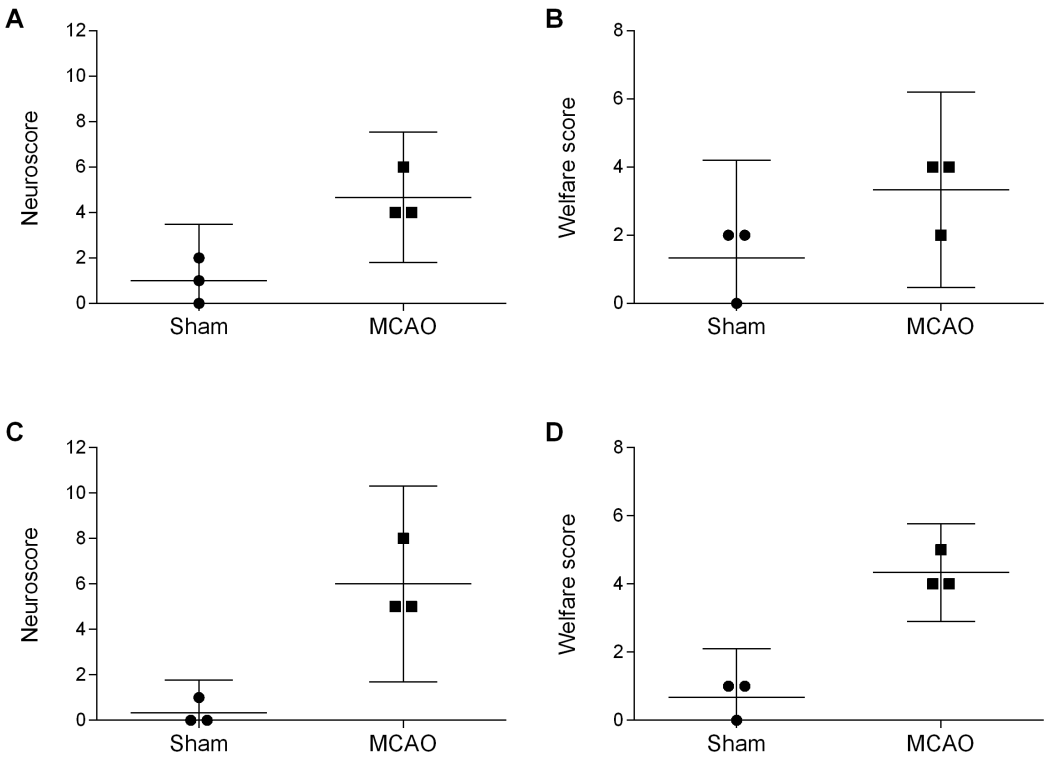

Figure 2.2: Neurological test scores and general welfare assessment in the 6-hour and 24-hour groups following sham or tMCAO indicate greater impairment in ischaemic animals. **(A)** Neurological impairment in sham and tMCAO animals of the 6-hour group, evaluated at approximately 3 hours after tMCAO onset. **(B)** Welfare scores in sham and tMCAO animals of the 6-hour group. **(C)** Neurological impairment in sham and tMCAO animals of the 24-hour group, evaluated at approximately 21 hours after tMCAO onset. **(D)** Welfare scores in sham and tMCAO animals of the 24-hour group. Mean ± 95% CI; $p>0.05$ for all comparisons. n=3 per group

2.3.3 Whisker stimulation responses are largely unaltered by tMCAO

The CBF response to whisker stimulation was investigated as an indicator of neurovascular coupling. At 6 hours following tMCAO onset, electrical stimulation at 3 Hz resulted in robust CBF increases in both contralateral (CL; Fig. 2.3A) and ipsilateral (IL; Fig. 2.3B) hemispheres. Surprisingly, the response was smallest in the IL hemisphere of the sham group; however, this did not reach significance when quantified as AUC (Fig. 2.3C; treatment p=0.1955, hemisphere p=0.9383) or peak ΔCBF (Fig. 2.3D; treatment p=0.1399, hemisphere p=0.6826). The CBF changes during 10 Hz stimulation in the same group were also similar in both hemispheres (Fig. 2.4A, 2.4B), with no differences between hemispheres in terms of AUC (Fig. 2.4C; treatment p=0.4750, hemisphere p=0.8998) or maximal responses (Fig. 2.4D; treatment p=0.5966, hemisphere p=0.5362).

At 24 hours after ischaemia, 3 Hz stimulation demonstrated a trend towards exaggerated ΔCBF in the CL hemisphere (Fig. 2.6A), with no difference between sham and ischaemic animals in the IL hemisphere (Fig. 2.6B). The enhanced CL response was non-significant when quantified as AUC (Fig. 2.6C; treatment p=0.1287, hemisphere p=0.1102), but there was a significant difference between CL and IL ΔCBF maxima in the MCAO group (Fig. 2.6D; treatment p=0.0902, hemisphere p=0.0446, treatment:hemisphere p=0.0350; MCAO CL vs. MCAO IL $p<0.05$). Intriguingly, the same trend of MCAO animals showing larger CBF changes was also evident for 10 Hz stimulation (Fig. 2.7A, 2.7B), but did not reach significance in terms of AUC (Fig. 2.7C; treatment p=0.2671, hemisphere p=0.9986) or peak ΔCBF (Fig. 2.7D; treatment p=0.1859, hemisphere p=0.9990).

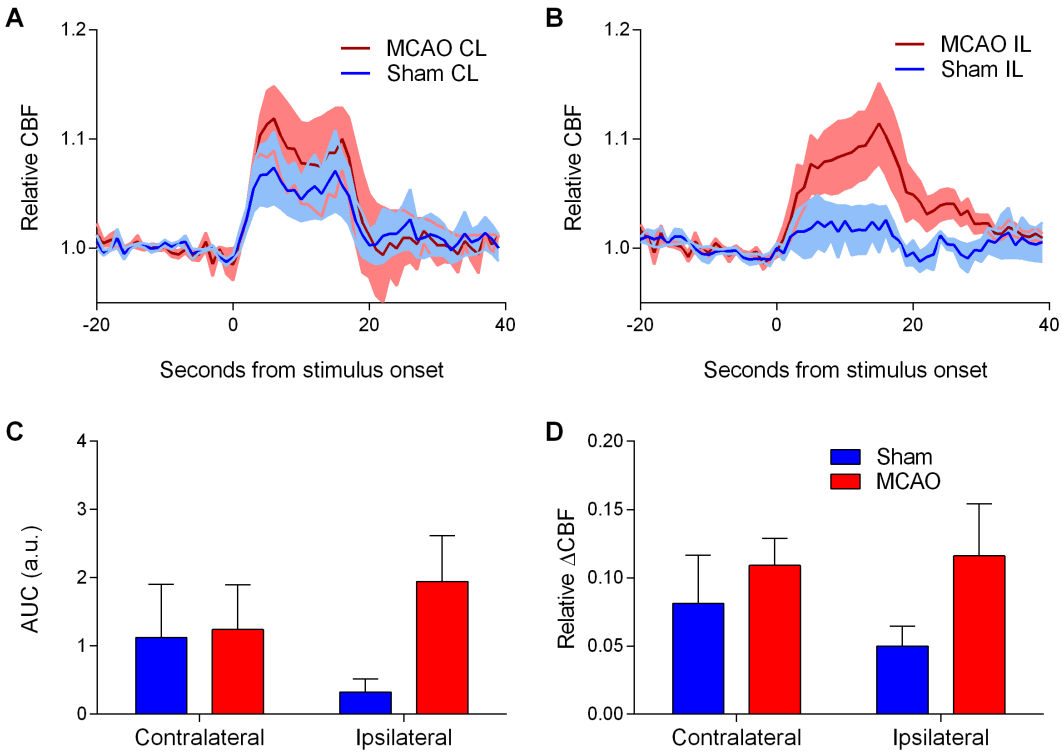

Figure 2.3: CBF responses to 3 Hz whisker stimulation at 6 hours following tMCAO show no significant differences between sham and ischaemic animals. **(A)** CBF response time courses in the CL (left) hemispheres of sham and tMCAO animals. **(B)** CBF response time courses in the IL (right) hemispheres of sham and tMCAO animals. **(C)** Overall CBF response size, quantified as area under the CBF curve for sham and tMCAO animals. **(D)** Peak ΔCBF in sham and tMCAO animals. Mean ± SEM; $p>0.05$ for all comparisons. n=3 per group.

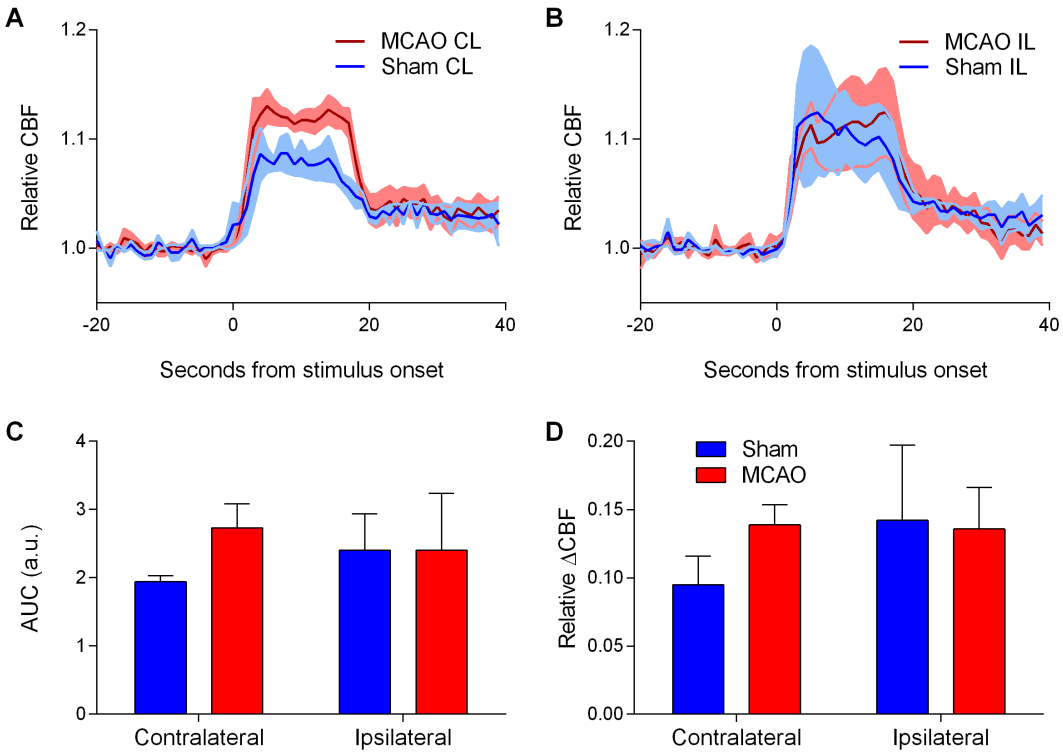

Figure 2.4: CBF responses to 10 Hz whisker stimulation at 6 hours following tMCAO show no significant differences between sham and ischaemic animals. **(A)** CBF response time courses in the CL (left) hemispheres of sham and tMCAO animals. **(B)** CBF response time courses in the IL (right) hemispheres of sham and tMCAO animals. **(C)** Overall CBF response size, quantified as area under the CBF curve for sham and tMCAO animals. **(D)** Peak ΔCBF in sham and tMCAO animals. Mean ± SEM; $p>0.05$ for all comparisons. n=3 per group.

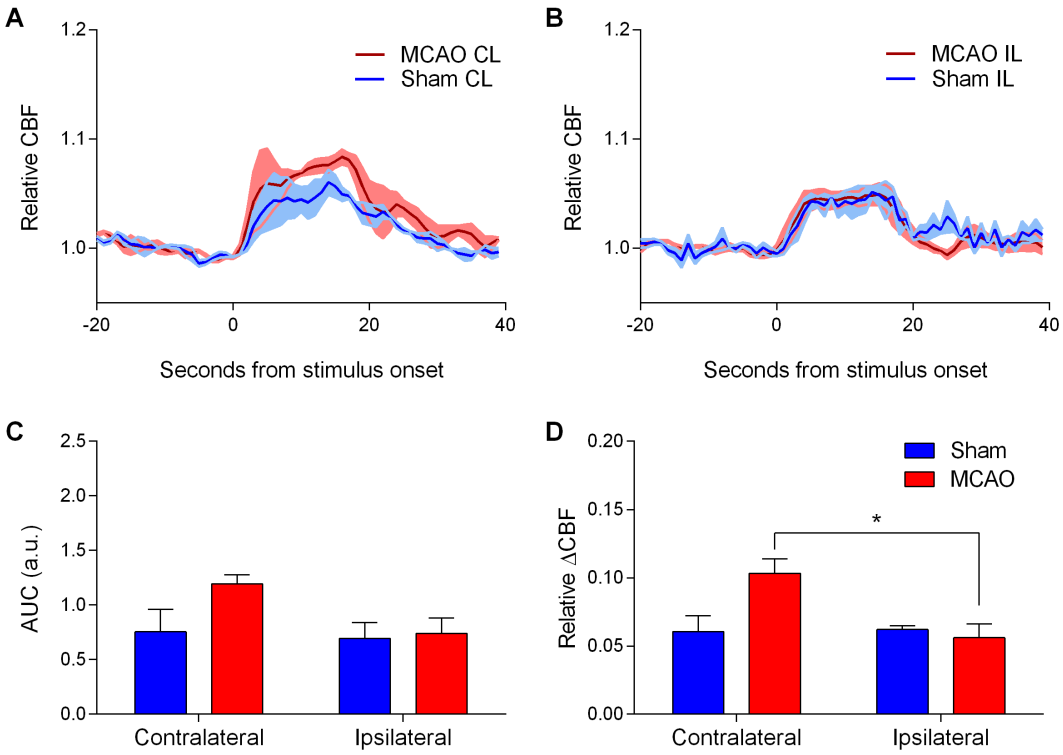

Figure 2.5: CBF responses to 3 Hz whisker stimulation at 24 hours following tMCAO show enhancement of CL CBF in the tMCAO group. **(A)** CBF response time courses in the CL (left) hemispheres of sham and tMCAO animals. **(B)** CBF response time courses in the IL (right) hemispheres of sham and tMCAO animals. **(C)** Overall CBF response size, quantified as area under the CBF curve for sham and tMCAO animals. **(D)** Peak ΔCBF in sham and tMCAO animals. Mean ± SEM; * $p<0.05$. n=3 per group.

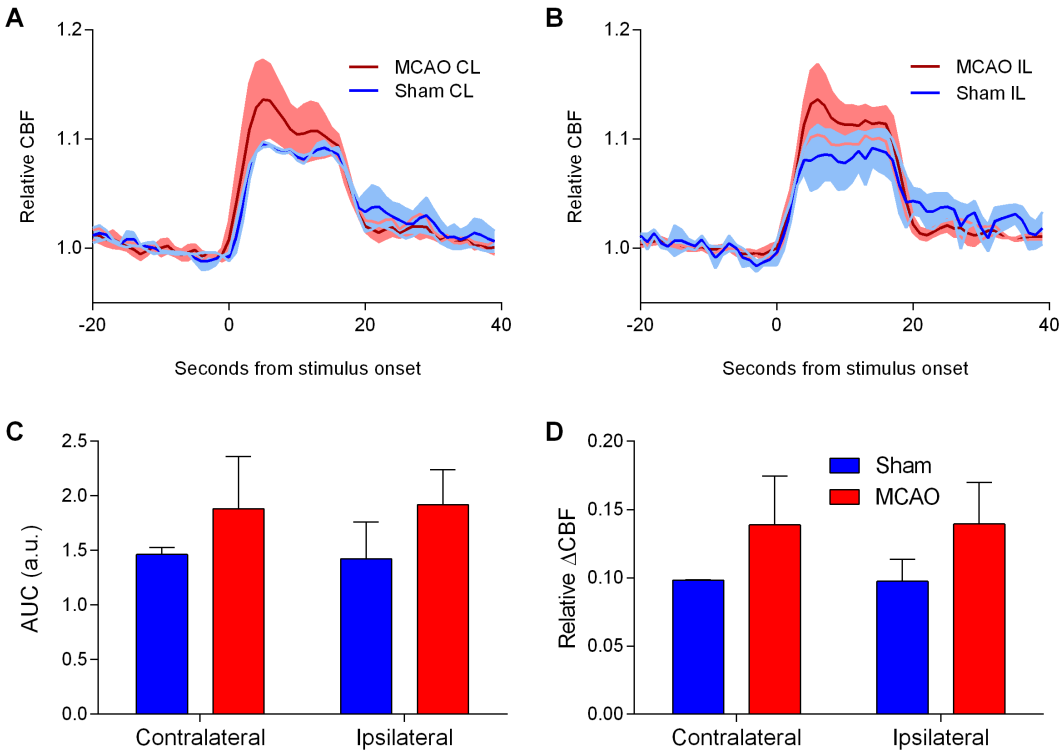

Figure 2.6: CBF responses to 10 Hz whisker stimulation at 24 hours following tMCAO show no significant differences between sham and ischaemic animals. **(A)** CBF response time courses in the CL (left) hemispheres of sham and tMCAO animals. **(B)** CBF response time courses in the IL (right) hemispheres of sham and tMCAO animals. **(C)** Overall CBF response size, quantified as area under the CBF curve for sham and tMCAO animals. **(D)** Peak ΔCBF in sham and tMCAO animals. Mean ± SEM; $p>0.05$ for all comparisons. n=3 per group.

2.3.4 Hypercapnic CBF responses are diminished following tMCAO

The effects of 10% CO_2 inhalation were then examined to establish CBF regulation changes independently of neural activity (Fig. 2.5A, 2.5B). At 6 hours after tMCAO, the variability in responses was very large, and there was no evident trend in AUC differences (Fig. 2.5C; treatment p=0.4151, hemisphere p=0.9996). There was a non-significant trend towards reduced peak ΔCBF in the MCAO group, on both the IL and CL sides compared to sham groups (Fig. 2.5D; treatment p=0.2889, hemisphere p=0.8034).

At 24 hours after tMCAO, the CBF response to 10% CO_2 exhibited a bilateral reduction in MCAO animals, compared to sham controls. The nonlinear regression curves were significantly different between sham and tMCAO groups in both the CL (Fig. 2.8A; $p<0.001$) and the IL hemispheres (Fig. 2.8B; $p<0.0001$). The difference in AUC was not significant in 2-way ANOVA (Fig. 2.8C; treatment p=0.0558, hemisphere p=0.9299); peak responses were significantly different, but post-hoc testing did not reveal specific intergroup differences (Fig. 2.8D; treatment p=0.0131, hemisphere p=0.8017).

2.3.5 Electrophysiological responses do not differ after tMCAO

To confirm that the tissue in the LSCI region of interest was still viable at 24 hours following onset of ischaemia, electrophysiological recordings were performed during 3 Hz and 10 Hz whisker stimulation, and quantified as ΣLFP. Similarly to the CBF changes, ΣLFPs from the IL hemisphere were not significantly different between sham and tMCAO groups, but there was a trend towards greater responses in ischaemic animals (Fig. 2.9; treatment p=0.2947, hemisphere p=0.7642).

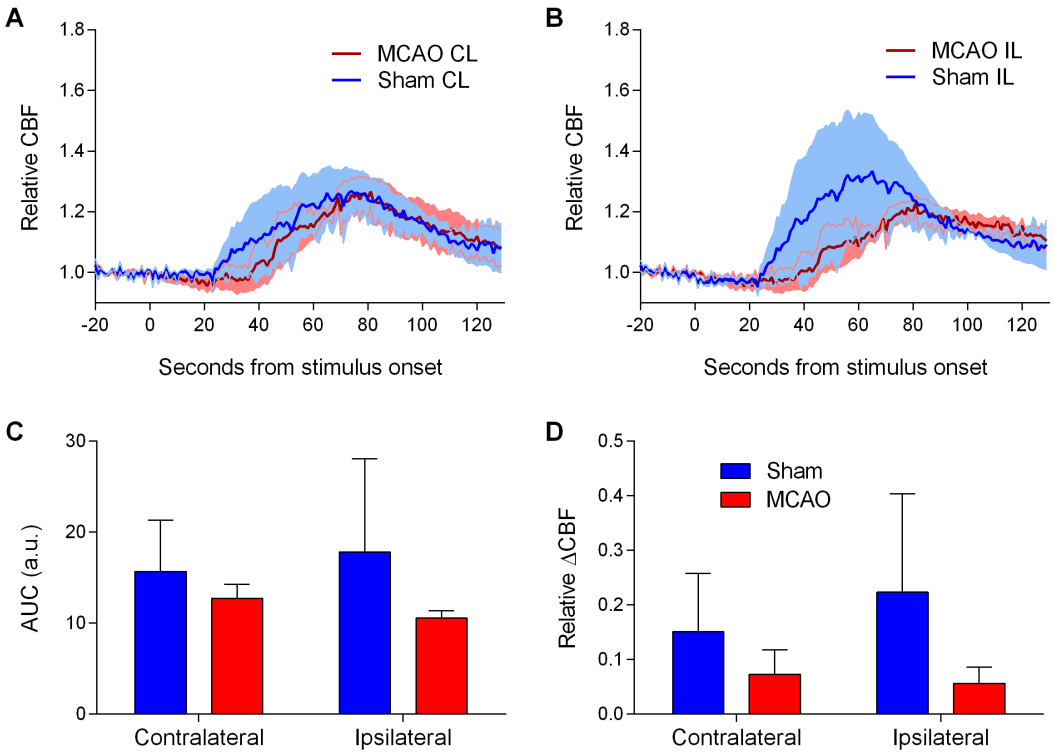

Figure 2.7: CBF responses to 10% CO_2 inhalation at 6 hours following tMCAO show no significant differences between sham and ischaemic animals. **(A)** CBF response time courses in the CL (left) hemispheres of sham and tMCAO animals. **(B)** CBF response time courses in the IL (right) hemispheres of sham and tMCAO animals. **(C)** Overall CBF response size, quantified as area under the CBF curve for sham and tMCAO animals. **(D)** Peak ΔCBF in sham and tMCAO animals. Mean ± SEM; $p>0.05$ for all comparisons. n=3 per group.

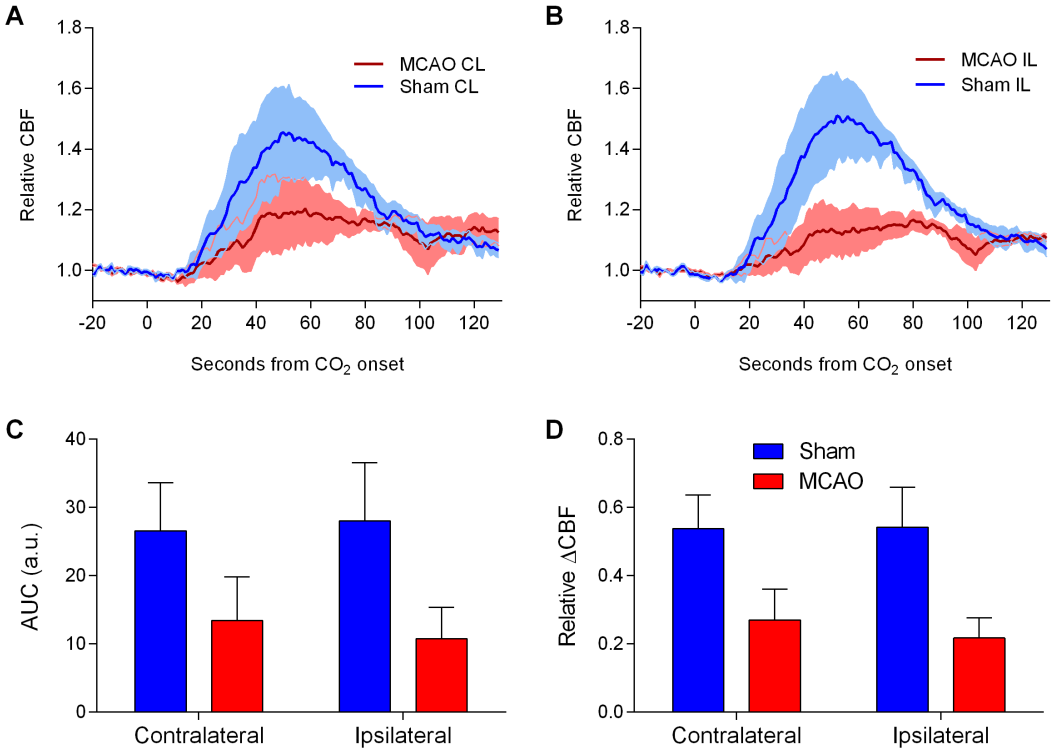

Figure 2.8: CBF responses to 10% CO_2 inhalation at 24 hours following tMCAO show a significant reduction in CBF in ischaemic animals. **(A)** CBF response time courses in the CL (left) hemispheres of sham and tMCAO animals. Nonlinear regression curves are significantly different ($p<0.001$) between groups. **(B)** CBF response time courses in the IL (right) hemispheres of sham and tMCAO animals. Nonlinear regression curves are significantly different ($p<0.0001$) between groups. **(C)** Overall CBF response size, quantified as area under the CBF curve for sham and tMCAO animals. **(D)** Peak ΔCBF in sham and tMCAO animals; 2-way ANOVA indicates significant differences based on surgical group ($p<0.05$). Mean $\pm$ SEM; n=3 per group.

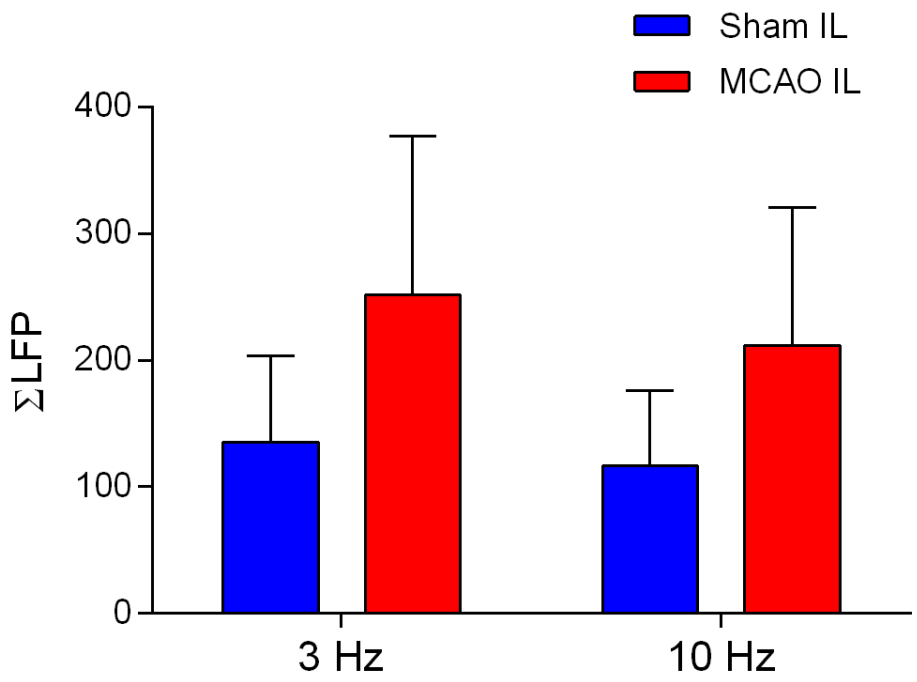

Figure 2.9: Electrophysiological responses to whisker stimulation, quantified as ΣLFP, did not differ between groups. Mean ± SEM; $p>0.05$ for all comparisons. n=3 per group.

2.3.6 Isolated vessel reactivity is bilaterally impaired after tMCAO

To investigate whether the *in vivo* differences in CBF responses were due to vascular changes, isolated MCA responses to vasoactive substances were measured *ex vivo*. Dilatory responses to bradykinin were significantly reduced in IL and CL vessels from MCAO rats compared to sham vessels (Fig. 2.10A; treatment $p=0.0118$, concentration $p<0.0001$, treatment:concentration $p<0.0001$; $p<0.0001$ for sham vs. MCAO CL and sham vs. MCAO IL at 10^{-6} M). The same was observed for histamine at the two highest doses (Fig. 2.10B; treatment $p<0.0001$, concentration $p<0.0001$, treatment:concentration $p=0.0006$; $p<0.01$ for sham vs. MCAO CL and sham vs. MCAO IL at 10^{-7} M, $p<0.0001$ for 10^{-6} M).

The nitric oxide donor vasodilator SNP had little effect on the vessels, and there were no evident differences between groups (Fig. 2.10C; treatment $p=0.6429$, concentration $p<0.0001$; treatment:concentration $p=0.7788$). Vasoconstriction was tested using 5-HT, which again showed differences between groups (Fig. 2.10D; treatment $p=0.0006$, concentration $p<0.0001$; treatment:concentration $p=0.3345$); at 10^{-7} M, there was a significant difference between sham and IL MCAO vessels ($p<0.01$), and between IL and CL MCAO vessels ($p<0.05$), whereas at 10^{-7} M 5-HT, only sham and IL MCAO vessels differed significantly ($p<0.05$).

The dose-response curves were also analysed using nonlinear regression, to assess the overall change in curve shape, with the null hypothesis that all data sets could be described by the same equation. The null hypothesis was rejected for bradykinin ($p<0.0001$), histamine ($p<0.0001$) and 5-HT ($p<0.01$), but not for SNP ($p=0.7069$).

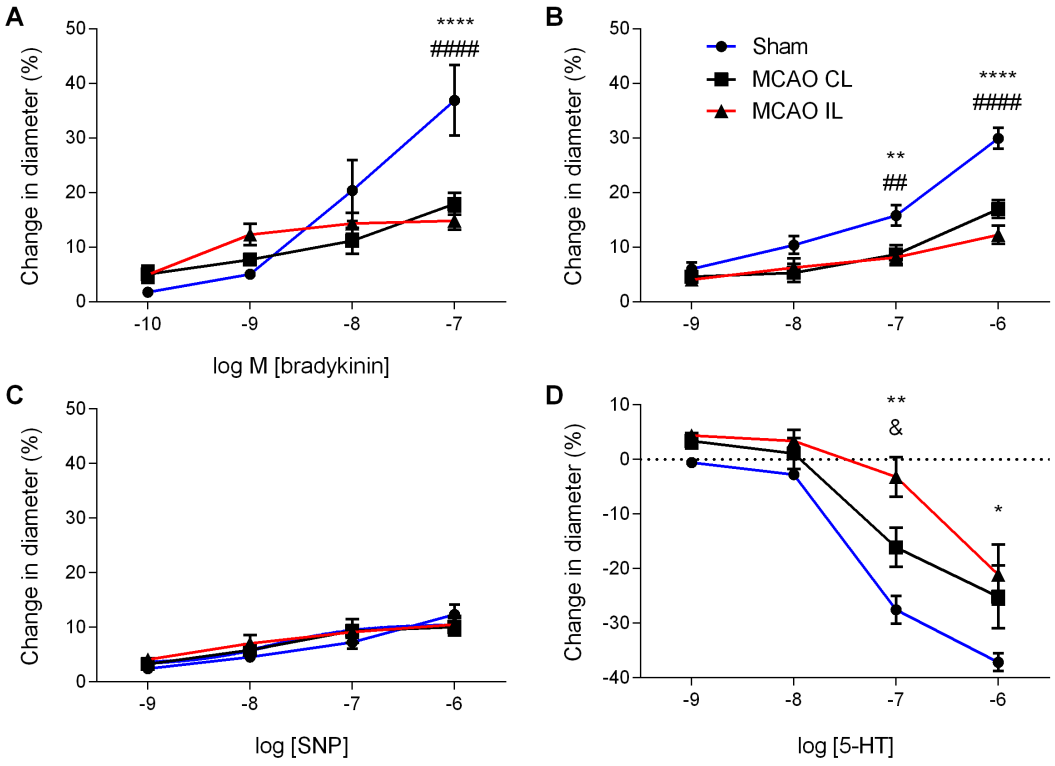

Figure 2.10: MCAs isolated from both the IL and CL hemispheres of ischaemic animals at 48 hours following tMCAO showed reduced reactivity compared to sham vessels. **(A)** Dose-response curve for bradykinin. **(B)** Dose-response curve for histamine. **(C)** Dose-response curve for SNP. **(D)** Dose-response curve for 5-HT. Mean ± SEM; * $p<0.05$ between MCAO IL and sham, ** $p<0.01$, **** $p<0.0001$. ## $p<0.01$ between MCAO CL and sham, #### $p<0.0001$. & $p<0.05$ between MCAO IL and MCAO CL. n=4-6 per group.

2.3.7 20-HETE production is not increased following tMCAO

To establish whether there was an increase in 20-HETE production that might account for altered CBF responses, brain 20-HETE content was assessed in a separate cohort of tMCAO animals. tMCAO animals had significant greater neurological impairment at 6 hours (Fig. 2.11A; p=0.0095), with no difference in welfare scores (Fig. 2.11B; p=0.3238). At 24 hours, the tMCAO group exhibited increases in both Neuroscore (Fig. 2.11C; p=0.0079) and welfare score (Fig. 2.11D; p=0.0159).

Samples were taken from brain regions corresponding to the affected territory (lateral cortex, striatum) and from equivalent areas in the contralateral hemisphere. 20-HETE content (normalised to the sham group) did not differ between sham and tMCAO groups at 24 hours following tMCAO (Fig. 2.12; treatment p=0.2064, location p=0.3702).

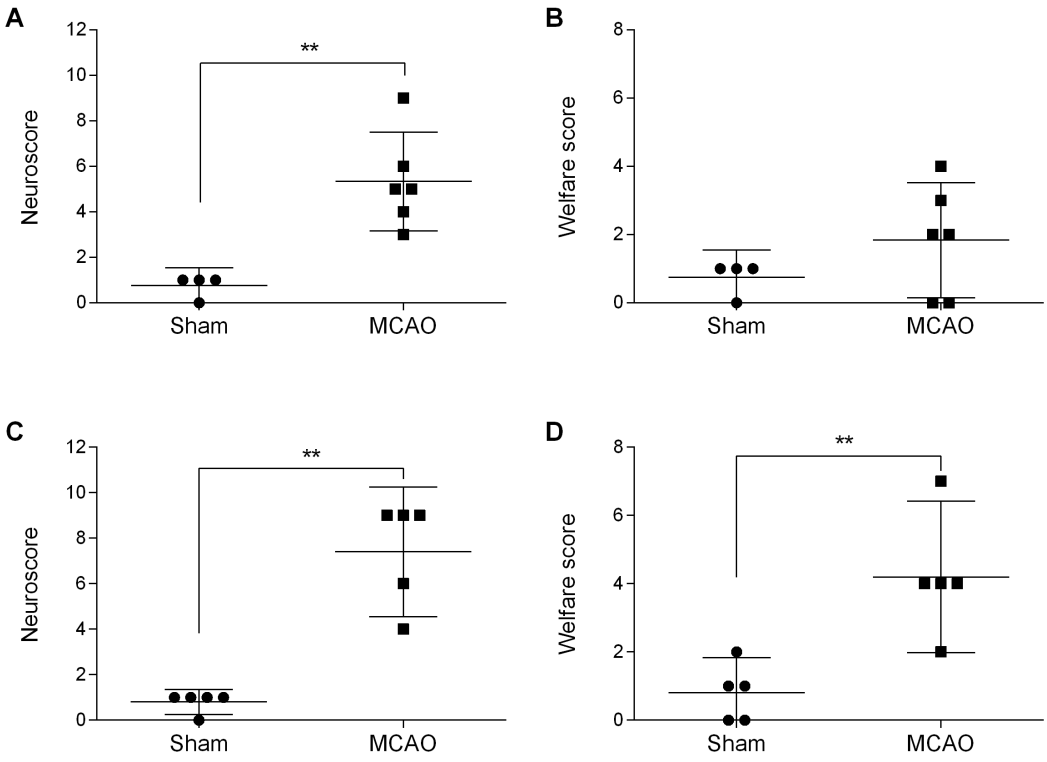

Figure 2.11: tMCAO resulted in significant neurological impairment and worsened general welfare. **(A)** Neurological impairment in sham and tMCAO animals of the 6-hour group. **(B)** Welfare scores in sham and tMCAO animals of the 6-hour group. **(C)** Neurological impairment in sham and tMCAO animals of the 24-hour group. **(D)** Welfare scores in sham and tMCAO animals of the 24-hour group. Mean ± 95% CI; ** $p<0.01$. n=4-6 per group

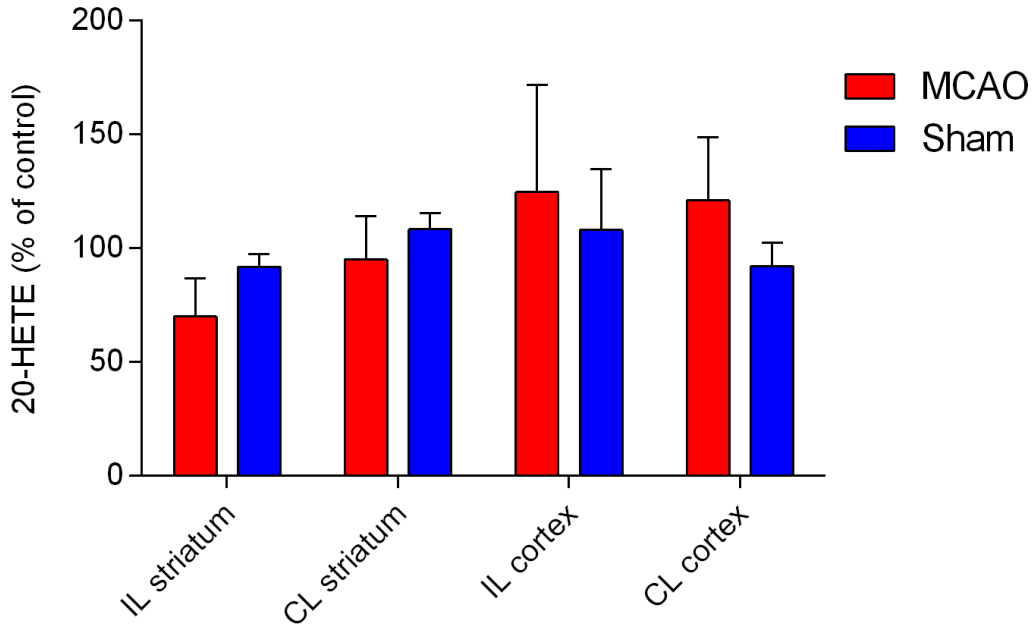

Figure 2.12: Brain 20-HETE content does not differ between shams and tMCAO animals at 24 hours after surgery. Mean ± SEM; $p>0.05$ for all comparisons. n=3-4 per group.

2.4 Discussion

The results described in this chapter suggest that while CBF responses to somatosensory stimulation were largely unaltered following focal ischaemia, there was a substantial and statistically significant reduction in reactivity to hypercapnic challenge at 24 hours in the tMCAO group. This change was evident in both the hemisphere ipsilateral to the stroke and, to a lesser extent, in the contralateral hemisphere. In agreement with this observation, the *ex vivo* data suggested that even in the absence of blood flow, systemic blood gas alterations or neural activity, isolated vessels from both ischaemic and control hemispheres of tMCAO animals exhibited diminished responses to vasoactive compounds. However, the initial hypothesis that these phenomena could be accounted for by an increase in cerebral 20-HETE production was not supported by ELISA results, showing no difference in whole-brain 20-HETE concentrations between shams and tMCAO rats.

Previous studies examining post-ischaemic responses to somatosensory stimulation and/or CO_2 inhalation have generally suggested that there is an initial impairment in cerebrovascular reacitivity following tMCAO (Sicard et al., 2006; Sauter et al., 2002; Reese et al., 2000); however, the dynamics of this process are not clear and may vary between stimuli. One study observed that BOLD and CBF responses to whisker stimulation were impaired 3 hours after ischaemia, but not at 24 hours. Conversely, hypercapnia-induced CBF and BOLD changes were impaired at 30 minutes into reperfusion, but not at 3 hours (Sicard et al., 2006). In addition, these studies have usually not observed a reduction in CL responsiveness (Sicard et al., 2006; Reese et al., 2000).

However, there is evidence from clinical studies that cerebrovascular dysfunction can occur in distant areas. In recovering stroke patients, reduced reactivity to CO_2 and diminished BOLD responses have been observed in non-lesioned areas (de Haan et al., 2013b; Krainik et al., 2005), including in the bilateral hemisphere (Pineiro

et al., 2002). This could be a consequence of either direct vascular changes or altered neural responses. Most clinical studies have not included measurements of electrophysiological activity during stimulation, but there are examples where BOLD and neural response intensities become dissociated following stroke, despite the spatial distributions of activity remaining similar (Altamura et al., 2007). The preclinical literature is equivocal – there are reports that CBF responses are lost before SEPs (Baker et al., 2013), while others have observed the two decreasing in parallel (Burnett et al., 2005). At more subacute and chronic time points (>2 days post-MCAO), SEPs and BOLD responses are correlated in their impairment (Weber et al., 2008).

The observation of bilateral cerebrovascular dysfunction is supported the isolated vessel studies, performed at 48 hours following tMCAO (a time point chosen based on preliminary results). It has previously been reported that in MCAs isolated from the IL side, ischaemia diminished responses to 5-HT, acetylcholine, and reduced spontaneous myogenic tone (Cipolla et al., 1997). The same group observed that ipsilateral myogenic tone was more severely impaired than contralateral tone, but both were below sham values (Cipolla and Curry, 2002); others have found that structural properties, such as wall volume and adventitial volume, are also increased in both IL and CL MCAs of Wistar rats subjcted to tMCAO (Jiménez-Altayó et al., 2007). These effects indicate that the ischaemic hemisphere is releasing mediators that are able to regulate vascular function at distant sites; the molecular basis of this is not known.

Based on observations from CSD experiments, 20-HETE is a candidate mediator of post-ischaemic hypoperfusion (Fordsmann et al., 2013). Although the role of 20-HETE in post-ischaemic neurovascular coupling has not been directly examined, inhibition of its synthesis appears to alleviate hypoperfusion after tMCAO and recanalisation (Poloyac et al., 2006; Renic et al., 2009). In vivo 2-photon microscopy showed that inhibition of 20-HETE production prevents a decrease in microvascular

CBF velocity at 1 and 7 hours following MCAO, as well as reducing an increase in CBF velocity at 24 h, suggesting its effects on the vasculature may be multiphasic (Marumo et al., 2010). It should be noted that both the detectable upregulation of 20-HETE following ischaemia, as well as its effects on CBF, are controversial (Renic et al., 2009). This may be due to a discrepancy between whole-brain and microvascular measurements of concentration, as well as different methodologies of CBF measurement (Marumo et al., 2010).

There are caveats to the experiments described in this chapter. First, this study did not examine NVC as a direct relationship of electrophysiological and CBF responses per se, as it was not possible to bilaterally record SEPs due to technical limitations of the setup. Second, these conclusions only apply to the cortical vasculature; as LSCI can only measure surface CBF, to a depth of no more than 1 mm, investigating responses in the striatum would have required different modalities such as BOLD-fMRI.

The approach taken to investigate 20-HETE in this study looked at whole-tissue 20-HETE concentrations rather than specifically looking at the vasculature. In future work, novel modalities such as imaging mass spectroscopy (McDonnell and Heeren, 2007) could potentially allow for maps of 20-HETE distribution to be compared to immunohistochemical labelling of vessels in adjacent sections, in order to determine its local concentrations in the vasculature. Moreover, measuring 20-HETE concentrations does not allow for mechanistic conclusions to be drawn about its contribution to post-ischaemic cerebrovascular reactivity. An alternative strategy that could have been used was LSCI in conjunction with pharmacological manipulation of 20-HETE after stroke, through inhibitors such as HET-0016 and TS-011 (Poloyac et al., 2006; Marumo et al., 2010), as well as antagonists such as WIT-002 (Yu et al., 2004).

In conclusion, these results indicate that cerebrovascular function is bilaterally

altered following 90-minute tMCAO in rats, based on both *in vivo* responses to whisker stimulation and hypercapnia, as well as isolated vessel reactivity to pharmacological challenges *ex vivo*. The molecular basis of this remains unknown and requires further investigation.

Chapter 3

Evaluating Pericyte Contractility *In Vitro*

3.1 Introduction

Evaluating the functional properties of vascular cell types remains technically challenging. While this would ideally be done *in vivo*, due to the dynamic nature of the vasculature, the physiological relevance of *in vivo* models is offset by numerous technical challenges. First, to achieve sufficient resolution for examining the microvasculature, the use of confocal and two-photon microscopes is necessary, which greatly increases the complexity of the experimental setup (Tran and Gordon, 2015). Second, image acquisition will be restricted to superficial cortical regions due to intrinsic limitations of optical microscopy in an opaque tissue. In addition, the neurovascular unit (NVU) itself complicates analysis of specific cell responses, particularly for pharmacological studies, as compounds may exerting effects indirectly via another cell type (e.g. a hypothetical vasculoprotective agent that could reduce pericyte constriction or death by causing release of endogenous protectants from endothelial cells or neurons), which would be extremely challenging to conclusively disentangle *in vivo*.

As a consequence, several models have been developed to assess vascular responses *ex vivo* and *in vitro*. Acute brain slices are commonly used to image vessel diameters

in response to pharmacological and electrical stimulation; the structure of the vessels or fluorescent labels can be used to determine pericyte location within the vascular tree, and define the specific cell types that are being examined (Hall et al., 2014). While acute slices retain the entire NVU (which can be seen as both an advantage and disadvantage, as mentioned), the throughput of acute slice experiments is limited by the ability to image on a few vessels at a time, and by the relatively elaborate experimental setup involved (Mishra et al., 2014), similar to *in vivo* setups. One can also use isolated vessels—as demonstrated in Chapter 2 of this thesis—to remove the NVU and simplify the microscopical analysis involved, but this nonetheless suffers from very limited throughput. In addition, the smallest vessels that can feasibly be isolated are parenchymal arterioles (Cipolla et al., 2014), making the study of capillary pericytes impossible with this method.

In order to overcome the limitations inherent to acute slice and *in vivo* studies, it is possible to use isolated pericyte cultures, which are relatively straightforward to prepare without the need for specialist equipment beyond typical cell culture facilities (Zhou et al., 2014). While most studies have used rodent or bovine pericytes (Zhou et al., 2014; McDonald et al., 1995), they can also be isolated from human brain biopsies (Paul et al., 2012), or differentiated from human pluripotent stem cells (Orlova et al., 2014), thus providing a more clinically relevant model system to investigate pericyte physiology.

However, assessing contraction and relaxation is challenging in isolated cultures. Conventionally, this relies on observing the effect on luminal diameter of the underlying vessel; this strategy is not feasible, as the cells are usually grown as a monolayer on a flat surface coated with extracellular matrix proteins, poly-lysine or similar compounds. While there are accurate quantitative methods, such as magnetic twisting cytometry, these require a highly specialised experimental setup, and the analysis is equally complex (Saxena et al., 2012; Fabry et al., 2001). To date, the main

method used for these experiments is to grow the cells on a deformable substrate, such as a relatively thick layer of silicone or collagen, which wrinkles at locations where the cells are exerting tension on it. Quantification of the response to vasoactive substances is performed through counting the number and size of wrinkles (Harris et al., 1980).

The substrate wrinkling method suffers from considerable drawbacks. First, the measurement is semiquantitative at best, as the exact correspondence between wrinkling and physical changes to the cells is not straightforward. Second, although the method has been used to quantify relaxation in pericytes (Matsugi et al., 1997), the relative lack of wrinkles at baseline makes it more difficult to accurately assess relaxation without the use of pre-constricting agents. Third, the silicone substrate might have confounding effects on pericyte physiology – in our pilot experiments attempting to culture pericytes on silicone, we observed a clear reduction in cell adhesion and viability, compared to cells grown on uncoated polystyrene dishes (unquantified observations). In the case of fixed samples, this is further complicated by the potential effects of the fixative – exposure time, exact molarity, temperature and other minor factors could alter the cell's morphology before fixation is complete.

Most importantly, these measures provide only a snapshot of the potentially complex and dynamic response a cell might have to a vasoactive compound. This greatly complicates time course studies, and makes it much more laborious and/or expensive to obtain a profile of responses with good temporal resolution. Therefore, it would be desirable to improve the methods available for evaluating pericyte contractility, and provide a superior platform to investigate both their physiological responses to vasoactive substances, and pathological changes in models of disease such as ischaemia.

3.1.1 Aims

The primary aim of this chapter was to develop a high-throughput, real-time and label-free assay to measure human pericyte contractility, using a commercially available device that records electrical impedance. The specific questions I sought to address were:

1. Can electrical impedance be used to quantify changes in area of the culture dish covered by human pericytes, directly corresponding to cell size in the acute context (i.e. with insufficient time for proliferation to become a confounding factor)?

2. Can time-course profiles of pericyte contraction and relaxation to various vasoactive substances be recorded with high temporal resolution?

3. Is it possible to measure both acute contractile effects and chronic proliferative changes in the same population of human pericytes?

3.2 Materials & Methods

3.2.1 Cell Culture

Standard incubation conditions (37°C, 5% CO_2 in humified air) were used for all experiments. Flasks and multiwell plates were obtained from Corning (USA).

3.2.1.1 Human pericytes

Human brain vascular pericytes (HBVP; Sciencell Research Laboratories, USA) were grown in pericyte medium (Sciencell) containing 2% foetal calf serum (FCS), 1% penicillin/streptomycin (P/S) and 1% pericyte growth supplement (Sciencell) on uncoated flasks and plates. HBVP were used at passages of <10, and did not exhibit differences in morphology or pericyte marker expression between early and late passages.

3.2.1.2 Human endothelial cells

Immortalised human temporal lobe endothelial cells (hCMEC/D3; Millipore, USA) were grown in EGM-2 medium (Lonza, USA) on flasks & plates coated with collagen I (Sigma, USA).

3.2.1.3 Rat pericytes

Primary rat brain vascular pericytes (RBVP) were isolated as previously described (Redzic et al., 2015). Briefly, male Sprague-Dawley rats (approx. 250-350 g) were anaesthetised with 4% isoflurane in a 30% O_2/70% N_2O carrier gas and killed by cervical dislocation. The cerebral cortices were dissected and minced in ice-cold modified Hanks' balanced salt solution buffer, before incubation in 1 mg/mL collagenase-dispase for 1 hour. Microvessel fractions were extracted by centrifugation of the digest in a 30% bovine serum albumin solution, resulting in a microvessel pellet while neurons, astrocytes, microglia and myelin remained in the top layer. Microvessels were further dissociated in 1 mg/mL collagenase-dispase

for 2.5-3.5 hours, then seeded onto collagen I-coated T-25 flasks in Dulbecco's modified Eagle medium (1 g/L glucose) containing 1% P/S, 4 µg/mL vitamin C, 325 µg/mL glutathione (Sigma), 10% FCS and 1× insulin-transferrin-selenium supplement (Gibco, USA). These cells were defined as passage 1 RBVP. The medium was completely replaced on day 3, followed by half replacement every 2-3 days, depending on cell density. When the flasks reached 90-100% confluence, cells were detached with TrypLE (Life Technologies, UK) and plated onto flasks or plates treated with poly-D-lysine (Sigma). RBVP were used at passages of <3.

3.2.2 iCelligence impedance analysis

Pericyte contractility studies were conducted with the iCelligence electrical impedance assay (ACEA Biosciences, USA). Briefly, cells were cultured on a surface containing gold-coated electrodes (E-plates) and placed into the iCelligence device, housed in the cell culture incubator under standard conditions. Effectively, the cells formed part of an electrical circuit and the device detected changes in coverage of the culture surface, whether it's through alterations in the contractile state of cells or proliferation (Fig. 3.1). Impedance changes were expressed as a cell index (CI), derived from the equation

$$CI(t) = \frac{I_t - I_{t_0}}{Z_n}$$

where I_t is impedance measured at frequency f_n at time t, I_{t_0} is impedance measured at frequency f_n at time t_0 (background measurement in the absence of cells), and Z_n is the frequency factor of f_n in ohms. As such, the units cancel out and CI is a unitless parameter expressing relative impedance.

HBVP were initially plated onto E-plates at various densities—5,000, 10,000, 20,000 and 40,000 cells/well—to establish optimal culturing conditions, with the aim of using the cells while they were sufficiently dense to provide accurate measurements of contraction, but with sufficient space to monitor proliferation for at least 48

hours following treatment. For contractility and ischaemia experiments, HBVP were plated at 10,000 cells/well (approx. 16,000 cells/cm^2). The plates were left at room temperature in sterile conditions for 30 minutes, to avoid rapid warming and prevent the resulting convective flow from causing uneven distribution within wells, thus allowing cells to adhere uniformly to the electrode-coated surface. Cells were left to adhere and grow for approximately 40-48 hours before further experimentation. Recordings were paused for drug addition and then restarted immediately.

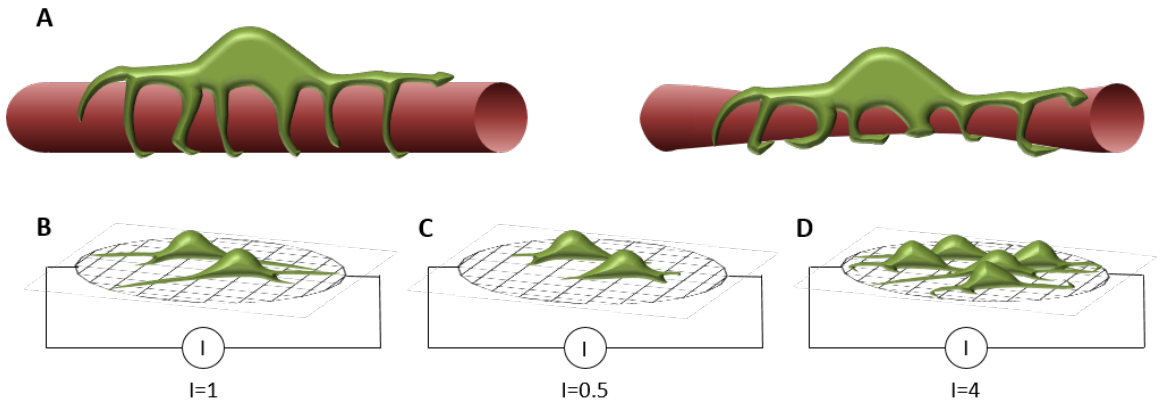

Figure 3.1: Schematic comparison of pericyte contractility *in vivo* and on the iCelligence platform *in vitro*. **(A)** Capillary constriction by pericytes (green). **(B)** Cultured pericytes on an E-plate at rest. **(C)** Pericytes can change following application of a vasoconstrictor, resulting in diminished contact area with the plate and the electrodes. **(D)** Impedance can increase following proliferation resulting in an increased contact area. 'I' refers to impedance.

3.2.3 Treatments

All drugs were added to wells as concentrates in pericyte medium (e.g. 4-fold concentrated when adding 100 µL of drug solution to 300 µL of culture medium on the cells); the concentrations presented herein refer to the final concentration in the well, unless otherwise specified. To minimise the effects of temperature differences on cell size, solutions were warmed to 37°C before administration. In all experiments, vehicle controls were added with water, phosphate-buffered saline (PBS) or dimethyl sulfoxide (DMSO) diluted in pericyte medium to match the concentration of carrier present in the drug groups.

3.2.3.1 Vasoactive compounds

Endothelin-1 (ET-1), sodium nitroprusside (SNP), and adenosine (Sigma) were dissolved in water (ET-1, SNP) or PBS (adenosine) before dilution in pericyte medium.

3.2.3.2 Antagonist experiments

For evaluation of specific receptor contributions to contractile responses, cells were pretreated with antagonists for 1 hour before administration of the relevant agonists. BQ-788 and CGS-15943 (Sigma) were dissolved in DMSO before dilution to a final concentration of $\leqslant$0.1% DMSO. BQ-123 (Abcam, UK) was dissolved in water before dilution.

3.2.4 Immunocytochemistry

Cells were seeded onto sterilised uncoated glass coverslips in 24-well plates, with 15,000 cells/well (approx. 8,000 cells/cm^2) in pericyte medium. After 24 hours, cells were washed with PBS and fixed with either 4% paraformaldehyde in PBS for 10 minutes at room temperature (confocal imaging) or ice-cold acetone for 20 minutes at -20°C. Cells were washed in PBS and left at 4°C in PBS with 0.1% sodium azide until

staining. After washing, cells were blocked in 10% normal donkey serum (DkS; Life Technologies) in PBS for 1 hour at room temperature, followed by primary antibody incubation in 1% DkS in PBS overnight at 4°C (see Table 3.1). Cells were then washed and secondary antibody (donkey anti-primary species conjugated to Alexa Fluor 488; Abcam) solution was added in 1% DkS. After 1 hour at room temperature, cells were washed, counterstained with Alexa Fluor 594-conjugated phalloidin (approx. 30 nM; Life Technologies) and 4',6-diamidino-2-phenylindole (DAPI, 1 µM; Sigma). Coverslips were mounted onto glass slides in anti-fade fluorescence mounting medium (Dako, USA) and imaged on a Zeiss LSM 510 inverted confocal microscope with 40× or 63× oil-immersion objectives and appropriate excitation/emission filters (Carl Zeiss, Germany) or a Nikon Eclipse E1000 epifluorescence microscope with 40× air objectives and appropriate excitation/emission filters (Nikon, Japan).

Table 3.1: Antibodies used for immunocytochemistry.

Antigen	**Manufacturer**	**Species**	**Concentration**
PDGFRβ	R&D Systems (af385)	Goat anti-human	1:100
CD31	Dako (M0823)	Mouse anti-human	1:200
GFAP	Abcam (ab53554)	Goat anti-human	1:500
Iba1	Abcam (ab5076)	Goat anti-human	1:500

3.2.5 Lactate dehydrogenase assay

Cell death and adherence were measured with a lactate dehydrogenase assay (LDH; Promega, UK), as the presence of an intracellular enzyme in the culture medium is indicative of membrane disruption or cell detachment from the culture surface. At the end of the treatment period, supernatant was collected and frozen on dry ice. An equivalent volume of lysis buffer (Promega) was added and plates were incubated at 37°C for 30 minutes before the lysate was collected and frozen. Samples were thawed

and plated into a 96-well plate with 2 technical replicates per sample. A tetrazolium salt LDH substrate was added and the plates were constantly agitated at room temperature for 30 minutes, at which point a stop solution was added. Absorbance values of the red formazan product were acquired at 492 nm on a SPECTROstar microplate reader (BMG Labtech, Germany) within 30 minutes of the reaction being stopped. Cell death was calculated as

$$\%\ cell\ death = \frac{AB_{Spnt} - BG_{Spnt}}{(AB_{Spnt} - BG_{Spnt}) + (AB_{Lys} - BG_{Lys})} = \frac{Released\ LDH}{Total\ LDH}$$

where AB is sample absorbance, BG is background absorbance (from culture medium or lysis buffer without cells), Spnt is supernatant and Lys is lysate.

3.2.6 qRT-PCR

Quantitative real-time polymerase chain reaction (qRT-PCR) was used to examine expression of pericyte genes in comparison with endothelial cells. Briefly, cells were cultured on 6-well plates (Corning) to approximately 90% confluency. Following washes with PBS, cells were lysed, lifted with cell scrapers and homogenised using QiaShredder columns (Qiagen, UK). RNA was extracted from the homogenate using RNeasy Plus Mini kits (Qiagen). Following RNA quantification on a Nanodrop UV spectrophotometer (Thermo Scientific, USA), 500 ng of complementary DNA (cDNA) was synthesised with a reverse transcription kit (Applied Biosystems, UK). qRT-PCR was performed using a SYBR Green based mastermix (Primerdesign, UK) on a Lightcycler 480 PCR machine (Roche, UK), with 5 ng of cDNA per reaction. Primers were targeted against GAPDH, CD31, PDGFRβ and αSMA (Primerdesign; see Table 3.2 for primer sequences).

Table 3.2: Primer sequences used for qRT-PCR.

Marker	Accession number	Primer sequences
PDGFRβ	NM_002609	5′-TGCTCACCATCATCTCCCTTA-3′ 3′-GCTCACAGACTCAATCACCTT-5′
αSMA	NM_001613	5′-AAGCACAGAGCAAAAGAGGAAT-3′ 3′-ATGTCGTCCCAGTTGGTGAT-5′
CD31	NM_000442	5′-AAGGAACAGGAGGGAGAGTATTA-3′ 3′-GTATTTTGCTTCTGGGGACACT-5′

3.2.7 Analysis

3.2.7.1 iCelligence

iCelligence data were analysed in RTCA Data Analysis Software v. 1.0 (ACEA Biosciences). Briefly, CI values were normalised to the last time point before treatment, to correct for minor variation in cell growth between wells. In the case of antagonist experiments, the last time point before application of the agonist was used for normalisation. ΔCI was defined as the difference between baseline (=1 by definition) and the highest or lowest value within the analysed period (1 hour in most experiments). Slope was calculated as the rate of change between baseline and peak response. For proliferation analysis, normalisation time points were selected based on the last time point where raw CI values were identical between groups; a strict temporal definition (i.e. a specific time after ET-1 application) was not possible due to batch-to-batch variation in rate of proliferation. Doubling time was calculated as the period required for CI to reach 2.

3.2.7.2 Image analysis

Confocal Z-stacks were extracted in ImageJ (NIH, USA); only contrast and brightness enhancements were applied, with equal parameters on all images.

3.2.7.3 qRT-PCR analysis

The relative standard curve method, based on 2-fold dilutions of pooled cDNA from all samples, was used to generate regression parameters for each target. Following exponentiation, relative fold differences were calculated in Excel (Microsoft, USA), normalised to the endothelial sample means.

3.2.7.4 Statistical analysis

Statistical analysis was carried out in Prism 6 (Graphpad, USA). For LDH results, 2-way ANOVA was used with Sidak's multiple comparison test, comparing treatment groups at a given time point. For iCelligence results, 1-way ANOVA was used with Tukey's multiple comparison test. In cases where the Brown-Forsythe test indicated heteroscedasticity, a Kruskal-Wallis test with Dunn's multiple comparison test was used instead of ANOVA. The significance level was set at α=0.05. Results are presented as mean $\pm$ standard error (SEM) for bar graphs, and mean with unidirectional SEM for time courses, in the interest of clarity and legibility.

3.3 Results

3.3.1 HBVP phenotyping confirms their pericyte identity

Confocal imaging showed that HBVP exhibited clear staining for the pericyte marker PDGFRβ; in contrast, the cells were negative for the endothelial marker CD31, astrocytic marker GFAP and microglial marker Iba1 (Fig. 3.2), consistent with HBVP being a pure pericyte population without glial or endothelial contamination. Under epifluorescence, HBVP did not express detectable levels of αSMA, whereas both desmin and NG2 showed strong expression (Fig. 3.3). To provide quantitative metrics of HBVP phenotype, their expression of CD31, PDGFRβ and αSMA was compared to the immortalised human brain endothelial cell line hCMEC/D3. HBVP had approximately 5-fold higher levels of PDGFRβ expression (Fig. 3.4A; $p=0.0378$). There were no clear differences in αSMA transcript levels (Fig 3.4B; $p=0.0507$). Conversely, expression of the endothelial marker CD31 was approximately 100-fold lower in HBVP (Fig. 3.4C; $p<0.0001$), consistent with HBVP exhibiting a pericyte phenotype.

3.3.2 ET-1 causes HBVP contraction and proliferation

The highly potent vasoconstrictor peptide ET-1 was used to validate the platform for assessment of pericyte contractility. A clear reduction in CI, as an indicator of reduced surface coverage, was observed when ET-1 was applied to the wells. The time course of normalised cell index (Fig. 3.5A) exhibited an interaction between factors (time $p<0.0001$, ET-1 concentration $p<0.0001$, time:concentration $p<0.0001$). ET-1-treated wells showed significant differences from vehicle-treated control wells, when quantified as a relative change in slope, which was notably steeper in the ET-1 groups (Fig. 3.5B; 0.5 nM $p<0.05$, 5 nM $p<0.01$, 50 nM $p<0.001$). The same was observed for relative changes in CI; wells treated with ET-1 demonstrated a significantly larger decrease in normalised CI (Fig. 3.5C; 0.5 nM $p<0.05$, 5 nM $p<0.01$, 50 nM $p<0.001$).

The cells were then monitored for an extended period after treatment, to examine the effects of ET-1 on proliferation. ET-1 enhanced proliferation of HBVP, which became evident approximately 70 h after treatment (Fig. 3.6A; time $p<0.0001$, ET-1 concentration $p=0.0002$, time:concentration $p<0.0001$). This effect was statistically significant when quantified as relative slope between approximately 70 and 110 hours after treatment (Fig. 3.6B; all concentrations $p<0.05$), as well as doubling time in that interval (Fig. 3.6C; 0.5 nM $p<0.0001$, 5 nM $p<0.001$, 50 nM $p<0.001$).

To confirm that the observed chronic CI changes were a consequence of proliferation and not artefactual, HBVP were detached and counted on the haemocytometer in a separate experiment. Vehicle-treated wells grew to an average of 18,750±4787 cells/well by 48 hours post-treatment, whereas 50 nM ET-1 resulted in proliferation to 40,000±4082 cells per well ($p=0.0278$; data not represented graphically).

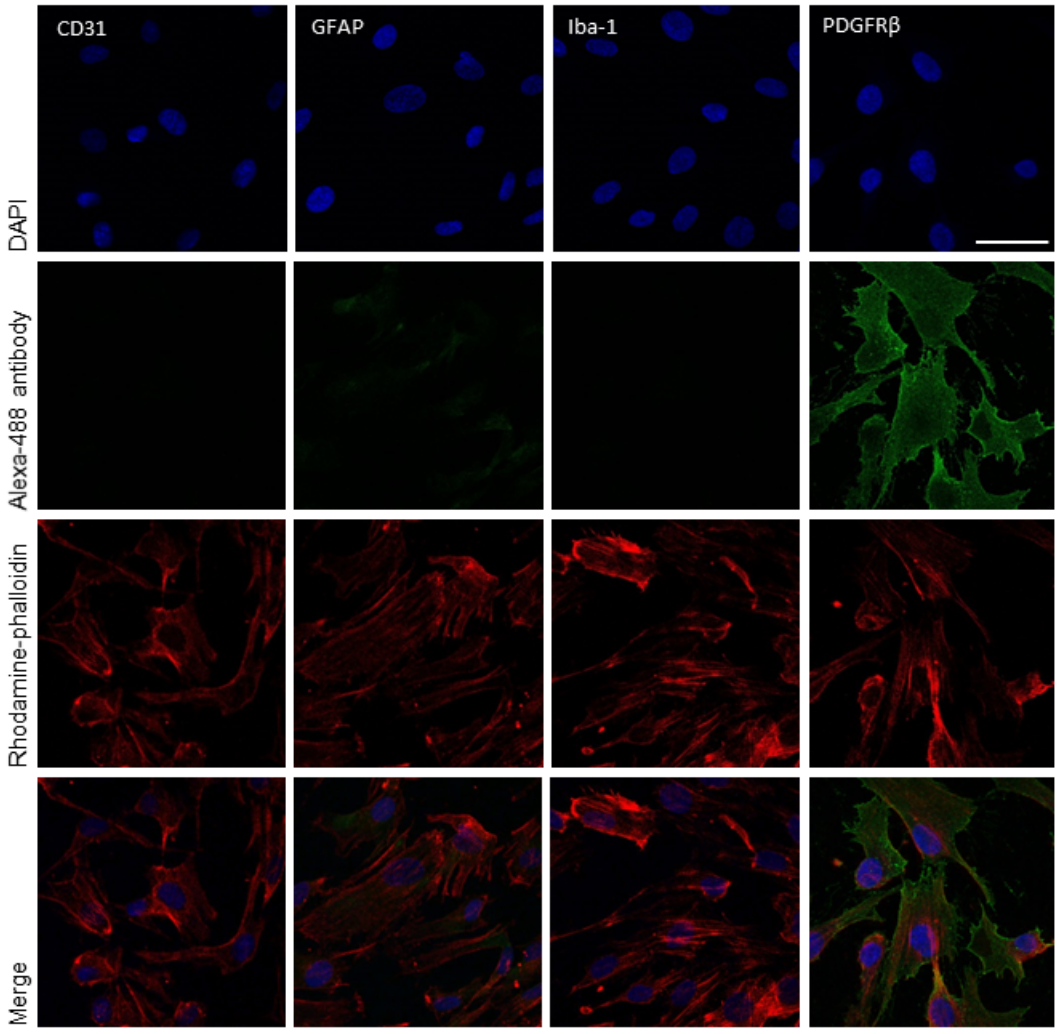

Figure 3.2: HBVP express typical pericyte markers in the absence of glial and endothelial markers. Immunocytochemistry for CD31, GFAP, Iba1 or PDGFRβ in the green channel, nuclear counterstaining in blue and cytoskeletal staining in red. Scale bar represents 30 µm.

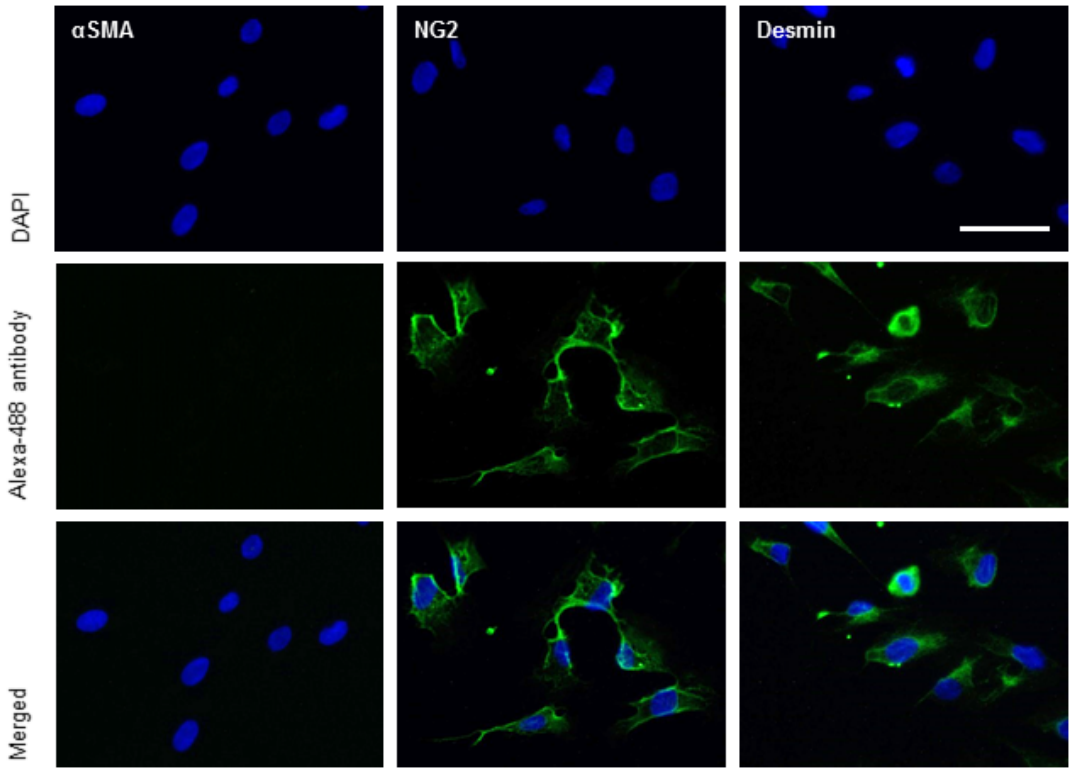

Figure 3.3: HBVP express the typical pericyte markers but are negative for αSMA. Immunocytochemistry for αSMA, desmin or NG2 in the green channel, nuclear counterstaining in blue . Scale bar represents 30 µm.

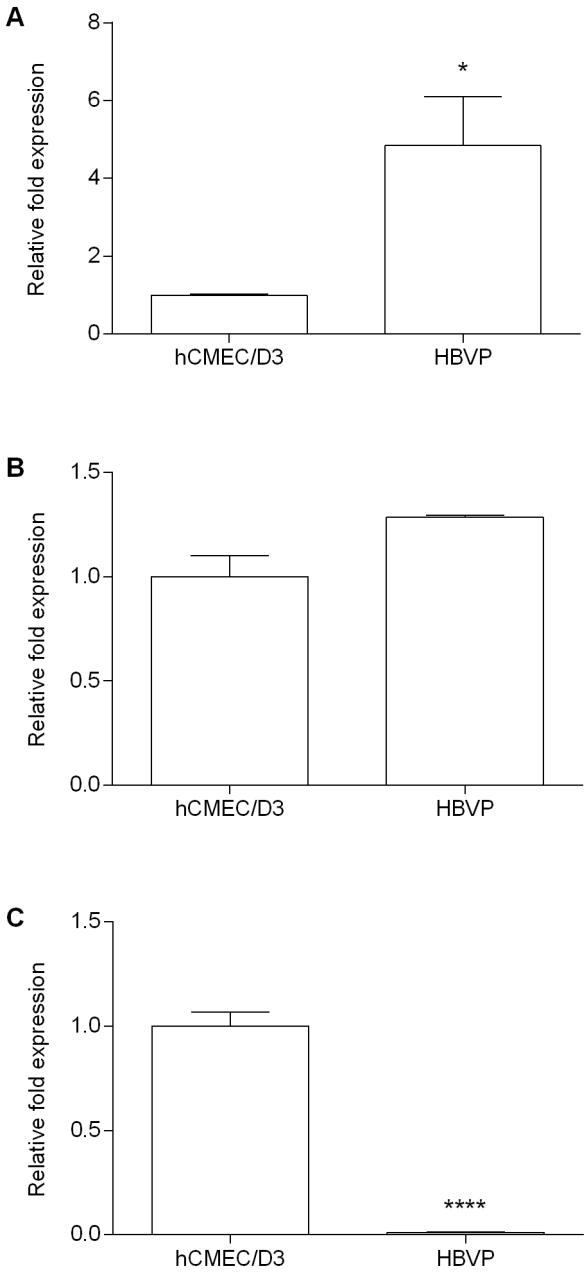

Figure 3.4: HBVP express higher levels of a typical pericyte marker, and markedly lower levels of a typical endothelial marker. **(A)** qRT-PCR of PDGFRβ, **(B)** αSMA and **(C)** CD31, normalised to hCMEC/D3 expression levels. Mean ± SEM; * $p<0.05$, ***$p<0.001$. n=3 per group.

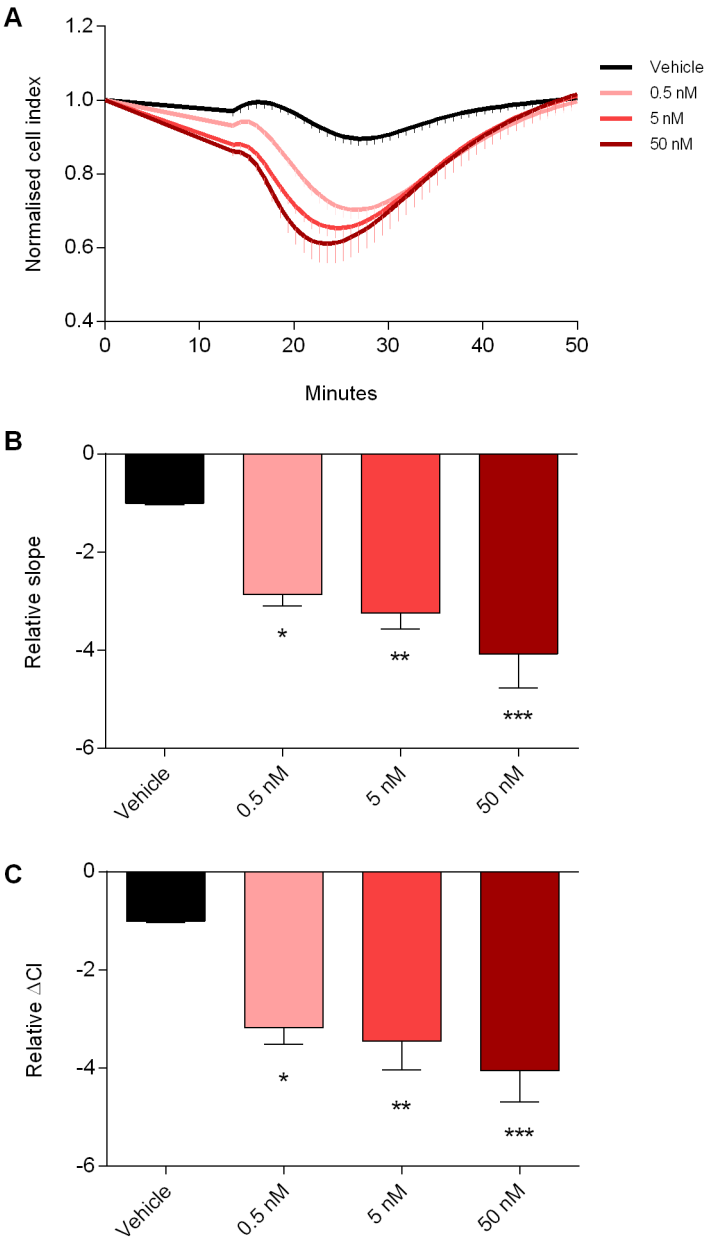

Figure 3.5: HBVP contract in response to ET-1. **(A)** Time course of acute CI changes after ET-1 application. Time $p<0.0001$, ET-1 concentration $p<0.0001$, time:concentration $p<0.0001$ **(B)** Change in slope of CI, normalised and compared to vehicle. **(C)** Reduction in cell index, normalised and compared to vehicle. Mean ± SEM; * $p<0.05$, ** $p<0.01$, *** $p<0.001$. n=4 per group

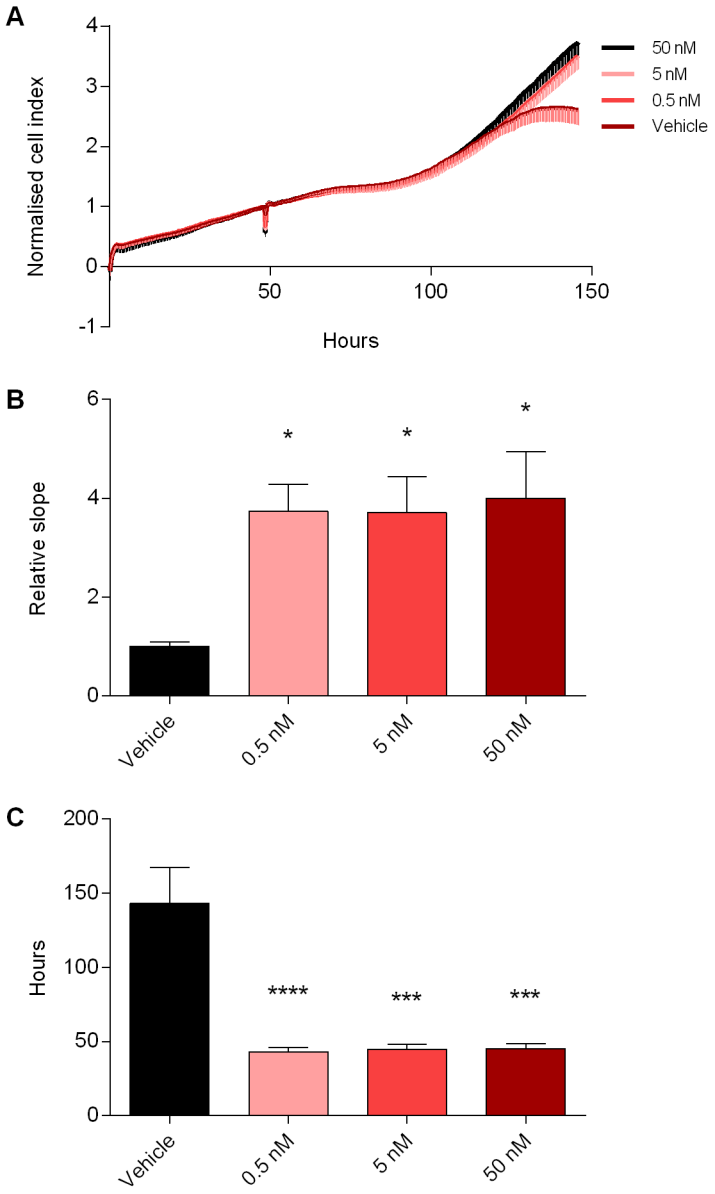

Figure 3.6: ET-1 increases HBVP proliferation. **(A)** Full time course of CI over the experiment. Time p<0.0001, ET-1 concentration p=0.0002, time:concentration p<0.0001 **(B)** Change in slope of CI, normalised and compared to vehicle. **(C)** Change in doubling time after ET-1 treatment, compared to vehicle. Mean ± SEM; * p<0.05, *** p<0.001, **** p<0.0001. n=4 per group.

3.3.3 ET-1 effects are mediated through ET_A receptors

To establish the mechanism through which ET-1 exerted its contractile effects, HBVP were pretreated with the ET_A antagonist BQ-123 (10 µM), the ET_B antagonist BQ-788 (10 µM) or a combination of BQ-123 and BQ-788 (each at 10 µM). When ET-1 was added to the wells 1 h later, the contractile effect was significantly reduced in wells pretreated with BQ-123 or both antagonists; BQ-788 alone had little effect (Fig. 3.7A). This reduction of ET-1-mediated contraction by BQ-123 and combination treatment compared to vehicle-treated cells was significant both in terms of slope (Fig. 3.7B; $p<0.0001$ for both groups compared to ET-1) and relative CI change (Fig. 3.7C; $p<0.0001$ for both groups compared to ET-1).

The chronic effects of ET-1 antagonism were also monitored in the same wells. The addition of BQ-123 reduced the rise in CI (seen onwards from 50 hours after treatment) compared to ET-1 alone, whereas BQ-788 showed a non-significant trend towards reduction (Fig. 3.8A). Similarly, a combination of the two antagonists did not show substantial differences compared to BQ-123 alone, also exhibiting a reduction in ET-1 mediated proliferation. The inhibitory effects of BQ-123 and the combination treatment compared to vehicle were significant when quantified as slope (Fig. 3.8B; $p<0.001$ for BQ-123, $p<0.0001$ for combination) and doubling time (Fig. 3.8C; $p<0.01$ for BQ-123, $p<0.001$ for combination).

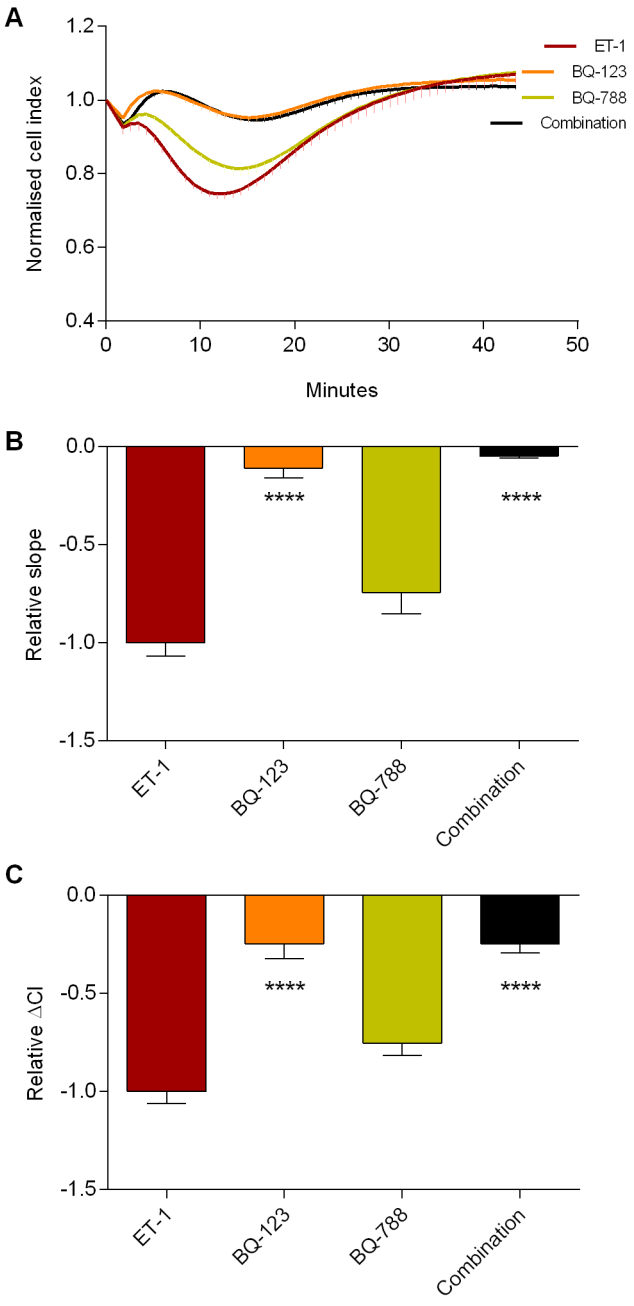

Figure 3.7: The contractile effects of ET-1 are mediated through ET_A receptors. **(A)** Time course of acute CI changes after ET-1 application, following pretreatment with vehicle (labelled 'ET-1'), ET_A antagonist BQ-123 (10 µM), ET_B antagonist BQ-788 (10 µM) or a mixture of BQ-123 and BQ-788 (labelled 'Combination'). **(B)** Change in slope of CI, normalised to ET-1 alone. **(C)** Reduction in cell index, normalised to ET-1 alone. Mean ± SEM; **** $p<0.0001$. n=4 per group.

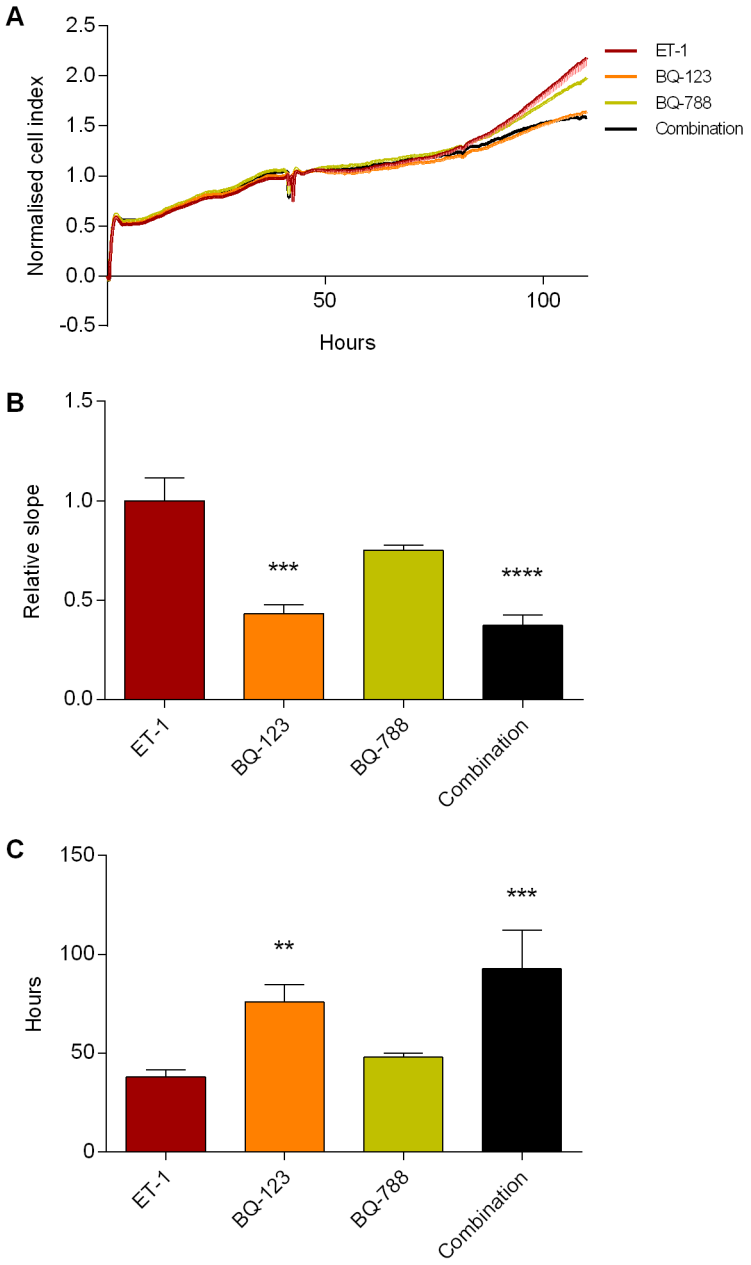

Figure 3.8: The proliferative effects of ET-1 are also mediated through ET_A receptors. **(A)** Full time course of CI over the experiment, following pretreatment with vehicle (labelled 'ET-1'), ET_A antagonist BQ-123 (10 µM), ET_B antagonist BQ-788 (10 µM) or a mixture of BQ-123 and BQ-788 (labelled 'Combination'). **(B)** Change in slope of CI, normalised to ET-1 alone. **(C)** Change in doubling time after ET-1 treatment. Mean ± SEM; ** $p<0.01$, *** $p<0.001$, **** $p<0.0001$. n=4 per group.

3.3.4 Adenosine and SNP cause HBVP relaxation

To demonstrate the utility of the method for detecting relaxation as well as contraction, the well-established vasodilators adenosine and SNP (a nitric oxide (NO) donor) were evaluated for impedance changes. A significant increase in CI following application of adenosine was observed at 1 mM and 10 µM doses, but not at 100 nM (Fig. 3.9A). This effect was significant in terms of both slope (Fig. 3.9B; $p<0.001$ for 10 µM and 1 mM compared to vehicle) and relative change in CI (Fig. 3.9C; $p<0.0001$ for both 10 µM and 1 mM compared to vehicle). SNP had a small relaxatory effect at very concentrations (Fig. 3.10A), which was statistically significant at 100 µM when quantified as slope (Fig. 3.10B; $p<0.001$), and at both 100 µM and 1 µM when quantified as relative ΔCI (Fig. 3.10C; $p<0.05$ for 1 µM, $p<0.0001$ for 100 µM).

3.3.5 Adenosine relaxes HBVP via A_1/A_{2A} receptors

To establish which adenosine receptor mediated these effecs, HBVP were pretreated with the adenosine A_1/A_{2A} receptor antagonist CGS-15943 (10 µM) or vehicle. CGS-15943 significantly reduced the effects of adenosine (1 mM), but did not completely abolish them (Fig. 3.11A). This was evident in both the diminished slope (Fig. 3.11B; $p<0.01$ for adenosine and CGS-15943, $p<0.0001$ for vehicle compared to either adenosine or CGS-15943) and smaller relative cell index change when HBVP were treated with CGS-15943 (Fig. 3.11C; $p<0.0001$ between all groups).

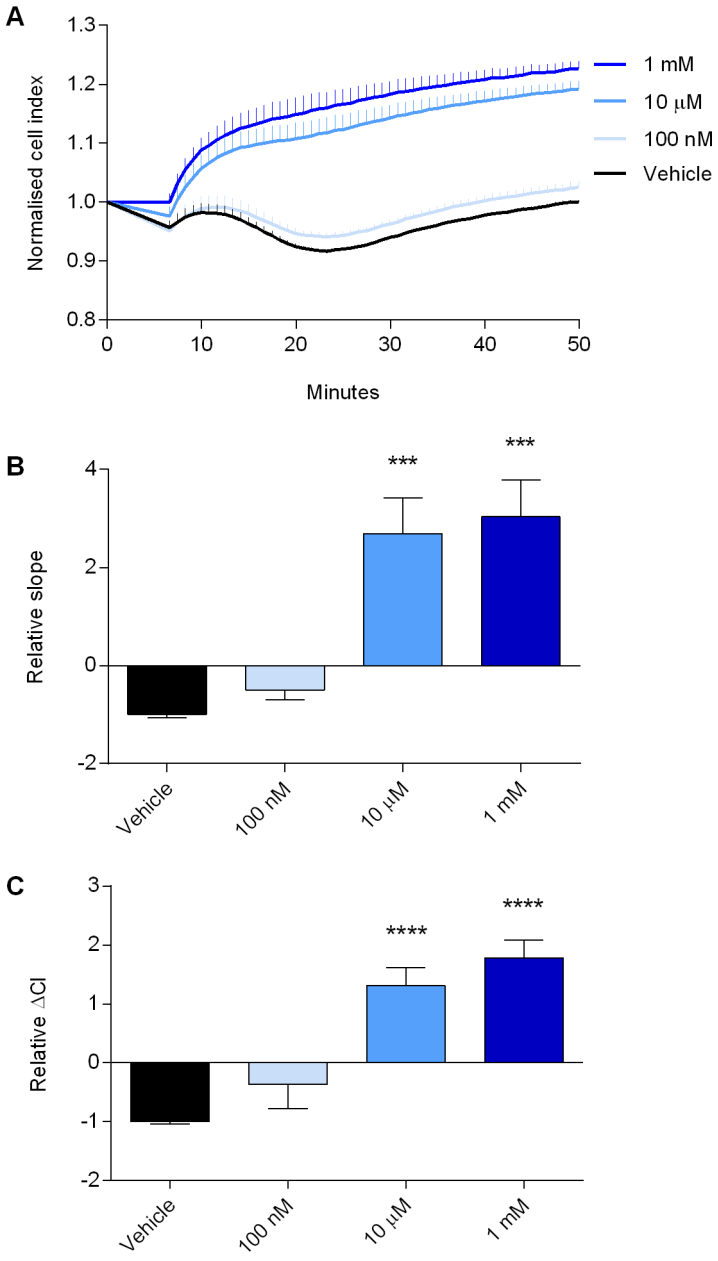

Figure 3.9: HBVP relax in response to adenosine. **(A)** Time course of acute CI changes after adenosine application. **(B)** Change in slope of CI, normalised to vehicle. **(C)** Increase in cell index, normalised to vehicle. Mean ± SEM; *** $p<0.001$, **** $p<0.0001$. n=4 per group

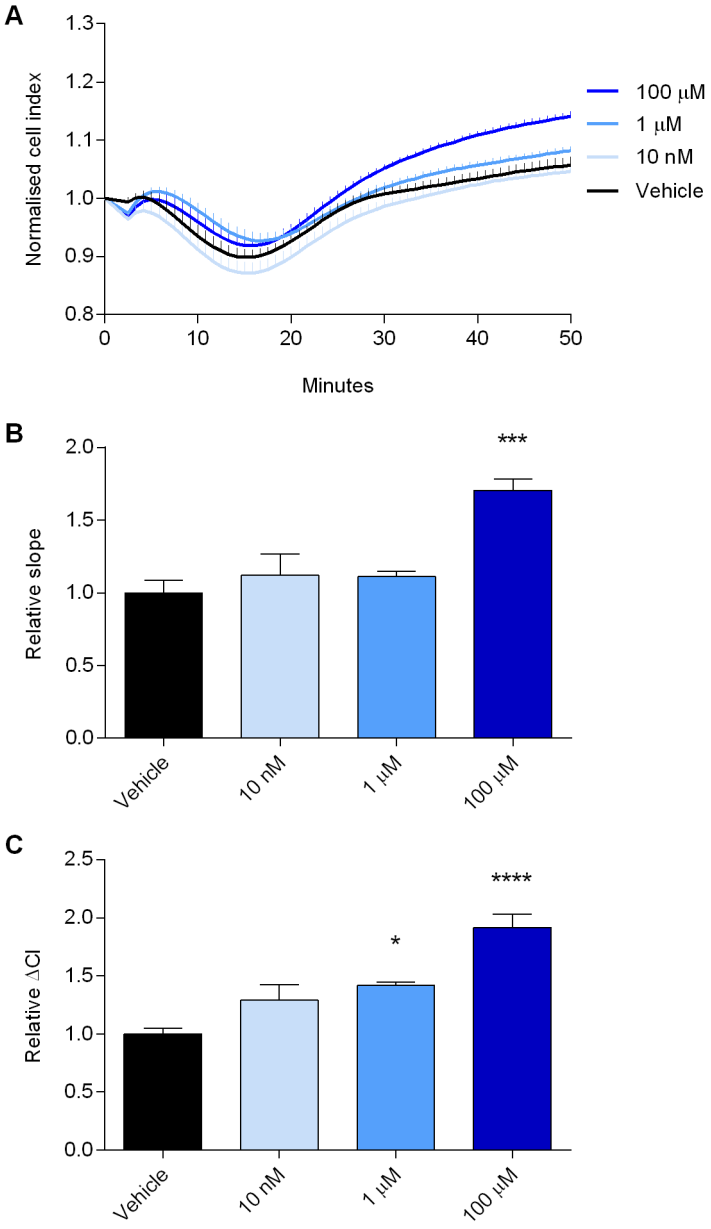

Figure 3.10: HBVP weakly relax in response to SNP. **(A)** Time course of acute CI changes after SNP application. **(B)** Change in slope of CI, normalised to vehicle. **(C)** Increase in cell index, normalised to vehicle. Mean ± SEM; * $p<0.05$, *** $p<0.001$, **** $p<0.0001$. n=4 per group

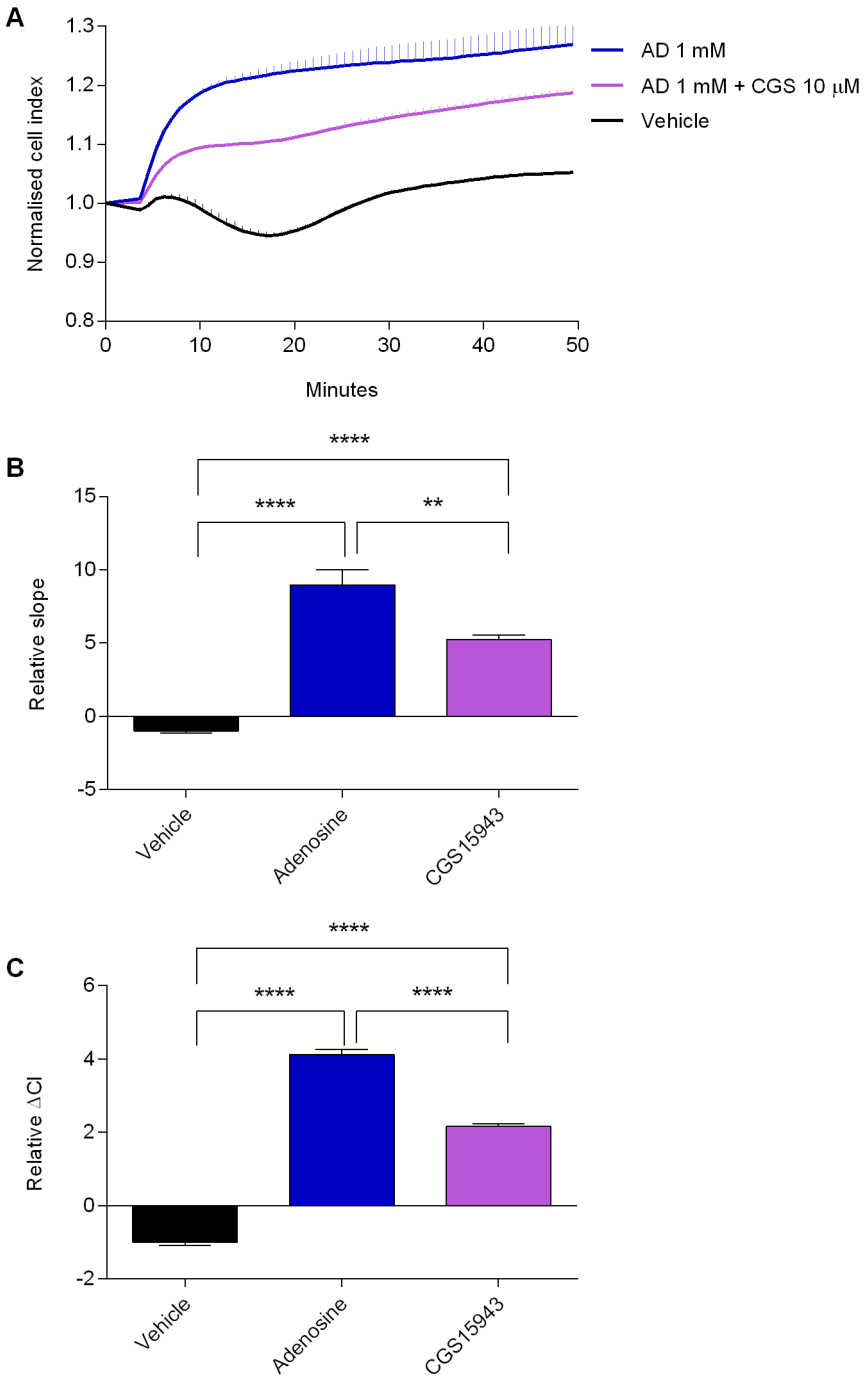

Figure 3.11: HBVP responses to adenosine are mediated through A_1/A_{2A} receptors. **(A)** Time course of acute CI changes after adenosine application, with or without pretreatment with 10 µM CGS-15943. **(B)** Change in slope of CI, normalised to vehicle. **(C)** Increase in cell index, normalised to vehicle. Mean ± SEM; ** $p<0.01$, **** $p<0.0001$. n=4 per group

3.3.6 ET-1 causes RBVP contraction

The method was further validated in a cell type other than HBVP, in order to exclude the results being the consequence of some HBVP-specific property. RBVP treated with 25 nM ET-1 demonstrated a small but detectable contraction compared to vehicle (Fig. 3.12A); as was the case with HBVP, the contraction was almost entirely prevented by the ET_A antagonist BQ-123 (10 µM), but only partly inhibited by the ET_B antagonist BQ-788 (10 µM). When quantified as relative slope, all pairwise comparisons except vehicle & BQ-123 showed highly significant differences (Fig. 3.12B; $p>0.05$ for vehicle and BQ-123; $p<0.0001$ for all other groups). In the case of relative CI change, ET-1-treated cells showed a significantly higher peak contraction than vehicle or antagonist groups; the latter were not significantly different from one another (Fig. 3.12C; $p>0.05$ for vehicle and BQ-123 or BQ-788; $p<0.0001$ for ET-1 and vehicle, BQ-123 or BQ-788).

3.3.7 Impedance changes are not due to cell detachment

An LDH assay was performed, in order to look for differences in cell adhesion following treatment that might introduce artefactual changes in CI, as detached cells would be present in the supernatant. No differences were observed in supernatant LDH content, relative to total LDH content, at 2 or 24 hours following application of ET-1 (50 nM), suggesting that cell detachment does not account for the impedance changes seen in ET-1 contractility experiments (Fig. 3.13; $p>0.05$ for all comparisons).

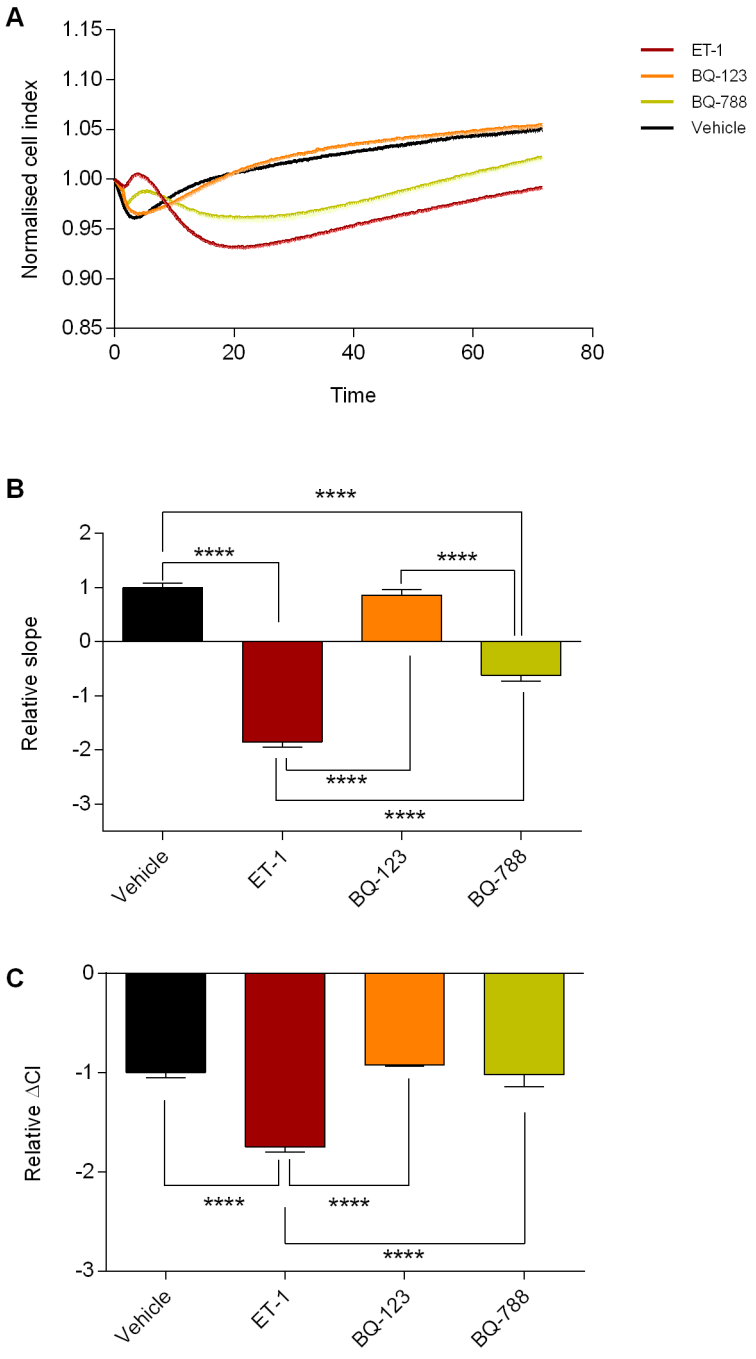

Figure 3.12: RBVP contract in response to ET-1, primarily through the activation of ET_A receptors. **(A)** Time course of acute CI changes after ET-1 application. **(B)** Change in slope of CI, normalised to vehicle. **(C)** Reduction in cell index, normalised to vehicle. Mean ± SEM; **** $p<0.0001$. n=4 per group

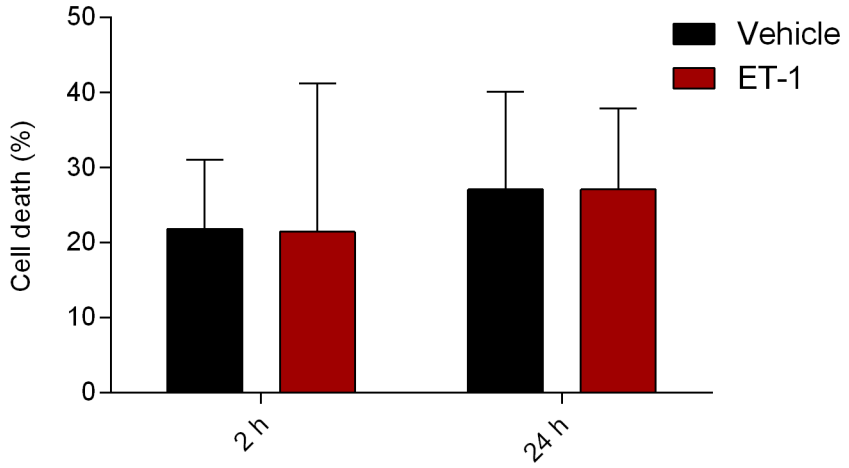

Figure 3.13: ET-1 does not cause cell detachment.There is no increase in LDH concentration in the supernatant (capturing both cell death and detachment) at 2 or 24 hours following application of ET-1. Mean ± SEM; $p>0.05$ for both 2 h and 24 h comparisons. n=3 per group.

3.4 Discussion

The results described in this chapter demonstrate that electrical impedance recording, as a surrogate of culture surface coverage and therefore cell size, provides a novel method of evaluating pericyte contractility *in vitro*. The iCelligence platform enabled higher throughput than classical microscopy-based approaches, and allowed for multiparametric quantitative descriptions of pericyte responses to vasoactive substances. These data demonstrate for the first time that human pericytes constrict in response to ET-1 acutely, that ET-1 increases their proliferation chronically, and that these effects are mediated via ET_A receptors. They also relax in response to application of adenosine (via A_1/A_{2A} receptors) and high-dose SNP.

Ideally, one would investigate pericyte function through *in vivo* microscopy and measurement of vessel diameter at pericyte locations, in combination with transgenic constructs that enable us to examine pericyte morphology, record calcium responses, selectively depolarise and activate them via optogenetics, and use various other transgenic technologies (Hill et al., 2015). However, these require elaborate experimental setups that are not widely available to most researchers. The iCelligence/xCelligence platform has previously been used to investigate cardiomyocyte contractility (Xi et al., 2011), but the aim of this work was to extend its use, from spontaneously and rhytmically contracting cells, to pharmacologically induced single events in a vascular mural cell population. Importantly, this approach enabled evaluation of both contractility and proliferation in the same cell population over an extended period of time, with minimal user input following application of the compounds. The impedance recording method described here is also label-free, reducing any potential toxic or otherwise artefactual effects that dyes or other labels might have on pericyte physiology.

The method was first validated using ET-1, an endothelium-derived vasoconstrictor that is able to evoke Ca^{2+} responses and cytoskeletal rearrangements in

cultured pericytes, and reduce their surface area (Dehouck et al., 1997; Chakravarthy et al., 1994). These results were replicated in both primary human and rat brain pericytes, although the response was much more prominent in human cells. Due to the normalisation procedure, and the extremely consistent patterns observed between replicates, the effects were nonetheless significant in both cell types. Pericytes from bovine retina express both ET_A and ET_B receptors (McDonald et al., 1995). It has been reported that contractile responses to ET-1 are mediated primarily through the G_q-coupled ET_A receptors (McDonald et al., 1995); by contrast, G_q-coupled ET_B receptors are associated with modulatory effects and may counteract ET_A-mediated vasoconstriction (Feger et al., 1997). Again, the results were in agreement with these observations, showing that the ET_A-selective antagonist BQ-123 was able to abolish or significantly reduce the contraction evoked by ET-1, whereas ET_B receptor inhibition did not alter the contractile response.

The more chronic effects of ET-1 on pericyte physiology include an increase in proliferation, as the addition of ET-1 reportedly increased pericyte growth, whereas antiserum against it diminished the positive effects of endothelial co-culture on pericyte proliferation (Yamagishi et al., 1993). The same was observed in the experiments described in this chapter: ET_A antagonism by BQ-123 significantly reduced ET-1-evoked increases in slope and reductions in doubling time at chronic time points, whereas the ET_B antagonist BQ-788 had little effect. While expression of either receptor subtype in HBVP was not tested for, the results from these pharmacological experiments suggest that ET_A receptors are functionally more important for pericyte responses to ET-1 than ET_B receptors.

It was equally important to establish whether the method was able to detect cell relaxation and the corresponding increase in surface coverage. Adenosine has been reported to relax bovine retinal pericytes through G_s-coupled A_2 receptors (Matsugi et al., 1997), with maximal responses at 0.1 mM adenosine. Robust increases in cell

index were observed when HBVP were treated with 10 µM and 1 mM adenosine, an effect that was reversed by CGS-15943, a competitive A_1 and noncompetitive A_{2A} antagonist (Williams et al., 1987; Ghai et al., 1987). However, the relaxation was not fully abolished by the antagonist. It is possible that the concentration of adenosine in the antagonist experiments (1 mM) was too high, and using the lower dose of 10 µM, which produced very similar CI changes to 1 mM, might have demonstrated a more potent inhibition by CGS-15943. It is also possible that the responses were partly mediated by other receptor subtypes, although A_{2A} receptors are most commonly implicated in vasodilation in response to adenosine (Headrick et al., 2013).

It was not possible to reliably monitor proliferation in the adenosine-treated cells, as they remained persistently relaxed. This was in contrast to ET-1, where the response was short-lasting and group differences disappeared within less than an hour, allowing us to examine the chronic effects (>24 hours after application) in isolation from the acute contraction. The failure to return to baseline after adenosine application greatly complicated the interpretation of chronic CI; while there was no apparent effect on chronic slope or doubling time (data not shown), it was not possible to disentangle the changes related to contractile state from proliferation-dependent change. Thus, subsequent analyses were restricted to the acute stage, where proliferation is not an important contributor.

SNP, an NO donor, evokes robust vasodilation through its activation of guanylyl cyclase and resulting production of cyclic guanosine monophosphate. This causes protein kinase G (PKG) activation and a plethora of downstream phosphorylation-dependent effects, which lead to an overall hyperpolarisation and reduction in Ca^{2+} influx (Martínez-Ruiz et al., 2011). It has previously been reported that SNP relaxes pericytes with a median effective dose of approximate 1 µM (Haefliger et al., 1994). Surprisingly, these results could not be replicated using the impedance assay, and even at 100 µM, only a very minor relaxation was observed. It is possible that HBVP

tone is not dependent on PKG, and is more sensitive to cAMP-dependent signalling through adenosine receptors; however, definitive conclusions regarding this would require further investigation, such as the use of methylene blue to antagonise NO, or 8-bromo-guanosine monophosphate as a direct activator of PKG.

There are some technical details that must be pointed out in the analysis of impedance results. First, cell index values are normalised to the last time point pretreatment. This is necessary to account for minor variations in seeding density between wells in the same experiment (typically <5% of raw CI), which would falsely reduce the signal-to-noise ratio in post-treatment results. However, variation between batches was observed, in terms of pericyte growth during the initial 48 hours – particularly in later passages, growth was slower and correspondingly, the raw CI values were lower, an effect that is not apparent from normalised CI traces. To account for potential variation between batches, a control group was always used in all experiments, and the quantitative analyses were normalised to this group; as such, it was possible to combine results from multiple experiments with reduced noise from baseline physiological differences.Second, the approach described here is limited to 16 wells per experiment, due to the costs associated with the impedance recording platform; however, the same technology is available in 96-well format (xCelligence), which would allow substantially higher throughput.

In conclusion, these results provide a proof-of-concept for very high-throughput, quantitative evaluation of pericyte tone that does not rely on videomicroscopy, does not require the use of animal models, and is compatible with primary human pericytes. This approach was used to demonstrate that pericytes constrict in response to ET-1 through the activation of ET_A receptors, and dilate in response to adenosine through the activation of A_1/A_{2A} receptors. This method also enables investigations of pericyte tone in other conditions, such as models of ischaemia.

Chapter 4

Effects of Nimodipine in Ischaemia

4.1 Introduction

Treatment options for acute ischaemic stroke are limited, as discussed in chapter 1. Following the landmark trial by The National Institute of Neurological Disorders and Stroke rt-PA Stroke Study Group (NINDS) (1995), thrombolysis with intravenous recombinant tissue plasminogen activator (IV-rt-PA) became the gold standard for treating ischaemic stroke. When administered within 6 hours of stroke onset, thrombolysis improves long-term functional outcomes, despite the increased short-term risk of haemorrhagic transformation (Wardlaw et al., 2014). Stroke therapy underwent a further revolution in 2015, with 5 trials demonstrating that endovascular thrombectomy (EVT), in conjunction with thrombolysis, was superior to thrombolysis alone (reviewed in Balami et al., 2015; Badhiwala et al., 2015). Both approaches aim to recanalise the occluded artery, thus ostensibly restoring cerebral blood flow (CBF) to the affected region and preventing neuronal death in the penumbra – an area of hypoperfusion that is electrically silent but not yet irreversibly damaged (Dirnagl et al., 1999; Astrup et al., 1981).

Increasing reperfusion is therefore key to current neuroprotective strategies in stroke. However, despite the success of thrombolysis and subsequently EVT, recanalisation of an occluded vessel does not necessarily result in reperfusion of the downstream microvasculature and consequently, nutrient supply to the parenchyma

remains diminished. This abnormality was first reported following observations of ink perfusion patterns, which showed incomplete capillary labelling following global ischaemia in the rabbit, known as the 'no-reflow' phenomenon (Ames et al., 1968). A related concept is delayed post-ischaemic hypoperfusion, which follows a period of hyperperfusion (Hossmann, 1997).

On a single-vessel basis, loss of capillary patency is not a major problem. Elegant two-photon microscopy (2-PM) studies in mice have demonstrated that occluding single vessels more than two branch points from a penetrating arteriole did not cause tissue damage, whereas first-order branch occlusions resulted in small (~10-800 pL) lesions (Shih et al., 2013). However, the affected territory is much larger in large artery stroke, and reversal of flow from downstream capillaries cannot necessarily compensate for microvascular occlusion. The problem is compounded by network dynamics in the microvasculature, where changes in one microvessel affect flow through neighbouring capillaries supplied by the same arteriole. *In silico* modelling suggests that oxygen extraction is optimal when all vessels have similar flow; the greater capillary transit time heterogeneity (CTTH) becomes, the less efficiently oxygen is extracted (Jespersen and Østergaard, 2012). This can reach the paradoxical situation where CTTH becomes malignant, and oxygen extraction is reduced with increasing CBF – an event that has been proposed to occur in stroke (Østergaard et al., 2013).

While our ability to investigate microcirculatory changes in a clinical setting is more limited, there is evidence to suggest effects similar to the no-reflow phenomenon also occur in man. A meta-analysis of EVT patients showed that only 71% of patients receiving EVT reperfused >50% of the ischaemic territory (Goyal et al., 2016), and 26% of patients who are recanalised (spontaneously, with thrombolysis and/or with EVT) do not achieve reperfusion (Dalkara and Arsava, 2012). It has also been observed that radiographic estimates of recanalisation (e.g. Arterial Occlusive

Lesion (AOL) scores) and reperfusion (e.g. Thrombolysis in Cerebral Infarction (TICI) scores) only show moderate agreement ($\kappa = 0.30$; Khatri et al., 2005). It is reperfusion, and not recanalisation, that is the stronger predictor of functional outcome and infarct volume in stroke (Eilaghi et al., 2013; Marks et al., 2014; Soares et al., 2010). Moreover, ischaemic CBF in a rat model of middle cerebral artery occlusion (MCAO) does not correlate as closely with infarct volumes as post-ischaemic CBF does (Sutherland and Buchan, 2013).

These observations suggest that enhancing reperfusion in the context of recanalisation could be beneficial in a clinical setting. Targeting post-ischaemic hypoperfusion is complicated by our incomplete understanding of its mechanistic basis, with several competing hypotheses. It is possible that fragments of the clot move downstream, either spontaneously or as a consequence of thrombectomy, and occlude smaller arteries, arterioles and capillaries (Topol and Yadav, 2000; Chueh et al., 2016). Platelets are activated by many of the mediators released during stroke, such as adenosine triphosphate (ATP) and platelet-activating factor (reviewed in Iadecola and Anrather, 2011). Local fibrin deposition has been described in baboons after experimental MCAO, potentially leading to intravascular coagulation (Okada et al., 1994). Leukocyte adhesion could also contribute to luminal obstruction, with reports of single neutrophils occluding 5% of capillaries after stroke (del Zoppo et al., 1991).

It has also been proposed that in addition to obstruction, no-reflow could be mediated by microvascular compression – for example, astrocyte endfoot swelling can compress the juxtaposed endothelium (Garcia et al., 1994; Ito et al., 2011). Other reports indicate that capillary diameters are reduced following ischaemia even in the absence of overt glial swelling (Fischer et al., 1977), which may be a consequence of vascular tone. This could occur due to upstream arteriolar constriction and subsequent passive capillary collapse, or due to an active effect of the capillary wall (Hauck et al., 2004). The latter hypothesis has gained traction in recent years,

with observations of pericyte contractility *ex vivo* and *in vivo* (Peppiatt et al., 2006; Hall et al., 2014), and co-localisation of erythrocyte rouleaux (indicative of stasis) to capillaries with constricted pericytes following MCAO (Yemisci et al., 2009).

During ischaemia, pericytes have been reported to die through a Ca^{2+}-dependent mechanism and remain in a contracted state ('death in rigour'; Hall et al., 2014). Other insults relevant to ischaemic pathophysiology also cause Ca^{2+}-dependent pericyte death. For example, ischaemia results in elevated extracellular ATP concentrations (Melani et al., 2005), and ATP-mediated activation of $P2X_7$ receptors kills pericytes through L-type voltage-gated Ca^{2+} channel (VGCC) activation (Sugiyama et al., 2005). In a physiological context, Ca^{2+} is crucial for maintaining pericyte tone: removing extracellular Ca^{2+} causes pericyte relaxation and prevents capillary constriction in response to electrical stimulation in acute brain slices (Peppiatt et al., 2006). Vasoconstrictive compounds, such as endothelin-1 and angiotensin II, cause pericyte depolarisation through nonspecific cation channels, which subsequently leads to VGCC activation (McGinty et al., 1999; Kawamura et al., 2002; Sakagami et al., 1999; Kawamura et al., 2004; Kamouchi et al., 2004). Conversely, VGCC inhibition is important for vasodilatory pathways such as NO signalling, which suppresses Ca^{2+} influx in a cGMP-dependent manner (Sakagami et al., 2001).

Nimodipine is an L-type VGCC inhibitor, clinically used in hypertension to relax vascular tone, and in subarachnoid haemorrhage to prevent vasospasm and secondary ischaemia (Dorhout Mees et al., 2007). Nimodipine has also been shown to improve CBF in patients resuscitated from cardiac arrest (Forsman et al., 1989). Although there was no detectable clinical benefit in that small study, there is preclinical evidence demonstrating the neuroprotective effects of nimodipine in various models of ischaemia (reviewed by Tomassoni et al., 2008; Horn et al., 2001). Meta-analyses of nimodipine in acute stroke have not detected a protective effect, with some indication that higher doses resulted in worse outcomes (Zhang et al., 2012a). However, these

trials were mostly conducted in the pre-EVT era, where reductions in blood pressure could reduce cerebral perfusion pressure and exacerbate stroke. In the context of efficient recanalisation, it is possible that a beneficial effect on no-reflow would further reduce ischaemic damage and ameliorate neurological impairment.

4.1.1 Aims

The primary aim of this chapter was to provide a detailed overview of the effects of nimodipine on the cerebral microvasculature in an animal model of ischaemic stroke that closely resembles EVT (Sutherland et al., 2016). Specifically, the following questions were investigated:

1. Does nimodipine ameliorate post-ischaemic hypoperfusion?

2. Does nimodipine enhance functional outcomes following transient focal ischaemia?

3. Are the effects of nimodipine mediated through improved pericyte survival and diminished contraction?

4.2 Materials & methods

4.2.1 Animal care

All procedures were conducted in accordance with the Animals (Scientific Procedures) Act of 1986, under a valid project licence and personal licence, and approved by the University of Oxford Animal Ethics Committee. Male Wistar rats (270-310 g; Harlan, UK) were housed in individually ventilated cages under a 12:12 hour light-dark cycle, with *ad libitum* access to standard food pellets and water unless otherwise specified.

4.2.2 Laser Doppler flowmetry

Laser Doppler flowmetry (LDF; Oxford Optronix, UK) was used for confirmation of ischaemia and evaluation of post-ischaemic hypoperfusion, as described in section 2.2.2. To reduce noise, CBF data were binned into 5-minute intervals starting from 0 (the point of occlusion), based on the median relative CBF value in each interval.

4.2.3 Focal cerebral ischaemia

A modified variant of the transient middle cerebral artery occlusion (tMCAO) model of focal cerebral ischaemia was used, as previously described in other publications (Sutherland and Buchan, 2013; Hall et al., 2014) and section 2.2.3. Animals were allowed to recover and killed at 6 hours (pericyte death assessment), 3 days (CBF experiment) or 7 days (behavioural testing) following tMCAO.

4.2.4 Experimental design

Sample size calculations were performed to detect a statistically significant difference (α=0.05) with 80% power. Group sizes for the 3-day experiment (n=6) were were based on an estimate of 25% higher CBF following tMCAO in the nimodipine group. Group sizes for the 7-day experiment (n=9) were based on preliminary Neuroscore data from the 3-day group.

4.2.5 Drug administration

Nimodipine (Sigma, USA) was dissolved in polyethylene glycol 400 (PEG-400, Sigma) at 2 mg/mL (~4.78 mM), and diluted in phosphate-buffered saline (PBS) containing 15% 2-hydroxypropyl-β-cyclodextrin (Sigma) to a final concentration of 3% PEG-400 and 60 µg/mL nimodipine. During tMCAO, the left jugular was exposed and cannulated with polyethylene tubing (outer/inner ⌀ 0.8/0.4 mm) containing sterile heparinised saline. Upon filament withdrawal, nimodipine (2 µg/kg/min) or vehicle was infused intravenously for 30 minutes using a syringe pump (Kent Scientific, USA). Treatment group allocation was performed before surgery using automatically generated number lists (Urbaniak and Plous, 2013). The surgeon was blinded to treatment at all times.

4.2.6 Behavioural outcomes

Animals were evaluated for overall welfare, somatosensory and motor function using the adhesive removal test, and overall neurological function using Neuroscore. The assessor was blinded to treatment at all times.

4.2.6.1 Neurological assessment

Neurological impairment following tMCAO was assessed with a modified Neuroscore protocol (Garcia et al., 1995), as described in table 2.1.

4.2.6.2 Welfare assessment

General welfare was evaluated according to a composite score, as described in table 2.2. Rats scoring >7 points were considered severely impaired, whereas scores of <4 points were considered indicative of mild impairment.

4.2.6.3 Adhesive removal test

A 10×7 mm piece of adhesive wash-proof plaster (Boots, UK) was placed onto either forepaw, and the rat was placed into an empty cage. After 3 training sessions, baseline latency to initial contact and latency to removal were recorded from both forepaws, with 2 replicates per trial. Testing was repeated at 1, 3 and 7 days following tMCAO.

4.2.7 Histology

At 7 days following tMCAO, animals were perfused with saline containing heparin (5 IU/mL). Brains were removed and snap frozen in isopentane (Sigma). 16-µm-thick sections were prepared on a cryostat (Leica, Germany), collected onto positively charged slides and stored at -80°C for later use. For lesion volume measurements, sections were post-fixed in 4% paraformaldehyde (PFA) for 30 minutes. Endogenous peroxidase activity was quenched in 0.3% hydrogen peroxide for 10 minutes. Nonspecific secondary binding was blocked using 10% normal goat serum (GtS; Life Technologies) in PBS for 1 hour at room temperature. Primary antibody (rabbit anti-NeuN; ab177487, Abcam, UK) was applied at 1:500 in 1% GtS in PBS, and kept overnight at 4°C. Slides were then washed and secondary antibody (biotinylated goat anti-rabbit; Vector, USA) was added at 1:200 in 1% GtS for 1 hour. Slides were washed before incubation with a horseradish peroxidase and streptavidin conjugate (Vector, USA) for 30 minutes. Antibody binding was visualised with 3'3-diaminobenzidine (Sigma). Sections were dehydrated through graded ethanol solutions and cleared with Histo-Clear II (National Diagnostics, USA). Coverslips were applied with Surgipath mounting medium (Leica).

Slides were scanned on an Aperio ScanScope CS slide scanner (Leica) at 20× magnification. Lesion sizes were manually outlined in Aperio ImageScope software (Leica); the observer was blinded to treatment group at all times.

4.2.8 Pericyte death assessment

6 hours after reperfusion, animals were perfused with ice-cold phosphate-buffered saline (PBS) with heparin (5 IU/mL). Brains were dissected out on ice, placed into artificial cerebrospinal fluid (aCSF) and cut into 200-µm-thick slices on a vibratome (VT1000S, Leica Microsystems, Germany), as previously reported (Hall et al., 2014). Slices were placed into aCSF (equilibrated with 95% O_2/5% CO_2) containing Alexa Fluor 647-conjugated isolectin B_4 (IB_4, 10 µg/mL; Molecular Probes, USA) and propidium iodide (PI, 37 µM; Sigma). Following incubation for 1 hour, slices were washed in aCSF and fixed in 4% PFA in PBS for 40 minutes. Counterstaining for cell nuclei was performed with 4',6-diamidino-2-phenylindole (DAPI, 1 µM; Sigma). Slices were washed in PBS and mounted onto glass slides in anti-fade fluorescence mounting medium (Dako, USA). Staining was imaged on a Zeiss LSM 700 upright confocal microscope with a 20× water-immersion objective and appropriate excitation/emission filters (Carl Zeiss, Germany).

4.2.9 Cell culture experiments

All cell culture experiments were conducted as outlined in section 3.2, using human brain vascular pericytes (HBVP). Contractility analyses were performed as described in section 3.2.2.

4.2.9.1 Chemical ischaemia

Ischaemia was modelled by the simultaneous inhibition of glycolysis and mitochondrial respiration, using 5 µM sodium iodoacetate (IA) and 50 nM antimycin A (AmA), respectively (Sigma). AmA was dissolved in ethanol (15 µM stock) and stored at -20°C; IA was freshly prepared in water for each experiment. In some experiments, 10- and 100-fold dilutions of the standard ischaemia solution were used; these were referred to as 'medium-dose' and 'low-dose' , respectively, with the standard solution

being 'high-dose'.

4.2.9.2 Cell death measurements

Cell death and adherence were measured with a lactate dehydrogenase assay (LDH; Promega, UK), as previously described in section 3.2.5. In addition, apoptosis was evaluated using a terminal deoxynucleotidyl transferase dUTP nick-end labeling (TUNEL) assay. Following treatment with chemical ischaemia solution for 2 or 24 hours, cells were washed with PBS and fixed with 4% PFA in PBS for 10 minutes at room temperature. Cells were washed in PBS and the assay was performed according to manufacturer's instructions (Millipore, USA) before counterstaining with DAPI. Images were acquired on a Nikon Eclipse E1000 epifluorescence microscope with a 20× air objective and appropriate excitation/emission filters.

4.2.10 Analysis

In vivo, histological and cell death data were analysed using Excel 2010 (Microsoft, USA) and Prism 6.0 (Graphpad, USA). iCelligence data were extracted in RTCA Data Analysis Software 1.0 (ACEA Biosciences) and analysed using Prism 6.0. The significance level was set at α=0.05. For iCelligence results, 1-way ANOVA was used with Tukey's multiple comparison test. Nonparametric Mann-Whitney U tests were used for Neuroscore and welfare score, due to the ordinal scales used. Nonlinear regression and 2-way repeated-measures ANOVA were used for CBF analysis. For all other comparisons, 2-way ANOVA with Sidak's post-hoc testing was performed. Results are presented as mean ± 95% confidence intervals or mean ± standard error (SEM), as specified in figure legends.

4.3 Results

4.3.1 Nimodipine enhances post-ischaemic CBF

To establish the effects of nimodipine on CBF following tMCAO, LDF recordings were performed for the entire duration of ischaemia from the ipsilateral (right) cortex (Fig. 4.1). One rat was excluded from the vehicle group due to subarachnoid haemorrhage, a known surgical complication of the tMCAO surgery and extremely unlikely to be related to treatment. One CBF recording was excluded from the nimodipine group due to technical problems.

There was no difference in CBF during MCAO between vehicle and nimodipine groups (0-90 minutes). Following reperfusion and drug administration at 90 minutes following MCAO, the nimodipine group exhibited ~2-fold higher CBF compared to vehicle-treated rats (mean values 1.357 vs. 0.6836), resulting in a significant overall difference between CBF profiles in both repeated-measures 2-way ANOVA (time $p< 0.0001$, treatment $p=0.0316$, interaction $p< 0.0001$) and nonlinear regression ($p< 0.0001$).

4.3.2 Nimodipine improves outcomes at 3 days after stroke

The CBF cohort of animals was also used to investigate neurological outcomes 3 days following tMCAO. There was a significant improvement in Neuroscore with nimodipine treatment, compared to the vehicle group (Fig. 4.2A; median values 4 vs. 8; $p=0.0087$). Overall welfare was also improved (Fig. 4.2B; $p=0.0325$), primarily due to reduced neurological impairment. There was a trend towards reduced weight loss in the nimodipine group; however, this was not significant when analysed as relative weight change from baseline (Fig. 4.2C; treatment $p=0.4389$, time $p<0.0001$, interaction $p=0.2026$) or as absolute weight change (Fig. 4.2D; treatment $p=0.2758$, time $p<0.0001$, interaction $p=0.2044$).

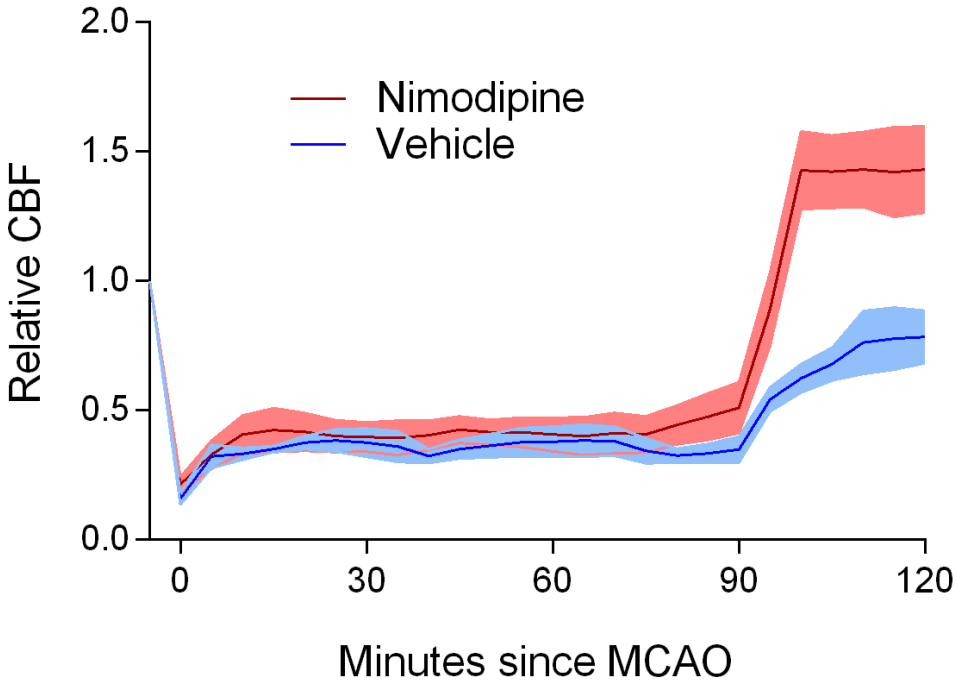

Figure 4.1: LDF recordings from ischaemic cortex in nimodipine- and vehicle-treated animals. There was no difference between groups during MCAO, but nimodipine-treated animals recovered to CBF levels above baseline (mean reperfused CBF 135.7% of baseline), whereas vehicle-treated animals exhibited post-ischaemic hypoperfusion (mean reperfused CBF 68.36% of baseline). Nonlinear regression curves are significantly different between groups ($p < 0.0001$). Mean ± SEM. n=5 per group.

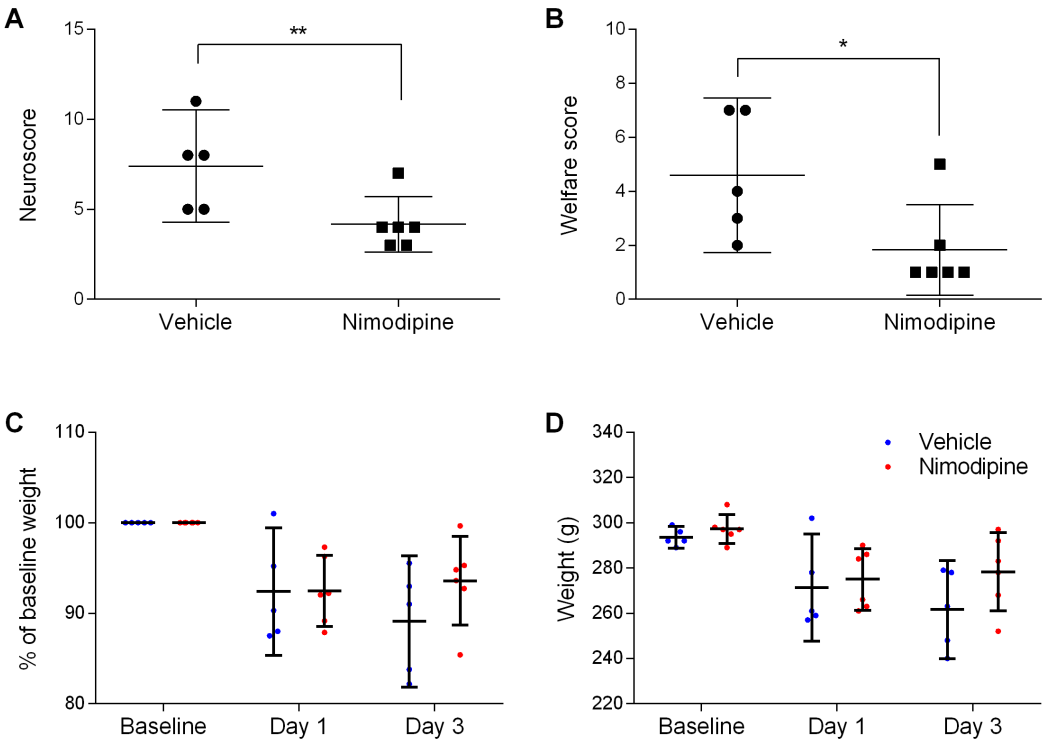

Figure 4.2: Nimodipine improves neurological outcome and general welfare at 3 days following stroke. **(A)** Neuroscores in the vehicle- and nimodipine-treated groups. **(B)** Welfare scores in the vehicle- and nimodipine-treated groups. **(C)** Relative weight change at 1 and 3 days post-tMCAO compared to baseline weight. **(D)** Absolute weight change at 1 and 3 days post-tMCAO in grams. Mean ± 95% CI; * $p<0.05$, ** $p<0.01$. n=5-6 per group.

4.3.3 Nimodipine ameliorates neurological impairment at 7 days after stroke

To validate these findings, a more chronic time point of 7 days was used in a separate cohort of animals. The animals were considerably less impaired at 7 days than the previous cohort had been at 3 days, but nimodipine treatment continued to exert a beneficial effect on neurological status compared to vehicle (Fig. 4.3A; median values 2 vs. 3; p=0.0015). There was no significant difference in welfare scores, although there was a trend towards benefit from nimodipine compared to vehicle (Fig. 4.3B; median values 0 vs. 2; p=0.1238). Weight change did not differ significantly between treatment groups when quantified as relative weight change from baseline (Fig. 4.3C; treatment p=0.4041, time p< 0.0001, interaction p=0.3523) or as absolute weight change (Fig. 4.3D; treatment p=0.3797, time p< 0.0001, interaction p=0.3273).

4.3.4 Nimodipine does not significantly alter infarct volume

To evaluate whether neurological improvement was related to a reduction in infarct volume, NeuN staining was performed and the lesion area quantified. Two animals were excluded from each group due to poor tissue morphology. Analysis of lesion volumes did not show significant differences between vehicle- and nimodipine-treated animals (Fig. 4.4; p=0.1045); however, there was a trend towards smaller lesions in the nimodipine group, with a mean infarct volume of 34.58 mm^3 in the vehicle group and 20.55 mm^3 in the nimodipine group.

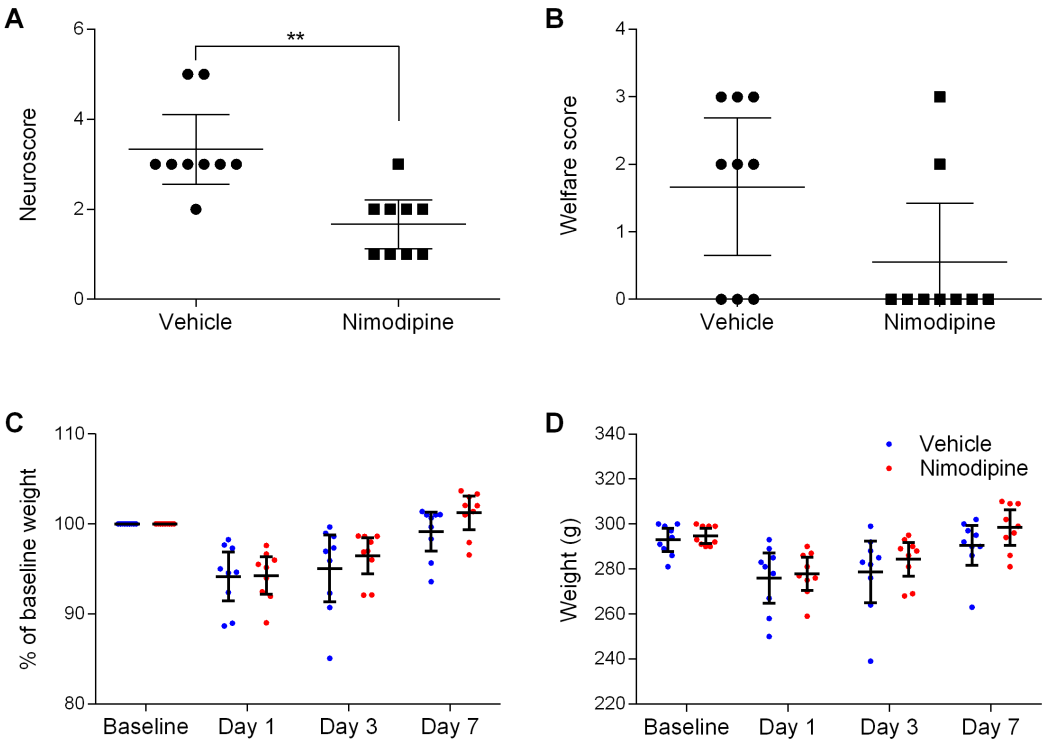

Figure 4.3: Nimodipine improves neurological outcome and general welfare at 7 days following stroke. **(A)** Neuroscores in the vehicle- and nimodipine-treated groups. **(B)** Welfare scores in the vehicle- and nimodipine-treated groups. **(C)** Relative weight change at 1, 3 and 7 days post-tMCAO compared to baseline weight. **(D)** Absolute weight change at 1, 3 and 7 days post-tMCAO in grams. Mean ± 95% CI; * $p<0.05$, ** $p<0.01$. n=5-6 per group.

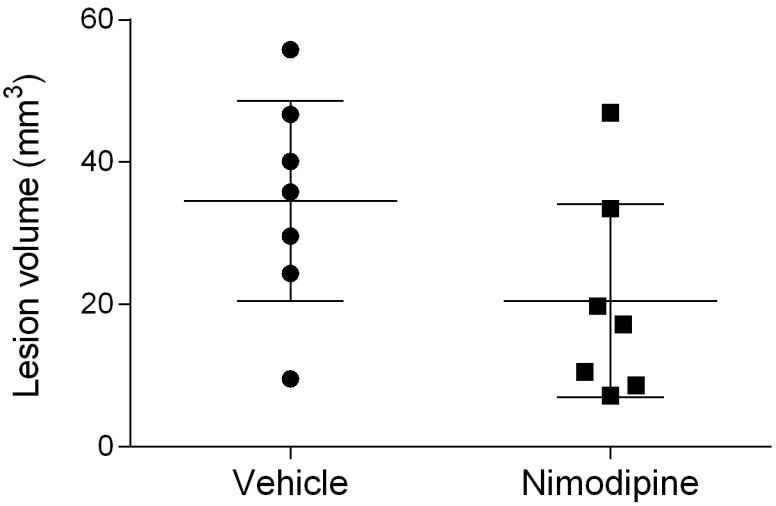

Figure 4.4: Nimodipine does not alter infarct volume at 7 days following tMCAO, based on NeuN staining. Mean ± 95% CI; n=7 per group.

4.3.5 Nimodipine does not improve behavioural task performance at 7 days after stroke

To examine the sensorimotor effects of nimodipine treatment in greater detail, rats were tested for adhesive tape removal, a task that requires them to detect the presence of a small adhesive strip on their affected (contralateral) forepaw and then remove it. When quantified as 'time to touch', rats exhibited severe impairment at day 1 after stroke compared to baseline. Both groups improved over time; however, here was no significant difference between treatment groups for time required for the rat to notice and touch the tape (Fig. 4.5A; time p=0.0036, treatment p=0.4149, interaction p=0.5630). The same was true for 'time to removal' – despite an apparent difference between groups at 7 days, hinting at a beneficial effect of nimodipine treatment, the results were not significant in 2-way ANOVA (Fig. 4.5B; time $p< 0.0001$, treatment p=0.3010, interaction p=0.5829).

4.3.6 Nimodipine reduces pericyte death at 6 hours after stroke

To investigate the effects of nimodipine treatment on pericyte death, acute brain slices were prepared from tMCAO rats treated with nimodipine or vehicle. Labelling for PI as a cell death marker (Fig. 4.6A) and IB_4 as a basement membrane marker (Fig. 4.6B) enabled quantification of dead pericytes in the lateral cortex and striatum of the ipsilateral hemisphere. By comparison, the contralateral hemisphere exhibited only background parenchymal PI labelling (Fig. 4.7A), with no apparent pericyte death (Fig. 4.7D). Nimodipine-treated animals exhibited a trend towards less neurological impairment at 6 hours (Fig. 4.8A), and significant reductions in cortical and striatal pericyte death (Fig. 4.8B). Although the sample size was too small to analyse correlations, the results from individual animals exhibited clustering for extent of pericyte death and neurological impairment (Fig. 4.8C).

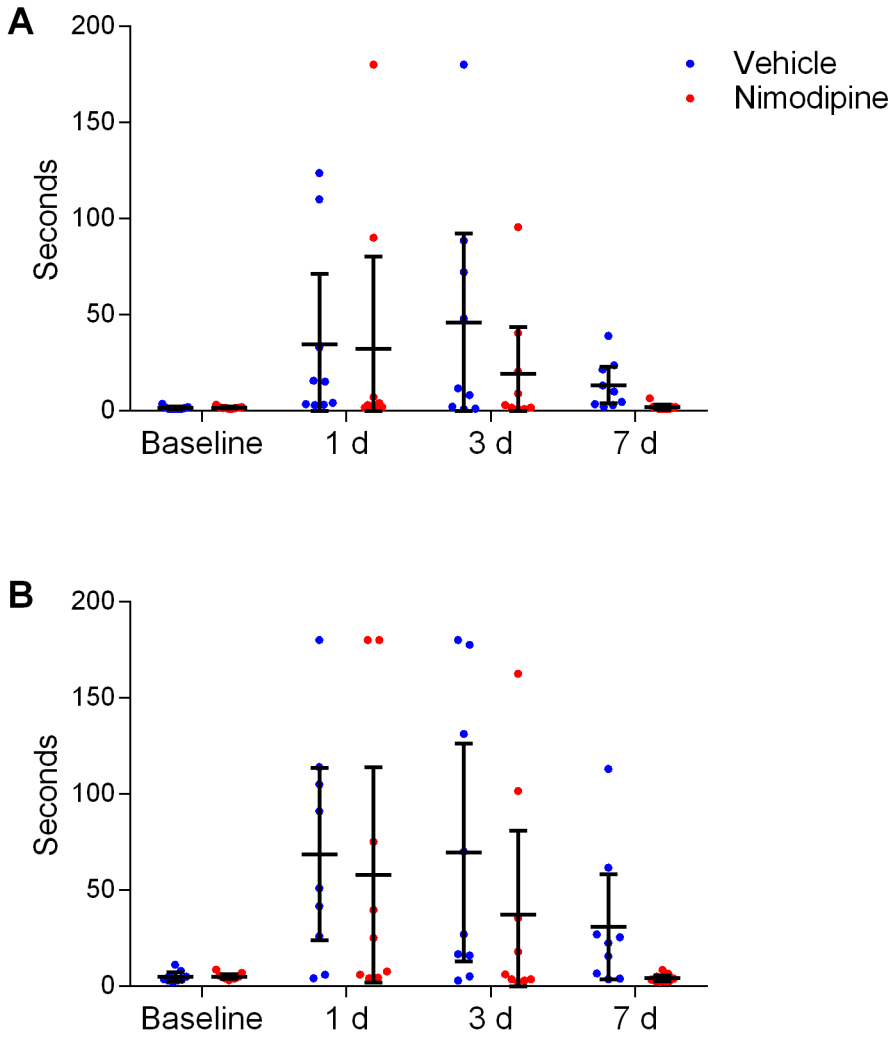

Figure 4.5: Nimodipine does not improve performance in adhesive tape testing of the affected limb. **(A)** 'Time to touch' as an indicator of somatosensory function. **(B)** 'Time to remove' as an indicator of motor function. Mean ± 95% CI; n=9 per group.

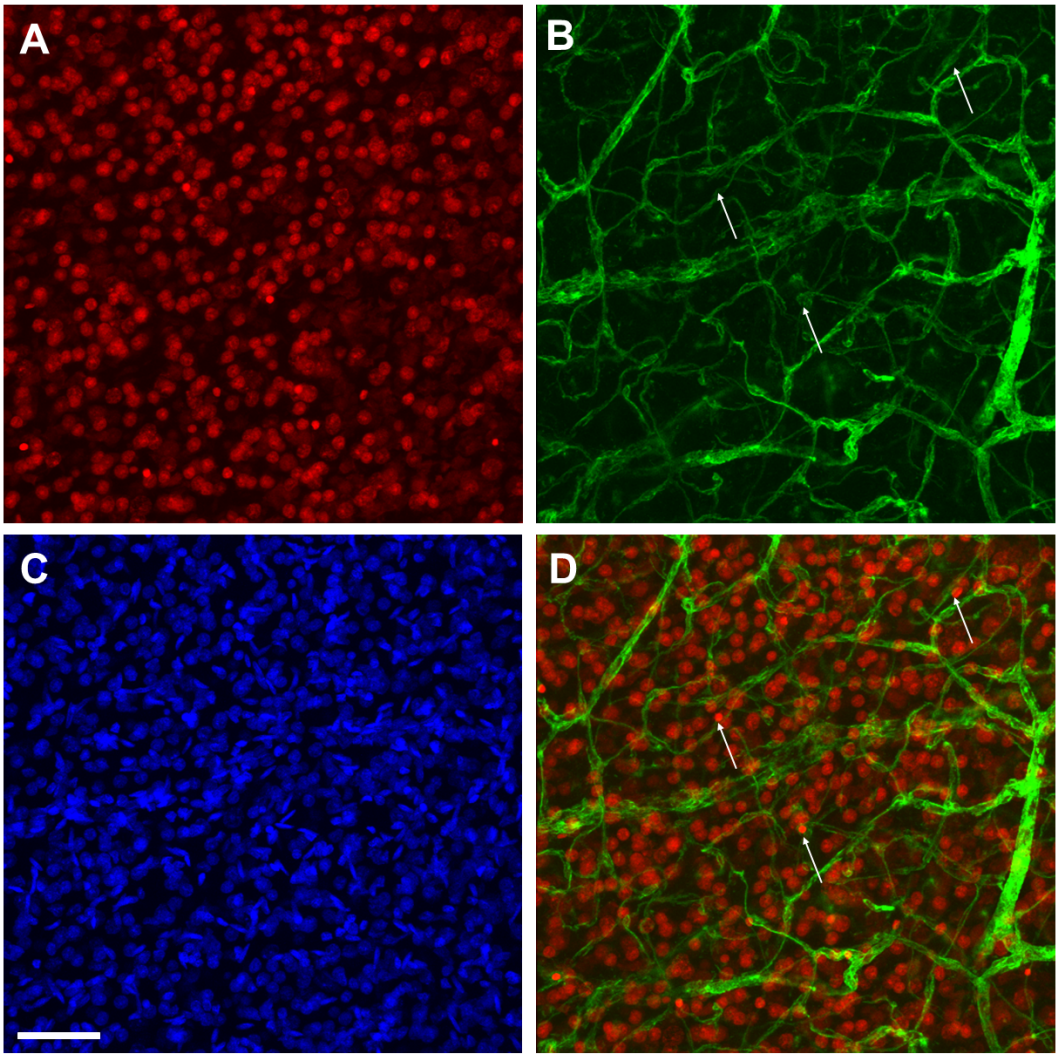

Figure 4.6: Example maximal Z-projections from confocal stacks of pericyte death staining from the ipsilateral (right) cortex. **(A)** PI labelling in ischaemic cortex, showing extensive cell death. **(B)** IB_4 staining for basement membrane allows for identification of pericytes as 'shadows' in the vasculature (white arrows). **(C)** DAPI labelling showing cell nuclei. **(D)** Merged PI and IB_4 labelling, indicating dead pericytes (white arrows). Scale bar, 50 µm.

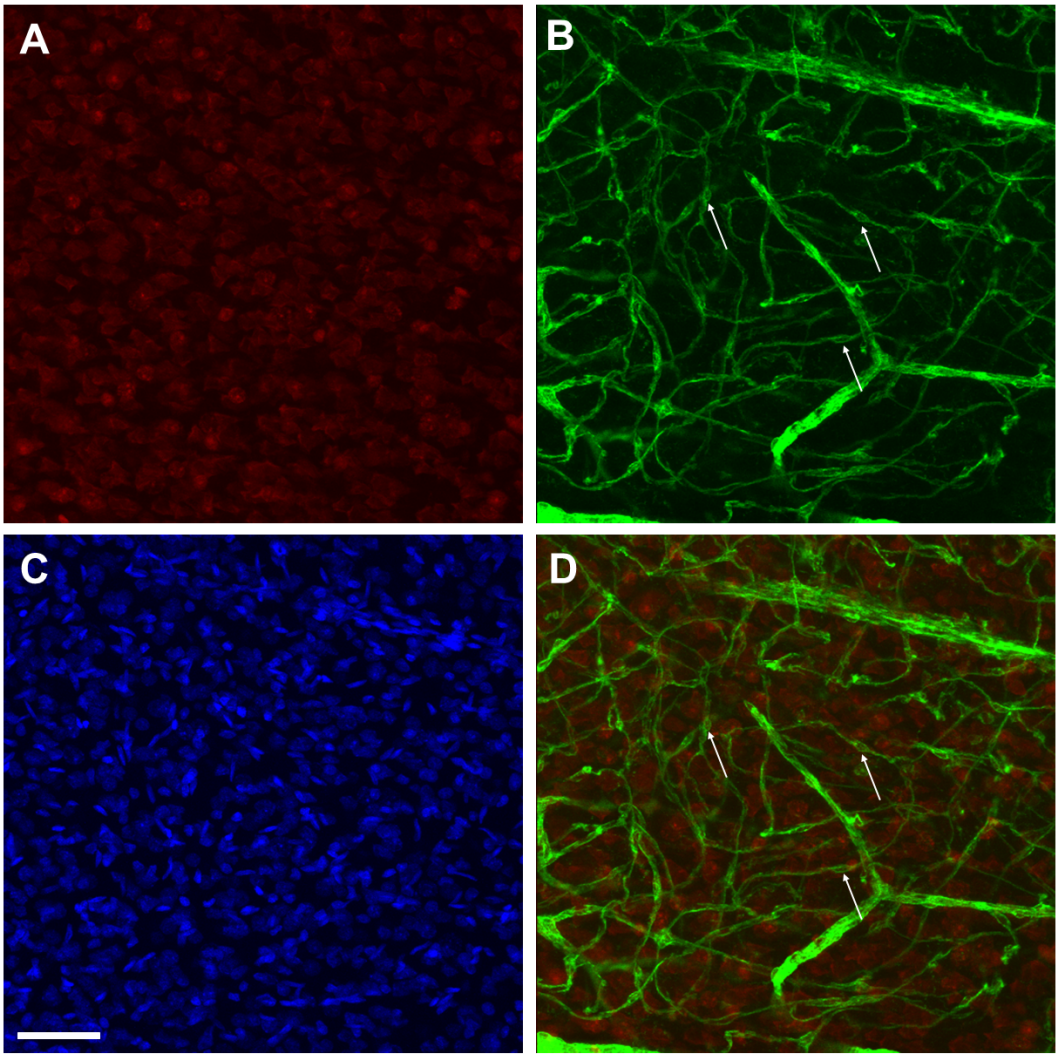

Figure 4.7: Example maximal Z-projections from confocal stacks of pericyte death staining from the contralateral (left) cortex. **(A)** PI labelling in non-ischaemic cortex, showing background PI labelling in the parenchyma, without concentrated foci that would indicate cell death. **(B)** IB_4 staining for basement membrane allows for identification of pericytes as 'shadows' in the vasculature (white arrows). **(C)** DAPI labelling showing cell nuclei. **(D)** Merged PI and IB_4 labelling, indicating live pericytes (white arrows). Scale bar, 50 µm.

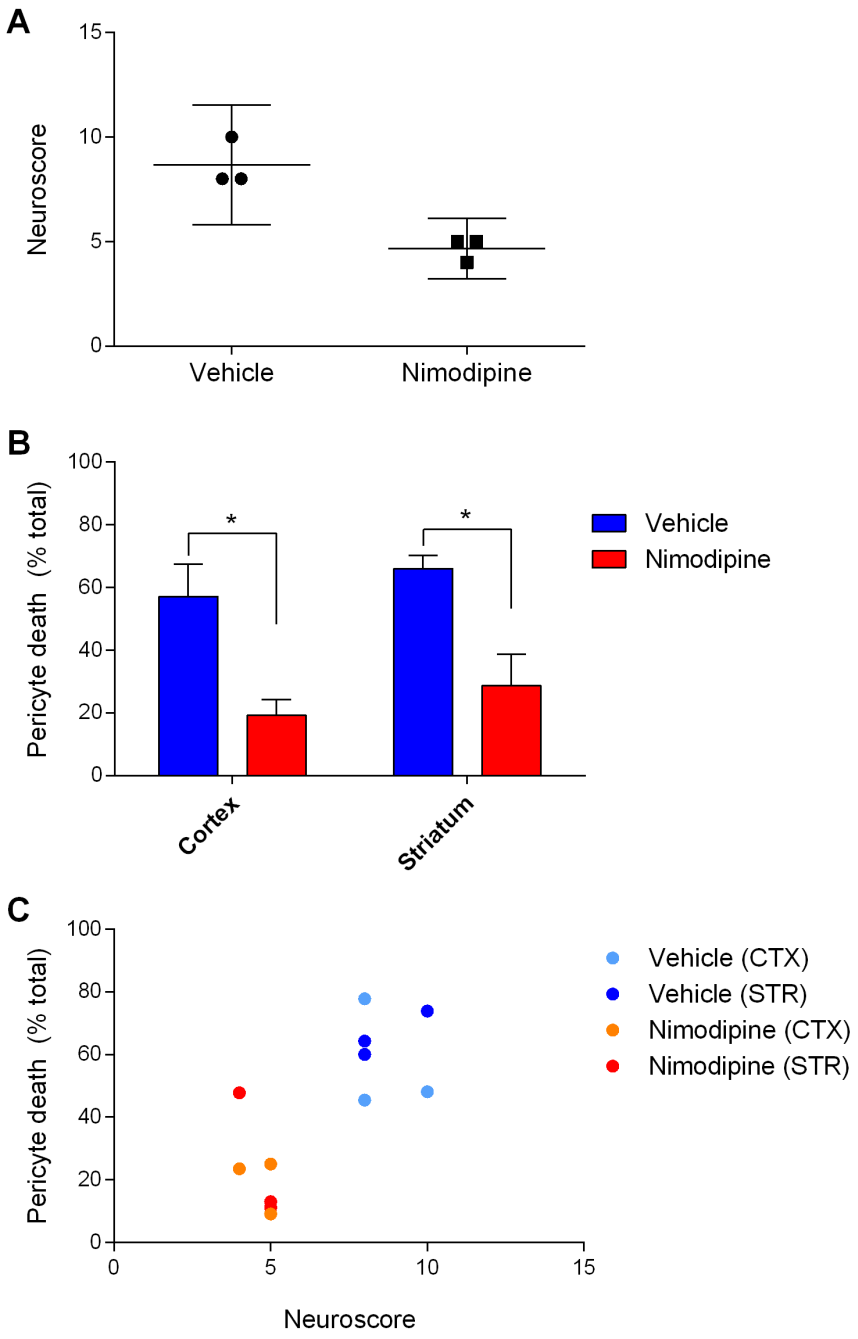

Figure 4.8: Nimodipine reduces pericyte death at 6 h after stroke. **(A)** Neuroscores in the vehicle- and nimodipine-treated groups. **(B)** Pericyte death in the cortex and striatum of vehicle- and nimodipine-treated groups. **(C)** Pericyte death and neurological impairment in individual animals. Mean ± 95% CI (neuroscore) or mean ± SEM (pericyte death); * $p<0.05$. n=3 per group.

4.3.7 Chemical ischaemia causes pericyte contraction *in vitro*

To evaluate the effects of ischaemia on pericyte tone, the contractility assay described in Chapter 3 was used in conjunction with a model of chemical ischaemia (ChI; combined blockade of mitochondrial respiration and glycolysis). Application of high-dose or medium-dose ChI resulted in a rapid decrease of cell index (CI), indicative of contraction (Fig. 4.9A). This was highly significant when quantified as relative slope (Fig. 4.9B; $p<0.0001$ for both high-dose and medium-dose ChI compared to either vehicle or low-dose ChI) or relative CI change (Fig. 4.9C; $p<0.0001$ for both high- and medium-dose ChI compared to either vehicle or low-dose ChI) at 1 hour after ChI application.

This effect was due to pericyte contraction, as the decrease in CI preceded cell death and detachment: even at 2 hours after treatment, LDH did not indicate the presence of cells or intracellular contents in the supernatant (Fig. 4.10A; $p>0.05$ for all comparisons), whereas there was extensive cell death at 24 hours after treatment (Fig. 4.10B; $p<0.001$ for high-dose ChI and $p<0.01$ for medium-dose ChI compared to vehicle). A similar pattern was observed with TUNEL staining (Fig. 4.11): while high-dose ChI resulted in positive TUNEL staining at 2 hours following treatment, nuclear integrity was retained based on DAPI staining. Medium-dose and low-dose ChI did not feature TUNEL staining.

4.3.8 Nimodipine does not prevent pericyte contraction *in vitro*

To investigate whether this contraction could be prevented by nimodipine, medium-dose ChI was applied together with 3 µM nimodipine or 0.01% DMSO vehicle. A clear effect of ischaemia was observed in both vehicle (Fig. 4.12A) and nimodipine-treated groups (Fig. 4.12B); however, there was no effect of treatment on contraction when quantified as relative slope (Fig. 4.12C) or relative CI change (Fig. 4.12D).

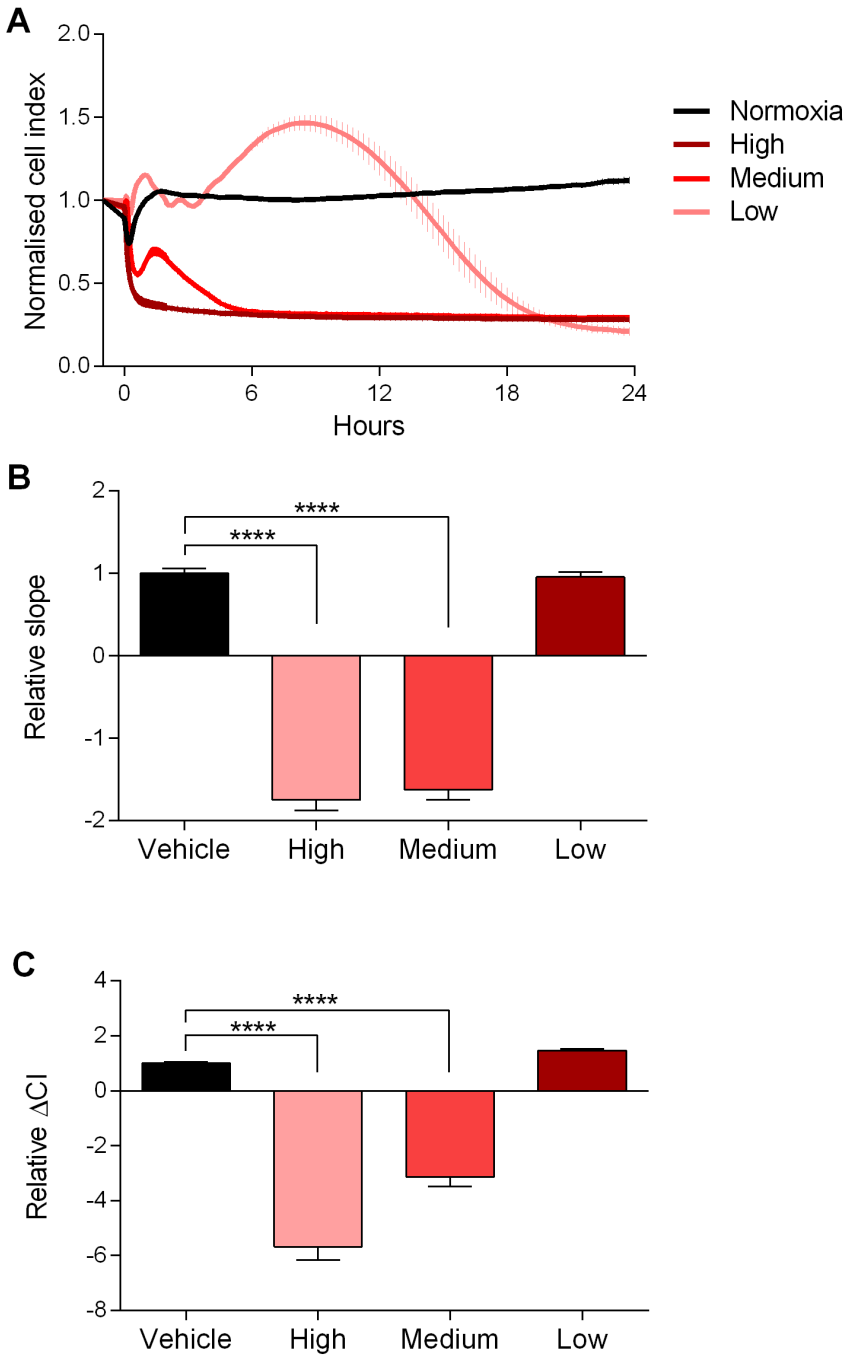

Figure 4.9: Chemical ischaemia causes pericyte contraction. **(A)** Time course of acute CI changes after ChI application. Time $p<0.0001$, treatment $p<0.0001$, time:treatment $p<0.0001$. **(B)** Change in slope of CI, normalised and compared to vehicle. **(C)** Reduction in cell index, normalised and compared to vehicle. Mean ± SEM; **** $p<0.0001$. n=4 per group.

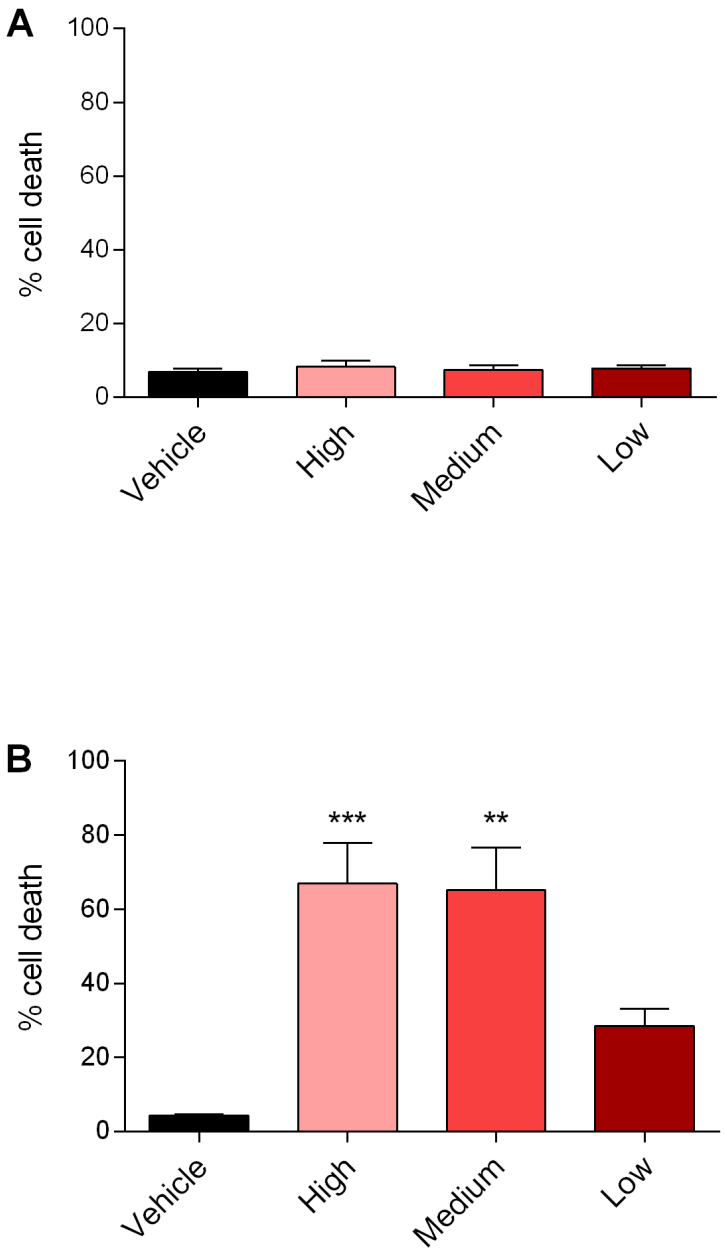

Figure 4.10: Chemical ischaemia does not cause pericyte death at 2 hours following treatment, based on LDH release. **(A)** Cell death at 2 hours following treatment with vehicle, high-dose, medium-dose or low-dose ChI. **(B)** Cell death at 24 hours following treatment with vehicle, high-dose, medium-dose or low-dose ChI. Mean ± SEM; ** $p<0.01$, *** $p<0.001$. n=4 per group.

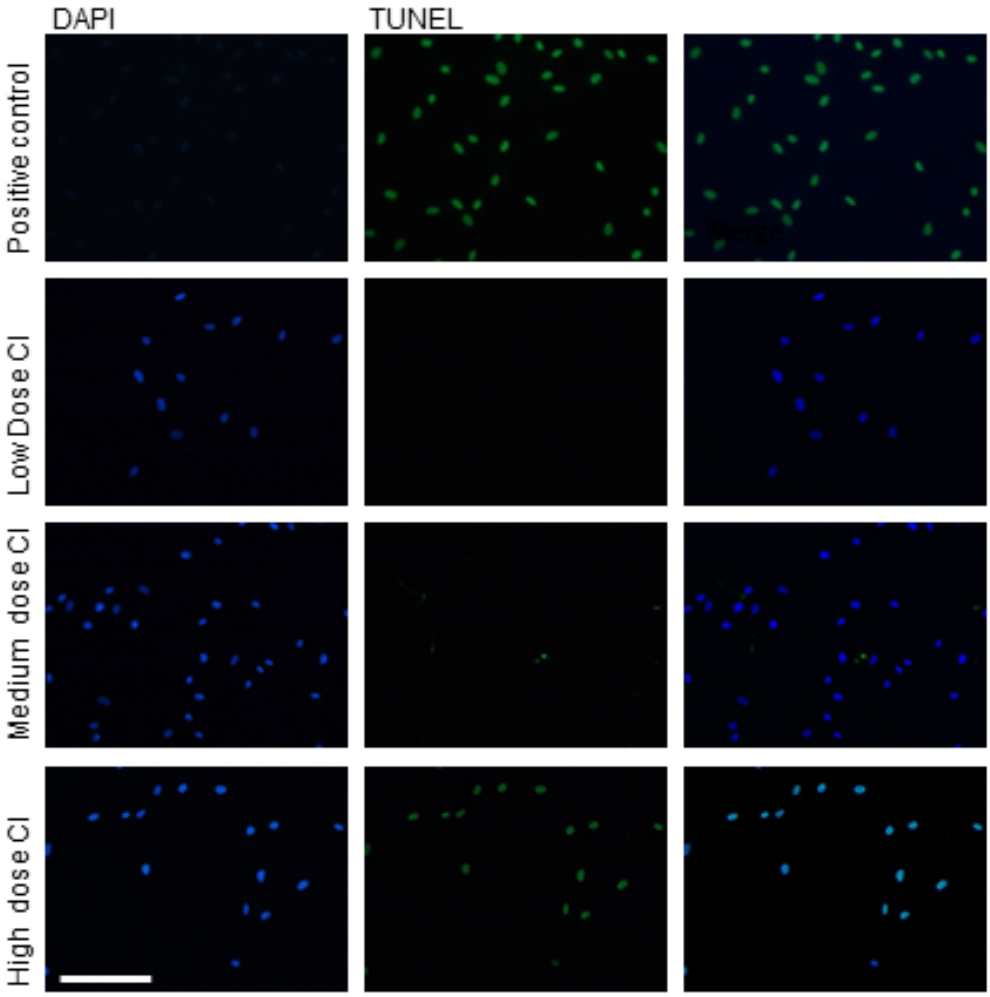

Figure 4.11: Medium-dose or low-dose chemical ischaemia do not cause pericyte apoptosis at 2 hours following treatment, based on TUNEL staining for DNA damage. High-dose chemical ischaemia causes more extensive apoptotic changes, but nuclei remain intact based on DAPI staining. Treatment with DNAse (positive control) causes extensive DNA damage and loss of nuclear DAPI staining. Representative images from an n=3 experiment. Scale bar, 50 µm.

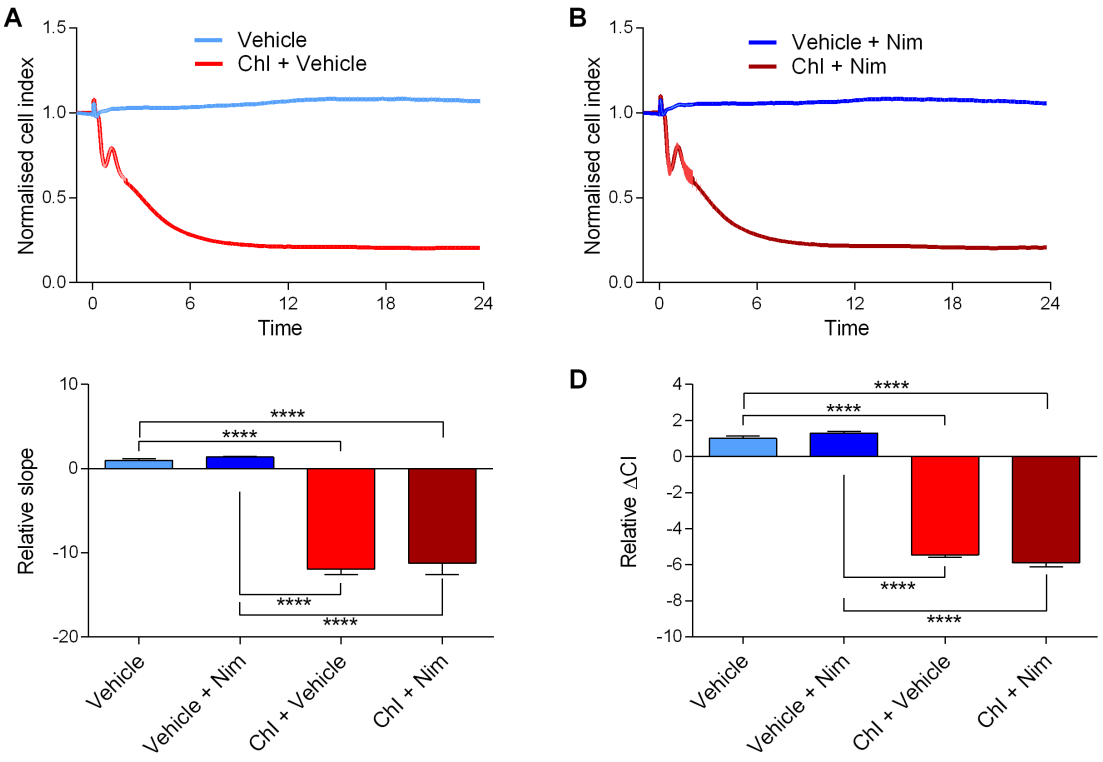

Figure 4.12: Nimodipine does not affect pericyte contraction during medium-dose chemical ischaemia. **(A)** Time course of acute CI changes after control solution or ChI application in conjunction with 0.01% DMSO vehicle. **(B)** Time course of acute CI changes after control solution or ChI application in conjunction with 3 µM nimodipine. Time $p<0.0001$, treatment $p<0.0001$, time:treatment $p<0.0001$. Panels A and B are derived from the same experiment, but plotted separately for clarity. **(C)** Change in slope of CI, normalised to control solution with DMSO vehicle. **(D)** Reduction in cell index, normalised to control solution with DMSO vehicle. Mean ± SEM; * $p<0.05$, ** $p<0.01$, *** $p<0.001$. n=4 per group.

4.4 Discussion

The results described in this chapter demonstrate that nimodipine, an antihypertensive L-type VGCC inhibitor, substantially and significantly enhances post-ischaemic CBF in rats subjected to tMCAO. Nimodipine treatment also exerted a neuroprotective effect at 3 and 7 days following stroke, based on neurological impairment scores, and reduced pericyte death in typical MCAO-affected areas (the lateral cortex and striatum) at 6 hours after stroke. However, there was no significant change in lesion volume or behavioural outcomes at 7 days. In addition, the *in vitro* data suggest that reduced pericyte death *iv vivo* could be an indirect effect mediated through neuronal or glial protection, as isolated pericyte constriction and death during chemical ischaemia was not significantly altered by the presence of nimodipine.

Although there are numerous Ca^{2+} inhibitors that relax vascular tone, nimodipine was chosen for this study due to its preferential action on the cerebral vasculature (Langley and Sorkin, 1989). Nimodipine is known to increase resting CBF in primates, at doses as low as 2 µg/kg/min i.v. (Harper et al., 1981). In agreement with this, experiments investigating the haemodynamic effects of nimodipine in global forebrain ischaemia have reported enhancement of CBF during reperfusion. In rats subjected to bilateral carotid occlusion and hypotension, pretreatment with nimodipine increased post-ischaemic CBF in a regionally heterogenous way, but did not restore electrophysiological responses to stimulation (Smith et al., 1983). Even when nimodipine was administered after global ischaemia in dogs, it resulted in ~2-fold higher CBF, accompanied by improvements in neurological function (Steen et al., 1983; Newberg et al., 1986).

However, global ischaemia is a more closely related to cardiac arrest injury, rather than stroke. Nimodipine has also been tested in more clinically relevant focal ischaemia models with mixed results – in one meta-analysis, 50% of *in vivo* studies found nimodipine to be protective in stroke, but many of the reports were of

low methodological quality (reviewed by Horn et al., 2001). Some publications have reported an amelioration of ischaemic CBF decrease in nimodipine-treated animals, with the drug administered before (Mohamed et al., 1985; Jacewicz et al., 1990) or after onset of ischaemia (Nishikibe, 1988; Meyer et al., 1986). Others, however, failed to detect an effect on CBF when treatment was started following occlusion (de la Torre, 1991; Dirnagl et al., 1990; Gotoh et al., 1986; Hakim, 1986; Berger and Hakim, 1988; Date and Hossmann, 1984). These studies used permanent occlusions, where the CBF deficit is obviously much more severe than the post-ischaemic hypoperfusion seen in transient models; as such, an effect on microcirculatory dysfunction could be masked by the much larger problem of persistent large vessel occlusion.

There is less evidence regarding the effects of nimodipine in transient models of focal ischaemia – to the best of the author's knowledge, this is the first report investigating the effects of nimodipine on CBF in the filament tMCAO model in rats. Previous work using the rat distal MCAO model showed that nimodipine treatment reduced infarct volumes when started immediately before reperfusion (Roda et al., 1995). In another report, nimodipine treatment during reperfusion reduced oedema and early mortality in a severe model of distal MCAO in cats, without improving 24-hour mortality (Hara et al., 1990). Enhancement of post-ischaemic CBF in nimodipine-treated cats has also been described; drug administration was started shortly after MCAO, continued for the ischaemic period (1 hour) and during 2.5 hours of reperfusion, yet CBF was improved by nimodipine only following reperfusion (Uematsu et al., 1989).

These reports are consistent with the observations presented in this chapter, and suggest that nimodipine improves outcomes in models of transient ischaemia. The cellular mechanism through which nimodipine exerts its effects is not clear-cut, and the disparate results from permanent and transient MCAO studies have presented two distinct options. Nimodipine could be ameliorating neuronal damage by preventing

no-reflow, consequently improving blood flow and nutrient supply after the insult. Alternatively, the primary effect could be through inhibition of neuronal Ca^{2+} influx, a key step in the ischaemic cascade (Dirnagl et al., 1999; Lipton, 1999). In the latter case, improved post-ischaemic CBF could be coincidental, or a consequence of improved tissue viability.

This dichotomy also has implications for the pericyte results presented here. While reduced pericyte death was observed in the cortex and striatum at an early time point, it was not possible to obtain reliable measurements of infarct size and location from these sections. As imaging was performed at fixed locations, improved pericyte survival could be a direct effect of nimodipine treatment, or an indirect effect due to reduced overall tissue damage, or improved neuronal/glial function. *In vitro* approaches were used to probe this question, and did not demonstrate any effect of nimodipine on isolated pericyte contraction. It should be noted that chemical ischaemia is irreversible and therefore a closer mimic of permanent ischaemia. The question of pericyte contraction in ischaemia-reperfusion, and any effects nimodipine may have on this process, require further investigation. One option would be to record capillary diameters *in vivo* using 2-PM before and after tMCAO, in conjunction with transgenic mice to label vascular mural cells (Hill et al., 2015). This would enable a more definitive assessment of microvascular tone in stroke, and whether nimodipine administration alters capillary diameter during ischaemia and/or reperfusion.

In conclusion, these results support the use of nimodipine for ameliorating post-ischaemic hypoperfusion and improving neurological outcomes. Further preclinical trials with larger sample sizes are required to validate these results – based on the data presented here, detecting a significant difference in lesion volume with 90% power would require 25 animals per group. In addition to larger confirmatory studies, the exact mechanistic basis of the actions exerted by nimodipine also requires clarification, to conclusively determine whether the effect is primarily vascular or neuroprotective.

Chapter 5

General Discussion

The work presented in this thesis employed a multimodal approach to investigate several key questions regarding cerebrovascular function following ischaemia. In particular, I sought to address the central hypothesis that post-ischaemic vascular dysfunction contributes to the outcome of stroke, and that the capillary pericyte is a potential target cell type for stroke therapy due to its contractile properties. The principal findings of the thesis are:

— focal ischaemia leads to dysfunction in both the ipsilateral and contralateral cerebrovasculature, based on responses to hypercapnia and somatosensory stimulation *in vivo* and isolated middle cerebral artery reactivity *ex vivo*;

— electrical impedance recording enables recording of contractile status in isolated pericytes *in vitro*, and demonstrates that human brain vascular pericytes are contractile even in the absence of α-smooth muscle actin (αSMA) expression;

— nimodipine treatment improves post-ischaemic blood supply and improves neurological outcomes following transient focal ischaemia in rats, but does not prevent pericyte contraction during chemical ischaemia *in vitro*.

5.1 Pericytes as contractile cells

The major unifying theme behind these experiments is the role of pericytes in the regulation of cerebral blood flow. Pericytes have many properties that are relevant to recovery from stroke, including their involvement in angiogenesis (von Tell et al., 2006), regulation of the blood-brain barrier (BBB) during aging (Bell et al., 2010), adoption of a microglial phagocytic phenotype after stroke (Özen et al., 2014), and attracting innate leukocytes during inflammation (Stark et al., 2013). However, their most relevant role in the hyperacute setting is the regulation of capillary blood flow. As discussed in section 1.4.3, there is considerable evidence that pericytes are contractile regulators of capillary diameter both in acute brain slices (Peppiatt et al., 2006) and in the cerebral cortex *in vivo* (Hall et al., 2014), and thus the primary controllers of regional cerebral blood flow (CBF).

The exact role of pericytes in neurovascular coupling (NVC) remains controversial (Wei et al., 2016, see section 1.4.3;), including issues raised by recent publications questioning their ability to contract *in vivo* and the absence of contractile apparatus proteins such as αSMA in mid-capillary pericytes (Hill et al., 2015; Wei et al., 2016; Hartmann et al., 2015a). The concept of mural cell heterogeneity along the vessel bed is not novel, and has been characterised since the 1990s in extensive detail, based on both morphological and molecular distinctions. It is well known that αSMA and smooth muscle myosin expression becomes weaker when progressing further along the branch order from the penetrating arteriole, before increasing again on the venular side Nehls and Drenckhahn (1993). Conversely, intermediate filament proteins desmin and vimentin are expressed at high levels in mid-capillary pericytes (Fujimoto and Singer, 1987), as is smooth muscle tropomyosin (Joyce et al., 1985). These are in agreement with my observations *in vivo*: although pericyte markers such as PDGFRβ and NG2 label all branches of the vasculature, I was unable to detect αSMA staining in most capillaries (data not presented).

The contractile properties of cultured pericytes are more widely accepted, based primarily on substrate-wrinkling assays, where cultured cells deform the silicone or collagen matrix on which they are grown (Kutcher and Herman, 2009), as well as the expression of contractility-associated proteins, including αSMA (Herman, 1985; Sieczkiewicz and Herman, 2003). This has primarily been investigated in retinal pericytes, particularly from bovine sources (Kelley et al., 1987; McDonald et al., 1995; Papetti et al., 2003). Although αSMA expression in retinal microvessels decreases with distance from the parent arteriole (Kornfield and Newman, 2014), similarly to observations in other tissues (Nehls and Drenckhahn, 1993), the use of retinal tissue in pericyte culturing protocols may not be representative of other organs or even other CNS regions.

The study reported in this thesis is the first quantitative assessment of human brain pericyte contractility *in vitro*, demonstrating that they contract and relax in response to a variety of vasoactive substances such as endothelin-1 (ET-1) and adenosine. The mechanism by which contraction occurs is uncertain: there was no evidence of αSMA transcript expression in human brain vascular pericytes (HBVP), compared to a human cerebral microvascular endothelial cell line, nor was it ever observed with immunocytochemical methods. The absence of αSMA in HBVP could reflect an interspecies difference between bovine, porcine or rodent pericytes and human pericytes, although there has been no comparative study examining this question. It could also be a phenotypic alteration that occurs during prolonged culturing, or a consequence of particular isolation methods – for example, it is known that vascular smooth muscle (VSM) cells can dedifferentiate over time *in vitro*, downregulating myosin expression (Chamley et al., 1977). It is also possible that HBVP are derived from mid-capillary fragments, whereas retinal isolation methods could favour proliferation of cells derived from branches closer to the arteriolar or venular side. Due to the proprietary nature of commercial HBVP, the exact

methods used to purify them are not publicly available. In general, current pericyte culturing protocols are mainly based on isolating microvessel fragments (e.g. by density gradient centrifugation) and thus cannot distinguish exact locations in the vascular tree (Redzic et al., 2015).

HBVP did, however, express the intermediate filament protein desmin, which might provide an alternative contractile pathway. Loss of desmin has been associated with impairment of both passive and active force development in microarterial smooth muscle (Wede et al., 2002), and similar observations have been made for other intermediate filament proteins such as vimentin (Wang et al., 2006a). The exact molecular composition of the contractile apparatus underlying pericyte responses vasoactive substances was not identified in this study, beyond demonstrating receptor-specificity of their responses to ET-1 and adenosine. Further work to address this question could utilise pharmacological tools such as cytochalasin B to disrupt actin filaments and establish whether HBVP responses require microfilament or intermediate filament function (Kelley et al., 1987). In addition, genetic tools such as lentiviral small hairpin RNA delivery or CRISPR-mediated gene editing could be used to prevent desmin expression in HBVP before characterising their responsiveness to ET-1 and other vasoactive substances. Identifying the exact contractile proteins would give us further experimental tools to target pericyte contractility *in vivo*, as well as potentially provide novel therapeutic targets for no-reflow (see section 5.2).

Resolving the question of how *in vitro* pericyte contractility relates to their exact origins within the microvasculature would require techniques such as laser capture microdissection from live tissue (Stich et al., 2003). This could be used specifically isolate capillaries or various branch orders (e.g. arteriolar-side vs. middle branch order vs. venular-side) for culturing, followed by functional characterisation. Alternatively, specific (or highly enriched) markers of distinct capillary populations could be used for antibody-based cell sorting (Zhou et al., 2014). However, while the mouse pericyte

transcriptome has recently been characterised using RNA-sequencing (Zhang et al., 2014), our understanding of pericyte gene expression heterogeneity along the vascular tree remains extremely limited. Therefore, such antibody-based methods cannot yet isolate specific subpopulations.

5.2 Pericytes in stroke

As discussed in section 1.6.2.2, it has been reported that pericytes also contract under ischaemic conditions. This has been observed both in mice subjected to transient middle cerebral artery occlusion (tMCAO), a model comparable to the one used in this work (Yemisci et al., 2009), and in acute brain slices exposed to the same chemical ischaemia solution that was used in Chapter 4 (Hall et al., 2014). While this has again been questioned by other publications (Vates et al., 2010; Hill et al., 2015), the *in vitro* results presented in chapter 4 are in agreement with observations from Hall et al. (2014), with contraction preceding pericyte death following chemical ischaemia *in vitro*.

Regardless of the exact mechanisms involved, both supporters and opponents of the pericyte hypothesis largely agree that there is a post-ischaemic constriction in microvessels towards the arteriolar side of the capillary bed, covered by discontinuous mural cells, thus distinguishing them from canonical arteriolar VSM cells. Moveover, the presence of αSMA is not necessarily a prerequisite for contraction, as demonstrated by the *in vitro* results described in this chapter. As such, we should not allow the field to be hindered by semantic disputes between 'terminal VSM cells' and 'early branch order pericytes', but rather agree that this cell population is a promising target to improve reperfusion in stroke (Attwell et al., 2016).

Chapter 4 investigated nimodipine as a potential vasculoprotectant, using a combined *in vivo* and *in vitro* approach. While nimodipine substantially enhanced post-ischaemic CBF and reduced ipsilateral cortical and striatal pericyte death in

the tMCAO model of stroke, it had no effect on isolated pericyte contraction when exposed to chemical ischaemia. However, chemical ischaemia is irreversible and therefore a model of permanent ischaemia, rather than the transient insult used for *in vivo* experiments. Therefore, it remains inconclusive whether nimodipine enhances CBF through arterial vasodilation, as has been suggested previously (Auer, 1981; Langley and Sorkin, 1989), prevention of pericyte constriction and death, as suggested by improved pericyte survival during chemical ischaemia in the absence of Ca^{2+} (Hall et al., 2014), or a direct neuroprotective effect by preventing neuronal Ca^{2+} influx and subsequent cell death (Scriabine et al., 1989).

The gold-standard approach to disentangle these effects would be to perform *in vivo* 2-photon imaging (2-PM) in animals. In transgenic mice expressing fluorescent pericyte markers—such as NG2-DsRed, $RGS5^{+/GFP}$, or PDGFRβ-Cre crossed with an appropriate reporter line—capillary diameters could be visualised with an appropriate circulating label such as fluorescent dextran, thus enabling determination of pericyte tone (Hall et al., 2014; Wei et al., 2016; Hartmann et al., 2015b). This could be performed before, during and following tMCAO (Hill et al., 2015), in conjunction with administration of nimodipine during reperfusion. The absence of nimodipine-induced pericyte relaxation in such an experiment would exclude that mechanism as the source of improved CBF and ameliorated stroke severity.

Nimodipine is already clinically used in subarachnoid haemorrhage, to prevent vasospasm and secondary ischaemia (Rowland et al., 2012). It is thought to preferentially affect the cerebral vasculature, but this specificity is imperfect (Haws et al., 1983). Unequivocal mechanistic proof that preventing Ca^{2+} influx ameliorates no-reflow would involve the use of BBB-impermeable L-type Ca^{2+} channel inhibitors to exclude any neuronal effects by restricting its access beyond the vasculature (which could, however, be confounded by stroke-induced BBB disruption). Alternatively, cell type contributions to the effects of nimodipine could be disentangled through

pericyte-specific expression of mutant L-type voltage-gated Ca^{2+} channel (VGCCs) that are insensitive to nimodipine due to mutations in the dihydropyridine binding site (Hockerman et al., 1997); however, such animal lines are not currently available.

In addition to understanding the cellular basis of nimodipine-induced CBF increases, its regional effects also require elucidation. It has been reported that nimodipine can cause redistribution of cerebral blood flow from non-ischaemic to ischaemic regions, whereas others have instead observed an increase in basal CBF without improving perfusion of the ischaemic region (Harris et al., 1982; Barnett et al., 1986). The data provided in chapter 4 used a single point measurement in the form of laser Doppler flowmetry, recording CBF in the ischaemic parietal cortex. Determining whether this reflected a general increase in cerebral perfusion or a specific enhancement of CBF in the ischaemic territory would require measuring cortical CBF in more dimensions, with either reflectance-based surface imaging approaches (as described in chapter 2 with laser speckle contrast) or magnetic resonance imaging (MRI), e.g. arterial spin labelling (Thomas et al., 2006).

MRI would also allow investigation of deeper structures affected by tMCAO, most notably the striatum. Compared to primates, rodents have more extensive neocortical collateral supply, whereas the caudate and putamen are true end-arterial territories supplied by the lenticulostriate arteries, and are thus more severely affected by proximal MCAO (Bederson et al., 1986b). It would therefore be of interest to examine whether the CBF effects observed in the cortex also apply to the striatal infarct core. Despite having poor spatial resolution compared to 2-PM, MRI would also enable more in-depth characterisation of other physiological parameteres, such as sequential multimodal measurements of lesion growth, metabolic status and pH change in tandem with CBF (Guo et al., 2016). This could provide detailed *in vivo* information on penumbral survival, including the dynamics of post-ischaemic perfusion changes, how these relate to infarct growth and the extent to which nimodipine alters these

processes.

5.3 Vascular changes distant to the lesion

It is also important to consider post-ischaemic abnormalities outside of the affected region. The *in vivo* results with nimodipine treatment mainly focussed on vascular changes in regions and cells directly affected by ischaemia; although there was no evidence of substantial pericyte death in the contralateral hemisphere, the experiments using *in vivo* blood flow imaging and pressurised isolated artery reactivity found a contralateral impairment of vascular responses following tMCAO. This was evident in both diminished *in vivo* reactivity to inhaled CO_2 and *ex vivo* reactivity to vasoactive substances. It is therefore unlikely that this phenomenon could be accounted for by maximal vasodilation following ischaemia, resulting in an exhaustion of the vessels' ability to further dilate, as this effect would not be evident in isolated arteries. I did not determine the mechanistic basis of diminished contralateral vascular reactivity, but there are some plausible hypotheses that might account for this.

Diaschisis (from the Greek for 'split across') was originally defined in 1914 by von Monakow, who described a remote loss of function in the context of a focal brain lesion (discussed in Carrera and Tononi, 2014). There is considerable evidence that stroke can lead to contralateral cerebellar and transhemispheric cortical diaschisis (Ito et al., 2002; Kamouchi et al., 2004; Dobkin et al., 1989; Lagreze et al., 1987). The mechanism is typically assumed to be neural deactivation, as extrapolated from altered cerebral metabolic rate of oxygen ($CMRO_2$) or CBF, in either the resting state (Dobkin et al., 1989; Lagreze et al., 1987) or during task-evoked responses (Ginsberg et al., 1989).

An alternative explanation would be an alteration in neurovascular coupling through diaschisis-like effects on the vasculature. There are extensive intercellular communication pathways between the constituent cell types of the vessel wall (Christ

et al., 1996; Figueroa and Duling, 2009), including the pericytes and their underlying endothelium (Cuevas et al., 1984). Vascular gap junctions have been proposed to mediate upstream propagation of vasodilation in response to local activity (Segal and Duling, 1986; Itoh and Suzuki, 2012; Chen et al., 2014), but could also explain how vascular dysfunction could occur beyond the ischaemic territory. It has been reported that ischaemia causes the closure of pericyte gap junctions (Oku et al., 2001), but the upstream and distant consequences of these changes have not been described.

Alternatively, remote vascular dysfunction could be mediated by diffusible signalling molecules, such as pro-inflammatory mediators. Stroke leads to a wide variety of inflammatory changes, including upregulation of numerous cytokines, recruitment of circulating leukocytes, and activation of microglial cells (reviewed by Jin et al., 2010), in ipsilateral non-infarcted areas (Pappata et al., 2000) and even on the contralateral side (Marks et al., 2001). This can lead to further neuronal damage through neuronophagia and removal of synapses by the activated microglia (Pappata et al., 2000), which could in turn affect NVC and blood flow responses to stimuli; however, this is likely to occur on a more chronic scale than the 6- and 24-hour time points used in the CBF imaging experiments in this study.

Although stroke is associated with systemic immunosuppression via autonomic nervous system activity (Anthony et al., 2012), there is nonetheless a substantial early increase in plasma concentrations of cytokines including interleukin 1β (IL-1β), IL-6 and tumour necrosis factor α (TNF-α; Mazzotta et al., 2004). These observations are particularly relevant to post-ischaemic vascular function due to the plethora of vasoactive substances whose expression is altered by inflammatory cytokines, including nitric oxide, ET-1 and arachidonic acid (AA) derivatives, which may in turn diminish vasodilatory signalling and promote vasoconstriction (Vila and Salaices, 2005). In agreement with this, one recent report suggested that striatal IL-1β injections can diminish cortical haemodynamic responses to whisker stimulation

(Bray et al., 2016).

In order to establish the mechanism underlying the observations made in chapter 2, the simplest approach would be to repeat the imaging and isolated vessel experiments, with animals subjected to tMCAO and treated with antagonists of specific pro-inflammatory pathways. One promising candidate would IL-1 receptor antagonist (Mulcahy et al., 2003). Targeting downstream mediators through inhibition of AA metabolism, including prostaglandin synthesis, would also be of interest; unfortunately, the involvement of AA derivatives in normal neurovascular function (Liu et al., 2012) would complicate interpretation of results, and make it very difficult to titrate the dose so that it prevents stroke-induced upregulation without disrupting basal signalling. A complementary strategy to antagonist studies would be to administer exogenous cytokines like IL-1β and determine whether they exacerbate vascular hyporeactivity. There is an intriguing report that systemic administration of IL-1β induces basal post-ischaemic hypoperfusion, through ET-1 acting on ET_A receptors (Murray et al., 2014), but the effects of this pathway on vascular reactivity have not been investigated.

Finally, the role of the microvasculature in this process should be considered. Although chapter 2 did not directly investigate microvascular structure or function on a single-vessel level, there are intriguing suggestions that contralateral hemisphere pericytes could be vulnerable to focal ischaemia. Using methods very similar to the acute brain slice experiments in chapter 4, quantification of pericyte death following 90-minute tMCAO in rats suggested that 70% of ipsilateral and 30% of contralateral pericytes had died after 24 hours of reperfusion; in sham animals, only 15-20% of pericytes died in each hemisphere (Hall et al., 2014), which was assumed to be a consequence of trauma during tissue preparation. Although there was still a considerable difference between the lesioned and contralateral sides, cell death is a relatively crude measure and could be obscuring more subtle effects

of pericyte function. Therefore, future experiments should investigate capillary responses bilaterally *in vivo* using 2-PM approaches, as outlined above.

5.4 Translational potential

After decades of immense investment of time and resources into neuroprotective strategies, the only efficacious therapies for acute ischaemic stroke revolve around restoration of vascular supply through the affected cerebral artery. Nonetheless, adjunct therapies to recanalisation remain highly desirable and, in some ways, more attainable than ever before. The field of stroke research, aided by novel methodological avenues and new conceptual insights, is continuing to provide us with a more detailed understanding of the very complex pathophysiology that follows a very simple insult.

This thesis further emphasises the importance of considering vascular effects beyond recanalisation, both in terms of the ischaemic microvasculature, as well as large vessel dysfunction in distant territories. In particular, it makes the important observation of enhanced reperfusion following nimodipine treatment, in an animal model that mimics endovascular thrombectomy, the new gold standard of stroke therapy. Although this study was conducted with diligent attention to minimising bias, including blinding, randomisation and appropriate sample size selection (Macleod et al., 2015a), these findings must be validated in a larger, 'phase II' preclinical trial, and preferably in other species as well.

Finally, although larger sample sizes and more rigorous quality control are essential overcoming the translational roadblock, this must be accompanied by smaller-scale studies that expand our understanding of basic stroke biology. Only by understanding the roles of particular cell types in the aftermath of ischaemia can we hope to delineate the mechanism by which no-reflow can be targeted, and provide novel adjunct therapeutic options for stroke.

5.5 Concluding remarks

This thesis made several novel observations concerning vascular function following cerebral ischaemia. First, I examined NVC and reactive hyperaemia on a macroscopic level, demonstrating that while NVC was largely unaltered at 6 or 24 hours after 90-minute tMCAO, CBF responses to hypercapnia were diminished bilaterally. In addition, middle cerebral artery responsiveness to vasoactive substances *ex vivo* was impaired on both sides as well, suggesting that focal ischaemia leads to global vascular dysfunction in the brain.

Then, I described the phenotype of HBVP cultured *in vitro*, which I used to develop a novel quantitative pericyte contractility assay. This allowed for detection of receptor-dependent changes in the contractile state and proliferation of HBVP in response to a wide variety of vasoactive substances, including ET-1 and adenosine. For the first time, this work demonstrated that human pericytes are contractile in response to a variety of vasoactive substances *in vitro*, despite lacking αSMA expression. The technique was further validated in primary rat brain vascular pericytes, which also exhibited contractile responses, as reported previously. Importantly, I demonstrated that application of chemical ischaemia resulted in pericyte contraction, which clearly preceded cell death, in agreement with previous reports of pericyte 'death in rigour' using different approaches.

Finally, I utilised both *in vivo* and *in vitro* models to investigate the effect of nimodipine, a VGCC inhibitor, on outcomes in tMCAO. While post-ischaemic CBF was enhanced, neurological outcomes were improved and pericyte death was reduced *in vivo* by nimodipine administration at reperfusion, there was no significant change in sensorimotor behavioural outcomes or lesion volume. Moreover, pericyte contraction in response to chemical ischaemia *in vitro* was not prevented by nimodipine, which may be due to differences between isolated cells and *in vivo* ischaemia, or it may indicate that the CBF augmentation I observed was a consequence of nimodipine

acting on arterial or arteriolar smooth muscle.

While further work is required to confirm the link between pericytes and post-ischaemic cerebrovascular dysfunction (and whether this is the true target of nimodipine) this thesis nonetheless highlights the importance of investigating vascular function following stroke, and suggests that nimodipine is a promising candidate for use as an adjunct therapy in the context of endovascular thrombectomy.

Appendices

Appendix A

List of abbreviations

2-PM	2-photon microscopy
4-VO	4-vessel occlusion
5-HT	5-hydroxytryptamine (serotonin)
20-HETE	20-hydroxyeicosatetraenoic acid
95% CI	95% confidence interval
αSMA	α-smooth muscle actin
A_1	Adenosine receptor type 1
A_2	Adenosine receptor type 2
A_{2A}	Adenosine receptor type 2A
AA	Arachidonic acid
ACh	Acetylcholine
aCSF	Artificial cerebrospinal fluid
AmA	Antimycin A
ANOVA	Analysis of variance
AOL	Arterial occlusive lesion
ASL	Arterial spin labelling
ATP	Adenosine triphosphate
AUC	Area under the curve
BBB	Blood-brain barrier
BK	Ca^{2+}-activated large conductance K^+ channel
BOLD-fMRI	Blood oxygen level-dependent functional magnetic resonance imaging
$[Ca^{2+}]_i$	Intracellular Ca^{2+} concentration
cAMP	Cyclic adenosine monophosphate
cBase(ECF)	Standard base excess
CBF	Cerebral blood flow
CBV	Cerebral blood volume
CCA	Common carotid artery
cDNA	Complementary DNA
cGMP	Cyclic guanosine monophosphate
ChI	Chemical ischaemia
CI	Cell index
CL	Contralateral

$CMRO_2$	Cerebral metabolic rate of oxygen
CNS	Central nervous system
COX-1	Cyclooxygenase-1
COX-2	Cyclooxygenase-2
CSD	Cortical spreading depression
CSI	Cortical spreading ischaemia
CTTH	Capillary transit time heterogeneity
CVRC	Cerebrovascular reserve capacity
CYP450	Cytochrome P450
DAPI	4',6-diamidino-2-phenylindole
DkS	Normal donkey serum
DMSO	Dimethyl sulfoxide
DREADD	Designer receptor selectively activator by designer drug
ECA	External carotid artery
EEG	Electroencephalography
EET	Epoxyeicosatrienoic acid
ELISA	Enzyme-linked immunosorbent assay
eNOS	Endothelial nitric oxide synthase
ET-1	Endothelin-1
ET_A	Endothelin type A receptor
ET_B	Endothelin type B receptor
EVT	Endovascular thrombectomy
GABA	γ-aminobutyric acid
$GABA_A$	GABA type A receptor
GECI	Genetically encoded Ca^{2+} indicator
GtS	Normal goat serum
Hb	Haemoglobin
HbO	Oxyhaemoglobin
HbR	Deoxyhaemoglobin
HbT	Total haemoglobin
HBVP	Human brain vascular pericytes
hCMEC/D3	Human cerebral microvascular endothelial cells
$[HCO_3^-]$	Bicarbonate concentration
IA	Iodoacetate
IB_4	Isolectin B_4
ICA	Internal carotid artery
IL	Ipsilateral
IL-1β	Interleukin 1β
IL-6	Interleukin 6
IP_3R_2	Inositol-3-phosphate receptor 2
IV-tPA	Intravenous tissue-type plasminogen activator
K_{ir}	Inward rectifying K^+ channel
LDF	Laser Doppler flowmetry
LDH	Lactate dehydrogenase
LFP	Local field potential

LSCI	Laser speckle contrast imaging
MCA	Middle cerebral artery
MCAO	Middle cerebral artery occlusion
mGluR	Metabotropic glutamate receptor
MPEP	2-methyl-6-(phenylethynyl)pyridine
MPTP	Mitochondrial permeability transition pore
MRI	Magnetic resonance imaging
MUA	Multi-unit activity
NADH	Nicotinamide adenine dinucleotide
NPY	Neuropeptide Y
NMDA	N-methyl-D-aspartate
nNOS	Neuronal nitric oxide synthase
NO	Nitric oxide
NVC	Neurovascular coupling
NVU	Neurovascular unit
OISI	Optical intrinsic signal imaging
P_aCO_2	Arterial carbon dioxide tension
P_aO_2	Arterial oxygen tension
pCO_2	Carbon dioxide tension
PCR	Polymerase chain reaction
PEG-400	Polyethylene glycol 400
PET	Positron emission tomography
PFA	Paraformaldehyde
PGD_2	Prostaglandin D_2
PGE_2	Prostaglandin E_2
PGF_2	Prostaglandin F_2
PGH_2	Prostaglandin H_2
PGI_2	Prostaglandin I_2
PI	Propidium iodide
PID	Peri-infarct depolarisation
PKG	Protein kinase G
pMCAO	Permanent middle cerebral artery occlusion
pO_2	Oxygen tension
P/S	Penicillin-streptomycin
qRT-PCR	Quantitative real-time polymerase chain reaction
RBVP	Rat brain vascular pericytes
ROS	Reactive oxygen species
SAH	Subarachnoid haemorrhage
SEM	Standard error of the mean
SEP	Somatosensory evoked potential
SNP	Sodium nitroprusside
STAIR	Stroke Therapy Academic Industry Roundtable
tACPD	Trans-1-amino-1,3-dicarboxycyclopentane
TCO_2	Total carbon dioxide content
TICI	Thrombolysis in cerebral infarction

tMCAO	Transient middle cerebral artery occlusion
TTC	2,3,5-triphenyltetrazolium chloride
TXA_2	Thromboxane A_2
VASO	Vascular space occupancy
VGCC	Voltage-gated Ca^{2+} channel
VIP	Vasoactive intestinal peptide
VSM	Vascular smooth muscle

Bibliography

Abbott, N. J., Patabendige, A. A. K., Dolman, D. E. M., Yusof, S. R., and Begley, D. J. (2010). Structure and function of the blood-brain barrier. *Neurobiol. Dis.*, 37(1):13–25.

Abbott, N. J., Rönnbäck, L., and Hansson, E. (2006). Astrocyte-endothelial interactions at the blood-brain barrier. *Nat. Rev. Neurosci.*, 7(1):41–53.

Aguzzi, A., Barres, B. a., and Bennett, M. L. (2013). Microglia: scapegoat, saboteur, or something else? *Science*, 339(6116):156–61.

Altamura, C., Reinhard, M., Vry, M.-S., Kaller, C. P., Hamzei, F., Vernieri, F., Rossini, P. M., Hetzel, A., Weiller, C., and Saur, D. (2009). The longitudinal changes of BOLD response and cerebral hemodynamics from acute to subacute stroke. A fMRI and TCD study. *BMC Neurosci.*, 10(1):151.

Altamura, C., Torquati, K., Zappasodi, F., Ferretti, A., Pizzella, V., Tibuzzi, F., Vernieri, F., Pasqualetti, P., Landi, D., Del Gratta, C., Romani, G.-L., Maria Rossini, P., and Tecchio, F. (2007). fMRI-vs-MEG evaluation of post-stroke interhemispheric asymmetries in primary sensorimotor hand areas. *Exp. Neurol.*, 204(2):631–9.

Ames, A., Wright, R. L., Kowada, M., Thurston, J. M., and Majno, G. (1968). Cerebral ischemia. II. The no-reflow phenomenon. *Am. J. Pathol.*, 52(2):437–53.

Amruthesh, S. C., Boerschel, M. F., McKinney, J. S., Willoughby, K. A., and Ellis, E. F. (1993). Metabolism of arachidonic acid to epoxyeicosatrienoic acids, hydroxyeicosatetraenoic acids, and prostaglandins in cultured rat hippocampal astrocytes. *J. Neurochem.*, 61(1):150–9.

Ances, B. M., Greenberg, J. H., Detre, J. A., and Dietrich, W. D. (2000). Acute carotid occlusion alters the activation flow coupling response to forepaw stimulation in a rat model. *Stroke.*, 31(4):955–960.

Andreone, B. J., Lacoste, B., and Gu, C. (2015). Neuronal and vascular interactions. *Annu. Rev. Neurosci.*, 38:25–46.

Anthony, D. C., Couch, Y., Losey, P., and Evans, M. C. (2012). The systemic response to brain injury and disease. *Brain. Behav. Immun.*, 26(4):534–40.

Araque, A., Parpura, V., Sanzgiri, R. P., and Haydon, P. G. (1999). Tripartite synapses: glia, the unacknowledged partner. *Trends Neurosci.*, 22(5):208–15.

Archer, S. L., Huang, J. M., Hampl, V., Nelson, D. P., Shultz, P. J., and Weir, E. K. (1994). Nitric oxide and cGMP cause vasorelaxation by activation of a charybdotoxin-sensitive K channel by cGMP-dependent protein kinase. *Proc. Natl. Acad. Sci. U. S. A.*, 91(16):7583–7.

Armulik, A., Genové, G., Mäe, M., Nisancioglu, M. H., Wallgard, E., Niaudet, C., He, L., Norlin, J., Lindblom, P., Strittmatter, K., Johansson, B. R., and Betsholtz, C. (2010). Pericytes regulate the blood–brain barrier. *Nature*, 468(7323):557–561.

Astrup, J., Siesjö, B. K., Symon, L., Siesjo, B. K., and Symon, L. (1981). Thresholds in cerebral ischemia - the ischemic penumbra. *Stroke.*, 12(6):723–725.

Attwell, D., Buchan, A. M., Charpak, S., Lauritzen, M., Macvicar, B. A., and Newman, E. A. (2010). Glial and neuronal control of brain blood flow. *Nature*, 468(7321):232–43.

Attwell, D. and Iadecola, C. (2002). The neural basis of functional brain imaging signals. *Trends Neurosci.*, 25(12):621–5.

Attwell, D. and Laughlin, S. B. (2001). An energy budget for signaling in the grey matter of the brain. *J. Cereb. Blood Flow Metab.*, 21(10):1133–45.

Attwell, D., Mishra, A., Hall, C. N., O'Farrell, F. M., and Dalkara, T. (2016). What is a pericyte? *J. Cereb. Blood Flow Metab.*, 36(2):451–5.

Auer, L. M. (1981). Pial arterial vasodilation by intravenous nimodipine in cats. *Arzneimittelforschung.*, 31(9):1423–5.

Ayata, C., Ma, J., Meng, W., Huang, P., and Moskowitz, M. A. (1996). L-NA-sensitive rCBF augmentation during vibrissal stimulation in type III nitric oxide synthase mutant mice. *J. Cereb. Blood Flow Metab.*, 16(4):539–41.

Badhiwala, J. H., Nassiri, F., Alhazzani, W., Selim, M. H., Farrokhyar, F., Spears, J., Kulkarni, A. V., Singh, S., Alqahtani, A., Rochwerg, B., Alshahrani, M., Murty, N. K., Alhazzani, A., Yarascavitch, B., Reddy, K., Zaidat, O. O., and Almenawer, S. A. (2015). Endovascular Thrombectomy for Acute Ischemic Stroke: A Meta-analysis. *JAMA*, 314(17):1832–43.

Baker, W. B., Sun, Z., Hiraki, T., Putt, M. E., Durduran, T., Reivich, M., Yodh, A. G., and Greenberg, J. H. (2013). Neurovascular coupling varies with level of global cerebral ischemia in a rat model. *J. Cereb. Blood Flow Metab.*, 33(1):97–105.

Balami, J. S., Chen, R.-L., Grunwald, I. Q., and Buchan, A. M. (2011). Neurological complications of acute ischaemic stroke. *Lancet Neurol.*, 10(4):357–71.

Balami, J. S., Hadley, G., Sutherland, B. A., Karbalai, H., and Buchan, A. M. (2013). The exact science of stroke thrombolysis and the quiet art of patient selection. *Brain*, 136(Pt 12):3528–53.

Balami, J. S., Sutherland, B. A., Edmunds, L. D., Grunwald, I. Q., Neuhaus, A. A., Hadley, G., Karbalai, H., Metcalf, K. A., DeLuca, G. C., and Buchan, A. M. (2015). A systematic review and meta-analysis of randomized controlled trials of endovascular thrombectomy compared with best medical treatment for acute ischemic stroke. *Int. J. Stroke*, 10(8):1168–78.

Bandettini, P. A. (2012). The BOLD Plot Thickens: Sign- and Layer-Dependent Hemodynamic Changes with Activation. *Neuron*, 76(3):468–469.

Barnett, G. H., Bose, B., Little, J. R., Jones, S. C., and Friel, H. T. (1986). Effects of nimodipine on acute focal cerebral ischemia. *Stroke*, 17(5):884–90.

Barone, F. C., Globus, M. Y., Price, W. J., White, R. F., Storer, B. L., Feuerstein, G. Z., Busto, R., and Ohlstein, E. H. (1994). Endothelin levels increase in rat focal and global ischemia. *J. Cereb. Blood Flow Metab.*, 14(2):337–42.

Bazargani, N. and Attwell, D. (2016). Astrocyte calcium signaling: the third wave. *Nat. Neurosci.*, 19(2):182–9.

Bederson, J. B., Pitts, L. H., Germano, S. M., Nishimura, M. C., Davis, R. L., and Bartkowski, H. M. (1986a). Evaluation of 2,3,5-triphenyltetrazolium chloride as a stain for detection and quantification of experimental cerebral infarction in rats. *Stroke.*, 17(6):1304–1308.

Bederson, J. B., Pitts, L. H., Tsuji, M., Nishimura, M. C., Davis, R. L., and Bartkowski, H. (1986b). Rat middle cerebral artery occlusion: evaluation of the model and development of a neurologic examination. *Stroke*, 17(3):472–476.

Begley, C. G. and Ioannidis, J. P. A. (2015). Reproducibility in Science: Improving the Standard for Basic and Preclinical Research. *Circ. Res.*, 116(1):116–126.

Behm, D. J., Ogbonna, A., Wu, C., Burns-Kurtis, C. L., and Douglas, S. A. (2009). Epoxyeicosatrienoic acids function as selective, endogenous antagonists of native thromboxane receptors: identification of a novel mechanism of vasodilation. *J. Pharmacol. Exp. Ther.*, 328(1):231–9.

Bell, R. D., Winkler, E. a., Sagare, A. P., Singh, I., LaRue, B., Deane, R., and Zlokovic, B. V. (2010). Pericytes Control Key Neurovascular Functions and Neuronal Phenotype in the Adult Brain and during Brain Aging. *Neuron*, 68(3):409–427.

Berger, L. and Hakim, A. M. (1988). Calcium channel blockers correct acidosis in ischemic rat brain without altering cerebral blood flow. *Stroke.*, 19(10):1257–61.

Berwick, J., Johnston, D., Jones, M., Martindale, J., Martin, C., Kennerley, A. J., Redgrave, P., and Mayhew, J. E. W. (2008). Fine detail of neurovascular coupling revealed by spatiotemporal analysis of the hemodynamic response to single whisker stimulation in rat barrel cortex. *J. Neurophysiol.*, 99(2):787–798.

Bhatia, R., Hill, M. D., Shobha, N., Menon, B., Bal, S., Kochar, P., Watson, T., Goyal, M., and Demchuk, A. M. (2010). Low rates of acute recanalization with intravenous recombinant tissue plasminogen activator in ischemic stroke: real-world experience and a call for action. *Stroke.*, 41(10):2254–8.

Binkofski, F. and Seitz, R. J. (2004). Modulation of the BOLD-response in early recovery from sensorimotor stroke. *Neurology*, 63(7):1223–1229.

Blicher, J. U., Stagg, C. J., O'Shea, J., Østergaard, L., MacIntosh, B. J., Johansen-Berg, H., Jezzard, P., Donahue, M. J., and Ostergaard, L. (2012). Visualization of altered neurovascular coupling in chronic stroke patients using multimodal functional MRI. *J. Cereb. Blood Flow Metab.*, 32(11):2044–54.

Boas, D. A. and Dunn, A. K. (2010). Laser speckle contrast imaging in biomedical optics. *J. Biomed. Opt.*, 15(1):011109.

Bochelen, D., Rudin, M., and Sauter, a. (1999). Calcineurin inhibitors FK506 and SDZ ASM 981 alleviate the outcome of focal cerebral ischemic/reperfusion injury. *J. Pharmacol. Exp. Ther.*, 288(2):653–9.

Bogousslavsky, J., Van Melle, G., and Regli, F. (1988). The Lausanne Stroke Registry: analysis of 1,000 consecutive patients with first stroke. *Stroke.*, 19(9):1083–92.

Bolotina, V. M., Najibi, S., Palacino, J. J., Pagano, P. J., and Cohen, R. A. (1994). Nitric oxide directly activates calcium-dependent potassium channels in vascular smooth muscle. *Nature*, 368(6474):850–3.

Bonakdarpour, B., Beeson, P. M., DeMarco, A. T., and Rapcsak, S. Z. (2015). Variability in blood oxygen level dependent (BOLD) signal in patients with stroke-induced and primary progressive aphasia. *NeuroImage. Clin.*, 8:87–94.

Bonder, D. E. and McCarthy, K. D. (2014). Astrocytic Gq-GPCR-Linked IP3R-Dependent Ca2+ Signaling Does Not Mediate Neurovascular Coupling in Mouse Visual Cortex In Vivo. *J. Neurosci.*, 34(39):13139–13150.

Bouvier, J., Detante, O., Tahon, F., Attye, A., Perret, T., Chechin, D., Barbieux, M., Boubagra, K., Garambois, K., Tropres, I., Grand, S., Barbier, E. L., and Krainik, A. (2015). Reduced CMRO2 and cerebrovascular reserve in patients with severe intracranial arterial stenosis: a combined multiparametric qBOLD oxygenation and BOLD fMRI study. *Hum. Brain Mapp.*, 36(2):695–706.

Bray, N., Burrows, F. E., Jones, M., Berwick, J., Allan, S. M., and Schiessl, I. (2016). Decreased haemodynamic response and decoupling of cortical gamma-band activity and tissue oxygen perfusion after striatal interleukin-1 injection. *J. Neuroinflammation*, 13(1):195.

Bredt, D. S. and Snyder, S. H. (1989). Nitric oxide mediates glutamate-linked enhancement of cGMP levels in the cerebellum. *Proc. Natl. Acad. Sci. U. S. A.*, 86(22):9030–3.

Broskova, Z., Sotnikova, R., Nedelcevova, J., and Bagi, Z. (2013). Effect of a novel stobadine derivative on isolated rat arteries. *Interdiscip. Toxicol.*, 6(2):63–6.

Buchan, A. and Pulsinelli, W. A. (1990). Hypothermia but not the N-methyl-D-aspartate antagonist, MK-801, attenuates neuronal damage in gerbils subjected to transient global ischemia. *J. Neurosci.*, 10(1):311–316.

Buchan, A. M., Slivka, A., and Xue, D. (1992). The effect of the NMDA receptor antagonist MK-801 on cerebral blood flow and infarct volume in experimental focal stroke. *Brain Res.*, 574(1-2):171–7.

Burnett, M. G., Detre, J. a., and Greenberg, J. H. (2005). Activation-flow coupling during graded cerebral ischemia. *Brain Res.*, 1047(1):112–8.

Busija, D. W. and Leffler, C. W. (1989). Dilator effects of amino acid neurotransmitters on piglet pial arterioles. *Am. J. Physiol.*, 257(4 Pt 2):H1200–H1203.

Caesar, K., Hashemi, P., Douhou, A., Bonvento, G., Boutelle, M. G., Walls, A. B., and Lauritzen, M. (2008). Glutamate receptor-dependent increments in lactate, glucose and oxygen metabolism evoked in rat cerebellum in vivo. *J. Physiol.*, 586(5):1337–1349.

Caesar, K., Thomsen, K., and Lauritzen, M. (2003). Dissociation of spikes, synaptic activity, and activity-dependent increments in rat cerebellar blood flow by tonic synaptic inhibition. *Proc. Natl. Acad. Sci. U. S. A.*, 100(26):16000–5.

Campbell, W. B., Gebremedhin, D., Pratt, P. F., and Harder, D. R. (1996). Identification of epoxyeicosatrienoic acids as endothelium-derived hyperpolarizing factors. *Circ. Res.*, 78(3):415–23.

Carey, L. M., Seitz, J., and Seitz, R. J. (2007). Functional neuroimaging in stroke recovery and neurorehabilitation: conceptual issues and perspectives. *Int. J. Stroke*, 2(4):245–64.

Carrera, E. and Tononi, G. (2014). Diaschisis: past, present, future. *Brain*, 137(9):2408–2422.

Cauli, B. and Hamel, E. (2010). Revisiting the role of neurons in neurovascular coupling. *Front. Neuroenergetics*, 2(June):9.

Cauli, B., Tong, X.-K., Rancillac, A., Serluca, N., Lambolez, B., Rossier, J., and Hamel, E. (2004). Cortical GABA interneurons in neurovascular coupling: relays for subcortical vasoactive pathways. *J. Neurosci.*, 24(41):8940–9.

Chakravarthy, U., McGinty, A., McKillop, J., Anderson, P., Archer, D. B., and Trimble, E. R. (1994). Altered endothelin-1 induced contraction and second messenger generation in bovine retinal microvascular pericytes cultured in high glucose medium. *Diabetologia*, 37(1):36–42.

Chamley, J. H., Campbell, G. R., McConnell, J. D., and Gröschel-Stewart, U. (1977). Comparison of vascular smooth muscle cells from adult human, monkey and rabbit in primary culture and in subculture. *Cell Tissue Res.*, 177(4):503–22.

Chan, P. H. (2001). Reactive oxygen radicals in signaling and damage in the ischemic brain. *J. Cereb. Blood Flow Metab.*, 21(1):2–14.

Chang, J. C., Shook, L. L., Biag, J., Nguyen, E. N., Toga, A. W., Charles, A. C., and Brennan, K. C. (2010). Biphasic direct current shift, haemoglobin desaturation and neurovascular uncoupling in cortical spreading depression. *Brain*, 133(Pt 4):996–1012.

Chen, B. R., Kozberg, M. G., Bouchard, M. B., Shaik, M. A., and Hillman, E. M. C. (2014). A critical role for the vascular endothelium in functional neurovascular coupling in the brain. *J. Am. Heart Assoc.*, 3(3):e000787–e000787.

Chen, Z. M., Sandercock, P., Pan, H. C., Counsell, C., Collins, R., Liu, L. S., Xie, J. X., Warlow, C., and Peto, R. (2000). Indications for early aspirin use in acute ischemic stroke : A combined analysis of 40 000 randomized patients from the chinese acute stroke trial and the international stroke trial. On behalf of the CAST and IST collaborative groups. *Stroke.*, 31(6):1240–9.

Chiang, J., Kowada, M., Ames, A., Wright, R. L., and Majno, G. (1968). Cerebral ischemia. III. Vascular changes. *Am. J. Pathol.*, 52(2):455–76.

Cholet, N., Seylaz, J., Lacombe, P., and Bonvento, G. (1997). Local uncoupling of the cerebrovascular and metabolic responses to somatosensory stimulation after neuronal nitric oxide synthase inhibition. *J. Cereb. Blood Flow Metab.*, 17(11):1191–201.

Christ, G. J., Spray, D. C., El-Sabban, M., Moore, L. K., and Brink, P. R. (1996). Gap Junctions in Vascular Tissues: Evaluating the Role of Intercellular Communication in the Modulation of Vasomotor Tone. *Circ. Res.*, 79(4):631–646.

Chueh, J.-Y., Puri, A. S., Wakhloo, A. K., and Gounis, M. J. (2016). Risk of distal embolization with stent retriever thrombectomy and ADAPT. *J. Neurointerv. Surg.*, 8(2):197–202.

Chuquet, J., Hollender, L., and Nimchinsky, E. a. (2007). High-resolution in vivo imaging of the neurovascular unit during spreading depression. *J. Neurosci.*, 27(15):4036–44.

Cipolla, M. J. and Bullinger, L. V. (2008). Reactivity of brain parenchymal arterioles after ischemia and reperfusion. *Microcirculation*, 15(6):495–501.

Cipolla, M. J., Chan, S.-L. S. L., Sweet, J., Tavares, M. J., Gokina, N., and Brayden, J. E. (2014). Postischemic reperfusion causes smooth muscle calcium sensitization and vasoconstriction of parenchymal arterioles. *Stroke*, 45(8):2425–2430.

Cipolla, M. J. and Curry, A. B. (2002). Middle cerebral artery function after stroke: the threshold duration of reperfusion for myogenic activity. *Stroke*, 33(8):2094–2099.

Cipolla, M. J., McCall, A. L., Lessov, N., and Porter, J. M. (1997). Reperfusion decreases myogenic reactivity and alters middle cerebral artery function after focal cerebral ischemia in rats. *Stroke.*, 28(1):176–80.

Cramer, S. C. (2008a). Repairing the human brain after stroke: I. Mechanisms of spontaneous recovery. *Ann. Neurol.*, 63(3):272–87.

Cramer, S. C. (2008b). Repairing the human brain after stroke. II. Restorative therapies. *Ann. Neurol.*, 63(5):549–60.

Cuevas, P., Gutierrez-Diaz, J. A., Reimers, D., Dujovny, M., Diaz, F. G., and Ausman, J. I. (1984). Pericyte endothelial gap junctions in human cerebral capillaries. *Anat. Embryol. (Berl).*, 170(2):155–159.

Dabertrand, F., Nelson, M. T., and Brayden, J. E. (2013). Ryanodine receptors, calcium signaling, and regulation of vascular tone in the cerebral parenchymal microcirculation. *Microcirculation*, 20(4):307–16.

Dalkara, T. and Alarcon-Martinez, L. (2015). Cerebral microvascular pericytes and neurogliovascular signaling in health and disease. *Brain Res.*, 1623:3–17.

Dalkara, T. and Arsava, E. M. (2012). Can restoring incomplete microcirculatory reperfusion improve stroke outcome after thrombolysis? *J. Cereb. Blood Flow Metab.*, 32(12):2091–2099.

Daneman, R., Zhou, L., Kebede, A. a., and Barres, B. a. (2010). Pericytes are required for blood-brain barrier integrity during embryogenesis. *Nature*, 468(7323):562–6.

Date, H. and Hossmann, K. A. (1984). Effect of vasodilating drugs on intracortical and extracortical vascular resistance following middle cerebral artery occlusion in cats. *Ann. Neurol.*, 16(3):330–6.

Davis, R. J., Murdoch, C. E., Ali, M., Purbrick, S., Ravid, R., Baxter, G. S., Tilford, N., Sheldrick, R. L. G., Clark, K. L., and Coleman, R. A. (2004). EP4 prostanoid receptor-mediated vasodilatation of human middle cerebral arteries. *Br. J. Pharmacol.*, 141(4):580–5.

Dawson, T. M., Steiner, J. P., Dawson, V. L., Dinerman, J. L., Uhl, G. R., and Snyder, S. H. (1993). Immunosuppressant FK506 enhances phosphorylation of nitric oxide synthase and protects against glutamate neurotoxicity. *Proc. Natl. Acad. Sci. U. S. A.*, 90(21):9808–12.

Dawson, V. L., Dawson, T. M., London, E. D., Bredt, D. S., and Snyder, S. H. (1991). Nitric oxide mediates glutamate neurotoxicity in primary cortical cultures. *Proc. Natl. Acad. Sci. U. S. A.*, 88(14):6368–6371.

de Haan, B., Rorden, C., and Karnath, H.-O. (2013a). Abnormal perilesional BOLD signal is not correlated with stroke patients' behavior. *Front. Hum. Neurosci.*, 7(October):1–10.

de Haan, B., Rorden, C., and Karnath, H.-O. (2013b). Abnormal perilesional BOLD signal is not correlated with stroke patients' behavior. *Front. Hum. Neurosci.*, 7(October):669.

de la Torre, J. C. (1991). Synergic activity of combined prostacyclin: dimethyl sulfoxide in experimental brain ischemia. *Can. J. Physiol. Pharmacol.*, 69(2):191–8.

Dehouck, M. P., Vigne, P., Torpier, G., Breittmayer, J. P., Cecchelli, R., and Frelin, C. (1997). Endothelin-1 as a mediator of endothelial cell-pericyte interactions in bovine brain capillaries. *J. Cereb. Blood Flow Metab.*, 17(4):464–9.

del Zoppo, G. J., Schmid-Schönbein, G. W., Mori, E., Copeland, B. R., and Chang, C. M. (1991). Polymorphonuclear leukocytes occlude capillaries following middle cerebral artery occlusion and reperfusion in baboons. *Stroke.*, 22(10):1276–83.

Derdeyn, C. P., Videen, T. O., Fritsch, S. M., Carpenter, D. a., Grubb, R. L., and Powers, W. J. (1999). Compensatory mechanisms for chronic cerebral hypoperfusion in patients with carotid occlusion. *Stroke.*, 30(5):1019–1024.

D'Esposito, M., Deouell, L. Y., and Gazzaley, A. (2003). Alterations in the BOLD fMRI signal with ageing and disease: a challenge for neuroimaging. *Nat. Rev. Neurosci.*, 4(11):863–872.

Devonshire, I. M., Papadakis, N. G., Port, M., Berwick, J., Kennerley, A. J., Mayhew, J. E. W., and Overton, P. G. (2012). Neurovascular coupling is brain region-dependent. *Neuroimage*, 59(3):1997–2006.

Devor, A., Dunn, A. K., Andermann, M. L., Ulbert, I., Boas, D. A., and Dale, A. M. (2003). Coupling of total hemoglobin concentration, oxygenation, and neural activity in rat somatosensory cortex. *Neuron*, 39(2):353–9.

Devor, A., Sakadžić, S., Srinivasan, V. J., Yaseen, M. A., Nizar, K., Saisan, P. A., Tian, P., Dale, A. M., Vinogradov, S. A., Franceschini, M. A., and Boas, D. A. (2012). Frontiers in optical imaging of cerebral blood flow and metabolism. *J. Cereb. Blood Flow Metab.*, 32(7):1259–76.

Dijkhuizen, R. M., Singhal, A. B., Mandeville, J. B., Wu, O., Halpern, E. F., Finklestein, S. P., Rosen, B. R., and Lo, E. H. (2003). Correlation between brain reorganization, ischemic damage, and neurologic status after transient focal cerebral ischemia in rats: a functional magnetic resonance imaging study. *J. Neurosci.*, 23(2):510–7.

Dijkhuizen, R. M. M., Ren, J., Mandeville, J. B. B., Wu, O., Ozdag, F. M. M., Moskowitz, M. A. a., Rosen, B. R. R., and Finklestein, S. P. P. (2001). Functional magnetic resonance imaging of reorganization in rat brain after stroke. *Proc. Natl. Acad. Sci. U. S. A.*, 98(22):12766–71.

Dirnagl, U., Hakim, A., Macleod, M., Fisher, M., Howells, D., Alan, S. M., Steinberg, G., Planas, A., Boltze, J., Savitz, S., Iadecola, C., and Meairs, S. (2013). A Concerted Appeal for International Cooperation in Preclinical Stroke Research. *Stroke*, 44(6):1754–1760.

Dirnagl, U., Iadecola, C., and Moskowitz, M. a. (1999). Pathobiology of ischaemic stroke: an integrated view. *Trends Neurosci.*, 22(9):391–7.

Dirnagl, U., Jacewicz, M., and Pulsinelli, W. (1990). Nimodipine posttreatment does not increase blood flow in rats with focal cortical ischemia. *Stroke.*, 21(9):1357–61.

Dirnagl, U., Lindauer, U., and Villringer, A. (1993). Role of nitric oxide in the coupling of cerebral blood flow to neuronal activation in rats. *Neurosci. Lett.*, 149(1):43–46.

Dirnagl, U., Niwa, K., Lindauer, U., and Villringer, A. (1994). Coupling of cerebral blood flow to neuronal activation: role of adenosine and nitric oxide. *Am. J. Physiol.*, 267(1 Pt 2):H296–H301.

Dobkin, J. a., Levine, R. L., Lagreze, H. L., Dulli, D. A., Nickles, R. J., and Rowe, B. R. (1989). Evidence for transhemispheric diaschisis in unilateral stroke. *Arch. Neurol.*, 46(12):1333–6.

Domoki, F., Perciaccante, J. V., Shimizu, K., Puskar, M., Busija, D. W., and Bari, F. (2002). N-methyl-D-aspartate-induced vasodilation is mediated by endothelium-independent nitric oxide release in piglets. *Am. J. Physiol. Heart Circ. Physiol.*, 282(4):H1404–H1409.

Donahue, M. J., Strother, M. K., and Hendrikse, J. (2012). Novel MRI approaches for assessing cerebral hemodynamics in ischemic cerebrovascular disease. *Stroke.*, 43(3):903–15.

Donnan, G. a., Davis, S. M., Parsons, M. W., Ma, H., Dewey, H. M., and Howells, D. W. (2011). How to make better use of thrombolytic therapy in acute ischemic stroke. *Nat. Rev. Neurol.*, 7(7):400–9.

Dorhout Mees, S. M., Rinkel, G. J. E., Feigin, V. L., Algra, A., van den Bergh, W. M., Vermeulen, M., and van Gijn, J. (2007). Calcium antagonists for aneurysmal subarachnoid haemorrhage. *Cochrane database Syst. Rev.*, (3):CD000277.

Draijer, M., Hondebrink, E., van Leeuwen, T., and Steenbergen, W. (2009). Review of laser speckle contrast techniques for visualizing tissue perfusion. *Lasers Med. Sci.*, 24(4):639–51.

Dreier, J. P., Ebert, N., Priller, J., Megow, D., Lindauer, U., Klee, R., Reuter, U., Imai, Y., Einhäupl, K. M., Victorov, I., and Dirnagl, U. (2000). Products of hemolysis in the subarachnoid space inducing spreading ischemia in the cortex and focal necrosis in rats: a model for delayed ischemic neurological deficits after subarachnoid hemorrhage? *J. Neurosurg.*, 93(4):658–666.

Dreier, J. P., Körner, K., Ebert, N., Görner, a., Rubin, I., Back, T., Lindauer, U., Wolf, T., Villringer, a., Einhäupl, K. M., Lauritzen, M., and Dirnagl, U. (1998). Nitric oxide scavenging by hemoglobin or nitric oxide synthase inhibition by N-nitro-L-arginine induces cortical spreading ischemia when K+ is increased in the subarachnoid space. *J. Cereb. Blood Flow Metab.*, 18(9):978–90.

Dreier, J. P., Major, S., Manning, A., Woitzik, J., Drenckhahn, C., Steinbrink, J., Tolias, C., Oliveira-Ferreira, A. I., Fabricius, M., Hartings, J. A., Vajkoczy, P., Lauritzen, M., Dirnagl, U., Bohner, G., and Strong, A. J. (2009). Cortical spreading ischaemia is a novel process involved in ischaemic damage in patients with aneurysmal subarachnoid haemorrhage. *Brain*, 132(Pt 7):1866–81.

Dreier, J. P., Windmüller, O., Petzold, G., Lindauer, U., Einhäupl, K. M., and Dirnagl, U. (2002). Ischemia caused by inverse coupling between neuronal activation and cerebral blood flow in rats. *Int. Congr. Ser.*, 1235:487–492.

Duchemin, S., Boily, M., Sadekova, N., and Girouard, H. (2012). The complex contribution of NOS interneurons in the physiology of cerebrovascular regulation. *Front. Neural Circuits*, 6(August):51.

Duffy, S. and MacVicar, B. a. (1996). In vitro ischemia promotes calcium influx and intracellular calcium release in hippocampal astrocytes. *J. Neurosci.*, 16(1):71–81.

Dunn, A. K. (2012). Laser speckle contrast imaging of cerebral blood flow. *Ann. Biomed. Eng.*, 40(2):367–77.

Eilaghi, A., Brooks, J., D'Esterre, C., Zhang, L., Swartz, R. H., Lee, T.-Y., and Aviv, R. I. (2013). Reperfusion is a stronger predictor of good clinical outcome than recanalization in ischemic stroke. *Radiology*, 269(1):240–8.

Ellis, E. F., Wei, E. P., and Kontos, H. A. (1979). Vasodilation of cat cerebral arterioles by prostaglandins D2, E2, G2, and I2. *Am. J. Physiol.*, 237(3):H381–H385.

Enager, P., Gold, L., and Lauritzen, M. (2004). Impaired neurovascular coupling by transhemispheric diaschisis in rat cerebral cortex. *J. Cereb. Blood Flow Metab.*, 24(7):713–9.

Enager, P., Piilgaard, H., Offenhauser, N., Kocharyan, A., Fernandes, P., Hamel, E., and Lauritzen, M. (2009). Pathway-specific variations in neurovascular and neurometabolic coupling in rat primary somatosensory cortex. *J. Cereb. Blood Flow Metab.*, 29(5):976–86.

Errede, M., Girolamo, F., Ferrara, G., Strippoli, M., Morando, S., Boldrin, V., Rizzi, M., Uccelli, A., Perris, R., Bendotti, C., Salmona, M., Roncali, L., and Virgintino, D. (2012). Blood-brain barrier alterations in the cerebral cortex in experimental autoimmune encephalomyelitis. *J. Neuropathol. Exp. Neurol.*, 71(10):840–54.

Estrada, C., Mengual, E., and González, C. (1993). Local NADPH-diaphorase neurons innervate pial arteries and lie close or project to intracerebral blood vessels: a possible role for nitric oxide in the regulation of cerebral blood flow. *J. Cereb. Blood Flow Metab.*, 13(6):978–84.

Fabricius, M., Akgoren, N., and Lauritzen, M. (1995). Arginine-nitric oxide pathway and cerebrovascular regulation in cortical spreading depression. *Am. J. Physiol.*, 269(1 Pt 2):H23–H29.

Fabry, B., Maksym, G. N., Butler, J. P., Glogauer, M., Navajas, D., and Fredberg, J. J. (2001). Scaling the microrheology of living cells. *Phys. Rev. Lett.*, 87(14):148102.

Faraci, F. M. and Breese, K. R. (1993). Nitric oxide mediates vasodilatation in response to activation of N- methyl-D-aspartate receptors in brain. *Circ. Res.*, 72(2):476–480.

Feger, G. I., Schilling, L., Ehrenreich, H., and Wahl, M. (1997). Endothelium-dependent relaxation counteracting the contractile action of endothelin-1 is partly due to ETB receptor activation. *Res. Exp. Med.*, 196(6):327–37.

Feigin, V. L., Forouzanfar, M. H., Krishnamurthi, R., Mensah, G. a., Connor, M., Bennett, D. a., Moran, A. E., Sacco, R. L., Anderson, L., Truelsen, T., O'Donnell, M., Venketasubramanian, N., Barker-Collo, S., Lawes, C. M. M., Wang, W., Shinohara, Y., Witt, E., Ezzati, M., Naghavi, M., and Murray, C. (2014). Global and regional burden of stroke during 1990–2010: findings from the Global Burden of Disease Study 2010. *Lancet*, 383(9913):245–255.

Fernández-Klett, F., Offenhauser, N., Dirnagl, U., Priller, J., and Lindauer, U. (2010). Pericytes in capillaries are contractile in vivo, but arterioles mediate functional hyperemia in the mouse brain. *Proc. Natl. Acad. Sci. U. S. A.*, 107(51):22290–5.

Ferro, J. M. and Fonseca, A. C. (2014). Clinical features of acute stroke. In *Oxford Textb. Stroke Cerebrovasc. Dis.*, pages 85–93. Oxford University Press.

Fields, R. D. (2008). Oligodendrocytes changing the rules: action potentials in glia and oligodendrocytes controlling action potentials. *Neuroscientist*, 14(6):540–3.

Figueroa, X. F. and Duling, B. R. (2009). Gap Junctions in the Control of Vascular Function. *Antioxid. Redox Signal.*, 11(2):251–266.

Filosa, J. A., Bonev, A. D., Straub, S. V., Meredith, A. L., Wilkerson, M. K., Aldrich, R. W., and Nelson, M. T. (2006). Local potassium signaling couples neuronal activity to vasodilation in the brain. *Nat. Neurosci.*, 9(11):1397–1403.

Fischer, E. G., Ames, A., Hedley-Whyte, E. T., and O'Gorman, S. (1977). Reassessment of cerebral capillary changes in acute global ischemia and their relationship to the "no-reflow phenomenon". *Stroke.*, 8(1):36–9.

Fischer, E. G., Ames, A., and Lorenzo, A. V. (1979). Cerebral blood flow immediately following brief circulatory stasis. *Stroke.*, 10(4):423–7.

Fisher, M., Feuerstein, G., Howells, D. W., Hurn, P. D., Kent, T. A., Savitz, S. I., and Lo, E. H. (2009). Update of the stroke therapy academic industry roundtable preclinical recommendations. *Stroke*, 40(6):2244–2250.

Ford, J. M., Johnson, M. B., Whitfield, S. L., Faustman, W. O., and Mathalon, D. H. (2005). Delayed hemodynamic responses in schizophrenia. *Neuroimage*, 26(3):922–31.

Fordsmann, J. C., Ko, R. W. Y., Choi, H. B., Thomsen, K., Witgen, B. M., Mathiesen, C., Lønstrup, M., Piilgaard, H., Macvicar, B. a., and Lauritzen, M. (2013). Increased 20-HETE Synthesis Explains Reduced Cerebral Blood Flow But Not Impaired Neurovascular Coupling after Cortical Spreading Depression in Rat Cerebral Cortex. *J. Neurosci.*, 33(6):2562–70.

Forsman, M., Aarseth, H. P., Nordby, H. K., Skulberg, A., and Steen, P. A. (1989). Effects of nimodipine on cerebral blood flow and cerebrospinal fluid pressure after cardiac arrest: correlation with neurologic outcome. *Anesth. Analg.*, 68(4):436–43.

Fox, P. T. and Raichle, M. E. (1986). Focal physiological uncoupling of cerebral blood flow and oxidative metabolism during somatosensory stimulation in human subjects. *Proc. Natl. Acad. Sci. U. S. A.*, 83(4):1140–4.

Fritzsch, C., Rosengarten, B., Guschlbauer, B., Weiller, C., Hetzel, A., and Reinhard, M. (2010). Neurovascular coupling and cerebral autoregulation in patients with stenosis of the posterior cerebral artery. *J. Neuroimaging*, 20(4):368–72.

Fujimoto, T. and Singer, S. J. (1987). Immunocytochemical studies of desmin and vimentin in pericapillary cells of chicken. *J. Histochem. Cytochem.*, 35(10):1105–15.

Garcia, J. H., Liu, K. F., Yoshida, Y., Chen, S., and Lian, J. (1994). Brain microvessels: factors altering their patency after the occlusion of a middle cerebral artery (Wistar rat). *Am. J. Pathol.*, 145(3):728–40.

Garcia, J. H., Wagner, S., Liu, K. F., and Hu, X. J. (1995). Neurological deficit and extent of neuronal necrosis attributable to middle cerebral artery occlusion in rats. Statistical validation. *Stroke.*, 26(4):627–34; discussion 635.

GBD 2013 Mortality and Causes of Death Collaborators (2015). Global, regional, and national age-sex specific all-cause and cause-specific mortality for 240 causes of death, 1990-2013: a systematic analysis for the Global Burden of Disease Study 2013. *Lancet (London, England)*, 385(9963):117–71.

Gebremedhin, D., Lange, a. R., Lowry, T. F., Taheri, M. R., Birks, E. K., Hudetz, a. G., Narayanan, J., Falck, J. R., Okamoto, H., Roman, R. J., Nithipatikom, K., Campbell, W. B., and Harder, D. R. (2000). Production of 20-HETE and its role in autoregulation of cerebral blood flow. *Circ. Res.*, 87(1):60–65.

Gebremedhin, D., Lange, A. R., Narayanan, J., Aebly, M. R., Jacobs, E. R., and Harder, D. R. (1998). Cat cerebral arterial smooth muscle cells express cytochrome P450 4A2 enzyme and produce the vasoconstrictor 20-HETE which enhances L-type Ca2+ current. *J. Physiol.*, 507(3):771–781.

Gebremedhin, D., Ma, Y. H., Falck, J. R., Roman, R. J., VanRollins, M., and Harder, D. R. (1992). Mechanism of action of cerebral epoxyeicosatrienoic acids on cerebral arterial smooth muscle. *Am. J. Physiol.*, 263(2 Pt 2):H519–H525.

Gebremedhin, D., Yamaura, K., Zhang, C., Bylund, J., Koehler, R. C., and Harder, D. R. (2003). Metabotropic glutamate receptor activation enhances the activities of two types of Ca2+-activated k+ channels in rat hippocampal astrocytes. *J. Neurosci.*, 23(5):1678–87.

Ghai, G., Francis, J. E., Williams, M., Dotson, R. A., Hopkins, M. F., Cote, D. T., Goodman, F. R., and Zimmerman, M. B. (1987). Pharmacological characterization of CGS 15943A: a novel nonxanthine adenosine antagonist. *J. Pharmacol. Exp. Ther.*, 242(3):784–90.

Ghosh, A., Wyss, M. T., and Weber, B. (2013). Somatotopic astrocytic activity in the somatosensory cortex. *Glia*, 61(4):601–10.

Ginsberg, M. D., Castella, Y., Dietrich, W. D., Watson, B. D., and Busto, R. (1989). Acute thrombotic infarction suppresses metabolic activation of ipsilateral somatosensory cortex: evidence for functional diaschisis. *J. Cereb. Blood Flow Metab.*, 9(3):329–41.

Girouard, H., Bonev, A. D., Hannah, R. M., Meredith, A., Aldrich, R. W., and Nelson, M. T. (2010). Astrocytic endfoot Ca2+ and BK channels determine both arteriolar dilation and constriction. *Proc. Natl. Acad. Sci. U. S. A.*, 107(8):3811–3816.

Goense, J., Merkle, H., and Logothetis, N. K. (2012). High-Resolution fMRI Reveals Laminar Differences in Neurovascular Coupling between Positive and Negative BOLD Responses. *Neuron*, 76(3):629–639.

Goldman, S. A. and Chen, Z. (2011). Perivascular instruction of cell genesis and fate in the adult brain. *Nat. Neurosci.*, 14(11):1382–9.

Gordon, G. R. J., Choi, H. B., Rungta, R. L., Ellis-Davies, G. C. R., and MacVicar, B. A. (2008). Brain metabolism dictates the polarity of astrocyte control over arterioles. *Nature*, 456(7223):745–9.

Gotoh, J., Kuang, T. Y., Nakao, Y., Cohen, D. M., Melzer, P., Itoh, Y., Pak, H., Pettigrew, K., and Sokoloff, L. (2001). Regional differences in mechanisms of cerebral circulatory response to neuronal activation. *Am. J. Physiol. Heart Circ. Physiol.*, 280(2):H821–9.

Gotoh, O., Mohamed, A. A., McCulloch, J., Graham, D. I., Harper, A. M., and Teasdale, G. M. (1986). Nimodipine and the Haemodynamic and Histopathological Consequences of Middle Cerebral Artery Occlusion in the Rat. *J. Cereb. Blood Flow Metab.*, 6(3):321–331.

Goyal, M., Menon, B. K., van Zwam, W. H., Dippel, D. W. J., Mitchell, P. J., Demchuk, A. M., Dávalos, A., Majoie, C. B. L. M., van der Lugt, A., de Miquel, M. A., Donnan, G. A., Roos, Y. B. W. E. M., Bonafe, A., Jahan, R., Diener, H.-C., van den Berg, L. A., Levy, E. I., Berkhemer, O. A., Pereira, V. M., Rempel, J., Millán, M., Davis, S. M., Roy, D., Thornton, J., Román, L. S., Ribó, M., Beumer, D., Stouch, B., Brown, S., Campbell, B. C. V., van Oostenbrugge, R. J., Saver, J. L., Hill, M. D., Jovin, T. G., and collaborators, H. (2016). Endovascular thrombectomy after large-vessel ischaemic stroke: a meta-analysis of individual patient data from five randomised trials. *Lancet (London, England)*, 387(10029):1723–31.

Grubb, R. L., Raichle, M. E., Eichling, J. O., and Ter-Pogossian, M. M. (1974). The Effects of Changes in PaCO2 Cerebral Blood Volume, Blood Flow, and Vascular Mean Transit Time. *Stroke*, 5(5):630–639.

Guiou, M., Sheth, S., Nemoto, M., Walker, M., Pouratian, N., Ba, A., and Toga, A. W. (2005). Cortical spreading depression produces long-term disruption of activity-related changes in cerebral blood volume and neurovascular coupling. *J. Biomed. Opt.*, 10(1):11004.

Guo, Y., Zhou, I. Y., Chan, S.-T., Wang, Y., Mandeville, E. T., Igarashi, T., Lo, E. H., Ji, X., and Sun, P. Z. (2016). pH-sensitive MRI demarcates graded tissue acidification during acute stroke – pH specificity enhancement with magnetization transfer and relaxation-normalized amide proton transfer (APT) MRI. *Neuroimage*, 141:242–249.

Gutiérrez-Jiménez, E., Cai, C., Mikkelsen, I. K., Rasmussen, P. M., Angleys, H., Merrild, M., Mouridsen, K., Jespersen, S. N., Lee, J., Iversen, N. K., Sakadzic, S., and Østergaard, L. (2016). Effect of electrical forepaw stimulation on capillary transit-time heterogeneity (CTH). *J. Cereb. Blood Flow Metab.*

Haapaniemi, E., Tatlisumak, T., Hamel, K., Soinne, L., Lanni, C., Opgenorth, T. J., and Kaste, M. (2000). Plasma endothelin-1 levels neither increase nor correlate with neurological scores, stroke risk factors, or outcome in patients with ischemic stroke. *Stroke.*, 31(3):720–5.

Hachinski, V., Donnan, G. A., Gorelick, P. B., Hacke, W., Cramer, S. C., Kaste, M., Fisher, M., Brainin, M., Buchan, A. M., Lo, E. H., Skolnick, B. E., Furie, K. L., Hankey, G. J., Kivipelto, M., Morris, J., Rothwell, P. M., Sacco, R. L., Smith, S. C., Wang, Y., Bryer, A., Ford, G. A., Iadecola, C., Martins, S. C. O., Saver, J., Skvortsova, V., Bayley, M., Bednar, M. M., Duncan, P., Enney, L., Finklestein, S., Jones, T. A., Kalra, L., Kleim, J., Nitkin, R., Teasell, R., Weiller, C., Desai, B., Goldberg, M. P., Heiss, W.-D., Saarelma, O., Schwamm, L. H., Shinohara, Y., Trivedi, B., Wahlgren, N., Wong, L. K., Hakim, A., Norrving, B., Prudhomme, S., Bornstein, N. M., Davis, S. M., Goldstein, L. B., Leys, D., and Tuomilehto, J. (2010). Stroke: working toward a prioritized world agenda. *Stroke.*, 41(6):1084–99.

Hachinski, V. C., Iliff, L. D., Zilhka, E., Du Boulay, G. H., McAllister, V. L., Marshall, J., Russell, R. W., and Symon, L. (1975). Cerebral blood flow in dementia. *Arch. Neurol.*, 32(9):632–7.

Haefliger, I. O., Zschauer, A., and Anderson, D. R. (1994). Relaxation of retinal pericyte contractile tone through the nitric oxide-cyclic guanosine monophosphate pathway. *Invest. Ophthalmol. Vis. Sci.*, 35(3):991–7.

Hahn, T., Heinzel, S., Plichta, M. M., Reif, A., Lesch, K.-P., and Fallgatter, A. J. (2011). Neurovascular coupling in the human visual cortex is modulated by cyclooxygenase-1 (COX-1) gene variant. *Cereb. Cortex*, 21(7):1659–66.

Hakim, A. M. (1986). Cerebral acidosis in focal ischemia: II. Nimodipine and verapamil normalize cerebral pH following middle cerebral artery occlusion in the rat. *J. Cereb. Blood Flow Metab.*, 6(6):676–83.

Hall, C. N., Reynell, C., Gesslein, B., Hamilton, N. B., Mishra, A., Sutherland, B. A., O'Farrell, F. M., Buchan, A. M., Lauritzen, M., and Attwell, D. (2014). Capillary pericytes regulate cerebral blood flow in health and disease. *Nature*.

Hamilton, N. B., Attwell, D., and Hall, C. N. (2010). Pericyte-mediated regulation of capillary diameter: a component of neurovascular coupling in health and disease. *Front. Neuroenergetics*, 2(May):1–14.

Hamzei, F., Knab, R., Weiller, C., and Röther, J. (2003). The influence of extra- and intracranial artery disease on the BOLD signal in FMRI. *Neuroimage*, 20(2):1393–9.

Hara, H., Onodera, H., Nagasawa, H., and Kogure, K. (1990). Effect of nimodipine on ischemia-induced brain edema and mortality in a novel transient middle cerebral artery occlusion model. *Jpn. J. Pharmacol.*, 53(2):247–53.

Harper, A. M., Craigen, L., and Kazda, S. (1981). Effect of the Calcium Antagonist, Nimodipine, on Cerebral Blood Flow and Metabolism in the Primate. *J. Cereb. Blood Flow Metab.*, 1(3):349–356.

Harris, A. K., Wild, P., and Stopak, D. (1980). Silicone rubber substrata: a new wrinkle in the study of cell locomotion. *Science*, 208(4440):177–9.

Harris, J. J. and Attwell, D. (2012). The energetics of CNS white matter. *J. Neurosci.*, 32(1):356–71.

Harris, R. J., Branston, N. M., Symon, L., Bayhan, M., and Watson, A. (1982). The effects of a calcium antagonist, nimodipine, upon physiological responses of the cerebral vasculature and its possible influence upon focal cerebral ischaemia. *Stroke.*, 13(6):759–66.

Harris, S., Bruyns-Haylett, M., Kennerley, A., Boorman, L., Overton, P. G., Ma, H., Zhao, M., Schwartz, T. H., and Berwick, J. (2013). The effects of focal epileptic activity on regional sensory-evoked neurovascular coupling and postictal modulation of bilateral sensory processing. *J. Cereb. Blood Flow Metab.*, 33(10):1595–604.

Hartmann, D. a., Underly, R. G., Grant, R. I., Watson, A. N., Lindner, V., and Shih, A. Y. (2015a). Pericyte structure and distribution in the cerebral cortex revealed by high-resolution imaging of transgenic mice. *Neurophotonics*, 2(4):041402.

Hartmann, D. A., Underly, R. G., Watson, A. N., and Shih, A. Y. (2015b). A murine toolbox for imaging the neurovascular unit. *Microcirculation*, 22(3):168–82.

Hata, A. N. and Breyer, R. M. (2004). Pharmacology and signaling of prostaglandin receptors: multiple roles in inflammation and immune modulation. *Pharmacol. Ther.*, 103(2):147–66.

Hauck, E. F., Apostel, S., Hoffmann, J. F., Heimann, A., and Kempski, O. (2004). Capillary flow and diameter changes during reperfusion after global cerebral ischemia studied by intravital video microscopy. *J. Cereb. Blood Flow Metab.*, 24(4):383–91.

Haws, C. W., Gourley, J. K., and Heistad, D. D. (1983). Effects of nimodipine on cerebral blood flow. *J. Pharmacol. Exp. Ther.*, 225(1):24–8.

He, B., Yang, L., Wilke, C., and Yuan, H. (2011). Electrophysiological imaging of brain activity and connectivity-challenges and opportunities. *IEEE Trans. Biomed. Eng.*, 58(7):1918–31.

Headrick, J. P., Ashton, K. J., Rose'meyer, R. B., and Peart, J. N. (2013). Cardiovascular adenosine receptors: expression, actions and interactions. *Pharmacol. Ther.*, 140(1):92–111.

Hein, T. W., Xu, W., and Kuo, L. (2006). Dilation of retinal arterioles in response to lactate: role of nitric oxide, guanylyl cyclase, and ATP-sensitive potassium channels. *Invest. Ophthalmol. Vis. Sci.*, 47(2):693–9.

Herman, I. M. (1985). Microvascular pericytes contain muscle and nonmuscle actins. *J. Cell Biol.*, 101(1):43–52.

Hill, R. A., Tong, L., Yuan, P., Murikinati, S., Gupta, S., and Grutzendler, J. (2015). Regional Blood Flow in the Normal and Ischemic Brain Is Controlled by Arteriolar Smooth Muscle Cell Contractility and Not by Capillary Pericytes. *Neuron*, 87(1):95–110.

Hillman, E. M. C. (2007). Optical brain imaging in vivo: techniques and applications from animal to man. *J. Biomed. Opt.*, 12(5):051402.

Hillman, E. M. C. (2014). Coupling Mechanism and Significance of the BOLD Signal: A Status Report. *Annu. Rev. Neurosci.*, 37:161–181.

Hirsch, S., Reichold, J., Schneider, M., Székely, G., and Weber, B. (2012). Topology and hemodynamics of the cortical cerebrovascular system. *J. Cereb. Blood Flow Metab.*, 32(6):952–67.

Hockerman, G. H., Peterson, B. Z., Johnson, B. D., and Catterall, W. A. (1997). Molecular determinants of drug binding and action on L-type calcium channels. *Annu. Rev. Pharmacol. Toxicol.*, 37:361–96.

Hoffmeyer, H. W., Enager, P., Thomsen, K. J., and Lauritzen, M. J. (2007). Nonlinear neurovascular coupling in rat sensory cortex by activation of transcallosal fibers. *J. Cereb. Blood Flow Metab.*, 27(3):575–87.

Horn, J., de Haan, R., Vermeulen, M., Luiten, P., and Limburg, M. (2001). Nimodipine in Animal Model Experiments of Focal Cerebral Ischemia: A Systematic Review. *Stroke*, 32(10):2433–2438.

Hossmann, K. A. (1997). Reperfusion of the brain after global ischemia: hemodynamic disturbances. *Shock*, 8(2):95–101; discussion 102–3.

Howarth, C., Gleeson, P., and Attwell, D. (2012). Updated energy budgets for neural computation in the neocortex and cerebellum. *J. Cereb. Blood Flow Metab.*, 32(7):1222–32.

Howells, D. W. and Macleod, M. R. (2013). Evidence-based translational medicine. *Stroke.*, 44(5):1466–1471.

Hristovska, A.-M. M., Rasmussen, L. E., Hansen, P. B. L., Nielsen, S. S., Nüsing, R. M., Narumiya, S., Vanhoutte, P., Skøtt, O., and Jensen, B. L. (2007). Prostaglandin E2 induces vascular relaxation by E-prostanoid 4 receptor-mediated activation of endothelial nitric oxide synthase. *Hypertension*, 50(3):525–530.

Hund-Georgiadis, M., Mildner, T., Georgiadis, D., Weih, K., and von Cramon, D. Y. (2003). Impaired hemodynamics and neural activation? A fMRI study of major cerebral artery stenosis. *Neurology*, 61(9):1276–9.

Iadecola, C. (2004). Neurovascular regulation in the normal brain and in Alzheimer's disease. *Nat. Rev. Neurosci.*, 5(5):347–60.

Iadecola, C. and Anrather, J. (2011). Stroke research at a crossroad: asking the brain for directions. *Nat. Neurosci.*, 14(11):1363–8.

Iadecola, C. and Nedergaard, M. (2007). Glial regulation of the cerebral microvasculature. *Nat. Neurosci.*, 10(11):1369–76.

Iannetti, G. D. and Wise, R. G. (2007). BOLD functional MRI in disease and pharmacological studies: room for improvement? *Magn. Reson. Imaging*, 25(6):978–88.

Imig, J. D., Simpkins, A. N., Renic, M., and Harder, D. R. (2011). Cytochrome P450 eicosanoids and cerebral vascular function. *Expert Rev. Mol. Med.*, 13(March 2011):e7.

Ito, H., Kanno, I., Shimosegawa, E., Tamura, H., Okane, K., and Hatazawa, J. (2002). Hemodynamic changes during neural deactivation in human brain: a positron emission tomography study of crossed cerebellar diaschisis. *Ann. Nucl. Med.*, 16(4):249–54.

Ito, U., Hakamata, Y., Kawakami, E., and Oyanagi, K. (2011). Temporary focal cerebral ischemia results in swollen astrocytic end-feet that compress microvessels and lead to focal cortical infarction. *J. Cereb. Blood Flow Metab.*, 31(1):328–338.

Itoh, Y. and Suzuki, N. (2012). Control of brain capillary blood flow. *J. Cereb. Blood Flow Metab.*, 32(7):1167–76.

Jacewicz, M., Brint, S., Tanabe, J., Wang, X. J., and Pulsinelli, W. A. (1990). Nimodipine pretreatment improves cerebral blood flow and reduces brain edema in conscious rats subjected to focal cerebral ischemia. *J. Cereb. Blood Flow Metab.*, 10(6):903–913.

Jay, T. M., Lucignani, G., Crane, A. M., Jehle, J., and Sokoloff, L. (1988). Measurement of local cerebral blood flow with [14C]iodoantipyrine in the mouse. *J. Cereb. Blood Flow Metab.*, 8(1):121–9.

Jespersen, S. N. and Østergaard, L. (2012). The roles of cerebral blood flow, capillary transit time heterogeneity, and oxygen tension in brain oxygenation and metabolism. *J. Cereb. Blood Flow Metab.*, 32(2):264–77.

Jiménez-Altayó, F., Martín, A., Rojas, S., Justicia, C., Briones, A. M., Giraldo, J., Planas, A. M., and Vila, E. (2007). Transient middle cerebral artery occlusion causes different structural, mechanical, and myogenic alterations in normotensive and hypertensive rats. *Am. J. Physiol. Heart Circ. Physiol.*, 293(1):H628–H635.

Jin, R., Yang, G., and Li, G. (2010). Inflammatory mechanisms in ischemic stroke: role of inflammatory cells. *J. Leukoc. Biol.*, 87(5):779–789.

Johnston, A. J., Steiner, L. A., Gupta, A. K., and Menon, D. K. (2003). Cerebral oxygen vasoreactivity and cerebral tissue oxygen reactivity. *Br. J. Anaesth.*, 90(6):774–86.

Jones, M., Berwick, J., Johnston, D., and Mayhew, J. (2001). Concurrent optical imaging spectroscopy and laser-Doppler flowmetry: the relationship between blood flow, oxygenation, and volume in rodent barrel cortex. *Neuroimage*, 13(6 Pt 1):1002–15.

Joyce, N. C., Haire, M. F., and Palade, G. E. (1985). Contractile proteins in pericytes. I. Immunoperoxidase localization of tropomyosin. *J. Cell Biol.*, 100(5):1379–86.

Kågström, E., Smith, M. L., and Siesjö, B. K. (1983a). Cerebral circulatory responses to hypercapnia and hypoxia in the recovery period following complete and incomplete cerebral ischemia in the rat. *Acta Physiol. Scand.*, 118(3):281–91.

Kågström, E., Smith, M. L., and Siesjö, B. K. (1983b). Recirculation in the rat brain following incomplete ischemia. *J. Cereb. Blood Flow Metab.*, 3(2):183–192.

Kagstrom, E., Smith, M.-L. L., Siesjö, B. K., Kågström, E., Smith, M.-L. L., and Siesjö, B. K. (1983). Local cerebral blood flow in the recovery period following complete cerebral ischemia in the rat. *J. Cereb. Blood Flow Metab.*, 3(2):170–182.

Kamouchi, M., Fujishima, M., Saku, Y., Ibayashi, S., and Iida, M. (2004). Crossed cerebellar hypoperfusion in hyperacute ischemic stroke. *J. Neurol. Sci.*, 225(1-2):65–9.

Karaki, H., Ozaki, H., Hori, M., Mitsui-Saito, M., Amano, K., Harada, K., Miyamoto, S., Nakazawa, H., Won, K. J., and Sato, K. (1997). Calcium movements, distribution, and functions in smooth muscle. *Pharmacol. Rev.*, 49(2):157–230.

Kasischke, K. A., Vishwasrao, H. D., Fisher, P. J., Zipfel, W. R., and Webb, W. W. (2004). Neural activity triggers neuronal oxidative metabolism followed by astrocytic glycolysis. *Science*, 305(5680):99–103.

Kawamura, H., Kobayashi, M., Li, Q., Yamanishi, S., Katsumura, K., Minami, M., Wu, D. M., and Puro, D. G. (2004). Effects of angiotensin II on the pericyte-containing microvasculature of the rat retina. *J. Physiol.*, 561(3):671–683.

Kawamura, H., Oku, H., Li, Q., Sakagami, K., and Puro, D. G. (2002). Endothelin-induced changes in the physiology of retinal pericytes. *Invest. Ophthalmol. Vis. Sci.*, 43(3):882–8.

Kawasaki, T., Marumo, T., Shirakami, K., Mori, T., Doi, H., Suzuki, M., Watanabe, Y., Chaki, S., Nakazato, A., Ago, Y., Hashimoto, H., Matsuda, T., Baba, A., and Onoe, H. (2012). Increase of 20-HETE synthase after brain ischemia in rats

revealed by PET study with 11C-labeled 20-HETE synthase-specific inhibitor. *J. Cereb. Blood Flow Metab.*, 32(9):1737–46.

Kelley, C., D'Amore, P., Hechtman, H. B., and Shepro, D. (1987). Microvascular pericyte contractility in vitro: comparison with other cells of the vascular wall. *J. Cell Biol.*, 104(3):483–90.

Kety, S. S. and Schmidt, C. F. (1948). The effects of altered arterial tensions of carbon dioxide and oxygen on cerebral blood flow and cerebral oxygen consumption of normal young men. *J. Clin. Invest.*, 27(4):484–492.

Khatri, P., Neff, J., Broderick, J. P., Khoury, J. C., Carrozzella, J., Tomsick, T., and IMS-I Investigators (2005). Revascularization end points in stroke interventional trials: recanalization versus reperfusion in IMS-I. *Stroke.*, 36(11):2400–3.

Knowles, R. G., Palacios, M., Palmer, R. M., and Moncada, S. (1989). Formation of nitric oxide from L-arginine in the central nervous system: a transduction mechanism for stimulation of the soluble guanylate cyclase. *Proc. Natl. Acad. Sci. U. S. A.*, 86(13):5159–62.

Ko, K. R., Ngai, A. C., and Winn, H. R. (1990). Role of adenosine in regulation of regional cerebral blood flow in sensory cortex. *Am. J. Physiol.*, 259(6 Pt 2):H1703–8.

Koehler, R. C., Roman, R. J., and Harder, D. R. (2009). Astrocytes and the regulation of cerebral blood flow. *Trends Neurosci.*, 32(3):160–9.

Koide, M., Bonev, A. D., Nelson, M. T., and Wellman, G. C. (2012). Inversion of neurovascular coupling by subarachnoid blood depends on large-conductance Ca2+-activated K+ (BK) channels. *Proc. Natl. Acad. Sci. U. S. A.*, 109(21):E1387–95.

Kornfield, T. E. and Newman, E. A. (2014). Regulation of blood flow in the retinal trilaminar vascular network. *J. Neurosci.*, 34(34):11504–13.

Krainik, A., Hund-georgiadis, M., Zysset, S., and Cramon, D. Y. V. (2005). Regional Impairment of Cerebrovascular Reactivity and. *Stroke*, pages 1146–1152.

Krueger, M. and Bechmann, I. (2010). CNS pericytes: concepts, misconceptions, and a way out. *Glia*, 58(1):1–10.

Kutcher, M. E. and Herman, I. M. (2009). The pericyte: cellular regulator of microvascular blood flow. *Microvasc. Res.*, 77(3):235–46.

Lagreze, H. L., Levine, R. L., Pedula, K. L., Nickles, R. J., Sunderland, J. S., and Rowe, B. R. (1987). Contralateral flow reduction in unilateral stroke: evidence for transhemispheric diaschisis. *Stroke*, 18(5):882–886.

Langhorne, P., Stott, D. J., Robertson, L., MacDonald, J., Jones, L., McAlpine, C., Dick, F., Taylor, G. S., and Murray, G. (2000). Medical complications after stroke: a multicenter study. *Stroke.*, 31(6):1223–9.

Langley, M. S. and Sorkin, E. M. (1989). Nimodipine. A review of its pharmacodynamic and pharmacokinetic properties, and therapeutic potential in cerebrovascular disease. *Drugs*, 37(5):669–99.

Lauritzen, M. (2001). Relationship of Spikes, Synaptic Activity, and Local Changes of Cerebral Blood Flow. *J. Cereb. Blood Flow Metab.*, 21(12):1367–1383.

Lecoq, J., Parpaleix, A., Roussakis, E., Ducros, M., Houssen, Y. G., Vinogradov, S. A., and Charpak, S. (2011). Simultaneous two-photon imaging of oxygen and blood flow in deep cerebral vessels. *Nat. Med.*, 17(7):893–898.

Lecrux, C. and Hamel, E. (2011). The neurovascular unit in brain function and disease. *Acta Physiol. (Oxf).*, 203(1):47–59.

Lecrux, C., Kocharyan, A., Sandoe, C. H., Tong, X.-K., and Hamel, E. (2012). Pyramidal cells and cytochrome P450 epoxygenase products in the neurovascular coupling response to basal forebrain cholinergic input. *J. Cereb. Blood Flow Metab.*, 32(5):896–906.

Lecrux, C., Toussay, X., Kocharyan, A., Fernandes, P., Neupane, S., Lévesque, M., Plaisier, F., Shmuel, A., Cauli, B., and Hamel, E. (2011). Pyramidal neurons are "neurogenic hubs" in the neurovascular coupling response to whisker stimulation. *J. Neurosci.*, 31(27):9836–47.

Leithner, C., Royl, G., Offenhauser, N., Füchtemeier, M., Kohl-Bareis, M., Villringer, A., Dirnagl, U., and Lindauer, U. (2010). Pharmacological uncoupling of activation induced increases in CBF and CMRO2. *J. Cereb. Blood Flow Metab.*, 30(2):311–22.

LeMaistre, J. L., Sanders, S. a., Stobart, M. J., Lu, L., Knox, J. D., Anderson, H. D., and Anderson, C. M. (2012). Coactivation of NMDA receptors by glutamate and D-serine induces dilation of isolated middle cerebral arteries. *J. Cereb. Blood Flow Metab.*, 32(3):537–547.

Lind, B. L., Brazhe, A. R., Jessen, S. B., Tan, F. C. C., and Lauritzen, M. J. (2013). Rapid stimulus-evoked astrocyte Ca2+ elevations and hemodynamic responses in mouse somatosensory cortex in vivo. *Proc. Natl. Acad. Sci.*, 110(48):E4678–E4687.

Lindauer, U., Megow, D., Matsuda, H., and Dirnagl, U. (1999). Nitric oxide: a modulator, but not a mediator, of neurovascular coupling in rat somatosensory cortex. *Am. J. Physiol.*, 277(2 Pt 2):H799–811.

Lipton, P. (1999). Ischemic cell death in brain neurons. *Physiol. Rev.*, 79(4):1431–568.

Liu, X., Li, C., Falck, J. R., Harder, D. R., and Koehler, R. C. (2012). Relative contribution of cyclooxygenases, epoxyeicosatrienoic acids, and pH to the cerebral blood flow response to vibrissal stimulation. *AJP Hear. Circ. Physiol.*, 302(5):H1075–H1085.

Liu, X., Li, C., Gebremedhin, D., Hwang, S. H., Hammock, B. D., Falck, J. R., Roman, R. J., Harder, D. R., and Koehler, R. C. (2011). Epoxyeicosatrienoic acid-dependent cerebral vasodilation evoked by metabotropic glutamate receptor activation in vivo. *Am. J. Physiol. Heart Circ. Physiol.*, 301(2):H373–81.

Llovera, G., Hofmann, K., Roth, S., Salas-Pérdomo, A., Ferrer-Ferrer, M., Perego, C., Zanier, E. R., Mamrak, U., Rex, A., Party, H., Agin, V., Fauchon, C., Orset, C., Haelewyn, B., De Simoni, M.-G., Dirnagl, U., Grittner, U., Planas, A. M., Plesnila, N., Vivien, D., and Liesz, A. (2015). Results of a preclinical randomized controlled multicenter trial (pRCT): Anti-CD49d treatment for acute brain ischemia. *Sci. Transl. Med.*, 7(299):299ra121.

Logothetis, N. K. (2003). The underpinnings of the BOLD functional magnetic resonance imaging signal. *J. Neurosci.*, 23(10):3963–71.

Logothetis, N. K. (2008). What we can do and what we cannot do with fMRI. *Nature*, 453(7197):869–878.

Logothetis, N. K. (2010). Neurovascular Uncoupling: Much Ado about Nothing. *Front. Neuroenergetics*, 2(June):1–4.

Logothetis, N. K., Pauls, J., Augath, M., Trinath, T., and Oeltermann, A. (2001). Neurophysiological investigation of the basis of the fMRI signal. *Nature*, 412(6843):150–7.

Logothetis, N. K. and Wandell, B. A. (2004). Interpreting the BOLD signal. *Annu. Rev. Physiol.*, 66(1):735–769.

Lovick, T. A., Brown, L. A., and Key, B. J. (1999). Neurovascular relationships in hippocampal slices: physiological and anatomical studies of mechanisms underlying flow-metabolism coupling in intraparenchymal microvessels. *Neuroscience*, 92(1):47–60.

Lv, Y., Margulies, D. S., Cameron Craddock, R., Long, X., Winter, B., Gierhake, D., Endres, M., Villringer, K., Fiebach, J., and Villringer, A. (2013). Identifying the perfusion deficit in acute stroke with resting-state functional magnetic resonance imaging. *Ann. Neurol.*, 73(1):136–40.

Ma, H., Zhao, M., and Schwartz, T. H. (2012). Dynamic Neurovascular Coupling and Uncoupling during Ictal Onset, Propagation, and Termination Revealed by Simultaneous In Vivo Optical Imaging of Neural Activity and Local Blood Volume. *Cereb. Cortex*, 23(4):885–99.

Macleod, M. R., Lawson McLean, A., Kyriakopoulou, A., Serghiou, S., de Wilde, A., Sherratt, N., Hirst, T., Hemblade, R., Bahor, Z., Nunes-Fonseca, C., Potluru, A., Thomson, A., Baginskaite, J., Baginskitae, J., Egan, K., Vesterinen, H., Currie, G. L., Churilov, L., Howells, D. W., and Sena, E. S. (2015a). Risk of Bias in Reports of In Vivo Research: A Focus for Improvement. *PLoS Biol.*, 13(10):e1002273.

Macleod, M. R., Lawson McLean, A., Kyriakopoulou, A., Serghiou, S., de Wilde, A., Sherratt, N., Hirst, T., Hemblade, R., Bahor, Z., Nunes-Fonseca, C., Potluru, A., Thomson, A., Baginskitae, J., Egan, K., Vesterinen, H., Currie, G. L., Churilov, L., Howells, D. W., and Sena, E. S. (2015b). Risk of Bias in Reports of In Vivo Research: A Focus for Improvement. *PLOS Biol.*, 13(10):e1002273.

Marks, L., Carswell, H. V., Peters, E. E., Graham, D. I., Patterson, J., Dominiczak, A. F., and Macrae, I. M. (2001). Characterization of the Microglial Response to Cerebral Ischemia in the Stroke-Prone Spontaneously Hypertensive Rat. *Hypertension*, 38(1):116–122.

Marks, M. P., Lansberg, M. G., Mlynash, M., Kemp, S., McTaggart, R., Zaharchuk, G., Bammer, R., Albers, G. W., and DEFUSE 2 Investigators (2014). Correlation of AOL recanalization, TIMI reperfusion and TICI reperfusion with infarct growth and clinical outcome. *J. Neurointerv. Surg.*, 6(10):724–8.

Marrelli, S. P. (2002). Altered endothelial Ca2+ regulation after ischemia/reperfusion produces potentiated endothelium-derived hyperpolarizing factor-mediated dilations. *Stroke*, 33(9):2285–2291.

Martínez-Ruiz, A., Cadenas, S., and Lamas, S. (2011). Nitric oxide signaling: classical, less classical, and nonclassical mechanisms. *Free Radic. Biol. Med.*, 51(1):17–29.

Marumo, T., Eto, K., Wake, H., Omura, T., and Nabekura, J. (2010). The inhibitor of 20-HETE synthesis, TS-011, improves cerebral microcirculatory autoregulation impaired by middle cerebral artery occlusion in mice. *Br. J. Pharmacol.*, 161(6):1391–402.

Mathiesen, C., Caesar, K., Thomsen, K., Hoogland, T. M., Witgen, B. M., Brazhe, A., and Lauritzen, M. (2011). Activity-dependent increases in local oxygen consumption correlate with postsynaptic currents in the mouse cerebellum in vivo. *J. Neurosci.*, 31(50):18327–37.

Mathiisen, T. M., Lehre, K. P., Danbolt, N. C., and Ottersen, O. P. (2010). The perivascular astroglial sheath provides a complete covering of the brain microvessels: an electron microscopic 3D reconstruction. *Glia*, 58(9):1094–103.

Matsugi, T., Chen, Q., and Anderson, D. R. (1997). Adenosine-induced relaxation of cultured bovine retinal pericytes. *Invest. Ophthalmol. Vis. Sci.*, 38(13):2695–701.

Mazzetto-Betti, K. C., Leoni, R. F., Pontes-Neto, O. M., Santos, A. C., Leite, J. P., Silva, A. C., and de Araujo, D. B. (2010). The stability of the blood oxygenation level-dependent functional MRI response to motor tasks is altered in patients with chronic ischemic stroke. *Stroke.*, 41(9):1921–6.

Mazzotta, G., Sarchielli, P., Caso, V., Paciaroni, M., Floridi, A., Floridi, A., and Gallai, V. (2004). Different cytokine levels in thrombolysis patients as predictors for clinical outcome. *Eur. J. Neurol.*, 11(6):377–381.

McDonald, D. M., Bailie, J. R., Archer, D. B., and Chakravarthy, U. (1995). Characterization of endothelin A (ETA) and endothelin B (ETB) receptors in cultured bovine retinal pericytes. *Invest. Ophthalmol. Vis. Sci.*, 36(6):1088–94.

McDonnell, L. A. and Heeren, R. M. (2007). Imaging mass spectrometry. *Mass Spectrom. Rev.*, 26(4):606–643.

McGinty, A., Scholfield, C. N., Liu, W. H., Anderson, P., Hoey, D. E., and Trimble, E. R. (1999). Effect of glucose on endothelin-1-induced calcium transients in cultured bovine retinal pericytes. *J. Biol. Chem.*, 274(36):25250–3.

Melani, A., Turchi, D., Vannucchi, M. G., Cipriani, S., Gianfriddo, M., and Pedata, F. (2005). ATP extracellular concentrations are increased in the rat striatum during in vivo ischemia. *Neurochem. Int.*, 47(6):442–448.

Mendis, S., Davis, S., and Norrving, B. (2015). Organizational update: the world health organization global status report on noncommunicable diseases 2014; one more landmark step in the combat against stroke and vascular disease. *Stroke.*, 46(5):e121–2.

Menon, R. S. (2012). The great brain versus vein debate. *Neuroimage*, 62(2):970–4.

Metea, M. R. and Newman, E. A. (2006). Glial cells dilate and constrict blood vessels: a mechanism of neurovascular coupling. *J. Neurosci.*, 26(11):2862–70.

Meyer, F. B., Anderson, R. E., Yaksh, T. L., and Sundt, T. M. (1986). Effect of nimodipine on intracellular brain pH, cortical blood flow, and EEG in experimental focal cerebral ischemia. *J. Neurosurg.*, 64(4):617–26.

Minnerup, J., Sutherland, B. A., Buchan, A. M., and Kleinschnitz, C. (2012). Neuroprotection for stroke: current status and future perspectives. *Int. J. Mol. Sci.*, 13(9):11753–72.

Mishra, A., Hamid, A., and Newman, E. A. (2011). Oxygen modulation of neurovascular coupling in the retina. *Proc. Natl. Acad. Sci. U. S. A.*, 108(43):17827–31.

Mishra, A. and Newman, E. A. (2010). Inhibition of inducible nitric oxide synthase reverses the loss of functional hyperemia in diabetic retinopathy. *Glia*, 58(16):1996–2004.

Mishra, A., O'Farrell, F. M., Reynell, C., Hamilton, N. B., Hall, C. N., and Attwell, D. (2014). Imaging pericytes and capillary diameter in brain slices and isolated retinae. *Nat. Protoc.*, 9(2):323–36.

Mohamed, A. A., Gotoh, O., Graham, D. I., Osborne, K. A., McCulloch, J., Mendelow, A. D., Teasdale, G. M., and Harper, A. M. (1985). Effect of pretreatment with the calcium antagonist nimodipine on local cerebral blood flow and histopathology after middle cerebral artery occlusion. *Ann. Neurol.*, 18(6):705–711.

Moore, C. I. and Cao, R. (2008). The hemo-neural hypothesis: on the role of blood flow in information processing. *J. Neurophysiol.*, 99(5):2035–2047.

Mori, E., del Zoppo, G. J., Chambers, J. D., Copeland, B. R., and Arfors, K. E. (1992). Inhibition of polymorphonuclear leukocyte adherence suppresses no-reflow after focal cerebral ischemia in baboons. *Stroke.*, 23(5):712–8.

Mozaffarian, D., Benjamin, E. J., Go, A. S., Arnett, D. K., Blaha, M. J., Cushman, M., de Ferranti, S., Després, J.-P., Fullerton, H. J., Howard, V. J., Huffman, M. D., Judd, S. E., Kissela, B. M., Lackland, D. T., Lichtman, J. H., Lisabeth, L. D., Liu, S., Mackey, R. H., Matchar, D. B., McGuire, D. K., Mohler, E. R., Moy, C. S., Muntner, P., Mussolino, M. E., Nasir, K., Neumar, R. W., Nichol, G., Palaniappan, L., Pandey, D. K., Reeves, M. J., Rodriguez, C. J., Sorlie, P. D., Stein, J., Towfighi, A., Turan, T. N., Virani, S. S., Willey, J. Z., Woo, D., Yeh, R. W., Turner, M. B., and American Heart Association Statistics Committee and Stroke Statistics Subcommittee (2015). Heart disease and stroke statistics–2015 update: a report from the American Heart Association. *Circulation*, 131(4):e29–322.

Mulcahy, N. J., Ross, J., Rothwell, N. J., and Loddick, S. a. (2003). Delayed administration of interleukin-1 receptor antagonist protects against transient cerebral ischaemia in the rat. *Br. J. Pharmacol.*, 140(3):471–6.

Mulligan, S. J. and MacVicar, B. A. (2004). Calcium transients in astrocyte endfeet cause cerebrovascular constrictions. *Nature*, 431(7005):195–9.

Murata, Y., Sakatani, K., Hoshino, T., Fujiwara, N., Kano, T., Nakamura, S., and Katayama, Y. (2006). Effects of cerebral ischemia on evoked cerebral blood oxygenation responses and BOLD contrast functional MRI in stroke patients. *Stroke*, 37(10):2514–2520.

Murray, K. N., Girard, S., Holmes, W. M., Parkes, L. M., Williams, S. R., Parry-Jones, A. R., and Allan, S. M. (2014). Systemic Inflammation Impairs Tissue Reperfusion Through Endothelin-Dependent Mechanisms in Cerebral Ischemia. *Stroke*, 45(11):3412–3419.

Nakai, a., Kuroda, S., Kristián, T., and Siesjö, B. K. K. (1997). The immunosuppressant drug FK506 ameliorates secondary mitochondrial dysfunction following transient focal cerebral ischemia in the rat. *Neurobiol. Dis.*, 4(3-4):288–300.

Nakamura, H., Strong, A. J., Dohmen, C., Sakowitz, O. W., Vollmar, S., Sué, M., Kracht, L., Hashemi, P., Bhatia, R., Yoshimine, T., Dreier, J. P., Dunn, A. K., and Graf, R. (2010). Spreading depolarizations cycle around and enlarge focal ischaemic brain lesions. *Brain*, 133(Pt 7):1994–2006.

Nedergaard, M. and Verkhratsky, A. (2012). Artifact versus reality–how astrocytes contribute to synaptic events. *Glia*, 60(7):1013–23.

Needleman, P., Turk, J., Jakschik, B. A., Morrison, A. R., and Lefkowith, J. B. (1986). Arachidonic acid metabolism. *Annu. Rev. Biochem.*, 55:69–102.

Nehls, V. and Drenckhahn, D. (1993). The versatility of microvascular pericytes: from mesenchyme to smooth muscle? *Histochemistry*, 99(1):1–12.

Neuhaus, A. A., Couch, Y., Sutherland, B. A., and Buchan, A. M. (2016). Novel method to study pericyte contractility and responses to ischaemia in vitro using electrical impedance. *J. Cereb. Blood Flow Metab.*

Neuhaus, A. A., Rabie, T., Sutherland, B. A., Papadakis, M., Hadley, G., Cai, R., and Buchan, A. M. (2014). Importance of preclinical research in the development of neuroprotective strategies for ischemic stroke. *JAMA Neurol.*, 71(5):634–9.

Neuwelt, E. A., Bauer, B., Fahlke, C., Fricker, G., Iadecola, C., Janigro, D., Leybaert, L., Molnár, Z., O'Donnell, M. E., Povlishock, J. T., Saunders, N. R., Sharp, F., Stanimirovic, D., Watts, R. J., and Drewes, L. R. (2011). Engaging neuroscience to advance translational research in brain barrier biology. *Nat. Rev. Neurosci.*, 12(3):169–82.

Newberg, L., Milde, J. H., and Michenfelder, J. D. (1986). Delayed Treatment with Nimodipine Improves Cerebral Blood Flow After Complete Cerebral Ischemia in the Dog. *J. Cereb. Blood Flow Metab.*, 6(3):332–337.

Newman, E. A. (2003). Glial cell inhibition of neurons by release of ATP. *J. Neurosci.*, 23(5):1659–66.

Nicolakakis, N., Aboulkassim, T., Aliaga, A., Tong, X.-K., Rosa-Neto, P., and Hamel, E. (2011). Intact memory in TGF-β1 transgenic mice featuring chronic cerebrovascular deficit: recovery with pioglitazone. *J. Cereb. Blood Flow Metab.*, 31(1):200–211.

Nimmerjahn, A., Kirchhoff, F., Kerr, J. N. D., and Helmchen, F. (2004). Sulforhodamine 101 as a specific marker of astroglia in the neocortex in vivo. *Nat. Methods*, 1(1):31–7.

Nimmerjahn, A., Mukamel, E. A., and Schnitzer, M. J. (2009). Motor behavior activates Bergmann glial networks. *Neuron*, 62(3):400–12.

Nishikibe, M. (1988). Effect of the calcium entry blocker NB-818 on cerebral blood flow after unilateral carotid occlusion in the Mongolian gerbil. *J. Pharmacol. Exp. Ther.*, 246(2):719–25.

Niwa, K., Araki, E., Morham, S. G., Ross, M. E., and Iadecola, C. (2000). Cyclooxygenase-2 contributes to functional hyperemia in whisker-barrel cortex. *J. Neurosci.*, 20(2):763–70.

Niwa, K., Haensel, C., Ross, M. E., and Iadecola, C. (2001). Cyclooxygenase-1 Participates in Selected Vasodilator Responses of the Cerebral Circulation. *Circ. Res.*, 88(6):600–608.

Nizar, K., Uhlirova, H., Tian, P., Saisan, P. A., Cheng, Q., Reznichenko, L., Weldy, K. L., Steed, T. C., Sridhar, V. B., Macdonald, C. L., Cui, J., Gratiy, S. L., Sakadzic, S., Boas, D. A., Beka, T. I., Einevoll, G. T., Chen, J., Masliah, E., Dale, A. M., Silva, G. A., and Devor, A. (2013). In vivo Stimulus-Induced Vasodilation Occurs without IP3 Receptor Activation and May Precede Astrocytic Calcium Increase. *J. Neurosci.*, 33(19):8411–8422.

Norup Nielsen, A. and Lauritzen, M. (2001). Coupling and uncoupling of activity-dependent increases of neuronal activity and blood flow in rat somatosensory cortex. *J. Physiol.*, 533(Pt 3):773–785.

O'Collins, V. E., Macleod, M. R., Donnan, G. a., Horky, L. L., van der Worp, B. H., and Howells, D. W. (2006). 1,026 Experimental treatments in acute stroke. *Ann. Neurol.*, 59(3):467–477.

Okada, Y., Copeland, B. R., Fitridge, R., Koziol, J. A., and del Zoppo, G. J. (1994). Fibrin contributes to microvascular obstructions and parenchymal changes during early focal cerebral ischemia and reperfusion. *Stroke.*, 25(9):1847–53; discussion 1853–4.

Oku, H., Kodama, T., Sakagami, K., and Puro, D. G. (2001). Diabetes-induced disruption of gap junction pathways within the retinal microvasculature. *Invest. Ophthalmol. Vis. Sci.*, 42(8):1915–20.

Omura, T., Tanaka, Y., Miyata, N., Koizumi, C., Sakurai, T., Fukasawa, M., Hachiuma, K., Minagawa, T., Susumu, T., Yoshida, S., Nakaike, S., Okuyama, S., Harder, D. R., and Roman, R. J. (2006). Effect of a new inhibitor of the synthesis of 20-HETE on cerebral ischemia reperfusion injury. *Stroke.*, 37(5):1307–13.

Orlova, V. V., van den Hil, F. E., Petrus-Reurer, S., Drabsch, Y., ten Dijke, P., and Mummery, C. L. (2014). Generation, expansion and functional analysis of endothelial cells and pericytes derived from human pluripotent stem cells. *Nat. Protoc.*, 9(6):1514–1531.

Østergaard, L., Jespersen, S. N. o. r. o. j., Mouridsen, K., aelig rke Mikkelsen, I. K., Jonsdottír, K. Ý., Tietze, A., Blicher, J. U., Aamand, R., Hjort, N., Iversen, N. K., Cai, C., Hougaard, K. D., Simonsen, C. Z., Von Weitzel-Mudersbach, P., Modrau, B., Nagenthiraja, K., Riisgaard Ribe, L., Hansen, M. B., Bekke, S. L., Dahlman, M. G., Puig, J., Pedraza, S., Serena, J. i. n., Cho, T.-H., Siemonsen, S., ouml tz Thomalla, G., Fiehler, J., Nighoghossian, N., Andersen, G., Ostergaard, L., Jespersen, S. N. o. r. o. j., Mouridsen, K., aelig rke Mikkelsen, I. K., iacute R, K. Y. r. J., Tietze, A., Blicher, J. U., Aamand, R., Hjort, N., Iversen, N. K., Cai, C., Hougaard, K. D., Simonsen, C. Z., Von Weitzel-Mudersbach, P., Modrau, B.,

Nagenthiraja, K., Ribe, L. R., Hansen, M. B., Bekke, S. L., Dahlman, M. G., Puig, J., Pedraza, S., Serena, J. i. n., Cho, T.-H., Siemonsen, S., ouml tz Thomalla, G., Fiehler, J., Nighoghossian, N., Andersen, G., Østergaard, L., Jespersen, S. N. o. r. o. j., Mouridsen, K., aelig rke Mikkelsen, I. K., Jonsdottír, K. Ý., Tietze, A., Blicher, J. U., Aamand, R., Hjort, N., Iversen, N. K., Cai, C., Hougaard, K. D., Simonsen, C. Z., Von Weitzel-Mudersbach, P., Modrau, B., Nagenthiraja, K., Riisgaard Ribe, L., Hansen, M. B., Bekke, S. L., Dahlman, M. G., Puig, J., Pedraza, S., Serena, J. i. n., Cho, T.-H., Siemonsen, S., ouml tz Thomalla, G., Fiehler, J., Nighoghossian, N., and Andersen, G. (2013). The role of the cerebral capillaries in acute ischemic stroke: the extended penumbra model. *J. Cereb. Blood Flow Metab.*, 33(5):1–14.

Otsu, Y., Couchman, K., Lyons, D. G., Collot, M., Agarwal, A., Mallet, J.-M., Pfrieger, F. W., Bergles, D. E., and Charpak, S. (2015). Calcium dynamics in astrocyte processes during neurovascular coupling. *Nat. Neurosci.*, 18(2):210–8.

Özen, I., Deierborg, T., Miharada, K., Padel, T., Englund, E., Genové, G., Paul, G., Ozen, I., Deierborg, T., Miharada, K., Padel, T., Englund, E., Genové, G., and Paul, G. (2014). Brain pericytes acquire a microglial phenotype after stroke. *Acta Neuropathol.*

Papetti, M., Shujath, J., Riley, K. N., and Herman, I. M. (2003). FGF-2 antagonizes the TGF-beta1-mediated induction of pericyte alpha-smooth muscle actin expression: a role for myf-5 and Smad-mediated signaling pathways. *Invest. Ophthalmol. Vis. Sci.*, 44(11):4994–5005.

Pappata, S., Levasseur, M., Gunn, R. N., Myers, R., Crouzel, C., Syrota, A., Jones, T., Kreutzberg, G. W., and Banati, R. B. (2000). Thalamic microglial activation in ischemic stroke detected in vivo by PET and [11C]PK1195. *Neurology*, 55(7):1052–4.

Park, L., Zhou, P., Koizumi, K., El Jamal, S., Previti, M. L., Van Nostrand, W. E., Carlson, G., and Iadecola, C. (2013). Brain and circulating levels of A??1-40 differentially contribute to vasomotor dysfunction in the mouse brain. *Stroke*, 44(1):198–204.

Paul, G., Özen, I., Christophersen, N. S., Reinbothe, T., Bengzon, J., Visse, E., Jansson, K., Dannaeus, K., Henriques-Oliveira, C., Roybon, L., Anisimov, S. V., Renström, E., Svensson, M., Haegerstrand, A., and Brundin, P. (2012). The Adult Human Brain Harbors Multipotent Perivascular Mesenchymal Stem Cells. *PLoS One*, 7(4):e35577.

Pauling, L. and Coryell, C. D. (1936). The Magnetic Properties and Structure of Hemoglobin, Oxyhemoglobin and Carbonmonoxyhemoglobin. *Proc. Natl. Acad. Sci. U. S. A.*, 22(4):210–6.

Pelligrino, D. A., Vetri, F., and Xu, H.-L. L. (2011). Purinergic mechanisms in gliovascular coupling. *Semin. Cell Dev. Biol.*, 22(2):229–236.

Peng, X., Carhuapoma, J. R., Bhardwaj, A., Alkayed, N. J., Falck, J. R., Harder, D. R., Traystman, R. J., and Koehler, R. C. (2002). Suppression of cortical functional hyperemia to vibrissal stimulation in the rat by epoxygenase inhibitors. *Am. J. Physiol. Heart Circ. Physiol.*, 283(5):H2029–37.

Peppiatt, C. M., Howarth, C., Mobbs, P., and Attwell, D. (2006). Bidirectional control of CNS capillary diameter by pericytes. *Nature*, 443(7112):700–4.

Perea, G., Navarrete, M., and Araque, A. (2009). Tripartite synapses: astrocytes process and control synaptic information. *Trends Neurosci.*, 32(8):421–31.

Petzold, G. C., Albeanu, D. F., Sato, T. F., and Murthy, V. N. (2008). Coupling of Neural Activity to Blood Flow in Olfactory Glomeruli Is Mediated by Astrocytic Pathways. *Neuron*, 58(6):897–910.

Petzold, G. C., Einhäupl, K. M., Dirnagl, U., and Dreier, J. P. (2003). Ischemia triggered by spreading neuronal activation is induced by endothelin-1 and hemoglobin in the subarachnoid space. *Ann. Neurol.*, 54(5):591–8.

Petzold, G. C. and Murthy, V. N. (2011). Role of astrocytes in neurovascular coupling. *Neuron*, 71(5):782–97.

Piilgaard, H. and Lauritzen, M. (2009). Persistent increase in oxygen consumption and impaired neurovascular coupling after spreading depression in rat neocortex. *J. Cereb. Blood Flow Metab.*, 29(9):1517–27.

Piilgaard, H., Witgen, B. M., Rasmussen, P., and Lauritzen, M. (2011). Cyclosporine A, FK506, and NIM811 ameliorate prolonged CBF reduction and impaired neurovascular coupling after cortical spreading depression. *J. Cereb. Blood Flow Metab.*, 31(7):1588–98.

Pineiro, R., Pendlebury, S., Johansen-Berg, H., and Matthews, P. M. (2002). Altered hemodynamic responses in patients after subcortical stroke measured by functional MRI. *Stroke*, 33(1):103–109.

Poloyac, S. M., Zhang, Y., Bies, R. R., Kochanek, P. M., and Graham, S. H. (2006). Protective effect of the 20-HETE inhibitor HET0016 on brain damage after temporary focal ischemia. *J. Cereb. Blood Flow Metab.*, 26(12):1551–61.

Promjunyakul, N.-O., Schmit, B. D., and Schindler-Ivens, S. (2013). Changes in hemodynamic responses in chronic stroke survivors do not affect fMRI signal detection in a block experimental design. *Magn. Reson. Imaging*, 31(7):1119–28.

Raichle, M. E. (2009). A brief history of human brain mapping. *Trends Neurosci.*, 32(2):118–126.

Raichle, M. E., Grubb, R. L., Gado, M. H., Eichling, J. O., and Ter-Pogossian, M. M. (1976). Correlation between regional cerebral blood flow and oxidative metabolism. In vivo studies in man. *Arch. Neurol.*, 33(8):523–6.

Raichle, M. E. and Mintun, M. a. (2006). Brain work and brain imaging. *Annu. Rev. Neurosci.*, 29:449–76.

Rajan, V., Varghese, B., Van Leeuwen, T. G., and Steenbergen, W. (2009). Review of methodological developments in laser Doppler flowmetry. *Lasers Med. Sci.*, 24(2):269–283.

Rasola, A. and Bernardi, P. (2011). Mitochondrial permeability transition in Ca(2+)-dependent apoptosis and necrosis. *Cell Calcium*, 50(3):222–33.

Redzic, Z. B., Rabie, T., Sutherland, B. A., and Buchan, A. M. (2015). Differential effects of paracrine factors on the survival of cells of the neurovascular unit during oxygen glucose deprivation. *Int. J. Stroke*, 10(3):407–14.

Reese, T., Bochelen, D., Baumann, D., Rausch, M., Sauter, A., and Rudin, M. (2002). Impaired functionality of reperfused brain tissue following short transient focal ischemia in rats. *Magn. Reson. Imaging*, 20(6):447–54.

Reese, T., Pórszász, R., Baumann, D., Bochelen, D., Boumezbeur, F., McAllister, K. H., Sauter, a., Bjelke, B., and Rudin, M. (2000). Cytoprotection does not preserve brain functionality in rats during the acute post-stroke phase despite evidence of non-infarction provided by MRI. *NMR Biomed.*, 13(6):361–70.

Renic, M., Klaus, J. a., Omura, T., Kawashima, N., Onishi, M., Miyata, N., Koehler, R. C., Harder, D. R., and Roman, R. J. (2009). Effect of 20-HETE inhibition on infarct volume and cerebral blood flow after transient middle cerebral artery occlusion. *J. Cereb. Blood Flow Metab.*, 29(3):629–39.

Ritter, P. and Villringer, A. (2006). Simultaneous EEG–fMRI. *Neurosci. Biobehav. Rev.*, 30(6):823–838.

Roc, A. C., Wang, J., Ances, B. M., Liebeskind, D. S., Kasner, S. E., and Detre, J. A. (2006). Altered hemodynamics and regional cerebral blood flow in patients with hemodynamically significant stenoses. *Stroke.*, 37(2):382–7.

Roda, J. M., Carceller, F., Díez-Tejedor, E., and Avendaño, C. (1995). Reduction of infarct size by intra-arterial nimodipine administered at reperfusion in a rat model of partially reversible brain focal ischemia. *Stroke.*, 26(10):1888–92.

Roman, R. J. (2002). P-450 metabolites of arachidonic acid in the control of cardiovascular function. *Physiol. Rev.*, 82(1):131–85.

Rombouts, S. A. R. B., Goekoop, R., Stam, C. J., Barkhof, F., and Scheltens, P. (2005). Delayed rather than decreased BOLD response as a marker for early Alzheimer's disease. *Neuroimage*, 26(4):1078–85.

Rosengarten, B., Krekel, D., Kuhnert, S., and Schulz, R. (2012). Early neurovascular uncoupling in the brain during community acquired pneumonia. *Crit. Care*, 16(2):R64.

Rossini, P. M., Altamura, C., Ferretti, a., Vernieri, F., Zappasodi, F., Caulo, M., Pizzella, V., Del Gratta, C., Romani, G.-L., and Tecchio, F. (2004). Does cerebrovascular disease affect the coupling between neuronal activity and local haemodynamics? *Brain*, 127(Pt 1):99–110.

Röther, J., Knab, R., Hamzei, F., Fiehler, J., Reichenbach, J. R., Büchel, C., and Weiller, C. (2002). Negative dip in BOLD fMRI is caused by blood flow–oxygen consumption uncoupling in humans. *Neuroimage*, 15(1):98–102.

Rowland, M. J., Hadjipavlou, G., Kelly, M., Westbrook, J., and Pattinson, K. T. S. (2012). Delayed cerebral ischaemia after subarachnoid haemorrhage: looking beyond vasospasm. *Br. J. Anaesth.*, 109(3):315–29.

Roy, C. S. and Sherrington, C. S. (1890). On the Regulation of the Blood-supply of the Brain. *J. Physiol.*, 11(1-2):85–158.17.

Ruitenberg, A., den Heijer, T., Bakker, S. L. M., van Swieten, J. C., Koudstaal, P. J., Hofman, A., and Breteler, M. M. B. (2005). Cerebral hypoperfusion and clinical onset of dementia: the Rotterdam Study. *Ann. Neurol.*, 57(6):789–94.

Sacco, R. L., Kasner, S. E., Broderick, J. P., Caplan, L. R., Connors, J. J. B., Culebras, A., Elkind, M. S. V., George, M. G., Hamdan, A. D., Higashida, R. T., Hoh, B. L., Janis, L. S., Kase, C. S., Kleindorfer, D. O., Lee, J.-M., Moseley, M. E., Peterson, E. D., Turan, T. N., Valderrama, A. L., Vinters, H. V., American Heart Association Stroke Council, C. o. C. S., Anesthesia, Council on Cardiovascular Radiology and Intervention, Council on Cardiovascular and Stroke Nursing, Council on Epidemiology and Prevention, Council on Peripheral Vascular Disease, Council on Nutrition, P. A., and Metabolism (2013). An updated definition of stroke for the 21st century: a statement for healthcare professionals from the American Heart Association/American Stroke Association. *Stroke.*, 44(7):2064–89.

Sakagami, K., Kawamura, H., Wu, D. M., and Puro, D. G. (2001). Nitric oxide/cGMP-induced inhibition of calcium and chloride currents in retinal pericytes. *Microvasc. Res.*, 62(2):196–203.

Sakagami, K., Wu, D. M., and Puro, D. G. (1999). Physiology of rat retinal pericytes: modulation of ion channel activity by serum-derived molecules. *J. Physiol.*, 521(3):637–650.

Sauter, A., Reese, T., Pórszász, R., Baumann, D., Rausch, M., and Rudin, M. (2002). Recovery of function in cytoprotected cerebral cortex in rat stroke model assessed by functional MRI. *Magn. Reson. Med.*, 47(4):759–65.

Saxena, H., Deshpande, D. A., Tiegs, B. C., Yan, H., Battafarano, R. J., Burrows, W. M., Damera, G., Panettieri, R. A., Dubose, T. D., An, S. S., and Penn, R. B. (2012). The GPCR OGR1 (GPR68) mediates diverse signalling and contraction of airway smooth muscle in response to small reductions in extracellular pH. *Br. J. Pharmacol.*, 166(3):981–90.

Schmitz, B., Bock, C., Hoehn-Berlage, M., Kerskens, C. M., Böttiger, B. W., and Hossmann, K. a. (1998). Recovery of the rodent brain after cardiac arrest: a functional MRI study. *Magn. Reson. Med.*, 39(5):783–8.

Schmitz, B., Böttiger, B. W., and Hossmann, K. a. (1997). Functional activation of cerebral blood flow after cardiac arrest in rat. *J. Cereb. Blood Flow Metab.*, 17(11):1202–9.

Schulz, K., Sydekum, E., Krueppel, R., Engelbrecht, C. J., Schlegel, F., Schröter, A., Rudin, M., and Helmchen, F. (2012). Simultaneous BOLD fMRI and fiber-optic calcium recording in rat neocortex. *Nat. Methods*, 9(6):597–602.

Schummers, J., Yu, H., and Sur, M. (2008). Tuned responses of astrocytes and their influence on hemodynamic signals in the visual cortex. *Science*, 320(5883):1638–43.

Schwab, S., Steiner, T., Aschoff, A., Schwarz, S., Steiner, H. H., Jansen, O., and Hacke, W. (1998). Early hemicraniectomy in patients with complete middle cerebral artery infarction. *Stroke.*, 29(9):1888–93.

Scremin, O. U., Rovere, A. A., Raynald, A. C., and Giardini, A. (1973). Cholinergic control of blood flow in the cerebral cortex of the rat. *Stroke.*, 4(2):233–9.

Scriabine, A., Schuurman, T., and Traber, J. (1989). Pharmacological basis for the use of nimodipine in central nervous system disorders. *FASEB J.*, 3(7):1799–806.

Segal, S. S. and Duling, B. R. (1986). Flow control among microvessels coordinated by intercellular conduction. *Science*, 234(4778):868–70.

Sena, E., van der Worp, H. B., Howells, D., and Macleod, M. (2007). How can we improve the pre-clinical development of drugs for stroke? *Trends Neurosci.*, 30(9):433–9.

Sena, E. S., van der Worp, H. B., Bath, P. M. W., Howells, D. W., and Macleod, M. R. (2010). Publication bias in reports of animal stroke studies leads to major overstatement of efficacy. *PLoS Biol.*, 8(3):e1000344.

Seo, B., Oemar, B. S., Siebenmann, R., von Segesser, L., and Lüscher, T. F. (1994). Both ETA and ETB receptors mediate contraction to endothelin-1 in human blood vessels. *Circulation*, 89(3):1203–8.

Shen, Q., Ren, H., Cheng, H., Fisher, M., and Duong, T. Q. (2005). Functional, perfusion and diffusion MRI of acute focal ischemic brain injury. *J. Cereb. Blood Flow Metab.*, 25(10):1265–79.

Shen, Z., Lu, Z., Chhatbar, P. Y., O'Herron, P., and Kara, P. (2012). An artery-specific fluorescent dye for studying neurovascular coupling. *Nat. Methods*, 9(3):273–6.

Sheth, S., Nemoto, M., Guiou, M., Walker, M., Pouratian, N., and Toga, A. W. (2003). Evaluation of coupling between optical intrinsic signals and neuronal activity in rat somatosensory cortex. *Neuroimage*, 19(3):884–894.

Sheth, S. A., Nemoto, M., Guiou, M., Walker, M., Pouratian, N., and Toga, A. W. (2004). Linear and nonlinear relationships between neuronal activity, oxygen metabolism, and hemodynamic responses. *Neuron*, 42(2):347–55.

Shih, A. Y., Blinder, P., Tsai, P. S., Friedman, B., Stanley, G., Lyden, P. D., and Kleinfeld, D. (2013). The smallest stroke: occlusion of one penetrating vessel leads to infarction and a cognitive deficit. *Nat. Neurosci.*, 16(1):55–63.

Shih, A. Y., Driscoll, J. D., Drew, P. J., Nishimura, N., Schaffer, C. B., and Kleinfeld, D. (2012). Two-photon microscopy as a tool to study blood flow and neurovascular coupling in the rodent brain. *J. Cereb. Blood Flow Metab.*, 32(7):1277–309.

Shin, H. K., Dunn, A. K., Jones, P. B., Boas, D. A., Moskowitz, M. A., and Ayata, C. (2006). Vasoconstrictive neurovascular coupling during focal ischemic depolarizations. *J. Cereb. Blood Flow Metab.*, 26(8):1018–30.

Shin, H. K., Salomone, S., Potts, E. M., Lee, S.-W., Millican, E., Noma, K., Huang, P. L., Boas, D. A., Liao, J. K., Moskowitz, M. a., and Ayata, C. (2007). Rho-kinase inhibition acutely augments blood flow in focal cerebral ischemia via endothelial mechanisms. *J. Cereb. Blood Flow Metab.*, 27(5):998–1009.

Sicard, K. M., Henninger, N., Fisher, M., Duong, T. Q., and Ferris, C. F. (2006). Differential recovery of multimodal MRI and behavior after transient focal cerebral ischemia in rats. *J. Cereb. Blood Flow Metab.*, 26(11):1451–62.

Sieczkiewicz, G. J. and Herman, I. M. (2003). TGF-beta 1 signaling controls retinal pericyte contractile protein expression. *Microvasc. Res.*, 66(3):190–6.

Sierra-Paredes, G. and Sierra-Marcuño, G. (2008). Ascomycin and FK506: pharmacology and therapeutic potential as anticonvulsants and neuroprotectants. *CNS Neurosci. Ther.*, 14(1):36–46.

Sirotin, Y. B. and Das, A. (2009). Anticipatory haemodynamic signals in sensory cortex not predicted by local neuronal activity. *Nature*, 457(7228):475–9.

Smith, M.-L., Kågström, E., Rosén, I., and Siesjö, B. K. (1983). Effect of the Calcium Antagonist Nimodipine on the Delayed Hypoperfusion Following Incomplete Ischemia in the Rat. *J. Cereb. Blood Flow Metab.*, 3(4):543–546.

Soares, B. P., Tong, E., Hom, J., Cheng, S.-C., Bredno, J., Boussel, L., Smith, W. S., and Wintermark, M. (2010). Reperfusion is a more accurate predictor of follow-up infarct volume than recanalization: a proof of concept using CT in acute ischemic stroke patients. *Stroke.*, 41(1):e34–40.

Somjen, G. G. (1979). Extracellular potassium in the mammalian central nervous system. *Annu. Rev. Physiol.*, 41(184):159–77.

Song, W., Zukor, H., Lin, S.-H., Hascalovici, J., Liberman, A., Tavitian, A., Mui, J., Vali, H., Tong, X.-K., Bhardwaj, S. K., Srivastava, L. K., Hamel, E., and Schipper, H. M. (2012). Schizophrenia-like features in transgenic mice overexpressing human HO-1 in the astrocytic compartment. *J. Neurosci.*, 32(32):10841–53.

Srinivasan, R., Huang, B. S., Venugopal, S., Johnston, A. D., Chai, H., Zeng, H., Golshani, P., and Khakh, B. S. (2015). Ca(2+) signaling in astrocytes from Ip3r2(-/-) mice in brain slices and during startle responses in vivo. *Nat. Neurosci.*, 18(5):708–17.

Stark, K., Eckart, A., Haidari, S., Tirniceriu, A., Lorenz, M., von Brühl, M.-L., Gärtner, F., Khandoga, A. G., Legate, K. R., Pless, R., Hepper, I., Lauber, K., Walzog, B., and Massberg, S. (2013). Capillary and arteriolar pericytes attract innate leukocytes exiting through venules and 'instruct' them with pattern-recognition and motility programs. *Nat. Immunol.*, 14(1):41–51.

Steen, P. A., Newberg, L. A., Milde, J. H., and Michenfelder, J. D. (1983). Nimodipine Improves Cerebral Blood Flow and Neurologic Recovery After Complete Cerebral Ischemiain the Dog. *J. Cereb. Blood Flow Metab.*, 3(1):38–43.

Stefanovic, B., Bosetti, F., and Silva, A. C. (2006). Modulatory role of cyclooxygenase-2 in cerebrovascular coupling. *Neuroimage*, 32(1):23–32.

Stefanovic, B., Hutchinson, E., Yakovleva, V., Schram, V., Russell, J. T., Belluscio, L., Koretsky, A. P., and Silva, A. C. (2008). Functional reactivity of cerebral capillaries. *J. Cereb. Blood Flow Metab.*, 28(5):961–72.

Stefanovic, B., Schwindt, W., Hoehn, M., and Silva, A. C. (2007). Functional uncoupling of hemodynamic from neuronal response by inhibition of neuronal nitric oxide synthase. *J. Cereb. Blood Flow Metab.*, 27(4):741–54.

Stich, M., Thalhammer, S., Burgemeister, R., Friedemann, G., Ehnle, S., Lüthy, C., and Schütze, K. (2003). Live cell catapulting and recultivation. *Pathol. Res. Pract.*, 199(6):405–9.

Stobart, J. L. and Anderson, C. M. (2013). Multifunctional role of astrocytes as gatekeepers of neuronal energy supply. *Front. Cell. Neurosci.*, 7(April):38.

Stroke Therapy Academic Industry Roundtable (STAIR) (1999). Recommendations for standards regarding preclinical neuroprotective and restorative drug development. *Stroke.*, 30(12):2752–8.

Stroke Unit Trialists Collaboration (1997). How do stroke units improve patient outcomes? A collaborative systematic review of the randomized trials. *Stroke.*, 28(11):2139–44.

Strong, A. J., Anderson, P. J., Watts, H. R., Virley, D. J., Lloyd, A., Irving, E. a., Nagafuji, T., Ninomiya, M., Nakamura, H., Dunn, A. K., and Graf, R. (2007). Peri-infarct depolarizations lead to loss of perfusion in ischaemic gyrencephalic cerebral cortex. *Brain*, 130(Pt 4):995–1008.

Stubbs, D., DeProto, J., Nie, K., Englund, C., Mahmud, I., Hevner, R., and Molnár, Z. (2009). Neurovascular congruence during cerebral cortical development. *Cereb. Cortex*, 19 Suppl 1(July):i32–41.

Sugiyama, T., Kawamura, H., Yamanishi, S., Kobayashi, M., Katsumura, K., and Puro, D. G. (2005). Regulation of P2X7-induced pore formation and cell death in pericyte-containing retinal microvessels. *Am. J. Physiol. Cell Physiol.*, 288(3):C568–76.

Sun, H., Kosaras, B., Klein, P. M., and Jensen, F. E. (2013). Mammalian target of rapamycin complex 1 activation negatively regulates Polo-like kinase 2-mediated homeostatic compensation following neonatal seizures. *Proc. Natl. Acad. Sci. U. S. A.*, pages 1–6.

Sutherland, B., Neuhaus, A., Couch, Y., Balami, J., Deluca, G., Hadley, G., Harris, S., Grey, A., and Buchan, A. (2016). The transient intraluminal filament middle cerebral artery occlusion model as a model of endovascular thrombectomy in stroke. *J. Cereb. Blood Flow Metab.*, 36(2):363–369.

Sutherland, B. A. and Buchan, A. M. (2013). Alteplase treatment does not increase brain injury after mechanical middle cerebral artery occlusion in the rat. *J. Cereb. Blood Flow Metab.*, 33(11):e1–7.

Sutherland, B. A., Minnerup, J., Balami, J. S., Arba, F., Buchan, A. M., and Kleinschnitz, C. (2012). Neuroprotection for ischaemic stroke: Translation from the bench to the bedside. *Int. J. Stroke*, 7(5):407–418.

Sweetnam, D. A. A. and Brown, C. E. E. (2012). Stroke induces long-lasting deficits in the temporal fidelity of sensory processing in the somatosensory cortex. *J. Cereb. Blood Flow Metab.*, 33(May):1–6.

Szydlowska, K. and Tymianski, M. (2010). Calcium, ischemia and excitotoxicity. *Cell Calcium*, 47(2):122–129.

Takano, T., Tian, G.-F., Peng, W., Lou, N., Libionka, W., Han, X., and Nedergaard, M. (2006). Astrocyte-mediated control of cerebral blood flow. *Nat. Neurosci.*, 9(2):260–7.

Takano, T., Tian, G.-F., Peng, W., Lou, N., Lovatt, D., Hansen, A. J., Kasischke, K. A., and Nedergaard, M. (2007). Cortical spreading depression causes and coincides with tissue hypoxia. *Nat. Neurosci.*, 10(6):754–62.

Takata, N., Nagai, T., Ozawa, K., Oe, Y., Mikoshiba, K., and Hirase, H. (2013). Cerebral blood flow modulation by Basal forebrain or whisker stimulation can occur independently of large cytosolic Ca2+ signaling in astrocytes. *PLoS One*, 8(6):e66525.

Tanaka, Y., Omura, T., Fukasawa, M., Horiuchi, N., Miyata, N., Minagawa, T., Yoshida, S., and Nakaike, S. (2007). Continuous inhibition of 20-HETE synthesis by TS-011 improves neurological and functional outcomes after transient focal cerebral ischemia in rats. *Neurosci. Res.*, 59(4):475–80.

The National Institute of Neurological Disorders and Stroke rt-PA Stroke Study Group (NINDS) (1995). Tissue plasminogen activator for acute ischemic stroke. *N Engl J Med*, 333(24):1581–1587.

Thomas, D. L., Lythgoe, M. F., van der Weerd, L., Ordidge, R. J., and Gadian, D. G. (2006). Regional variation of cerebral blood flow and arterial transit time in the normal and hypoperfused rat brain measured using continuous arterial spin labeling MRI. *J. Cereb. Blood Flow Metab.*, 26(2):274–82.

Tomassoni, D., Lanari, A., Silvestrelli, G., Traini, E., and Amenta, F. (2008). Nimodipine and Its Use in Cerebrovascular Disease: Evidence from Recent Preclinical and Controlled Clinical Studies. *Clin. Exp. Hypertens.*, 30(8):744–766.

Topol, E. J. and Yadav, J. S. (2000). Recognition of the Importance of Embolization in Atherosclerotic Vascular Disease. *Circulation*, 101(5):570–580.

Tran, C. H. T. and Gordon, G. R. (2015). Acute two-photon imaging of the neurovascular unit in the cortex of active mice. *Front. Cell. Neurosci.*, 9(February):11.

Tremblay, M.-È., Stevens, B., Sierra, A., Wake, H., Bessis, A., and Nimmerjahn, A. (2011). The role of microglia in the healthy brain. *J. Neurosci.*, 31(45):16064–9.

Tsacopoulos, M. and Magistretti, P. J. (1996). Metabolic coupling between glia and neurons. *J. Neurosci.*, 16(3):877–885.

Tsai, Y.-H., Yuan, R., Huang, Y.-C., Weng, H.-H., Yeh, M.-Y., Lin, C.-P., and Biswal, B. B. (2014). Altered resting-state FMRI signals in acute stroke patients with ischemic penumbra. *PLoS One*, 9(8):e105117.

Ueki, M., Linn, F., and Hossmann, K. a. (1988). Functional activation of cerebral blood flow and metabolism before and after global ischemia of rat brain. *J. Cereb. Blood Flow Metab.*, 8(4):486–94.

Uematsu, D., Greenberg, J. H., Hickey, W. F., and Reivich, M. (1989). Nimodipine attenuates both increase in cytosolic free calcium and histologic damage following focal cerebral ischemia and reperfusion in cats. *Stroke.*, 20(11):1531–7.

Urbaniak, G. C. and Plous, S. (2013). Research Randomizer (Version 4.0) [Computer software], http://www.randomizer.org.

Vangilder, R. L., Rosen, C. L., Barr, T. L., and Huber, J. D. (2011). Targeting the neurovascular unit for treatment of neurological disorders. *Pharmacol. Ther.*, 130(3):239–247.

Vanzetta, I. and Grinvald, A. (2001). Evidence and lack of evidence for the initial dip in the anesthetized rat: implications for human functional brain imaging. *Neuroimage*, 13(6 Pt 1):959–67.

Vates, G. E., Takano, T., Zlokovic, B., and Nedergaard, M. (2010). Pericyte constriction after stroke: the jury is still out. *Nat. Med.*, 16(9):959; author reply 960.

Vaucher, E. and Hamel, E. (1995). Cholinergic basal forebrain neurons project to cortical microvessels in the rat: electron microscopic study with anterogradely transported Phaseolus vulgaris leucoagglutinin and choline acetyltransferase immunocytochemistry. *J. Neurosci.*, 15(11):7427–7441.

Veldsman, M., Cumming, T., and Brodtmann, A. (2015). Beyond BOLD: Optimizing functional imaging in stroke populations. *Hum. Brain Mapp.*, 36(4):1620–1636.

Vila, E. and Salaices, M. (2005). Cytokines and vascular reactivity in resistance arteries. *Am. J. Physiol. Heart Circ. Physiol.*, 288(3):H1016–21.

Villringer, A. (2012). The intravascular susceptibility effect and the underlying physiology of fMRI. *Neuroimage*, 62(2):995–9.

von Tell, D., Armulik, A., and Betsholtz, C. (2006). Pericytes and vascular stability. *Exp. Cell Res.*, 312(5):623–9.

Wang, R., Li, Q., and Tang, D. D. (2006a). Role of vimentin in smooth muscle force development. *Am. J. Physiol. Cell Physiol.*, 291(3):C483–9.

Wang, X., Lou, N., Xu, Q., Tian, G.-F., Peng, W. G., Han, X., Kang, J., Takano, T., and Nedergaard, M. (2006b). Astrocytic Ca2+ signaling evoked by sensory stimulation in vivo. *Nat. Neurosci.*, 9(6):816–23.

Wardlaw, J. M. and Dennis, M. S. (2015). Thrombectomy for Acute Ischemic Stroke. *JAMA*, 314(17):1803–5.

Wardlaw, J. M., Murray, V., Berge, E., del Zoppo, G., Sandercock, P., Lindley, R. L., and Cohen, G. (2012). Recombinant tissue plasminogen activator for acute ischaemic stroke: an updated systematic review and meta-analysis. *Lancet (London, England)*, 379(9834):2364–72.

Wardlaw, J. M., Murray, V., Berge, E., and del Zoppo, G. J. (2014). Thrombolysis for acute ischaemic stroke. *Cochrane database Syst. Rev.*, (7):CD000213.

Weber, R., Ramos-Cabrer, P., Justicia, C., Wiedermann, D., Strecker, C., Sprenger, C., and Hoehn, M. (2008). Early prediction of functional recovery after experimental stroke: functional magnetic resonance imaging, electrophysiology, and behavioral testing in rats. *J. Neurosci.*, 28(5):1022–9.

Wede, O. K., Löfgren, M., Li, Z., Paulin, D., and Arner, A. (2002). Mechanical function of intermediate filaments in arteries of different size examined using desmin deficient mice. *J. Physiol.*, 540(Pt 3):941–9.

Wei, H. S., Kang, H., Rasheed, I.-Y. D., Zhou, S., Lou, N., Gershteyn, A., McConnell, E. D., Wang, Y., Richardson, K. E., Palmer, A. F., Xu, C., Wan, J., and Nedergaard, M. (2016). Erythrocytes Are Oxygen-Sensing Regulators of the Cerebral Microcirculation. *Neuron*, 91(4):851–62.

Williams, M., Francis, J., Ghai, G., Braunwalder, A., Psychoyos, S., Stone, G. A., and Cash, W. D. (1987). Biochemical characterization of the triazoloquinazoline, CGS 15943, a novel, non-xanthine adenosine antagonist. *J. Pharmacol. Exp. Ther.*, 241(2):415–20.

Winters, A., Taylor, J. C., Ren, M., Ma, R., Liu, R., and Yang, S.-H. (2012). Transient Focal Cerebral Ischemia Induces Long-Term Cerebral Vasculature Dysfunction in a Rodent Experimental Stroke Model. *Transl. Stroke Res.*, 3(2):279–285.

Wyss, M. T., Jolivet, R., Buck, A., Magistretti, P. J., and Weber, B. (2011). In vivo evidence for lactate as a neuronal energy source. *J. Neurosci.*, 31(20):7477–85.

Xi, B., Wang, T., Li, N., Ouyang, W., Zhang, W., Wu, J., Xu, X., Wang, X., and Abassi, Y. A. (2011). Functional cardiotoxicity profiling and screening using the xCELLigence RTCA Cardio System. *J. Lab. Autom.*, 16(6):415–21.

Yamagishi, S., Hsu, C. C., Kobayashi, K., and Yamamoto, H. (1993). Endothelin 1 mediates endothelial cell-dependent proliferation of vascular pericytes. *Biochem. Biophys. Res. Commun.*, 191(3):840–6.

Yanagisawa, M., Kurihara, H., Kimura, S., Tomobe, Y., Kobayashi, M., Mitsui, Y., Yazaki, Y., Goto, K., and Masaki, T. (1988). A novel potent vasoconstrictor peptide produced by vascular endothelial cells. *Nature*, 332(6163):411–5.

Yang, G., Zhang, Y., Ross, M. E., and Iadecola, C. (2003). Attenuation of activity-induced increases in cerebellar blood flow in mice lacking neuronal nitric oxide synthase. *Am. J. Physiol. Heart Circ. Physiol.*, 285(1):H298–304.

Yang, Y. and Rosenberg, G. a. (2011). Blood-brain barrier breakdown in acute and chronic cerebrovascular disease. *Stroke*, 42(11):3323–3328.

Yemisci, M., Gursoy-Ozdemir, Y., Vural, A., Can, A., Topalkara, K., and Dalkara, T. (2009). Pericyte contraction induced by oxidative-nitrative stress impairs capillary reflow despite successful opening of an occluded cerebral artery. *Nat. Med.*, 15(9):1031–7.

Yu, M., Cambj-Sapunar, L., Kehl, F., Maier, K. G., Takeuchi, K., Miyata, N., Ishimoto, T., Reddy, L. M., Falck, J. R., Gebremedhin, D., Harder, D. R., and Roman, R. J. (2004). Effects of a 20-HETE antagonist and agonists on cerebral vascular tone. *Eur. J. Pharmacol.*, 486(3):297–306.

Yu, X., He, Y., Wang, M., Merkle, H., Dodd, S. J., Silva, A. C., and Koretsky, A. P. (2016). Sensory and optogenetically driven single-vessel fMRI. *Nat. Methods*.

Zhang, J., Chen, Y.-m., and Zhang, Y.-t. (2011). Blood-oxygenation-level-dependent-(BOLD-) based R2' MRI study in monkey model of reversible middle cerebral artery occlusion. *J. Biomed. Biotechnol.*, 2011:318346.

Zhang, J., Yang, J., Zhang, C., Jiang, X., Zhou, H., and Liu, M. (2012a). Calcium antagonists for acute ischemic stroke. *Cochrane database Syst. Rev.*, (5):CD001928.

Zhang, Y., Chen, K., Sloan, S. a., Bennett, M. L., Scholze, A. R., O'Keeffe, S., Phatnani, H. P., Guarnieri, P., Caneda, C., Ruderisch, N., Deng, S., Liddelow, S. a., Zhang, C., Daneman, R., Maniatis, T., Barres, B. a., and Wu, J. Q. (2014). An RNA-Sequencing Transcriptome and Splicing Database of Glia, Neurons, and Vascular Cells of the Cerebral Cortex. *J. Neurosci.*, 34(36):11929–47.

Zhang, Y.-P., Zhang, H., and Duan, D. D. (2012b). Chloride channels in stroke. *Acta Pharmacol. Sin.*, pages 1–7.

Zhou, C., Shimazu, T., Durduran, T., Luckl, J., Kimberg, D. Y., Yu, G., Chen, X.-H., Detre, J. a., Yodh, A. G., and Greenberg, J. H. (2008). Acute functional recovery of cerebral blood flow after forebrain ischemia in rat. *J. Cereb. Blood Flow Metab.*, 28(7):1275–84.

Zhou, L., Sohet, F., and Daneman, R. (2014). Purification and culture of central nervous system pericytes. *Cold Spring Harb. Protoc.*, 2014(6):pdb.top070888.

Zimmermann, H. and Braun, N. (1996). Extracellular metabolism of nucleotides in the nervous system. *J. Auton. Pharmacol.*, 16(6):397–400.

Ziv, I., Fleminger, G., Djaldetti, R., Achiron, A., Melamed, E., and Sokolovsky, M. (1992). Increased plasma endothelin-1 in acute ischemic stroke. *Stroke.*, 23(7):1014–6.

Zonta, M., Angulo, M. C., Gobbo, S., Rosengarten, B., Hossmann, K.-A., Pozzan, T., and Carmignoto, G. (2003). Neuron-to-astrocyte signaling is central to the dynamic control of brain microcirculation. *Nat. Neurosci.*, 6(1):43–50.

Zou, a. P., Fleming, J. T., Falck, J. R., Jacobs, E. R., Gebremedhin, D., Harder, D. R., and Roman, R. J. (1996). 20-HETE is an endogenous inhibitor of the large-conductance Ca(2+)-activated K+ channel in renal arterioles. *Am. J. Physiol.*, 270(1 Pt 2):R228–37.